



MONASH University

Oxy-Fuel Combustion of Victorian Brown Coal

Wirhan Prationo

B.Eng. (Chemical Engineering (Hons))

A thesis submitted in fulfilment of the requirement for the degree
of

Doctor of Philosophy

Department of Chemical Engineering

Faculty of Engineering

MONASH UNIVERSITY

September 2015

Copyright notice

© Wirhan Prationo (2015). Except as provided in the Copyright Act 1968, this thesis may not be reproduced in any form without the written permission of the author.

I certify that I have made all reasonable efforts to secure copyright permissions for third-party content included in this thesis and have not knowingly added copyright content to my work without the owner's permission.

DECLARATION

I hereby declare that this thesis contains no material which has been accepted for the award of any other degree or diploma at any university or equivalent institution and that, to the best of my knowledge and belief, this thesis contains no material previously published or written by another person, except where due reference is made in the text of the thesis.

This thesis includes three original papers published in peer reviewed journals and one unpublished publication. The core theme of the thesis is the investigation of the ignition characteristic of Victorian brown coal during oxy fuel combustion. The ideas, development and writing up of all the papers in the thesis were the principal responsibility of my own, the candidate, working within the Department of Chemical Engineering under the supervision of Dr. Lian Zhang.

(The inclusion of co-authors reflects the fact that the work came from active collaboration between researchers and acknowledges input into the team-based research)

In the case of following chapters:

Chapter 4: *Influence of External Clay and Inherent Minerals on Lignite Optical Ignition and Volatile Flame Propagation in Air-Firing and Oxy-Firing*

Chapter 5: *Influence of inherent moisture on the ignition and combustion of wet Victorian brown coal in air-firing and oxy-fuel modes: Part 1: The volatile ignition and flame propagation*

Chapter 6: *Clarifying the influence of moisture on the ignition and combustion of wet Victorian brown coal in air-firing and oxy-fuel modes: Part 2: Contribution of gasification reaction to char oxidation rate*

Chapter 7: *Influence of steam on ignition of Victorian brown coal particle stream in oxy-fuel combustion*

My contribution to the work involved the following:

Thesis chapter	Publication title	Publication status*	Nature and extent (%) of students contribution
4	Influence of External Clay and Inherent Minerals on Lignite Optical Ignition and Volatile Flame Propagation in Air-Firing and Oxy-Firing	Published	90% - Experiment, analysis, writing up the paper
5	Influence of inherent moisture on the ignition and combustion of wet Victorian brown coal in air-firing and oxy-fuel modes: Part 1: The volatile ignition and flame propagation	Published	99% - Experiment, analysis, writing up the paper
6	Clarifying the influence of moisture on the ignition and combustion of wet Victorian brown coal in air-firing and oxy-fuel modes: Part 2: Contribution of gasification reaction to char oxidation rate	Published	99% - Experiment, analysis, writing up the paper
7	Influence of steam on ignition of Victorian brown coal particle stream in oxy-fuel combustion	Submitted for Publication	100% - Experiment, analysis, writing up the paper

I have / have not renumbered sections of submitted or published papers in order to generate a consistent presentation within the thesis.

Student signature:

Date: 22-09-2015

The undersigned hereby certify that the above declaration correctly reflects the nature and extent of the student and co-authors' contributions to this work.

Main Supervisor signature:



Date: 22-09-2015

ACKNOWLEDGEMENTS

First and foremost, I would like to express my deepest gratitude to my supervisor Dr. Lian Zhang, for the support and guidance to establish this research project, for his limitless patience to revise my work over and over, and also for conveying his ambition to research, which has strongly influenced myself during my research. Without your guidance, this research project would not have been possible.

I also would like to thank my co supervisor Dr. Meng Wai Woo for your help and aid that helped me to complete the mathematical modelling studies. I really appreciate your willingness to listen to my concern and thank you for always giving constructive comments. To Professor Brian Haynes at University of Sydney, thank you for your feedback on my work during my visit to your university two years ago. My special gratitude goes to the postdoctoral research fellow in our research group, Dr. Jian Zhang, who has left to his hometown in China to take on an Associate Professor position. You have provided huge assistance in establishing my foundation in mathematical modelling and also provide directions in this most difficult part of my studies. I doubt I would be able to finish this project without your guidance in this aspect.

My acknowledgement also goes to Brown Coal Innovation Australia (BCIA), ANLEC R&D (Australia National Low Emission Coal Research & Development) and Department of Chemical Engineering, Monash University who has offered me an opportunity to take on this PhD project and also for the financial supports.

I would also like to take this opportunity to extend my gratitude to the staffs in the Department of Chemical Engineering; Kim Phu, Ronald Graham, Garry Thunder, Ross Ellingham, Gamini Ganegoda, Lilyanne Price, Martin Watkins, Jill Crisfield and specially Harry Bouwmeester. Thank you so much for your assistance and support in the laboratory and also patiently helping with a lot of technical problems that I have to deal with. Without your help, I would not be able to finish up my project in time.

To my friends in my research group, Teck Kwang and Anthony, for being my coffee and dinner buddies during stressful time, Baiqian, for always initiating this session and also

cooking us some amazing food, Niken, for her assistance when I just started my PhD project, Fiona, for listening to my personal issues (although your feedbacks are irrelevant, I still appreciate that you are willing to listen to me), Tahereh, for your feedback on my work during the group meeting. Thank you to all of you guys for being there throughout my studies these years.

Sharmen and Willie, we started our research projects around the same time. It was quite stressful initially as we were totally clueless on our project. However, having buddies to talk with and providing each other feedbacks and encouragements indeed has provided a great help. Thank you for being there. To Kenneth, I always come to you whenever I had a problem, either personal or academic. Thank you for always listening to me.

Finally, I would like to thank my family, for your spiritual support and confidence in me, which has made me who I am. To Fensuny Chan, you have always been there through easy and hard time. It is thanks to your constant support throughout these years that always back me up when I am down. Thank you for your unwavering belief in me that made it possible to finish this project.

PUBLICATIONS

Peer reviewed journal (s):

LIST OF PUBLICATION FROM THIS RESEARCH THAT IS INCLUDED IN THIS THESIS:

- **Pratono, W.,** Zhang, J., Abbas, H.A.A., Wu, X., Chen. X.D., and Zhang, L., *Influence of external clay and inherent minerals on lignite optical ignition and flame propagation in air-firing and oxy-firing.*, Industrial Engineering & Chemistry Research, 2014, 53(7), pp 2594-2604.
- **Pratono, W.,** Zhang, J., Cui, J.F., Wang, Y.T., and Zhang, L., *Influence of inherent moisture on the ignition and combustion of wet Victorian brown coal in air-firing and oxy-fuel modes: Part 1: The volatile ignition and flame propagation.*, Fuel Processing Technology, 2015, 138, pp 670-679.
- **Pratono, W.,** Zhang, J., Cui, J.F., Wang, Y.T., and Zhang, L., *Clarifying the influence of moisture on the ignition and combustion of wet Victorian brown coal in air-firing and oxy-fuel modes: Part 2: Contribution of gasification reaction to char oxidation rate.*, Fuel Processing Technology, 2015, 138, pp 680-686.
- **Pratono, W.,** Zhang, L., *Influence of steam on ignition of Victorian brown coal particle stream in oxy-fuel combustion: In-situ Diagnosis and Transient ignition modelling.*, Fuel, 2016, Special Issues ISCC 8 (**Submitted for Publication**).

LIST OF PUBLICATION FROM THIS RESEARCH THAT IS NOT INCLUDED IN THIS THESIS:

- Zhang,J., **Pratono, W.,** Zhang, L., and Zhang, Z.X., *Computational fluid dynamics modelling on the air-firing and oxy-fuel combustion of dried Victorian brown coal.*, Energy Fuels, 2013, 27(8), pp. 4258-4269.

CONFERENCE PUBLICATION (s):

- **Pratono, W.** and Zhang, L., *Advancing Oxy-fuel combustion of Victorian brown coal for Low Carbon Emission*. AIE Postgraduate Energy Awards 2012, Melbourne, Victoria. 10-11 October 2012.
- Zhang, J., **Pratono, W.**, and Zhang, L., *CFD Modelling of the Oxy-Fuel Combustion of Victorian Brown Coal in Lab-Scale Drop-Tube Furnace and 3MW Pilot-Scale Boiler*". 9th International Conference of CFD on the Minerals and Process Industry, CSIRO, Melbourne, Victoria. 10-12 December 2012.
- **Pratono, W.**, Zhang, L., and Zhang, J., *Ignition and Combustion characteristics of wet Victorian brown coal in oxy-firing and air-firing conditions*". 30th Annual International Pittsburgh Coal Conference, Beijing, China. 16-18th September 2013.
- **Pratono, W.**, Zhang, L., and Zhang, J., *Modelling Studies to clarify the influence of moisture in wet Victorian brown coal combustion in air-firing and oxy-firing*". JCG Australia-China Oxy-fuel combustion workshop. 6-7th February 2014.
- **Pratono, W.** and Zhang, L., *"Influence of Steam on ignition of Victorian brown coal particle stream in oxy-fuel combustion"*. 8th International Symposium on Coal Combustion, Beijing, China. 19-22nd July 2015. Note: Recommended for publication as special issues in Energy Fuels

AWARDS:

- Encouragement Awards (3rd place) from AIE Postgraduate Energy Awards 2012, held in Melbourne, Australia. Poster titled: *"Advancing oxy-fuel combustion of Victorian brown coal for low carbon emission"*.

LIST OF TABLES

Table 1-1 World recoverable coal reserves as of 1st January 2010 (billions tonnes), adapted from (IEO, 2011).....	5
Table 1-2 Proximate and Ultimate analysis of brown coal from Australia, China, Germany and Indonesia (Li, 2004; Liu, 2012; Prationo, 2014; Young, 1988).....	8
Table 1-3 Summary of GCCSI costing study (GSSCI, 2009).....	15
Table 2-1 Properties of N ₂ , CO ₂ and H ₂ O at 1400K and atmospheric pressure, adapted from (Khare, 2008, Shaddix, 2011).....	26
Table 2-2 Advantages and disadvantages of different coal devolatilisation model, adapted from (Edge, 2011).....	36
Table 2-3 Advantages and Disadvantages of several char combustion models, adapted from (Edge, 2011).....	38
Table 4-1 Proximate analysis of Xinjiang lignite tested.....	74
Table 4-2 Properties of the ash-forming metals in the raw lignite and its sequential leaching residues, unit mg/kg.....	74
Table 4-3 Activation energy (KJ/mol) and pre-factor (s ⁻¹) for raw coal, coal with 3 wt% clay and HA-washed coal (Xinjiang Coal as the test sample) and comparison with other coals (Copalakrishman, 1994, Morgan, 1986, Zhang, 2013).....	79
Table 4-4 Combustion rate for liquid fuels in the literature (Smith, 1982, Tewarson, 1995).....	97
Table 5-1 Properties of brown coal sample used in this study.....	108
Table 5-2 Summary of the experimental condition in this study.....	109
Table 5-3 Particle shape distribution in air, 21%O ₂ /CO ₂ and 31%O ₂ /CO ₂	127
Table 6-1 Summary of the CO ₂ and H ₂ O gasification reaction evaluated in this study compared with literature data (Hetch, 2011, Hetch, 2012, Kim, 2014).....	153
Table 7-1 Proximate and Ultimate analysis of coal samples.....	162

This page is intentionally left blank

LIST OF FIGURES

Figure 1-1 Total world energy demand (Quadrillion Btu per year) by fuel types from 1990-2035, taken from (EIA, 2010)	4
Figure 1-2 World coal consumption by region and reserve-to-production ratio by the end of 2010, adapted from (Hasegawa, 2013)	7
Figure 1-3 CO ₂ capture options (IPCC, 2005)	9
Figure 1-4 Oxy-Fuel Combustion Process from (Hackett, 2015)	10
Figure 1-5 Schematic diagram for oxy-fuel combustion regimes as a function of oxygen mole fraction and preheat temperature of reactant stream, adapted from (Chen, 2012) ...	11
Figure 1-6 Historical development of oxy-fuel demonstration plant, adapted from (Wall, 2011)	12
Figure 1-7 Process Flow Diagram (PFD) for oxy-fuel combustion with CO ₂ capture, adapted from (Nsakala, 2001)	14
Figure 1-8 Flue gas composition during the combustion of dried VBC in 3MWt pilot scale power plant in oxy-firing with 27% O ₂ (Zhang, 2015)	17
Figure 1-9 Influence of Flue gas recycle ratio on Oxygen concentration	20
Figure 2-1 Required O ₂ molar fraction in the burner inlet to achieve similar AFT in oxy-fuel combustion to that in air-firing case for wet and dry flue gas recycle (Wall, 2009) .	27
Figure 2-2 Experimental and modelling results of total gas radiation intensity, cited from (Andersson, 2008a)	28
Figure 2-3 Coal combustion process, adapted from (Wu, 2005)	29
Figure 2-4 Measurement of soot cloud size of Pittsburgh bituminous coal in air and oxy-fuel combustion with different oxygen concentration, cited from (Shaddix, 2009)	32
Figure 2-5 Average temperature and burnout time of bituminous coal volatiles under O ₂ /N ₂ and O ₂ /CO ₂ atmospheres, cited and adapted from (Bejarano, 2008, Chen, 2012) ..	33
Figure 2-6 Average char particle temperature at 50% char burnout at elevated oxygen concentration, cited from (Timothy, 1982)	34
Figure 2-7 Char combustion temperature of Anthracite coal in air and oxy-fuel combustion, adapted from (Riaza, 2014)	35

Figure 2-8 Three different mechanism for coal ignition proposed by Essenheigh (1989), (a). Homogeneous Ignition, (b) Hetero-Homogeneous Ignition, (c) Heterogeneous ignition, from (Essenheigh, 1989)	41
Figure 2-9 Variation of ignition delay at elevated oxygen concentration in O ₂ /CO ₂ atmosphere, from (Shaddix, 2009).....	45
Figure 2-10 Combustion sequence of Victorian brown coal at 1073K in DTF in different O ₂ /N ₂ and O ₂ /CO ₂ mixtures, adapted from (Zhang, 2010)	46
Figure 2-11 Brown coal particle temperature history in hot gas, from (Stevenson, 1973)47	
Figure 2-12 Comparison between experimentally measured ignition time in Flat flame burner with calculated ignition time using spherical cloud model for Bituminous coal, from (Ye, 2014)	49
Figure 2-13 Development of flame profile over time predicted using cylindrical cloud model, from (Du, 1995)	49
Figure 3-1 Snapshot of the facilities employed in this research	55
Figure 3-2 Full-view of FFBR facility	56
Figure 3-3 Piezoelectric coal feeding system located at the lower level bench.....	56
Figure 3-4 Hencken flat flame burner schematic, adapted from (Kastelis, 2008).....	57
Figure 3-5 Schematic of McKenna flat flame burner	59
Figure 3-6 Combustion region segmentation based on flame structure	60
Figure 3-7 Typical curves obtained from TGA experiments in this research.....	65
Figure 4-1 Schematics of the flat flame burner reactor used throughout this study	76
Figure 4-2 Comparison of measured kinetics of lignite and its acid-washed residues here and those reported in literatures (Kobayashi, 1977, Quyn, 2003, Ubhayakar, 1977, Zhang, 2013). Panels (a) and (b) are for devolatilisation and char oxidation, respectively.....	78
Figure 4-3 Representative flame patterns and flame lengths for raw coal, coal doped with 3 wt% clay and HA-washed coal in air versus oxy-fuel modes	81
Figure 4-4 The distance for coal ignition (a) and oxidation (b) as a function of bulk gas composition for raw coal, acid-washed coal and coal added with 3 wt% clay.....	83

Figure 4-5 High-speed camera observations of the initial igniting particles for three cases at the height of 5 cm from burner base.	85
Figure 4-6 Igniting volatile cloud sizes as a function of bulk gas composition for three cases, raw coal (a), HCl-washed coal (b) and coal with 3 wt% clay (c). Measurement was done for the luminous spots observed at a height of 5 cm from burner base.	86
Figure 4-7 Particle velocity profiles in the early stage of coal combustion, as a function of bulk gas composition for three different cases, raw coal (a), HCl-washed coal (b) and coal mixed with 3 wt% clay (c)	88
Figure 4-8 Coal ignition time (ms) as a function of bulk gas composition for three different cases, raw coal, acid-washed coal and coal mixed with 3 wt% clay	89
Figure 4-9 Calculated percentage of volatiles ignited initially on coal particle surface at the low temperatures	91
Figure 4-10 Dynamic oxidation of the liquid volatiles on coal particle surface, at a shutter speed of 500 fps for the interval of 2 ms between two adjacent photographs. Series (a) ~ (d) are for raw coal in air, acid-washed coal in air, raw coal in oxy-21 and acid-washed coal in oxy-21, respectively. Measurements were taken from high speed camera images at 5 cm above the burner base.....	92
Figure 4-11 Liquid volatile combustion time (ms) on coal particle surface and its combustion rate (mg/s)	94
Figure 4-12 Predicted devolatilisation mass loss and rate of the raw coal and acid-washed coal in air and oxy-21 cases. The TGA data in table 3 were used for prediction based on first – order reaction.....	96
Figure 5-1 Centre-line gas temperature profile in air and 21% O ₂ /CO ₂	109
Figure 5-2 Calculated average particle velocity of dried and wet coal.....	111
Figure 5-3 Calculation procedures to determine the extent of wet coal moisture evaporation.....	113
Figure 5-4 Method to determine the brown coal volatile release time with the variation of the drying extent to calculate the coal ignition time.	114
Figure 5-5 Combustion of dried coal, semi-dried coal and wet coal in air (21% O ₂ /N ₂); Panel (a): flame structure; Panel (b): Measured axial gas temperature with coal burning in the reactor with relative to the blank gas temperature	116

Figure 5-6 Representative images of the flame structure captured with digital camera in oxy-fuel combustion case for (a) dried coal, (b) semi-dried coal, and (c) wet coal	118
Figure 5-7 Difference between measured axial gas temperature with and without coal burning for dried and wet coal samples in oxy-fuel case.....	119
Figure 5-8 Comparison of the combustion time for all coal samples in all combustion cases, (a) ignition time, (b) volatile oxidation time, (c) char oxidation time.....	120
Figure 5-9 Effect of the extent of moisture evaporation on the ignition time of all three brown coal samples in air	122
Figure 5-10 Experimental and prediction of ignition time for all combustion cases (a) dried coal, (b) semi-dried coal, (c) wet coal	123
Figure 5-11 Representative images of dried coal captured near the burner base	125
Figure 5-12 Representative images of wet coal captured near the burner base.....	127
Figure 5-13 Measured volatiles cloud size for all coal samples in the axial centre line of the FFBR for three different bulk gases.....	129
Figure 6-1 Linear plot of Coats-Redfern method for Loy Yang coal to determine the kinetic parameters for its char-steam gasification rate	140
Figure 6-2 Comparison of measured gasification rate with other brown coals available in the literature (Otto, 1979, Sandars, 1984, Ye, 1998)	140
Figure 6-3 Schematic of the numerical procedure applied to determine the contribution of gasification reaction	142
Figure 6-4 Distribution of measured char particle temperature of dried and wet coal in Air	143
Figure 6-5 Method to determine the contribution of steam gasification reaction in air-firing case.....	145
Figure 6-6 Measured pyrometer data for dried and wet brown coal at 50 mm and 75 mm height for (a) oxy-21 case and (b) oxy-31 case.....	146
Figure 6-7 Predicted char particle temperature for dried coal and wet coal at 75mm at oxy-fuel combustion case with the consideration of char-CO ₂ gasification reaction ONLY. The extent of char-CO ₂ reaction is shown above the prediction bars in the figure.	148

Figure 6-8 Contribution of char - CO ₂ and char - steam gasification reactions for dried coal and wet coals in oxy-21 case	149
Figure 6-9 Contribution of char-CO ₂ and char-steam gasification reaction for dried coal and wet coal in oxy-26 case	150
Figure 6-10 Contribution of char-CO ₂ and char-steam gasification reaction for dried coal and wet coal in oxy-31 case	151
Figure 7-1 Schematic of Mckenna flat flame burner facility used in this study	164
Figure 7-2 Centre-line gas temperature profile measured using the B-type thermocouple, corrected for radiation loss (Shaddix, 1999).....	165
Figure 7-3 Photographs of brown coal burning in 21% O ₂ in O ₂ /N ₂ (top panel) and O ₂ /CO ₂ (bottom panel).....	169
Figure 7-4 Ignition time of Victorian brown coal in air and oxy-fuel as the function of coal feeding rate in 21% O ₂ without and with steam injection.....	170
Figure 7-5 Photographs of brown coal ignition in air-firing mode (top panel) and oxy-firing mode (bottom panel). The coal feeding rate was fixed at 0.5g/min.....	172
Figure 7-6 Measured brown coal ignition time at various oxygen concentration with fixed coal mass feeding rate of 0.5g/min	173
Figure 7-7 Images of XJC and BC burned in 21% oxygen, with fixed coal mass flow rate of 0.5g/min.	174
Figure 7-8 Quantitative measurements of the ignition time for all coals at a fixed coal loading rate of 0.5 g/min in all cases. (Data for Coal A was replicated from Figure 7.4)	175
Figure 7-9 Comparison between calculated ignition time and experimental ignition time in the steam injection case with 21vol% O ₂ for Victorian brown coal. Note that R-3 refers to water-gas shift reaction	176
Figure 7-10 Comparison between calculated and experimental brown coal ignition time at varied oxygen concentration in steam-injection case	177
Figure 7-11 Ignition modelling case studies for higher rank coals for (top panel) sub-bituminous coal and (bottom panel) bituminous coal. Two modelling approach were used, with and without the inclusion of water-gas shift reaction, R-3	178

Figure 7-12 Measured particle temperature in 21% oxygen at 65 mm above the burner base. Coal feeding rate was fixed at 0.5g/min.	180
Figure 7-13 Method to determine the contribution of char gasification reaction towards total char consumption rate. An example of the simulation was shown here with brown coal as the test subject.	181
Figure 7-14 Contribution of char gasification to char-consumption rate at 21% oxygen concentration in oxy-firing mode. The calculation was done by comparison of measured particle temperature with the theoretically predicted particle temperature.	182

TABLE OF CONTENTS

DECLARATION	i
ACKNOWLEDGEMENTS	iii
PUBLICATIONS.....	v
LIST OF TABLES	vii
LIST OF FIGURES	ix
TABLE OF CONTENTS.....	xv
ABSTRACT.....	xxi
1 INTRODUCTION	3
1.1 Background	4
1.2 Oxy-fuel combustion as a promising CCS technology	8
1.3 State-of-the-art of oxy-fuel combustion.....	10
1.4 Techno-economic analysis of oxy-fuel combustion.....	13
1.5 Feasibility and applicability of oxy-fuel combustion.....	15
1.6 Oxy-fuel burner design for applicability of VBC	17
1.7 Motivations.....	19
1.8 Key focuses of research.....	21
1.9 Research frameworks	21
1.10 Thesis outlines	22
2 LITERATURE REVIEW	25
2.1 Oxy-fuel combustion versus air combustion.....	25

2.2	Fundamentals of oxy-fuel combustion mechanism.....	28
2.2.1	Drying of single coal particles	29
2.2.2	Coal pyrolysis	30
2.2.3	Volatile oxidation.....	31
2.2.4	Char combustion and oxidation	33
2.3	Combustion modelling	35
2.3.1	Devolatilisation model	35
2.3.2	Volatile combustion model	37
2.3.3	Char combustion model	37
2.4	Coal ignition.....	40
2.4.1	Ignition mechanism.....	41
2.4.2	Review on experimental ignition study	42
2.4.3	Modelling criteria for ignition	46
2.5	Impacts of mineral matters and solid additives on coal ignition.....	50
2.6	Summary	51
3.	RESEARCH METHODOLOGIES	55
3.1.	Heating devices	55
3.1.1.	Hencken burner	57
3.1.2.	McKenna burner	58
3.2.	Diagnostic devices.....	59
3.2.1.	Digital camera.....	59

3.2.2.	High-speed camera.....	61
3.2.3.	High-speed infrared pyrometer	62
3.2.4.	Thermocouple	62
3.3.	Analytical Device	64
3.4.	Modeling approach.....	65
4.	INFLUENCE OF EXTERNAL CLAY AND INHERENT MINERALS ON LIGNITE OPTICAL IGNITION AND VOLATILE FLAME PROPAGATION IN AIR- FIRING AND OXY-FIRING	71
4.1.	Introduction	71
4.2.	Experimental	73
4.2.1.	Coal properties	73
4.2.2.	Determination of coal devolatilisation, ignition and char oxidation by TG- DTA	75
4.2.3.	Coal ignition and in-situ optical diagnosis.....	75
4.3.	Results and discussion.....	77
4.3.1.	Devolatilisation and char oxidation reactivity of coal samples	77
4.3.2.	High-resolution camera observation of flame characteristics in FFBR.....	80
4.3.3.	High-speed camera observation of coal devolatilisation and ignition in FFBR	84
4.3.4.	Burning particle velocity profiles in FFBR	87
4.4.	General discussion.....	88
4.5.	Conclusions	97

4.6. Nomenclature	99
5. INFLUENCE OF INHERENT MOISTURE ON VOLATILE IGNITION AND FLAME PROPAGATION OF WET VICTORIAN BROWN COAL IN OXY-FUEL COMBUSTION	105
5.1. Introduction	105
5.2. Experimental facility	107
5.2.1. Fuel properties	107
5.2.2. Non-premixed flat-flame burner reactor (FFBR)	108
5.2.3. Non-intrusive in- situ optical diagnostics facility	110
5.3. Mathematical formulation	111
5.4. Results and discussion.....	115
5.4.1. Experimental observation on flame structure and ignition characteristics	115
5.4.2. Comparison of experimental observations on coal ignition with modelling prediction	121
5.4.3. Influence of moisture on coal volatile combustion.....	123
5.5. Conclusion.....	129
6. INFLUENCE OF INHERENT MOISTURE ON CHAR-STEAM GASIFICATION RATE OF VICTORIAN BROWN COAL IN OXY-FUEL COMBUSTION.....	135
6.1. Introduction	135
6.2. Experimental set-up.....	136
6.2.1. High-speed pyrometer for coal particle temperature measurement	136
6.3. Mathematical model.....	137

6.3.1.	Modelling approach	137
6.3.2.	Numerical calculation procedure	141
6.4.	Results and discussions	142
6.4.1.	Influence of moisture and char-H ₂ O gasification on particle temperature in air-firing case	142
6.4.2.	Combined effect of char-H ₂ O and char-CO ₂ gasification reaction in oxy-fuel mode	145
6.5.	Conclusions	153
7.	INFLUENCE OF STEAM ON IGNITION OF VICTORIAN BROWN COAL PARTICLE STEAM IN OXY-FUEL COMBUSTION	159
7.1.	Introduction	159
7.2.	Materials and Experimental Methodology	161
7.2.1.	Fuel Properties	161
7.2.2.	Optical flat-flame McKenna burner experiments	163
7.2.3.	Non-intrusive optical diagnosis facility	165
7.3.	Modelling approach.....	166
7.3.1.	Transient cylindrical cloud combustion model.....	166
7.3.2.	Numerical procedure.....	168
7.4.	Experimental results and discussion	168
7.4.2.	Effect of oxygen concentration.....	172
7.4.3.	Effect of coal rank.....	174
7.5.	Experimental results validation using transient ignition model	175

7.6. Conclusions	182
8. CONCLUSIONS AND RECOMMENDATIONS	187
8.1. Conclusions	187
8.1.1. Influence of external clay and AAEM species on ignition	187
8.1.2. Influence of moisture on volatile flame propagation	187
8.1.3. Influence of moisture on char gasification reaction.....	188
8.1.4. Influence of external steam on combustion of dense cloud	189
8.2. Practical implications	189
8.3. Recommendation for future research	190
REFERENCES	193
APPENDIX A	- 213 -
APPENDIX B	228
APPENDIX C	260
APPENDIX D	274
D.1. MATLAB code for calculating the amount inherent moisture (Chapter 5).....	276
D.2. MATLAB code to calculate the contribution of steam gasification (Chapter 6).284	
D.3. MATLAB code to predict the ignition time of dense coal particle stream in a cylindrical cloud (Chapter 7)	298

ABSTRACT

The consistent use of coal as a fuel source for power generation results in the significant emission of greenhouse gases into the environment. Using a low-rank coal, such as Victorian brown coal, results in a much higher CO₂ emission rate. Oxy-fuel combustion is identified as the promising CO₂ abatement technology for cleaner coal combustion. With the replacement of air with the mixture of high-purity oxygen and flue gas, the overall process is nitrogen-lean and can generate a flue gas ready that is rich in CO₂ and ready for carbon capture and storage (CCS). Due to the altered ignition and combustion feature of coal under this environment, the oxy-fuel burner has to be re-designed.

With the construction and testing in various pilot-scale and demonstration-scale power plant, oxy-fuel combustion has been progressively advancing in recent years. However, most of these studies were centred towards the use of black coal as the main fuel source. Therefore, Victorian brown coal (VBC) is highlighted in this thesis due to the limited knowledge for its oxy-fuel combustion. VBC also possesses distinct properties and also burns distinctively from other coal. Although coal ignition has been widely studied, the impact of alkali and alkaline earth metal (AAEM) species and moisture, which are abundant in brown coal, are scarcely reported. The AAEM species are responsible for notorious slagging and fouling in the boiler which can be subsided via the injection of fuel additives. Additionally, the recirculation of flue gas is also likely to increase the overall steam concentration in the furnace. Understand of all these impacts on VBC ignition are essential for the deployment of oxy-fuel combustion in Latrobe Valley, Victoria.

The scope of this research involves both experimental and modeling studies. For the experimental aspects of this research, a bench-scale entrained flow reactor with flat flame burner is commissioned for ignition study. Using an advance in-situ non-intrusive diagnostics facility, coal ignition behavior is captured in a series of photograph to elucidate the transient phenomena occurring during the particle heat up, devolatilisation and ignition. For the modeling approach, series of mathematical equations for coal combustion are written in MATLAB, including a single-film model to quantitatively describe the contribution of the two gasification reactions on char burnout and a transient

ignition model for the ignition of dense particle stream. The calculated results are validated by experimental measurements.

The first part of this research involves the investigation of the effect of AAEM species on coal ignition. The Chinese lignite from Xinjiang, which is rich in AAEM species, is used for this experiment. Further to that, ignition of coal upon the addition of kaolinite and the removal of AAEM are also investigated. The injection of kaolinite has a negligible effect on coal ignition but enhances the volatile decomposition rate. With the removal of AAEM species, the demineralised coal ignites considerably slower. This delay, however, can be eliminated by increasing the oxygen concentration to 30% in oxy-firing mode.

Following that, the second distinct property in brown coal, abundant inherent moisture, is studied. Victorian brown coal with differing moisture content from 12% to 30% is prepared. It was later found that the coal ignition can occur although moisture in brown coal is not completely evaporated. This remaining moisture, referred to as inherent moisture, exerts influence on the subsequent devolatilisation and char combustion rate. Nonetheless, wet brown coal still ignites slightly later compared to its air-dried counterpart. An oxygen concentration of 30% in oxy-firing was also found sufficient to compensate for the detrimental effect of the inherent moisture on coal ignition.

Next, the impact of the remaining moisture is investigated during char combustion process. From a modeling approach, it has been clarified that the un-evaporated moisture in wet coal is further released with the volatiles simultaneously in the air-firing mode. On the other hand, a portion of the inherent moisture still remains even after coal devolatilisation in the oxy-firing case. This residing moisture on particle surface later triggers a char-steam gasification reaction and its contribution is quantified through the modeling study in MATLAB.

Finally, this research concludes with the ignition study of dense particle stream as means to extend these results to a real pulverized coal-fired burner. Here, it is more interesting to evaluate the effect of elevated steam concentration in the flue gas rather than evaluating the effect of the inherent moisture in the raw coal. Surprisingly, a faster ignition under the steam-rich condition was revealed from this research. This is later confirmed from

modeling approach that the homogenous water-gas shift reaction is influential in accelerating the ignition of the volatiles released from Victorian brown coal.

In summary, this thesis has identified a number of distinct features associated with the ignition and burnout of Victorian brown coal in the oxy-fuel combustion mode. Some of these findings can be further extended to commercial software for industrial applications. This research ultimately provides a clearer picture on ignition behavior of Victorian brown coal that is essential to develop an oxy-fuel burner.

This page is intentionally left blank

Chapter 1

Introduction

This page is intentionally left blank

1 INTRODUCTION

Globally, coal is one of the most widely distributed energy source with recoverable reserves. Coal-firing power stations are also known to be a major contributor to carbon dioxide (CO₂) emission. In Victoria, brown coal is the main energy source for electricity generation, which accounts for nearly 90% of electricity demand in the State (SGV, 2015). Its consumption in Victoria's coal-fired power stations contributes approximately 18% of the total greenhouse gas emission in Australia (ABS, 2011). Although oxy-fuel combustion has emerged as a promising technology to reduce CO₂ emission from coal power stations via CO₂ capture and sequestration, the combustion behavior of brown coal under the oxy-fuel combustion is still unclear. As brown coal is widely considered as an alternative fuel to black coal, the applicability of brown coal in oxy-fuel combustion needs to be thoroughly accessed. The successful commissioning of the oxy-fuel combustion technology for brown coal can produce electricity in an environmental friendly manner in the long term. The applicability of the oxy-fuel combustion system and its techno-economic analysis has been investigated in-depth through numerous researches (Buhre, 2005, Toftegaard, 2010, Scheffknecht, 2011, Chen, 2012). However, the fundamental issue on brown coal, such as ignition, has not been widely studied. Understanding brown coal ignition behaviour under oxy-fuel combustion will provide a significant contribution to the design of oxy-fuel burners, which is an important parameter to control the flame stability. Therefore, this thesis aims to examine the ignition characteristic of brown coal under the condition that is typically encountered in the oxy-fuel combustion mode.

This chapter is made up of ten sections. Section 1.1 provides an overview of the coal and the demand for brown coal as an alternative energy source. Section 1.2 discusses options of clean coal technology and the advantages of oxy-fuel combustion. Section 1-3 is a review on the progression of oxy-fuel combustion development. Section 1.4 assesses the techno-economic study of oxy-fuel combustion. Section 1.5 describes the highlights of brown coal combustion characteristics in oxy-fuel combustion and its techno-economic study. Section 1.6 identifies the significance of ignition study for oxy-fuel burner design. The motivations for this research are addressed in Section 1.7. Section 1.8 states the key

focus of this research and expected contribution from this thesis. Section 1.9 outlines the research frameworks. This chapter concludes with a summary of thesis structure in Section 1.10.

1.1 Background

The wild population and economic growth in the recent decade have induced a significant increase in the world's energy demands. The report by U.S Department of Energy shows the projection of world energy consumption over the time, based on a selection of available energy sources (EIA, 2010). As illustrated in **figure 1-1**, the global energy consumption is expected to increase by 80%, from 400 quadrillion Btu in 1990 to 725 quadrillion Btu in 2035. Fossil fuels, such as coal, natural gas and liquid petroleum, are the main energy sources, supplying almost 80% of the total world energy demand between 1990 and 2035. Of all types of fossil fuels, liquid fuels are expected to remain as the largest sources of energy for the next two decades, although their world-wide share of energy consumption is likely to decline from 35% in 2007 to 30% in 2035. On the other hand, the demand for coal will escalate over time, particularly due to the quick growth in China's coal industry. Out of the total fossil fuel usage, coal powers 37% of the total energy demand in 2015, and will remain as the popular choice for the power generation industry towards 2035.

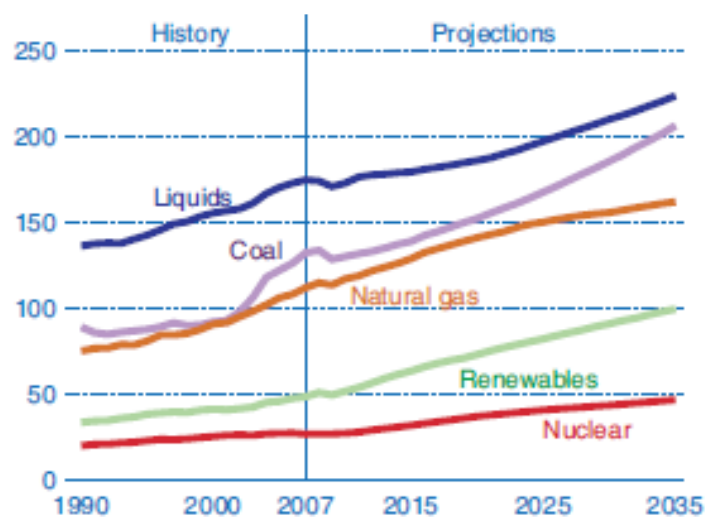


Figure 1-1 Total world energy demand (Quadrillion Btu per year) by fuel types from 1990-2035, taken from (EIA, 2010)

From IEO2011, the total world recoverable coal resources are abundant. As detailed in **table 1-1**, the coal reserves that are economically exploitable with current technology amounted to approximately 948 billion tonnes, equivalent to the 126.3 years of global energy output in 2011 (IEO, 2011). The large reserves-to-consumption ratio for coals indicates that sufficient coals will be available to meet the global energy demand in the long-term. Furthermore, the estimation on the total recoverable coal resources can increase substantially as mining technology improves and additional geological assessments of the coal resource base are completed. By coal rank basis, 78% of the total coal reserves are constituted from hard coal; anthracite, bituminous and sub-bituminous coal. Of all the total recoverable coal resources, 10% are located in Australia/ New Zealand, which makes it the fifth largest coal producer in the world. Having substantial coal reserves in this region, Australia relies heavily on coal as the main source of energy, with 69% of the nation's electricity requirement is currently supplied by coal-fired power plant.

Table 1-1 World recoverable coal reserves as of 1st January 2010 (billions tonnes), adapted from (IEO, 2011)

Region/ Country	Recoverable reserves by coal rank				2008 production	Reserves-to-production ratio (Years)
	Bituminous and Anthracite	Subbituminous	Lignite	Total		
World total	445.7	287.0	215.3	948.0	7.5	126.3
United States ^a	119.2	108.2	33.2	260.6	1.2	222.3
Russia	54.1	107.4	11.5	173.1	0.3	514.9
China	68.6	37.1	20.5	126.2	3.1	40.9
Other non-OECD	42.2	19.1	40.1	101.4	0.3	291.9
Europe and Eurasia						
Australia and New Zealand	40.9	2.5	41.4	84.8	0.4	191.1
India	61.8	0.0	5.0	66.8	0.6	117.5
OECD Europe	6.2	0.8	54.3	61.3	0.7	94.2
Africa	34.7	0.2	0.0	36.9	0.3	123.3
Other non-OECD	3.9	3.9	6.8	14.7	0.4	34.4
Asia						
Other Central and South America	7.6	1.0	0.0	8.6	0.1	95.8
Canada	3.8	1.0	2.5	7.3	0.1	97.2
Brazil	0.0	5.0	0.0	5.0	0.0	689.5
Other ^b	2.6	0.6	0.1	3.4	0.0	184.5

^aData for the U.S. represent recoverable coal estimates as of January 1, 2010

^bIncludes Mexico, Middle east, Japan and South Korea.

Sources: World Energy Council and EIA

Black coal, generally known as bituminous coal, is commonly used in coal-fired power stations for the purpose of electricity generation. As coal is a fossil fuel that is normally formed by decomposition of land plants over a million years, the rapid utilization of coal will result in the depletion of coal reserves. For instance, the demand for coal in Asia Pacific rose significantly in the recent years, from 500 million tonnes oil equivalent (Mtoe) in 1980 to 2000 Mtoe in 2010, as shown in **figure 1-2**(Hasegawa, 2013). Therefore, the coal reserve-to-production ratio will decrease remarkably and is expected to last for only another 110 years from now. Consequently, mining operations start to experience difficulties in reaching deeper coal seams, resulting in an upsurge of black coal prices in the global market. This has urged coal power stations to consider brown coal as an alternative fuels. Although brown coal is not commonly used in coal-fired power stations, it is vital in the energy sector of some countries and regions, where brown coal may be the only indigenous energy resources, such as Germany and Victoria, Australia. With an abundance of lignite occurring in the thick seams close to the earth surface, Victoria is home to one of the largest and lowest cost energy sources in the world.

Brown coal in Australia is naturally located in three major tertiary basins in the state of Victoria; the Murray Basin, the Otway Basin and the Gippsland Basin. The total recoverable brown coal reserves in these regions account for approximately 100,000 million tonnes (Mt) (Li, 2004). In 2013-2014 alone, the total production of brown coal in Victoria amounted to 57.8Mt (SGV, 2015). These abundant brown coal reserves are expected to last for approximately 500 years, based on the current brown coal utilization rate. In addition, the comparison between the Victorian brown coal (VBC) with lignite from other countries also indicates the brown coal reserves in Victoria are of the highest quality in the world (Barton, 1993).

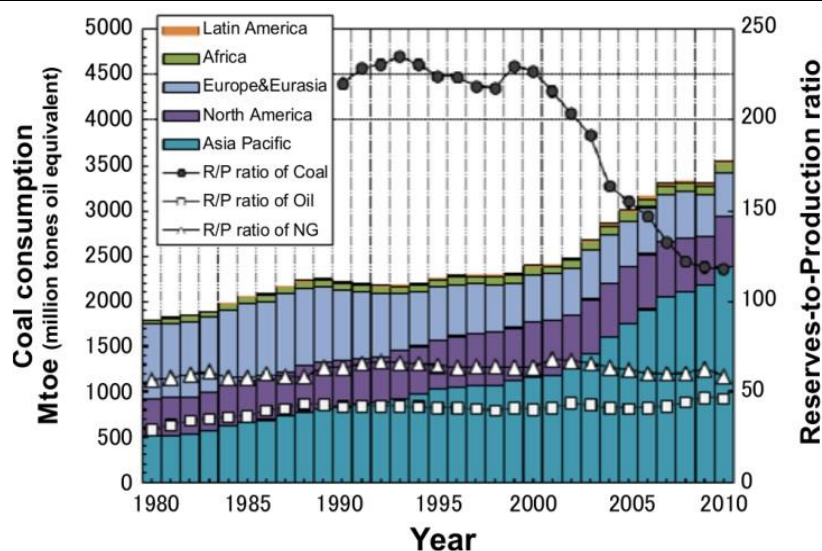


Figure 1-2 World coal consumption by region and reserve-to-production ratio by the end of 2010, adapted from (Hasegawa, 2013)

The properties of various brown coal mined from different parts of the globe are shown in **table 1-2** (Li, 2004, Liu, 2012, Prationo, 2014, Young, 1988). Generally, brown coal has less organic carbon content, higher moisture content, lower in ash and sulphur and is of poorer quality than black coal. The high moisture content of brown coal, up to 70% water, means that long-term transportation is not viable and also generates less energy compared to black coal. Accordingly, using brown coal in coal-fired power stations contributes to higher greenhouse gas emissions in order to meet the energy requirement rather than using black coal. While brown coal procures numerous problems in its utilization, it has been used in the nearby coal power station in Latrobe Valley, which has operated since the 1920s and generates nearly 90% of the total state's electricity demand (Li, 2004). Based on the data summarized by the Australian Bureau of Statistics, Victoria generated third highest carbon dioxide equivalent emissions of all states in 2009, producing up to 22.5% of total emissions in Australia. Of the total CO₂ emission in Victoria, energy productions account for 84.4% (ABS, 2011). The escalated brown coal consumption will intensify the rate of CO₂ emission unless carbon capture and storage (CCS) technologies are implemented. Therefore, there is a need to develop CCS technology for cleaner brown coal utilisation to achieve the sustainable future.

Table 1-2 Proximate and Ultimate analysis of brown coal from Australia, China, Germany and Indonesia (Li, 2004; Liu, 2012; Prationo, 2014; Young, 1988)

Properties	Australia (Loy Yang)	China (XinJiang)	US (Beulah)	Indonesia
Moisture, % (ar)	62.5	19.1	33.4	24.06
Ash, % (db)	1.5	5	9.6	3.1
Volatiles, % (db)	51.3	30.77	56	48.1
Fixed carbon, % (db)	47.2	64.2	34.4	48.8
C, % (daf)	65.7	66.7	56.8	71.51
H, % (daf)	6.8	4.7	4.1	4.97
N, % (daf)	0.6	0.6	1.1	1.03
S, % (daf)	0.5	0.3	0.7	0.24
O (by-difference), % (daf)	25.8	27.7	15.8	22.25

1.2 Oxy-fuel combustion as a promising CCS technology

As illustrated in **figure 1-3**, there are three commonly considered CCS technologies, namely, post-combustion capture, pre-combustion capture, and oxy-fuel combustion (IPCC, 2005). In a post-combustion capture (PCC) process, the CO₂ from flue/exhaust gas from power plant is captured by means of chemical absorption, mainly via amine absorption using either ammonia-containing or alkali-containing solvents. However, the cost of solvents, including the solvent regeneration process and cooling, is high and energy intensive (Davison, 2007, Varagani, 2005, Wall, 2007). The second option, pre-combustion capture, commonly known as Integrated-Gasification-Combined-Cycle (IGCC), refers to electricity generation via gasification of coal with a mixture of oxygen/steam to produce flue gas mixtures of carbon monoxide (CO) and hydrogen (H₂). However, the gas separation technology to produce CO₂-rich stream requires enormous energy and electricity. Moreover, the overall process is complex and high in capital costs (Kanniche, 2010, McDonald, 2008). Lastly, in the oxy-fuel combustion process, the high-purity oxygen, which is generated from air-separation units (ASU), is mixed with the flue gas recycled (FGR) from the furnace and used as an oxidizing agent for coal combustion instead of air. Subsequently, the resulting flue/exhaust gas consists of CO₂, water vapour and trace amount of emission gases, such as NO_x and SO_x. By eliminating the majority of nitrogen from the oxidant gas stream, it is possible to produce a CO₂-concentrated flue gas after water and other impurities have been removed.

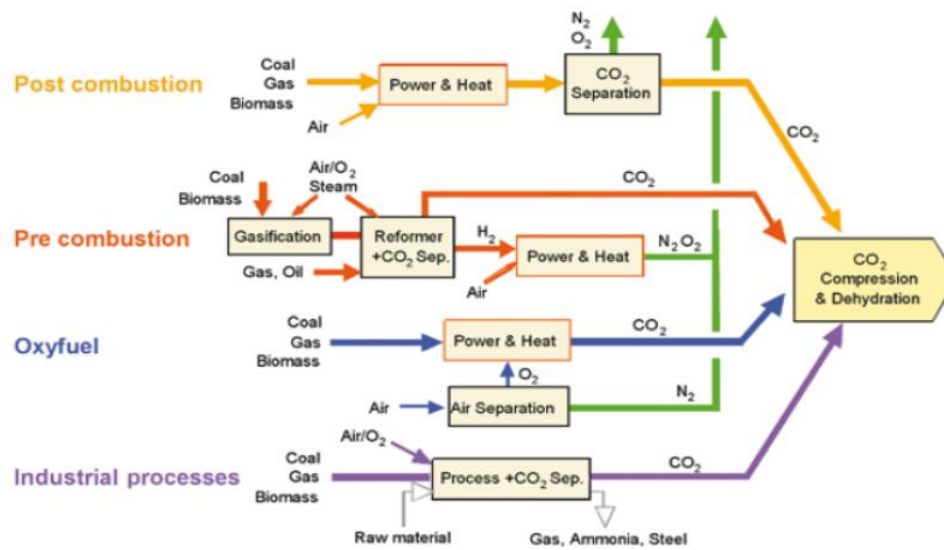


Figure 1-3 CO₂ capture options (IPCC, 2005)

Among these three options, the oxy-fuel combustion is the most promising solution to generate highly concentrated CO₂ streams in the flue gas for easier capture and storage of CO₂ (Buhre, 2005, Chen, 2012, Toftgaard, 2010, Wall, 2009). Compared with other CCS technologies, oxy-fuel combustion is simple, elegant and readily available technology. This differs from post-combustion capture, where an addition of major chemical process for CO₂ capture is required, and pre-combustion capture, where the technology itself is still relatively new (Zheng, 2011). **Figure 1-4** illustrates the oxy-fuel combustion process based on a conventional power plant steam cycle (Hackett, 2015). As the major components of oxy-fuel combustion, i.e air-separation and coal combustion, are mature technologies that have been extensively employed, the retraining requirement for personnel and costs are minimal. Furthermore, the absence of nitrogen from the process also reduces the rate of NO_x emission and amount of flue gas volume to one-quarter or one-fifth to that of air-combustion (Wall, 2007, Wall, 2009). Subsequently, much smaller flue gas emissions control equipment is required in oxy-fuel combustion, which substantially reduces capital and annual operating costs (White, 2009, Zheng, 2011). In addition to these advantages, oxy-fuel combustion operation is also highly flexible and able to operate in dual-firing capability, which provides the possibility to switch to air-firing mode in order to meet peak load demand. The remainder of this chapter will mainly

discuss the progress and feasibility of oxy-fuel combustion technology, particularly for brown coal.

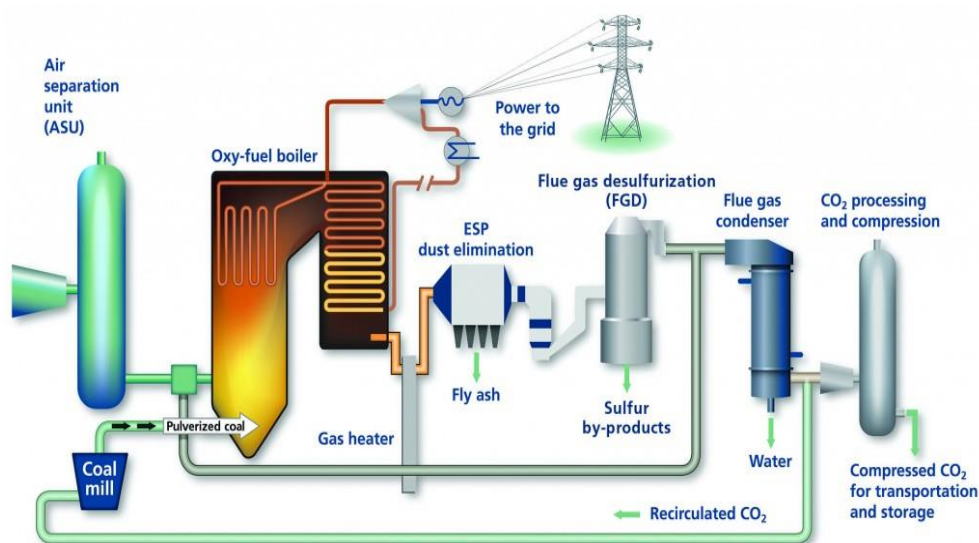


Figure 1-4 Oxy-Fuel Combustion Process from (Hackett, 2015)

1.3 State-of-the-art of oxy-fuel combustion

Even before the concern regarding CO₂ emission arose, forms of oxy-fuel combustion had been applied in different industry sectors, including glass melting furnaces, steel scrap melting, aluminium melting furnaces, copper smelting, hazardous waste incinerators and lead melting furnaces. Initially introduced in 1970s, an oxidizer stream containing oxygen concentration higher than 21% was widely applied in glass and metal industries because of its advantages in NO_x reduction and cost effectiveness (Baukal, 1998, Santos, 2005, Tsuji, 2003). However, with the complete removal of nitrogen from the process, although it can generate a highly-concentrated CO₂ stream, it is likely to result in furnace material failure, as illustrated in **figure 1-5**(Chen, 2012). In oxy-fuel combustion application for CCS, the CO₂-concentrated flue gas from the combustion stack-gas is typically used to replace air in the furnace and to control the combustion temperature. This idea was first proposed in 1982 for the purpose of enhanced oil recovery (EOR) in depleted oil field using a high concentration of CO₂(Abraham, 1982, Horn, 1982).

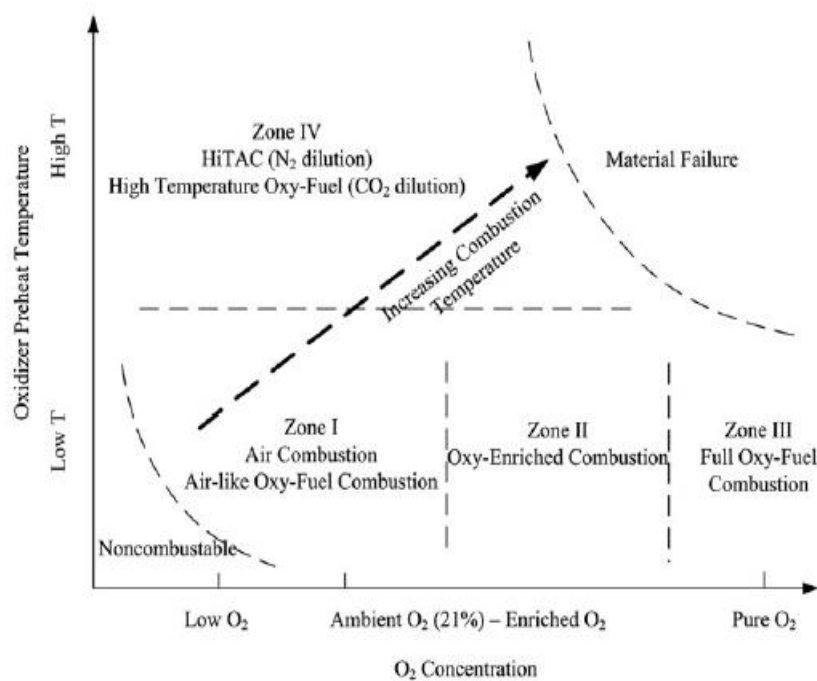


Figure 1-5 Schematic diagram for oxy-fuel combustion regimes as a function of oxygen mole fraction and preheat temperature of reactant stream, adapted from (Chen, 2012)

Following this proposal, the Argonne National Laboratory (ANL) pioneered the first-ever oxy-fuel combustion testing in a 3MW_t pilot-scale test facility, focusing on its process and combustion characteristics (Payne, 1988, Wang, 1988). The research soon led to a renewed interest in the 1990s, where considerable contributions to understanding the process were made by International Flame Research Foundation (IFRF), CANMET, IHI, and other institutes through their pilot-scale facility. **Figure 1-6** shows the timeline of the oxy-fuel combustion development, including some of the notable oxy-fuel projects around the world and recently announced demonstration plants (Wall, 2011). The majority of the projects are pulverized coal fired, showing the centred-focus of the research area. It can be noted that although several industrial-scale demonstrations have operated since the 1990s, it was not until 2008 where the Vattenfall's Schwarze Pumpe commissioned the world's first full-chain oxy-fuel demonstration plant. The results from this demonstration plant were to serve as a basis for the design and operation of a 250MW_t fully integrated oxy-fuel demonstration plant in Janschwaide, which was later cancelled in 2012 due to the lack of political support for the project's proposed CO₂ storage site (Anheden, 2011, Global_CCS_Institute, 2012). Since then, more large-scale

demonstrations in industrial-scale coal-fired boiler have been planned or are already underway.

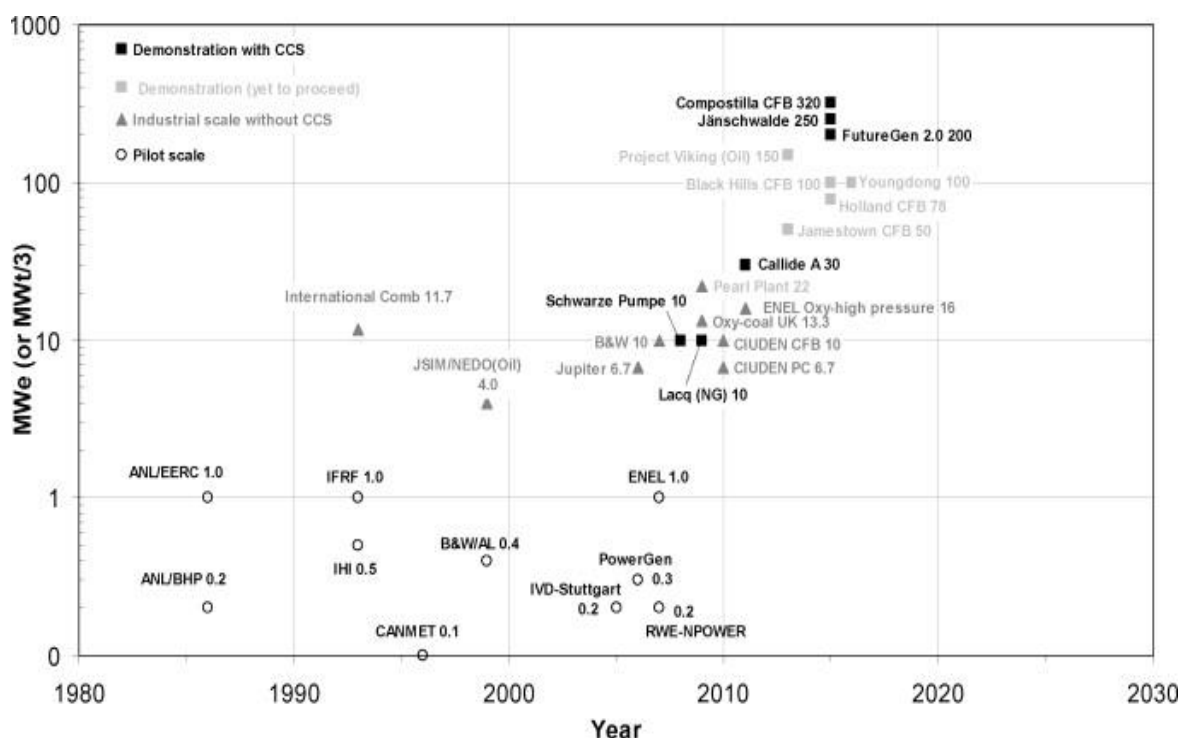


Figure 1-6 Historical development of oxy-fuel demonstration plant, adapted from (Wall, 2011)

The next major milestone for this technology is the commissioning of Callide Oxy-Fuel Project 3.0 in Australia, which started its operation in 2012 with FutureGen2.0 in USA to follow in 2015. The Callide Oxy-Fuel project is the first oxy-fuel pilot plant that supplies the generated electricity to the open market (Wall, 2011). Key results from this project indicated CO₂ recovery rate of 87% from the process, which was later concentrated to 99.9% after gas cleaning and purification. Overall, the findings from Callide pilot tests exhibited good performance over 1100 hours of operations. Part of these results will serve as reference for FutureGen2.0 design (Beasse, 2013). The FutureGen2.0 is expected to be the world's first commercial scale power plant with near zero emission level totalling \$US 1.65 billion (Shah, 2014). This project is scheduled for four phases with the start-up phase to commission between January 2014 and August 2017 (McDonald, 2012). These projects and milestones indicate a pathway for the development of the scale of technology. To date, no full scale demonstration plant based on this technology has been built. Due to

the lack of demonstrations, oxy-fuel is still in the early stage of development since its conceptualization back in 1980s.

Through the numerous tests conducted in the pilot-scale oxy-fuel facility, oxy-fuel pulverized coal (pf)-fired technology shows promising results for its implementation in the near future (Chui, 2003, Khare, 2008, Sarofim, 2007, Sturgeon, 2009, White, 2013). Recent reviews also agree that oxy-fuel pf combustion is economically promising and technologically feasible with current technology (Buhre, 2005, Molina, 2007). However, there is still a need to address the fundamental issues before this technology can reach its full potential and full scale operation (Toftegaard, 2010, Wall, 2009). A successful operation of O₂/CO₂ combustion technology relies heavily on the understanding the differences that result from replacing the main diluting gas in air-firing, N₂ with dominant gas in oxy-firing, CO₂.

1.4 Techno-economic analysis of oxy-fuel combustion

To re-iterate, a full-scale oxy-coal power plant with CO₂ capture and storage will consist of four major systems, such as air-separation unit (ASU), oxy-coal steam generator process, steam turbine cycle, and CO₂ purification unit. Although oxy-fuel combustion has been identified as the most promising CCS technology for CO₂ mitigation, the decision to deploy this process in preference to others will largely be made based on a comparative cost basis. The cost bases for power plants can vary widely depending on fuel types, plant designs, construction prices, geographical labour rate, and other factors. Therefore, there are enormous difficulties in an attempt to compare relevant costs produced from different studies. The most useful cost studies are those that compare technology options with the common baseline.

Buhre (2005) presented reviews on the techno-economic assessments on full-scale applications of oxy-fuel combustion technology (Buhre, 2005). It was emphasized that many uncertainties on the evaluations were identified due to lack-of commercial experience of the process at large-scale magnitude. Most studies were based on a comparison between oxy-fuel technology and air-combustion equipped with CO₂ scrubbing facility using either Mono-Ethanol-Amine (MEA) or Methyl Diethanol-Amine

(MDEA) (Anderssen, 2002, Marin, 2003, Okawa, 1997, Singh, 2003). In the study covered by Chalmers University on 865MWe lignite power plant in Germany, the retrofit of oxy-fuel combustion and CO₂ recovery decreased the power output and net efficiency from 865MW and 42.6% to 623MW and 30.7%, respectively (Anderssen, 2003a, Anderssen, 2003b, Birkestad, 2002). However, through process optimisation, it is possible to increase the power output and net efficiency to 696.7MW and 34.3%, respectively.

ALSTOM adopted different approaches by developing a computer simulation of oxy-fuel combustion to evaluate technical and economic issues. The developed flow diagram is shown in **figure 1-7**(Nsakala, 2001). The main findings can be summarized as follows:

- Comparable technical practicality to that of air-firing with MEA or MDEA for CO₂ capture
- Reduction in plant thermal efficiency from 35% in the normal air-firing to 23% in oxy-fuel combustion, due to additional energy requirements from ASU and CO₂ compression units. However, the overall plant efficiency is equivalent to that of air-firing with post-combustion capture
- Similar CO₂ recovery rate of 94% in oxy-fuel combustion to that in air-firing with CO₂ capture facility.

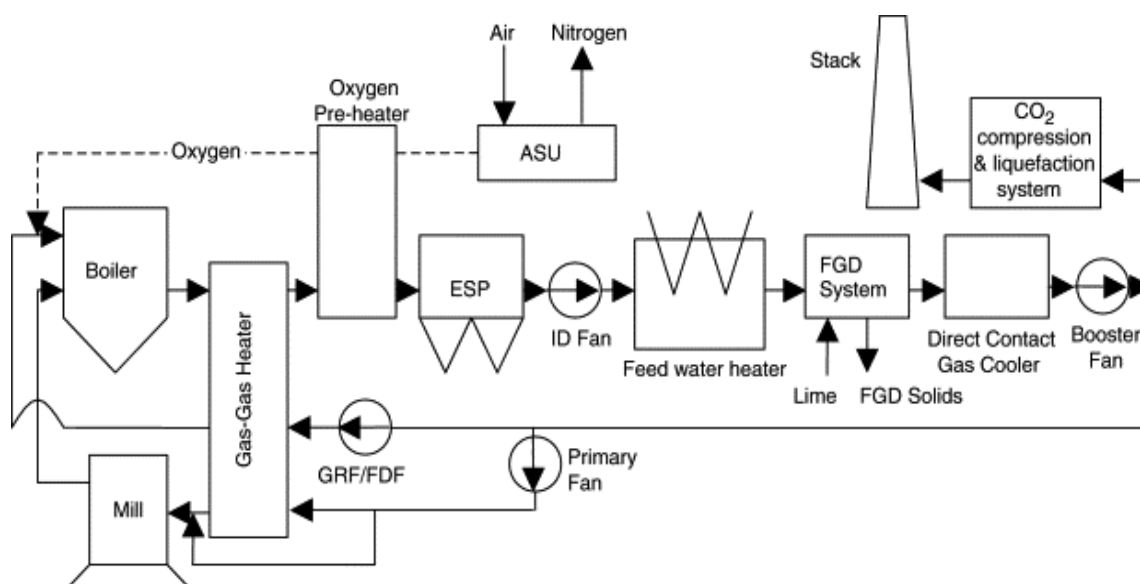


Figure 1-7 Process Flow Diagram (PFD) for oxy-fuel combustion with CO₂ capture, adapted from (Nsakala, 2001)

In another independent study, the Global Carbon Capture and Storage Institute (GCCSI) reviewed the economic assessment on pulverized fuel firing of bituminous coal between the three CCS options including the assessment of ultra-super critical steam (USC) and advanced ultra-supercritical steam (AUSC) boiler technology. From this assessment, the plant capital cost, levelized cost of electricity generated (COE) and cost of CO₂ avoided are listed in **Table 1-3**(GCCSI, 2009). The total valuation of oxy-fuel plant was marginally lower than the capital cost for post-combustion capture and IGCC facility. Also, the levelized COE was also approximately 7% lower than the levelized COE for air-firing process employing the same steam cycle. In terms of the cost of CO₂ avoided, oxy-coal combustion procures lowest amount of approximately US\$60/ tonne of CO₂ emission, compared to other CCS options. It is to be noted that the published results are indicative, not conclusive, due to ambiguous assumptions in estimating operational costs, such as scale-up of ASU unit, CO₂ purification and CO₂ storage costs. While these costs and estimations cannot be considered definite, there is a promising indication that oxy-coal technology is economically viable and is likely to be competitive with the pre- and post-combustion capture for new power plants (Thimsen, 2011).

Table 1-3 Summary of GCCSI costing study (GCCSI, 2009)

	Estimated Cost		
	Total plant cost (US\$/kW)	30-year levelized COE (US\$/MWh)	Cost of CO ₂ avoided (US\$/tonne CO ₂)
USC air-firing	1900	79	-
USC air-firing, with PCC	3400	136	88
AUSC air-firing	2000	76	-
AUSC air-firing, with PCC	3350	126	83
Oxy-fuel USC	3185	125	60
Oxy-fuel AUSC	3190	121	63
IGCC	3345	133	78

1.5 Feasibility and applicability of oxy-fuel combustion

The techno-economic analysis on full-scale oxy-fuel combustion power plants has indicated likelihood for oxy-fuel combustion as a near-zero carbon emission technology in the future. To successfully develop oxy-combustion technology, it is necessary to study

the combustion characteristics using a variety of coal, including brown coals. The unique properties of brown coal, i.e. rich in alkali and alkaline earth metal (AAEM) species and high moisture content, is expected to change the combustion characteristics in oxy-fuel furnace due to the flue-gas recirculation system.

The first unique property of brown coal, which is abundant in brown coal and sub-bituminous coal, is the AAEM species. During the combustion, the vaporisation of these metals is prone to intensify the slagging and fouling propensity in the oxy-fuel boiler (Dai, 2015, Kosminski, 2006). Additionally, the presence of AAEM species, which can also act as catalyst for coal combustion, may significantly alter the ignition and combustion behaviour (Gupta, 1999, Wan, 2009). Furthermore, the AAEM species are also catalysts for char-steam gasification, which may be promoted at high H₂O concentration in oxy-fuel combustion (Bayarsaikhan, 2006, Kajitani, 2010). The ash slagging problem can be averted by the installation of soot blowers that use a high-pressure superheated steam, saturated steam, water or compressed air to remove ash deposits (Babcock, 1978). However, the process is energy intensive and is likely to reduce overall boiler efficiency (Gordon, 2006). The injection of solid sorbents is another practical method to mitigate fouling through capture of AAEM species (Gale, 2002).

Another important attribute of brown coal is its high moisture content. Its release during the combustion is expected to significantly increase the steam concentration in the oxy-firing furnace due to the continuous recirculation of flue gas. As illustrated in **figure 1-8**, the flue gas component from the oxy-firing furnace in a 3MW_t pilot scale power plant in China contains 35vol% steam in comparison to air-firing flue gas containing 10vol% steam (Zhang, 2015). In another study, the results from the demonstration operation at Callide Oxy-fuel power plant with 3 types of Australian coals also indicated higher H₂O concentration in oxy-fuel combustion, which was 2.5 times higher than the H₂O concentration obtained from systems operated in air-firing mode (Yamada, 2010). The high H₂O concentration alerts some issues in the operation of oxy-fuel furnace, including the change of fundamental ignition behaviour and burnout, and the selection of furnace material due to the change in the dew points of sulphuric acid in the flue gas (Yamada, 2010).

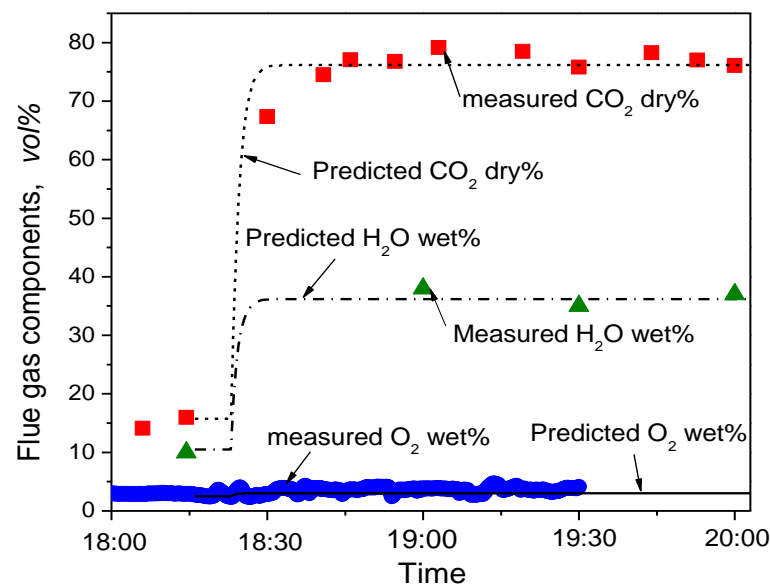


Figure 1-8 Flue gas composition during the combustion of dried VBC in 3MWt pilot scale power plant in oxy-firing with 27% O₂ (Zhang, 2015)

Due to its high moisture content, the power plant system facilitating Victorian brown coal is likely to encounter some technological challenges in order to maintain the current power plant net thermal efficiency. In light of this, the techno-economic study has been performed to assess the feasibility of brown coal in oxy-combustion in various design configurations including integration of coal pre-drying process and state of the flue gas recycle, either wet or dry. The approximated cost of electricity and cost of CO₂ abatement were US\$100/MWh and US\$50-60/ tonne of CO₂, respectively, which were considerably lower compared with the estimated cost on bituminous coal shown in **Section 1.5**. In terms of plant thermal efficiency, the integration of pre-drying and supercritical steam cycle was able to compensate the energy penalty cause by ASU and CO₂ compression, with comparable net efficiency of 25-29%LHV with that in the existing power plant process (Zhang, 2014).

1.6 Oxy-fuel burner design for applicability of VBC

Section 1.5 has indicated that oxy-fuel combustion using Victorian brown coal as a fuel is indeed practical. As coal burns distinctively from each other due to its individual characteristics, the design of coal-fired boiler differs depend on the type of coal used.

Fundamentally, the particles undergo rapid heating, volatile releases, ignition and combustion of volatiles and residual chars in the sequential order after being introduced to the furnace. These combustion-related effects are manifest and play important roles in practical furnace operations, including flame stability and flame shape, burner stability, heat transfer distribution, water-wall corrosion and carbon burnout (Liu, 2005b, Liu, 2005a, Nozaki, 1996). In particular, the topic of coal ignition, including considerations of homogeneous (gas-phase) versus heterogeneous (solid-phase) is a problem of interest and concern over many years for researchers (Essenheigh, 1989, Gururajan, 1990, Kim, 2014b, Zou, 2014). The early research on coal-dust ignition originates with concerns for fire safety and coal mine explosions. Nevertheless, it has little relevance to the application of flame holdings in pulverized coal (pc) burners, where high velocity streams of coal particles turbulently are mixed with surrounding hot gases.

For application to pc-burners, the characteristic ignition delay of coal particles, which influences coal flame stability, may be instrumental for predicting the performance of oxy-coal burners (Khatami, 2012b, Liu, 2011). Flame stability refers to the ability of the existing flame to remain ignited despite variations in the furnace operating condition. Therefore, it is an important concept in burner design and operation as burners have to stay ignited through a reasonable range of fuel and oxidizer flow characteristics and over the range of heat release rates. In fact, the design of pc-burners for conventional air-firing was well-established in the 1960s although the pc-combustion technologies had begun to emerge in the early 1900s (Shan, 2011). For the oxy-combustion, the number of independently controlled streams entering the furnace has increased by one due to the replacement of air by oxygen and FGR. This has posed additional operational constraints in oxy-fuel due to the change in burner aerodynamics (Beer, 1972). Furthermore, potential use of low-oxygen concentration in the primary oxidizer stream in oxy-fuel combustion is expected to pose further challenges for burner designers and operators to maintain flame stability. In addition, the high moisture content in brown coal provides additional degree of freedom in engineering the practical burner for VBC. The implementation of integrated drying system for brown coal and wet-recycle flue gas are also additional variables to be considered in the burner development for low-rank coal.

1.7 Motivations

Comprehensive reviews in **section 1-1** to **section 1-5** have designated oxy-fuel combustion as the most favorable CCS method for carbon mitigation. The practicality of Victorian brown coal in oxy-combustion has also been assessed and shows promising results. Accelerating the deployment of this technology for brown coal in the near future involves the design of a practical burner that can generate a stable flame under oxy-combustion atmosphere. The coal ignition characteristic has been identified as a crucial parameter for burner design and is the main subject for investigation in this thesis. Although many studies on the coal ignition mechanisms in oxy-fuel combustion have been instigated, most of them focused on the black coal. Therefore, the ignition behavior of brown coal under this combustion condition, especially with its unique properties, is still not fully understood (Gururajan, 1990, Howard, 1967, Khatami, 2012b, Liu, 2011, Molina, 2007, Shaddix, 2009). Thermodynamically, coal of different ranks exhibits different combustion behavior and cannot be treated equally (Khatami, 2012b, Khatami, 2012a). Also, as most practical combustors implement dense sprays/suspensions of particles, the ignition behavior of group particles, rather than the common single particle study in literature (Khatami, 2012b, Rathnam, 2009, Schiemann, 2009, Shaddix, 2009, Zhang, 2010b, Khatami, 2012a, Maffei, 2013), also needs to be investigated. The ignition of group particles is different from the ignition of single particle since volatile reactions in the gas phase are strongly affected by the coal concentration and total volatile yields (Liu, 2011, Lucas, 1994, Taniguchi, 2001). From literature (Buhre, 2005, Chen, 2012), some promising research aspects in the field of oxy-fuel combustion are promoted:

- Combustion characteristics of different coal types as an integral part of accelerating oxy-coal burner design
- Development of models for sub-processes under oxy-fuel combustion condition
- Combustion characteristics under wet recycle ($O_2/CO_2/H_2O$) atmosphere

In addition, with the impending establishment of oxy-fuel technology for brown coal, there is a pressing need to elucidate the fate of moisture and role of mineral matters derived from brown coal under oxy-fuel conditions. Firstly, the current drying systems in brown coal-fired power stations in Latrobe Valley reveals moisture content of

approximately 25% after first stage of drying, which is still far higher than that of black coal (McIntosh, 1976a, McIntosh, 1976b). Also, the abundant steam condensed during brown coal combustion may have the potential to reduce boiler operational expenses through the reduction of flue gas recycle ratio, shown in **figure 1-9**. By comparing brown coal containing 30% and 60% moisture, approximately twice the amount of flue gas is required for 30% moisture coal compared with that for 60% moisture coal to achieve the oxygen level of 24vol% in the boiler. Although considerable amount of operating costs can be avoided, the impact of moisture during the high temperature combustion is still unknown. Furthermore, wet coal combustion simulations in commercial computational fluid dynamics (CFD) software over-simplify the coal drying mechanism such that it has little or no overlap with the subsequent coal combustion stage (Ansys, 2011, Kurose, 2001). Obviously, a novel approach to predict the combustion behavior of wet coal is needed. Secondly, the injection of mineral-additives in coal has been proven to minimize the slagging and fouling propensity in the boiler. Surprisingly, to date, no research has been done to investigate the impact of these silica-additives, although beneficial, on ignition.

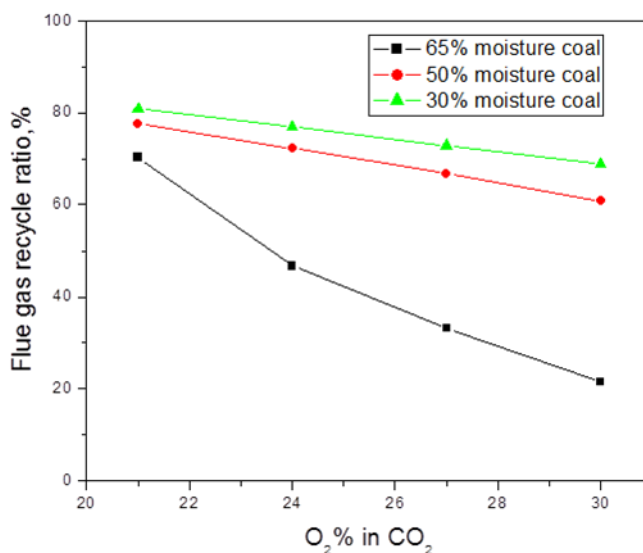


Figure 1-9 Influence of Flue gas recycle ratio on Oxygen concentration

1.8 Key focuses of research

The objective of this research is to fill the research needs highlighted in **section 1.7**. The key focuses are:

1. To develop a specific understanding of the key issues associated with the differing properties in brown coal, such as moisture, AAEM species and clay additives, on its ignition in air-firing and oxy-firing conditions.
2. To investigate differences between the gaseous properties formed under oxy-firing conditions, either wet-recycle or dry-recycle, on coal ignition.

The novelty of this research project derives from the usage and application of low-rank coal as opposed to high-rank coal. To reiterate, the coal in focus is the Victorian brown coal from Australia and the Chinese lignite from Xinjiang province. Both fuels are abundant in moisture and are rich in AAEM species. Overall, this research project is expected to deliver significant contribution in accelerating the development of oxy-fuel burner for low-rank coal.

1.9 Research frameworks

To achieve the research objectives stated in **Section 1.8**, a systematic research framework was designed and subdivided into four distinct parts as shown below:

- I. Chinese lignite ignition experiments** which focus on the role of mineral matters and silica-additives on ignition in air and oxy-fuel combustion conditions
- II. Wet VBC combustion experiments** in single particle mode, which aimed to clarify the role of moisture under air-firing and oxy-firing mode
- III. Mathematical modelling on ignition of wet VBC** in MATLAB which utilised the results obtained in Part II to elucidate the role of moisture on three combustion stages; ignition, volatile release and oxidation, and char combustion.
- IV. Group ignition experiments of dried VBC in wet recycle condition** which extend the single particle studies in part II to mimic the real condition in industrial furnace
- V. Mathematical modelling on group ignition of VBC under $O_2/CO_2/H_2O$ atmosphere** to explain the role of steam on ignition based on results achieved in part IV

1.10 Thesis outlines

Chapter 1 of this study has briefly outlined the background of CCS technologies and stated the motivation behind the research. **Chapter 2** gives a summary of related literature to the study ignition mechanisms of low-rank coal during oxy-fuel combustion, the controlled mechanisms governing coal ignition and also the progress and concept of the mathematical modeling for coal combustion. This chapter concludes with the summary of the knowledge gaps based on the reports presented. **Chapter 3** gives a description and general overview of the experimental method and setup for (1) single particle ignition experiments and (2) group particle ignition experiments. The mathematical modeling approach on (1) wet coal ignition and (2) group particle ignition is also outlined. The main experimental results are presented in Chapter 4-7

Chapter 4 describes the influence of mineral matter and silica-additives on low-rank coal ignition in air-firing and oxy-firing

Chapter 5 presents the study on the influence of moisture in wet VBC, concentrating on the volatile ignition and flame propagation in air-firing and oxy-firing through experimental and modeling study

Chapter 6 provides the complete analysis method to determine the contribution of moisture in wet VBC on the char-steam gasification reaction in air-firing and oxy-firing through experimental and modeling study

Chapter 7 provides detailed discussions that focus on the role of steam on group ignition of low-rank coal.

Chapter 8 summarizes the conclusions from the findings from this thesis, and how they will impact the practical operations on power plant. Also included are some recommendations for future research.

Chapter 2

Literature Review

This page is intentionally left blank

2 LITERATURE REVIEW

In the previous chapter, background information of coal power generation industry and some available technologies for carbon mitigation were discussed. Although these technologies have their own advantages and disadvantages, oxy fuel combustion emerges as a favorable option due to its design flexibility and ease of retrofitting to the current power plant system. Several techno-economic studies also have indicated oxy-fuel as the preferred technology option. Therefore, this chapter provides in detail a comprehensive review of related research that has been undertaken in oxy-fuel combustion. Firstly, differences between air-firing and oxy-firing are identified followed by the review of related experimental and numerical research in oxy-fuel combustion. In the next section, coal ignition are discussed in-depth as the main scope of this research. This includes comprehensive review on experimental and modelling studies. Furthermore, literature summary on the silica-based sorbents as fuel additives to reduce slagging and fouling in the boiler are also presented. To sum it up, the research gaps, which will be addressed in this thesis, are identified based on the reviewed literatures.

2.1 Oxy-fuel combustion versus air combustion

To reiterate, nitrogen is completely removed from oxy-fuel boilers by replacing the air in oxidizer stream with the mixture of pure oxygen and CO₂-rich flue gas. The replacement of nitrogen with CO₂ in dry recycle oxy-fired condition and with CO₂/H₂O in wet recycle oxy-fired condition were reported to significantly change combustion characteristic in oxy-fuel combustion, such as reduced flame temperature, delayed ignition, and reduced pollutant emissions (Chen, 2012, Wall, 2009).

The difference in ignition and combustion characteristic in conventional air and oxy-combustion can be explained by the difference in thermo-physical properties of bulk gas in air-firing, N₂, and in oxy-firing, CO₂ and H₂O. The values of thermo-physical property of these gases at 1400K are given in Table 2-1 (Khare, 2008, Shaddix, 2011). From this table, thermal conductivity of H₂O is two-fold higher compared to the other two gases. Therefore, the rate of particle heat up is likely to increase with the implementation of wet

recycle loop in oxy-fuel. However, this does not suggest accelerated ignition under wet recycle loop as other property, such as heat capacity, may be significant.

Table 2-1 Properties of N_2 , CO_2 and H_2O at 1400K and atmospheric pressure, adapted from (Khare, 2008, Shaddix, 2011)

	N_2	CO_2	H_2O
Density (ρ) (kg/m³)	0.24	0.38	0.17
Thermal conductivity (k) (W/m.K)	8.2e-02	9.7e-02	1.6e-01
Specific heat capacity (Cp) (kJ/kmol.K)	34.18	57.83	45.93
Dynamic viscosity (μ) (kg/m.s)	4.9e-05	5.0e-05	3.9e-05
Kinematic viscosity (ν) (m²/s)	2.0e-04	1.3e-04	6.6e-05
Binary diffusion coefficient of O_2 (m²/s)	3.0e-04	2.5e-04	3.8e-04

According to the auto-ignition theory, particle ignition is strongly influenced by the gas specific heat capacity (Law, 2006). The higher specific heat capacity of CO_2 and H_2O , 57.83kJ/mole and 45.93kJ/mole compared with that of N_2 , 34.18kJ/mole, was accredited to the delayed ignition and lower combustion temperature in oxy-fuel (Molina, 2007, Shaddix, 2009). Apart from ignition, it is also necessary to maintain the similar heat transfer characteristics with that in air-firing for retrofitting a conventional air-fired power plant to oxy-fuel furnace. A good indicator of matched temperature profile is when a similar adiabatic flame temperature (AFT) is attained. Using an equilibrium calculation procedure, a higher proportion of O_2 in the feed gas, typically 35vol% in wet recycle and 28vol% in dry recycle, is required in oxy-fuel combustion to main the similar AFT, shown in **Figure 2-1**(Wall, 2009).

Nonetheless, it should be noted that the required oxygen molar fraction to match the combustion temperature in air-firing highly depends on the proximate and ultimate analysis of specific coal. For example, sub-bituminous coal and bituminous coal require O_2 molar fraction of 28% and 35%, respectively, in oxy-fuel to match the gas temperature and heat fluxes in air-combustion mode (Croiset, 2000, Croiset, 2001). In another independent study, a relatively lower oxygen molar fraction of 25% was found sufficient in lignite oxy-fuel tests to generate equivalent combustion temperature to that in air-firing (Andersson, 2008a). The gas temperature increased by 50K and 100K, respectively, when oxygen concentration was elevated to 27% and 29%, respectively, in the flue gas.

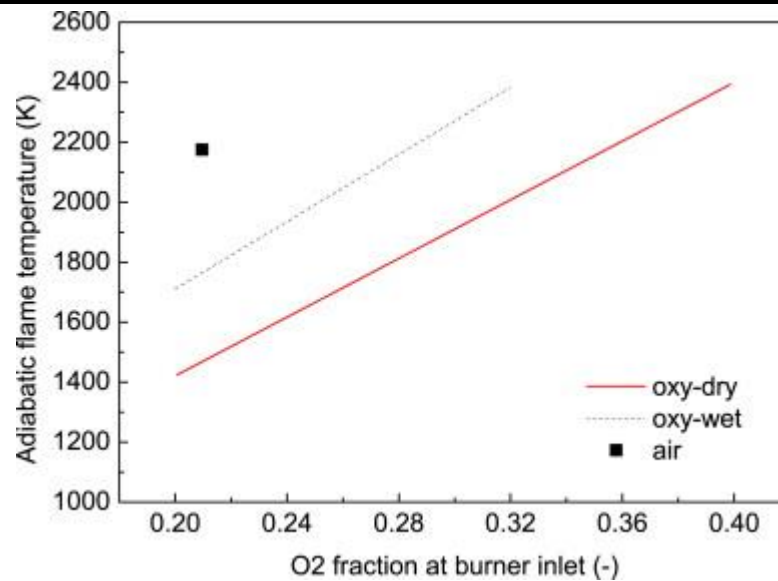


Figure 2-1 Required O₂ molar fraction in the burner inlet to achieve similar AFT in oxy-fuel combustion to that in air-firing case for wet and dry flue gas recycle (Wall, 2009)

Another important factor that may alter required O₂ concentration to match temperature field is the state of flue gas recycle, either dry or wet. With similar O₂ concentration, the gas temperature in dry flue gas recycle is likely to be lower due to the higher heat capacity of CO₂ compared to H₂O (**Table 2-1**). Some experimental results from pilot scale testing facilities indicated a slightly lower O₂ mole fraction of 23%-27% in wet recycle and 25%-35% in dry recycle (Andersson, 2008a, Croiset, 2001, Hjartstam, 2009, Payne, 1988, Rehfeldt, 2009, Wall, 2009, Wang, 1988). However, no explicit relation between the oxygen mole fraction and the scale of test facility can be drawn (Chen, 2012).

In addition to these, the difference in the radiative properties of bulk gas is also an influencing factor that impacts heat transfer profile in oxy-fuel combustors. Diatomic gases, such as N₂ and O₂, are transparent to radiation while triatomic gases, such as CO₂ and H₂O radiate considerably (Abdul-Gani, 2011). The Chalmers University of Technology measured the gas radiation intensity in a 100kW test facility, shown in **Figure 2-2** (Andersson, 2008a), and indicated a significantly higher radiation intensity in oxy-fuel combustion, regardless of oxygen mole fraction (Andersson, 2007, Andersson, 2008a, Andersson, 2008b, Hjartstam, 2009). Therefore, radiation from soot and particles (coal, char and fly-ash) is prominent in oxy-fuel boilers (Andersson, 2008b, Gupta, 1985, Hjartstam, 2009, Wall, 1973). Comparing the radiation energy contributed from both

particles and gas, the particle radiation is more important and contributes to approximately 60%-70% of the total radiation (Andersson, 2007, Andersson, 2008a). It was later suggested that similar radiation heat transfer to air-firing could be achieved in lignite oxy-fuel combustion if the gas temperature is maintained similar as in air combustion.

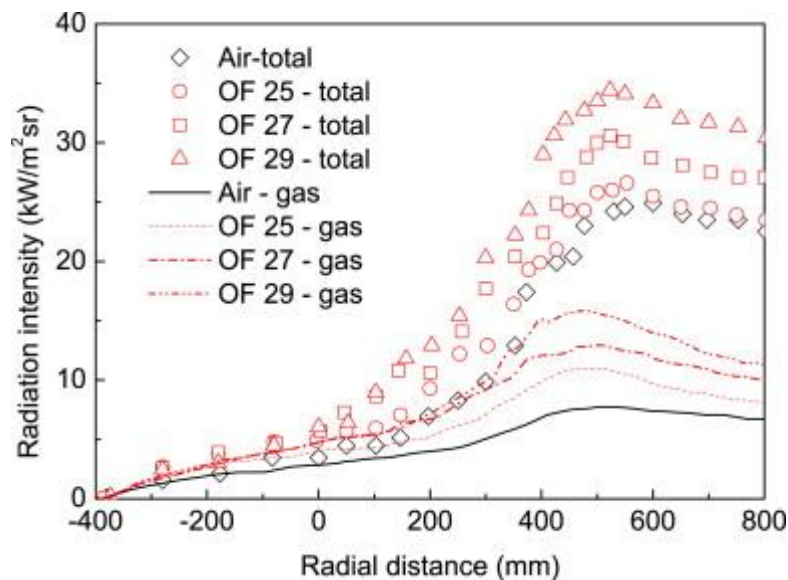


Figure 2-2 Experimental and modelling results of total gas radiation intensity, cited from (Andersson, 2008a)

2.2 Fundamentals of oxy-fuel combustion mechanism

To comprehend how coal combustion characteristic differs in oxy-fuel combustion, it is of utmost importance to understand how coal particles behave during normal combustion process. Coal combustion is a complex physical and chemical process. For coal particles undergoing a combustion process, four well-defined steps have been identified, illustrated in **figure 2-3**(Wu, 2005). The combustion processes, in sequences, are:

1. Drying of original coal particle and then, heating up to the pyrolysis temperature. Some coal types may exhibit particle shrinking, pore size reduction, internal cracking or particle break-up
2. Pyrolysis of coal particles to produce non-condensable volatiles (light gases), condensable volatiles (tar) and a carbonaceous char

3. Rapid oxidation of the combustible volatiles with the oxygen in surroundings, producing CO_2 and H_2O
4. Combustion of the residual char.

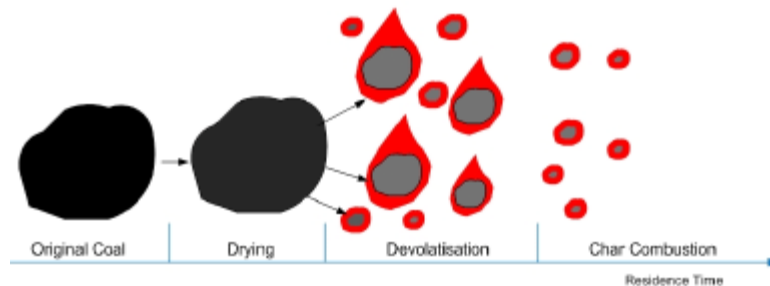


Figure 2-3 Coal combustion process, adapted from (Wu, 2005)

2.2.1 Drying of single coal particles

Pulverized coal (pc) particles are generally heated and partially dried by primary air or hot recycled flue gas in the milling system (McIntosh, 1976a, McIntosh, 1976b). The temperature of hot flue gas is typically preheated to 250°C or above to ensure full drying capacity and maintained at around $60\text{--}90^\circ\text{C}$ at the mill exit (Dillon, 2005). The remaining moisture, or water in the case of coal water-slurry (CWS) system, is evaporated in the furnace prior to combustion. The process of moisture evaporation is mainly controlled by physical mechanism governing heat and mass transfer rather than chemical reaction (Turns, 2000). For drying of small coal particles in pc boiler, convective heat transfer is more dominant than radiative heat transfer (Cen, 1997). The numerical study on pulverized coal drying in 1000°C furnace showed similar drying time of 2.5ms in both air and CO_2 environment (Chen, 2012). Given the small size of typical pc particles such that the Nusselt number is close to 2, the gas thermal conductivity dominates the heat transfer rate. This also suggested the shorter moisture evaporation time under wet recycle configuration. However, this analysis is solely based on drying of an isolated single particle/droplet. The drying process of particle group may be different and is proposed as a subject of study for future research.

2.2.2 Coal pyrolysis

Following moisture evaporation, some volatile matters, including condensable and non-condensable matters, are subsequently released to the gas phase at a temperature above 300°C. These account for up to 70% of coal weight loss and are strongly dependent on the organic properties of the coal (Solomon, 1993). In general, pyrolysis process or devolatilisation is highly endothermic and its kinetics and yields are strongly influenced by heating rate, gas temperature, holding time, ambient gas composition and operating pressure (Chen, 2010, Gibbins-Matham, 1988, Matsuoka, 2003, Serio, 1987). The product yields and pyrolysis kinetics are typically investigated in inert gas, such as N₂ and helium. As CO₂ is considered a reactive species, significant alterations in pyrolysis characteristics due to high concentration of CO₂ is expected in oxy-fuel combustion.

Experimental studies on coal pyrolysis are normally conducted using a thermogravimetric analyzer (TGA) or a drop-tube furnace (DTF). The corresponding heating rate of TGA and DTF are approximately 10K min⁻¹ and 10⁴-10⁵K min⁻¹, respectively. This difference in heating rate also influences the total volatiles yield. In terms of application, the slow heating rate in TGA is normally used to obtain coal intrinsic kinetic data. Meanwhile, rapid heating in DTF is applied to simulate practical coal reaction process under similar condition to that encountered in an industrial furnace.

Several coal pyrolysis research in a high-temperature TGA have exhibited higher overall volatile yields in the CO₂ atmosphere (Duan, 2009, Li, 2009, Rathnam, 2009, Yuzbasi, 2011). However, these studies were performed over a wide range of temperature such that discrepancies between each study are prominent. For example, Rathnam (2009) and Yuzbasi (2011) showed similar weight loss behavior of coal samples in both air and CO₂ atmosphere at the temperature up to 700°C while Li (2009) revealed lower devolatilisation rate in CO₂ atmosphere at the similar temperature range. On the other hand, Duan (2009) indicated maximum volatile release rate at lower temperature of approximately 480°C. As conflicting results were achieved from various studies, no clear conclusion can be drawn regarding the impact of CO₂ at lower temperature. Nonetheless, these studies agree that the overall higher volatiles yield in CO₂ is linked to the char-CO₂ gasification reaction (Rathnam, 2009, Yuzbasi, 2011).

Similarly, several researchers also reported conflicting results in experimental works conducted in a DTF (Al-Makhadmeh, 2009, Borrego, 2007, Brix, 2010, Li, 2010, Rathnam, 2009). Both Rathnam (2009) and Al-Makhadmeh (2009) concluded the higher volatiles yield in CO₂ than those in N₂ atmosphere while Borrego (2007) observed the opposite. Borrego (2007) suggested that cross-linking of CO₂ to the char surface of the solidifying char reduces particle swelling and inhibits volatile release. Recent CO₂ gasification study also indicated the development of char structure at 800-950°C which support the earlier statement (Komarova, 2015). In another independent study, higher porosity char was found to be more reactive to gasification reaction (Liu, 2015). On the contrary, Brix (2010) observed no difference in char morphology, char N₂-BET surface area and volatile yields in both air and CO₂ atmosphere. The discrepancies between different studies can be related to different operating conditions between each study, such as total particle residence time employed in these experiments. The longer residence time increases the total volatile yields and char porosity (Al-Makhadmeh, 2009, Liu, 2015, Rathnam, 2009) while short residence time results in similar char characteristics under both N₂ and CO₂ atmosphere (Brix, 2010). From the studies reviewed above, although extensive research on oxy-fuel combustion were conducted, the impact of wet recycle on pyrolysis was not investigated and should be studied in future research.

2.2.3 Volatile oxidation

The flammable volatiles that are released during coal devolatilisation will react with oxidizer in the hot gas and burn in the gas-phase. The burning characteristics of volatiles vary significantly depending on coal size, coal rank and furnace operating conditions. In an entrained flow reactor (EFR) facility at Sandia National Laboratory (SNL), a large hot-volatiles burning soot was observed from bituminous coal combustion while sub-bituminous coal produced soot-less cloud and a relatively lower radiation intensity (Shaddix, 2009). Likewise, other studies also showed extensive soot formation from bituminous coal combustion. Additionally, fragmentation of lignite char during volatile combustion was also observed (Bejarano, 2008, Stivers, 2010). These differences in volatile combustion behavior can be correlated to different coal composition. The soot generated from bituminous coal combustion is produced from burning of long

hydrocarbon chain in bituminous coal tar while low-rank coal, such as lignite and sub-bituminous coal, is much lower in tar yields.

Additionally, the distinctive thermo-physical properties of CO_2 is also predicted to alter volatile combustion characteristic under oxy-fuel combustion. The replacement of N_2 by CO_2 increases soot cloud size, shown in **Figure 2-4**, and reduces soot burning temperature (Molina, 2007, Shaddix, 2009). In another independent study, lower volatiles burning temperature and longer volatiles burnout time, illustrated in **Figure 2-5**, were observed under oxy-firing mode over a range of oxygen mole fraction of 20%-80% (Bejarano, 2008). These observations are likely caused by lower O_2 diffusional rate in CO_2 , listed in **Table 2-1** above. As oxygen diffuses faster in H_2O , it is also necessary to investigate volatile combustion behavior under wet recycle configuration.

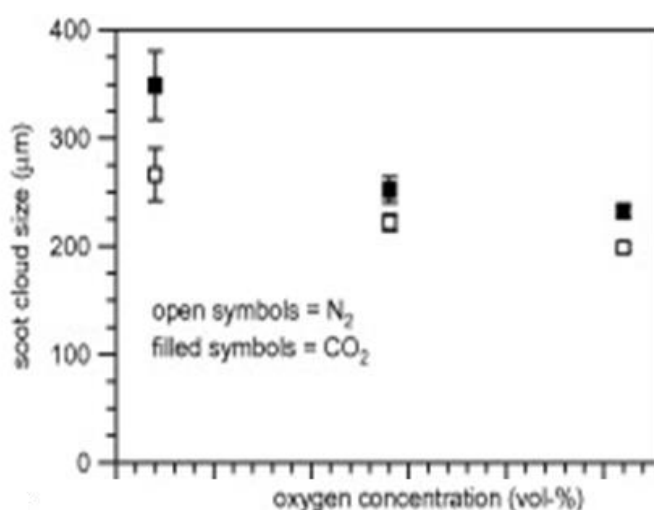


Figure 2-4 Measurement of soot cloud size of Pittsburgh bituminous coal in air and oxy-fuel combustion with different oxygen concentration, cited from (Shaddix, 2009)

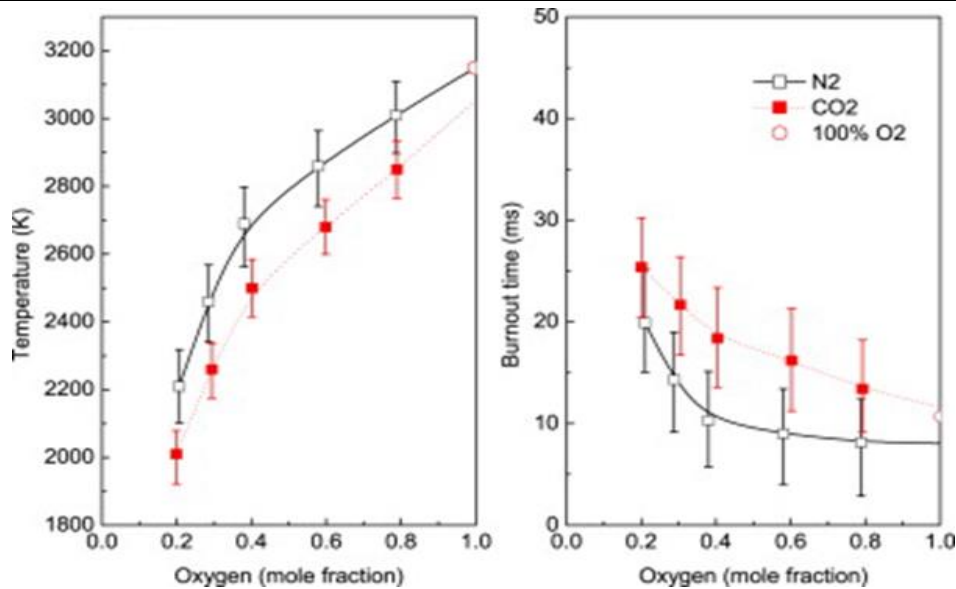


Figure 2-5 Average temperature and burnout time of bituminous coal volatiles under O₂/N₂ and O₂/CO₂ atmospheres, cited and adapted from (Bejarano, 2008, Chen, 2012)

2.2.4 Char combustion and oxidation

The residue left after volatile combustion which is rich in carbon is referred to as ‘char’. The residual char particles are oxidized heterogeneously through direct attack of oxygen to particle surface at sufficiently high temperature. While the pyrolysis step is usually rapid, the duration for char oxidation is relatively slow, in the order of seconds (Smith, 1971). Therefore, char oxidation influentially contributes to the radiative heat transfer in the boiler. The oxidation mechanism is complex and controlled by temperature, pressure, coal type, char size and structure, and oxygen molar fraction. Subjected to oxygen concentration, the particles may burn in different regimes, either kinetic-controlled (Zone I), diffusion-controlled (Zone III) or combination of both (Zone II).

In a kinetically-controlled oxidation, char oxidation reaction dominates the char consumption rate. This is typically encountered at low or intermediate temperature furnaces, such as TGA experiments (Liu, 2005a, Liu, 2009, Varhegyi, 1999). Meanwhile, in a diffusion-controlled regime, the char burning rate is proportional to the oxygen partial pressure in bulk gas and is controlled by char consumption rather than char oxidation reaction. This mechanism dominates at high temperature and high oxygen concentration condition, which are typically found in DTF and EFR experiments. The

combination of these two mechanisms are typically encountered in practical situations (Murphy, 2006).

In oxy-fuel combustion, the combustion rate of coal char is further influenced by the combined effects of mass transfer, internal oxygen diffusion to char surface, dissociative adsorption of CO_2 and H_2O on the char surface and char gasification by CO_2 and H_2O (Hetch, 2011, Hetch, 2012, Shaddix, 2011). Consequently, the extent to which of these effects influences the total char burning rate depends on the char particle temperature and change in char structure under oxy-firing mode (Hetch, 2011). Due to the exothermicity of the char oxidation reaction, a higher char particle temperature implies a higher char burning rate when char combustion takes place in the mixture of oxygen and inert gas, i.e. conventional air combustion. The dependence of char particle temperature on gaseous environment is demonstrated in **Figure 2-6** (Timothy, 1982), which shows pronounced trends in the increasing temperature at elevated oxygen concentration.

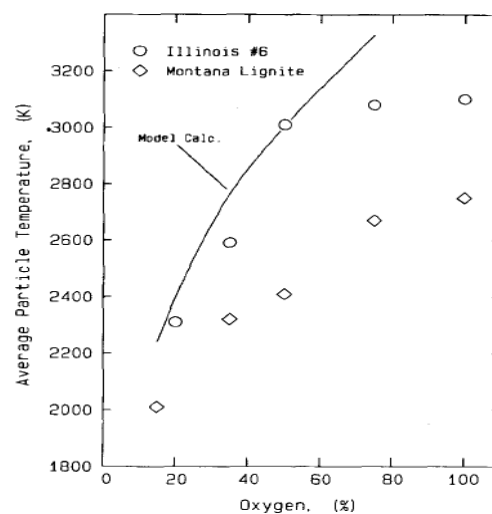


Figure 2-6 Average char particle temperature at 50% char burnout at elevated oxygen concentration, cited from (Timothy, 1982)

Conversely, char particle temperature is lower in oxy-fuel combustion because of high specific capacity of CO_2 . This is demonstrated in **Figure 2-7**, at which char particle temperature decreased by 125K under oxy-firing mode at similar oxygen concentration to that in air-firing (Riaza, 2014). As CO_2 is considered a reactive species, the lower combustion temperature in oxy-fuel does not necessarily infer lower char burning rate.

The possibility of endothermic char gasification reaction with CO_2 and H_2O in oxy-firing may confound the interpretation of char burning rate based on char burning temperature.

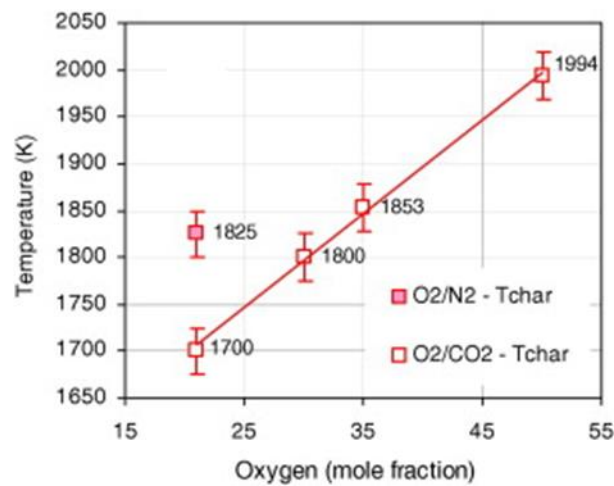


Figure 2-7 Char combustion temperature of Anthracite coal in air and oxy-fuel combustion, adapted from (Riaza, 2014)

2.3 Combustion modelling

A wide-ranging review in **section 2-2** provides comprehensive details on the progress and advancement of oxy-fuel combustion. Nonetheless, application of mathematical models in coal combustion process is less progressive although it received significant emphasis over the past decade (Edge, 2011, Williams, 2002). A panel of industrial and university professionals in U.S. department of energy recommended the development of combustion models to the point where they will find application in the management and control of practical systems (Smoot, 1984). Consequently, there is a necessity to develop a model to simulate the process of devolatilisation, volatile combustion and char oxidation for accurate prediction in oxy-fuel combustion.

2.3.1 Devolatilisation model

To reiterate, coal devolatilisation is the initial step in coal conversion process. The release of volatiles matter from coal is an endothermic process and affects the overall furnace operation. Devolatilisation models are used to predict the rate of volatile release from coal. Currently, there are four widely known coal devolatilisation models; constant rate model, single-rate Arrhenius model, two competing rate model and network models,

either FLASHCHAIN, Chemical percolation- devolatilisation (CPD) or Functional Group-Depolymerisation Vaporization Cross-linking (FG-DVC). Some of the advantages and disadvantages of each model are listed in **Table 2-2**.

From **Table 2-2**, network models are the most advanced model for coal devolatilisation. Although it is able to accurately predict the tar species and yield from pyrolysis (Fletcher, 2015, Guan, 2015, Stark, 2015), most studies on coal combustion modelling favored single-kinetic rate Arrhenius model due to its simplicity and short computational time (Al-Abbas, 2011, Al-Abbas, 2012b, Alvarez, 2011, Black, 2013, Chui, 2003). Also, the kinetic devolatilisation data for the studied coal in either air or oxy-fuel combustion can be easily derived from TGA experiments.

Table 2-2 Advantages and disadvantages of different coal devolatilisation model, adapted from (Edge, 2011)

	Constant rate model	Single-rate Arrhenius model	Two competing rate model	Network model
Reference(s)	(Baum, 1971)	(Badzioch, 1970)	(Kobayashi, 1977, Ubhayakar, 1977)	(Grant, 1989, Niksa, 1994, Solomon, 1994)
Description	Volatiles are release at constant rate	Devolatilisation rate is first order dependent on amount of volatile release and temperature	Rate of devolatilisation dependent on two competing rates at different temperature range	The most detailed and comprehensive model by considering chemical structure and coal functional group
Advantages	Simple	Easy to implement in either small-scale or large-scale simulation	This model considers different devolatilisation rate at different temperature range	Accurate prediction of mass loss rate and results are independent of coal proximate analysis and kinetics
Disadvantages	Error in predicting actual rate in practical simulation	Need to derive the kinetic data for individual coal, therefore limiting its application to certain type of coal	Need to derive the kinetic data for individual coal, therefore limiting its application to certain type of coal	Complex model and may be unnecessary in commercial software

2.3.2 Volatile combustion model

For the application in large-scale simulation, coal volatile combustion is typically modelled by using a mixture fraction/ PDF chemical equilibrium approach (Sivathanu, 1990). The main product from coal pyrolysis is anticipated as light hydrocarbon equivalent; either CH_4 or CO (Al-Abbas, 2011, Lockwood, 1998). This simplifies the homogeneous volatile reaction scheme as overall one-step reaction of volatiles with oxygen to produce CO_2 and water vapor. Nevertheless, discrepancies between simulated and experimental data were observed using this modelling approach (Al-Abbas, 2011, Al-Abbas, 2012a). A multi-step reaction scheme for volatile combustion was then developed and exhibited more accurate predictions of gas temperature and species concentration in the combustor (Al-Abbas, 2012b).

Unlike devolatilisation, modelling volatile combustion mechanism in oxy-firing has different approach than that in air-firing. Although the multi-step reaction scheme works well under air combustion, the exchange of inert N_2 with chemically reactive CO_2 is expected to alter the overall elementary reaction, especially at high temperature (Glarborg, 2008). The two-step mechanism (WD) and four-step mechanism (JL) hydrocarbon mechanism are widely applied for CFD modelling in industrial application and are directly available as default mechanism in commercial CFD package (Jones, 1988, Westbrook, 1981, Westbrook, 1984). Recently, these models were refined where changes were made in the CO-O_2 reaction subset to improve prediction of CO levels (Andersen, 2009). The improvement was more pronounced for WD mechanism while refined-JL reaction scheme showed a slightly results in predicting CO trends. Additionally, the latter also showed better prediction of propane flame behavior in oxy-fuel combustion.

2.3.3 Char combustion model

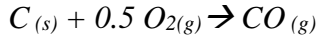
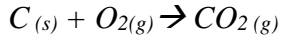
Char combustion is the limiting step on overall coal conversion process. Therefore, it has major impact on overall furnace heat transfer and combustion efficiency. Burning char particle temperature is balanced by char burning rate and heat transfer to/from the surroundings. An accurate prediction of the char burning rate is therefore essential in calculating the correct char particle temperature. As indicated in **Section 2.2.4**, char combustion process occurs under three controlling steps; either kinetic controlled,

diffusion controlled or combination of both. Generally, pulverized coal combustion falls under combination of both chemical and diffusion controlled regime (Baum, 1971). From extensive research in coal combustion, several char combustion models were proposed; kinetic-diffusion model, such as single film and double film model, the random-pore model, and the intrinsic reaction model. The advantages and disadvantages from each model are listed in **Table 2-3**. Of all the listed models, the simplistic single film model is favored in the simulation of pulverized coal combustion (Al-Abbas, 2012b, Murphy, 2006, Yu, 2009, Zhang, 2013). Following that regard, the rest of this section is dedicated to reviewing the development and application of single film model.

Table 2-3 Advantages and Disadvantages of several char combustion models, adapted from (Edge, 2011)

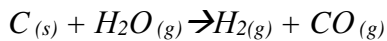
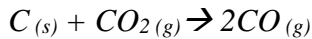
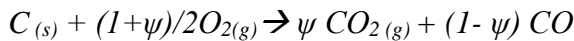
	Description	Advantages	Disadvantages	Reference(s)
Single-film model	Reaction of carbon with oxygen occurs in a frozen boundary layer with no gas-phase CO oxidation $C + O_2 \rightarrow CO$	A simplistic model to predict char burning rate for pulverized coal combustion (<100µm)	Not applicable to predict burning rate of larger particles (>100 µm). Also, structural change in char is not considered	(Field, 1969, Geier, 2012, Yu, 2009)
Double-film model	Carbon oxidation occurs in two-phase zone. particles react with O ₂ to produce CO. CO diffuses through film zone to gas-phase zone and further oxidized to CO ₂ $C + O_2 \rightarrow CO$ $CO + O_2 \rightarrow CO_2$	Able to accurately capture burning rate of larger particle and also more accurate compared to single film model	Similar to that of single-film model, assumption on constant char properties during combustion may not be accurate	(Annamalai, 1987, Mitchell, 1991)
Random pore model	This model consider the effect of pore size distribution in char particle and integrate in calculation for char burning rate	Able to predict physical changes of char particle during combustion	Difficulties in obtaining the data on char porosity for microporous char	(Fei, 2011, Mitchell, 2007)
Intrinsic model	A more advanced char combustion model that take into account the intrinsic reactivity of each pore in the char.	A more accurate prediction for char burnout due to consideration of diffusional effect in char porous structure	Application limited to certain type of coal. Also, the reaction order used in calculation may not be accurate	(Smith, 1982)

Char combustion process is commonly described as a heterogeneous reaction of carbon with oxygen, either



From literature studies, it is well understood that CO is the predominant product during combustion at high temperature (Arthur, 1951, Mitchell, 1991, Tognotti, 1990). Further CO oxidization to CO₂ is likely to occur at the boundary layer close to the particle surface which communicates a portion of heat released back to the particle. For small particles which size less than 100µm, CO₂ is principally generated at the particle surface rather than in the boundary layer (Mitchell, 1987). This confirms the applicability of single-film model to predict char combustion rate in pulverized coal-fired boiler.

Under oxy-fuel combustion mode, an oxygen-enriched environment is expected to significantly increase char particle temperature which alters the oxidation mechanism of CO to CO₂. Through recent computational study, the partial conversion of CO to CO₂ in particle boundary layer affected char particle temperature and char burning rate (Hetch, 2011). Additionally, the elevated concentration of CO₂ and H₂O in oxy-coal combustion is anticipated to trigger char-CO₂ and char-H₂O gasification reaction, respectively. Thus, an improvement in single-film model is recommended for suitable application in the simulation of char combustion in O₂/CO₂ atmosphere. Geier (2012) extended the conventional single-film model by considering the influence of CO₂/CO production ratio (ψ) on particle surface to calculate char particle temperature. The same author also considered char-CO₂ and char-H₂O gasification reaction in the simulation (Geier, 2012). The above-mentioned reactions were assumed to take place heterogeneously, as follows:



From above reactions, the overall char consumption rate equals to the sum of the carbon removal rate from individual reaction. It should be noted that the char consumption rate

calculated in the afore-mentioned study was modelled by n^{th} order Arrhenius kinetic without consideration for diffusion. The combination of both kinetic and diffusion mechanism should be applied when using single-film model to calculate the overall char consumption rate. The extended-model developed by Geier (2012) can be integrated to the initial single-film model developed by Field (Field, 1969).

The representative char burning rate highly depends on value of the kinetic data. Unlike char oxidation kinetic, which was already well-established in the literature (Field, 1969, Murphy, 2006, Patel, 1988, Smith, 1971, Smith, 1982, Stevenson, 1973, Timothy, 1982), the study on char gasification kinetic only emerged recently (Chen, 2013, Hetch, 2011, Hetch, 2012, Huo, 2014a, Huo, 2014b, Kim, 2014a, Roberts, 2000, Roberts, 2014, Ahn, 2001, Cristina, 2012, Jiang, 1991). Mostly, the measured char gasification rate from these studies was several order of magnitude lower than char oxidation rate. Consider that these data were generated from low-temperature study in TGA, the actual kinetic rate of these reactions at high temperature condition is still unknown. Nevertheless, char gasification reactions show a higher apparent activation energy, 148-255kJ/mole (Ahn, 2001, Cristina, 2012, Jiang, 1991) for char- CO_2 and 131kJ/mole for char- H_2O (Ye, 1998), in comparison with with activation energy for char oxidation, 57kJ/mole (Murphy, 2006). Therefore, these reactions are likely to be prominent at high temperature during oxy-fuel combustion.

2.4 Coal ignition

Combustion of coal particles is initiated by ignition. Following that, coal may be ignited in gas-phase or particle phase depending on furnace operating condition. Moreover, the replacement of air flow by O_2/CO_2 mixture in oxy fuel combustion may also influence coal ignition. This is likely to alter flame location, length and stability, and coal preheat temperature. Subsequently, oxy-fuel combustors have to be specially designed to account for these specific changes. The aforementioned impacts are more pronounced when ignition process occur near the burner in the pc-fired furnace. Consequently, the degree of carbon burnout may also be different (Costa, 1994). Therefore, it is essential to fully understand coal ignition mechanism for developing cleaner coal combustion technology. In this section, coal particle ignition will be discussed in-depth followed by review of the literature studies on coal ignition that are relevant to oxy-fuel combustion.

2.4.1 Ignition mechanism

When coal particles are heated in an oxidizing atmosphere, ignition takes place which is characterized by substantial energy release. As illustrated in **Figure 2-8**, coal particles are ignited via three different mechanisms (Essenheigh, 1989); either homogeneous ignition of volatiles, heterogeneous ignition of carbonaceous char, or combination of both.

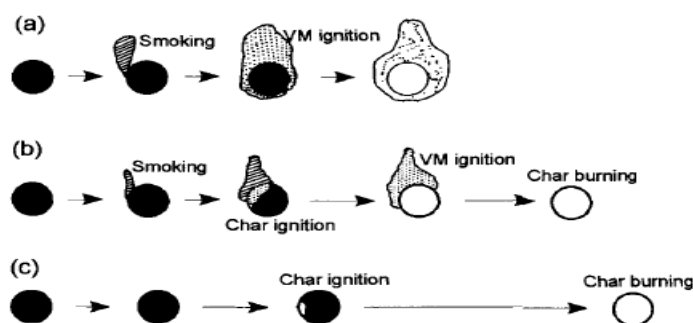


Figure 2-8 Three different mechanisms for coal ignition proposed by Essenheigh (1989), (a). Homogeneous Ignition, (b) Hetero-Homogeneous Ignition, (c) Heterogeneous ignition, from (Essenheigh, 1989)

Homogeneous ignition occurs when the rate of volatile release exceeds the heating rate of char particle surface. Visible sign of homogeneous ignition is the development of volatile flame surrounding coal particle. This provides enhanced heat feedback to char particle by conduction and also isolates char particle from the surrounding gaseous mixture. The latter forces the reaction flame sheet away from the solid surface, thereby preventing an oxygen attack to the solid char (Essenheigh, 1989, Howard, 1967). Finally, the residual char is oxidized after the volatiles are completely burned.

On the other hand, heterogeneous ignition follows once the particle heating rate surpasses the rate of volatile release. In this case, the particle surface temperature is high enough for char combustion to occur prior to evolution of volatiles. In heterogeneous ignition, char particle is oxidized via direct attack of oxygen to the char surface. The reaction continues until all the carbon in the residual char is consumed. Under specific conditions, the initial heterogeneous ignition of char may be quenched by sudden eruption of volatiles, known as 'heterogeneous-homogeneous ignition' (Essenheigh, 1989). In this case, both volatiles and char are consumed simultaneously.

Some critical variables influencing the mode of ignition have been suggested including volatile fraction in coal, particle size, particle loading and heating rate (Shaddix, 2011). The likelihood of heterogeneous ignition to occur depends on the ease of oxygen access to the char surface. For example, low volatile content, small particle, low particle loading, high oxygen concentration and slow heating rate favouring heterogeneous ignition. As the mode of particle ignition directly correlates to the particle heating rate, gas thermal conductivity is expected to influence ignition mode to a certain degree. Based on gas properties listed in **Table 2-1**, similar ignition mode is expected in both N₂ and CO₂ atmosphere at same temperature. In contrast, when wet recycle loop is applied in oxy-fuel combustion, the elevated steam concentration is likely to increase gas thermal conductivity; thereby favouring homogeneous ignition of coal particles. Additionally, coal of different ranks also exhibits different ignition behaviour. Recently, higher-rank coal, anthracite and bituminous coal, was reported to ignite homogeneously in gas-phase while lignite experienced extensive fragmentation prior to its heterogeneous ignition (Khatami, 2012b, Maffei, 2013, Riaza, 2014). However, this conclusion is not definite and there is a necessity to further clarify this observation.

2.4.2 Review on experimental ignition study

The most commonly reported ignition studies in literature have been the identification of ignition temperature, which is defined as minimum particle or gas temperature at where ignition occurs. Experimental techniques used for this measurement typically fall under two categories; either fixed bed experiment (i.e. TGA, electrically heated fixed bed reactor) or continuous feeding experiment (i.e fluidized bed reactor (FBR) or entrained flow reactor (EFR)). For the former technique, ignition temperature is detected by measuring coal mass loss over time in an oxidizing environment. Ignition temperature is taken as the temperature at which the derivative mass loss curve shows a peak at a specific temperature (Tognotti, 1985, Wall, 1991). Meanwhile, the latter approach is more favourable for ignition study in practical application as EFR and FBR can be subjected to conditions typically encountered in an industrial combustor. Commonly, characterisation of ignition behaviour in this facility is through measurement of light emissions using either photo detectors, such as radiation pyrometer or via imaging (Gupta,

1990). Some of the relevant experimental studies on coal ignition are reviewed in the next section.

IGNITION IN O_2/N_2

The first experimental ignition study dated back to the early 70s. Using a two-colour pyrometer, the temperature of size-graded anthracite coal particles was measured in a laminar flow reactor (Ayling, 1972). This study suggested the primary product of carbon oxidation as CO. Following this research, a similar pyrometry technique and a high speed camera were used to measure the burning times and temperature history of an individual coal particle (Timothy, 1982). By tracking the entire burning history of an individual coal particle, they reported the formation of soot flame during the initial stage of volatile combustion followed by char combustion. This indicated the initial coal ignition to occur in gas-phase rather than on particle surface. Another separate study also confirmed the formation of a layer of condensed matter or soot-like material surrounding the bituminous coal particles which defined homogeneous ignition prior to heterogeneous combustion of char (McLean, 1981). In the same study, lignite combustion showed the similar characteristic, but with no formation of a layer of condensed material surrounding coal particles. The same author later concluded the formation of soot is strongly dependant on coal type rather than local condition in the furnace.

A more recent study focused on the impact of different oxidizer concentration on coal ignition. Using a pelletized bituminous coal, Ponzio (2008) investigated the relation between oxygen concentration and ignition time in a high temperature batch reactor. The ignition time was reported to decrease remarkably with increasing oxygen concentration. Nevertheless, little variation in ignition time was observed at oxygen concentration of 21% or above (Ponzio, 2008).

The study described above focused on the ignition of single coal particle. Recently, Liu (2011) reported the ignition study of coal particle stream, which is more relevant to the application in pc burner. Prior to this research, only a single experimental study on coal stream ignition was ever conducted where a critical point for minimum coal ignition time was identified over a range of coal feeding rate (Ruiz, 1990). Liu (2011) later suggested

that concept of particle number density is more important in characterising ignition rather than coal feeding rate. Using a filtered charged coupled device (CCD) camera for ignition study, the same author reported that the minimum ignition time is found at a particle number density of $4 \times 10^9 \text{m}^{-3}$ in the coal feed line (Liu, 2011).

IGNITION IN O_2/CO_2

Most ignition studies in the last decade were on coal combustion in air or oxygen enhanced combustion with N_2 as the main diluting gas. As oxy-fuel combustion was prompted recently, a number of research facilities were built to investigate coal combustion under this condition. Nevertheless, the centred focus was on combustion study and the ignition characteristic under oxy-firing mode was scarcely reported.

The first reported ignition study in oxy-fuel combustion was conducted in a bench-scale 1.2MW tunnel furnace at IHI. They reported poor ignition quality due to the high specific heat capacity of CO_2 and water vapour (Kiga, 1997, Kimura, 1995). Following after, researchers at SNL initiated the single particle ignition study in O_2/CO_2 atmosphere using an entrained flow flat flame burner reactor (Molina, 2007, Shaddix, 2009). The ignition data was measured using a CCD camera to capture either the thermal emission of individual particles or the emission of CH^* chemiluminescence from ensemble of particles. The ignition data from this study is shown in **Figure 2-9** and exhibits a 2-3ms delay in O_2/CO_2 atmosphere (Shaddix, 2009). This also demonstrates the pronounced decrease in ignition time with increasing oxygen concentration. The conclusion was, increasing oxygen molar fraction to elevated concentration, which was 36% in that research, could match the ignition time as that in air combustion mode (Shaddix, 2009). Nonetheless, their subsequent study also revealed the less pronounced effect of oxygen concentration at higher temperature condition (Molina, 2009).

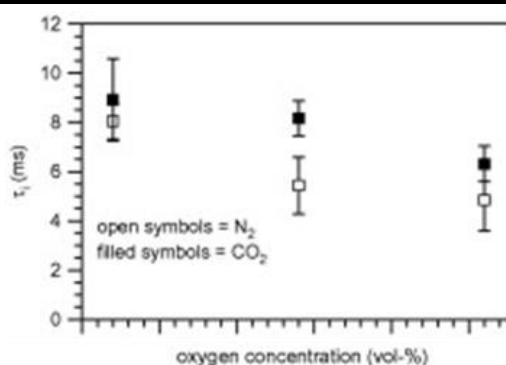


Figure 2-9 Variation of ignition delay at elevated oxygen concentration in O_2/CO_2 atmosphere, from (Shaddix, 2009)

In another study, the ignition behaviour of Victorian brown coal was studied in a DTF and captured with a high-speed imaging camera (Zhang, 2010b, Zhang, 2010a). This is the first study in oxy-coal combustion that presented coal ignition behaviour captured using a high speed photography technique. As illustrated in **Figure 2-10**, poor ignition quality was observed in 21% O_2/CO_2 atmosphere to which was improved by increasing the oxygen concentration to 27% and 36% in CO_2 diluent (Zhang, 2010b). From this research, the author reported an oxygen concentration of approximately 30% in oxy-fuel to match the flame intensity in air.

Following that after, a wire-mesh reactor was used in another study to investigate the effect of CO_2 on ignition using the temperature measurement approach. This was to study the effect of CO_2 on heterogeneous char ignition rather than homogeneous volatile ignition. Similar to the results discussed above, a delay in coal ignition was also observed. The ignition temperature increased by 21K, for brown coal, and 7K, for bituminous coal, in O_2/CO_2 atmosphere (Qiao, 2010). From these results, it should be noted that coal of different types may also ignite differently.

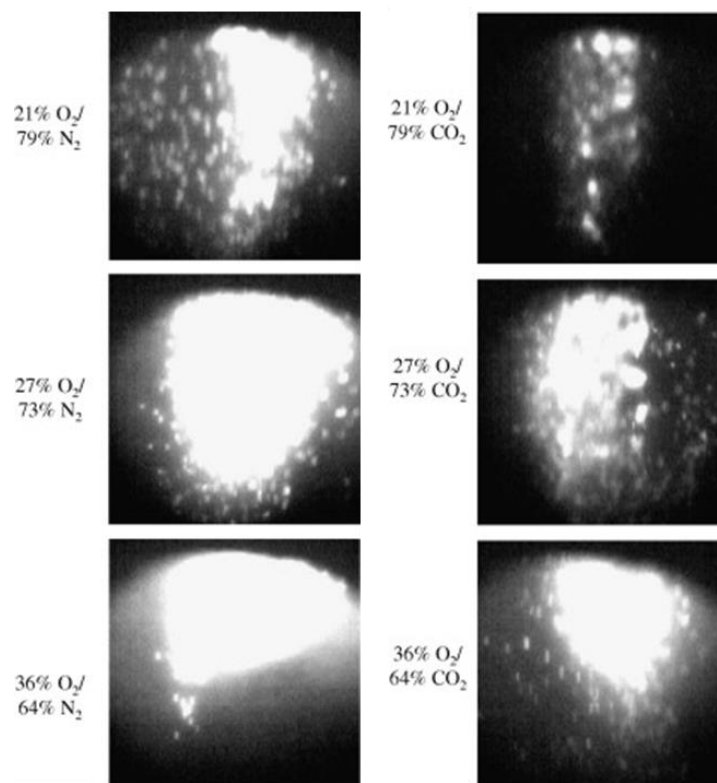


Figure 2-10 Combustion sequence of Victorian brown coal at 1073K in DTF in different O_2/N_2 and O_2/CO_2 mixtures, adapted from (Zhang, 2010)

The ignition characteristic of coal of different rank in O_2/CO_2 condition was later investigated by Khatami (2012) using a drop-tube reactor facility. Three different types of coal rank were used; bituminous coal, sub-bituminous coal and lignite. They also confirmed the ignition delay with the replacement of N_2 with CO_2 . However, higher rank coal was reported to exhibit a greater ignition delay compared to low-rank coal, which was approximately 100ms in bituminous coal and 60ms in lignite, at oxygen molar fraction of 30% (Khatami, 2012b). Nonetheless, this differences may be because of different coal composition from different coal type and the generalisation of this conclusion may not be accurate.

2.4.3 Modelling criteria for ignition

Complementary to the experimental study, modelling investigation also bears the same importance for the development of oxy-fuel technology. Initially, the first mathematical modelling study on coal ignition dated back to the 1920s (Nusselt, 1924). Back then, an

unsteady state energy balance equation was used to calculate the time required for coal particle to reach the ignition temperature. This simplistic statement regarding ignition was later re-defined as ‘the time required for coal particle to attain critical state which causes a sudden temperature rise’ (Stevenson, 1973). An illustration of particle temperature jump, from (Stevenson, 1973), is shown in **Figure 2-11**. This shows the predominance effect of gas temperature on particle ignition where an increase in gas temperature of 10K from 690K to 700K is critical. Since then, research on ignition breached out to numerically investigate the criterion behind homogeneous and heterogeneous ignition.

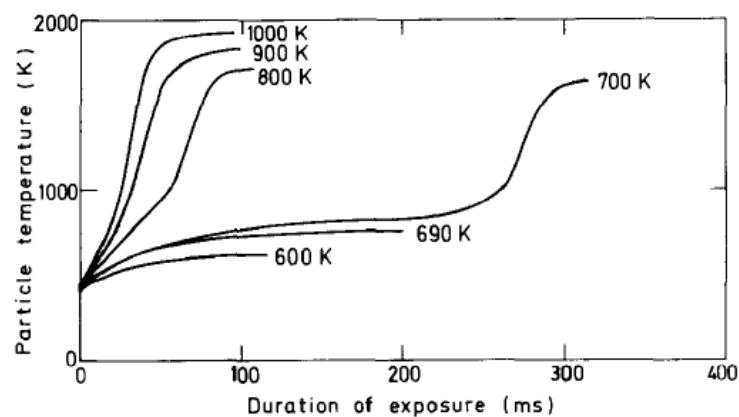


Figure 2-11 Brown coal particle temperature history in hot gas, from (Stevenson, 1973)

As discussed in **Section 2.4**, coal ignition mode, either heterogeneous or homogeneous, still need to be thoroughly assessed. One of the proposed methods is the characterization of ignition mode based coal intrinsic data derived from TGA. A theoretical basis for the ignition conditions was developed and tested (Ponzio, 2008). From this theory, three ignition regimes were constructed, which were defined as:

- Heterogeneous ignition of non-devolatilized coal; $r_{het, coal} > r_{devol}$
- Heterogeneous ignition of char; $r_{devol} > r_{het, coal}$ and $r_{het, char} > r_{hom, vol}$
- Homogeneous ignition of volatiles; $r_{devol} > r_{het, coal}$ and $r_{hom, vol} > r_{het, char}$

The above-mentioned approach was later adopted in CFD simulation (Jovanovic, 2011, Zou, 2014). In this model, the onset of particle ignition is generally identified by the drastic change in particle temperature over time (d^2T/dt^2) (Zou, 2014). The combustion process was simulated with different approaches depending on the ignition regime. For

homogeneous ignition, the combustion process was modeled as conventional process. The volatiles released from the coal initially, followed by combustion of the volatiles species and finally char oxidation. On the other hand, char oxidation was triggered as an initial process for heterogeneous ignition. Similarly, both char oxidation and coal devolatilisation process simultaneously progressed for heterogeneous-homogeneous ignition. Nonetheless, as this method was initiated for single particle investigation, a new methodology is needed to predict the ignition behavior in real combustors, where particle-particle interaction is significant.

Such approach was initially developed by Annamalai (1987) through establishment of quasi-steady (QS) model for group combustion of a spherical cloud of char particles (Annamalai, 1987). The theoretical model was constructed from gas phase conservation equation for mass, species and energy, particle-phase reaction and particle and gas energy balance. Two different criteria for ignition were established to distinguish between homogeneous and heterogeneous ignition (Du, 1995). The former was said to occur when the local heat generation in gas phase is higher than heat loss rate while the latter took place when particle temperature rose above gas temperature.

Other than spherical cloud, the particle clusters for group combustion can also be arrays of few particles or stream of many particles (Annamalai, 1988). Nevertheless, spherical cloud group combustion model has an advantage over other models as the burning rate of dense cloud can be approximated to the combustion rate of a large isolated particle of the same cloud size (Annamalai, 1987, Chiu, 1977). Several studies applied this model to predict the transient ignition behavior of coal particles (Ye, 2014, Zhao, 2007). As illustrated in **Figure 2-12**, spherical cloud model approximated reasonably well with the experimental data from the experiment conducted in an EFR to predict heterogeneous ignition time (Ye, 2014).

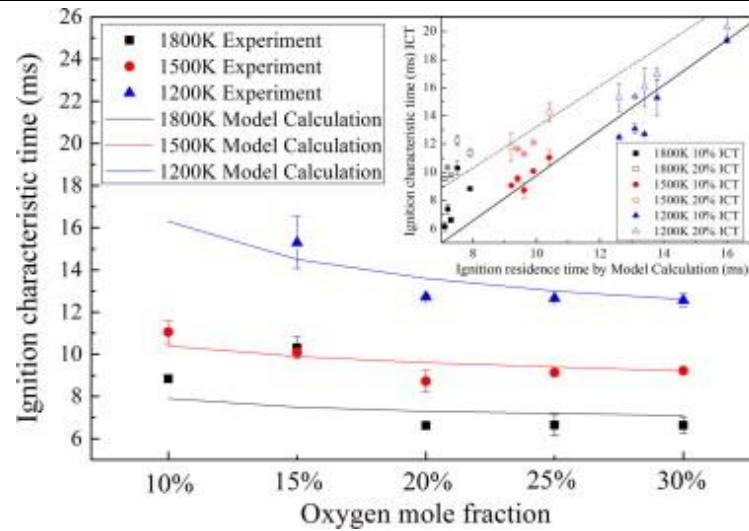


Figure 2-12 Comparison between experimentally measured ignition time in Flat flame burner with calculated ignition time using spherical cloud model for Bituminous coal, from (Ye, 2014)

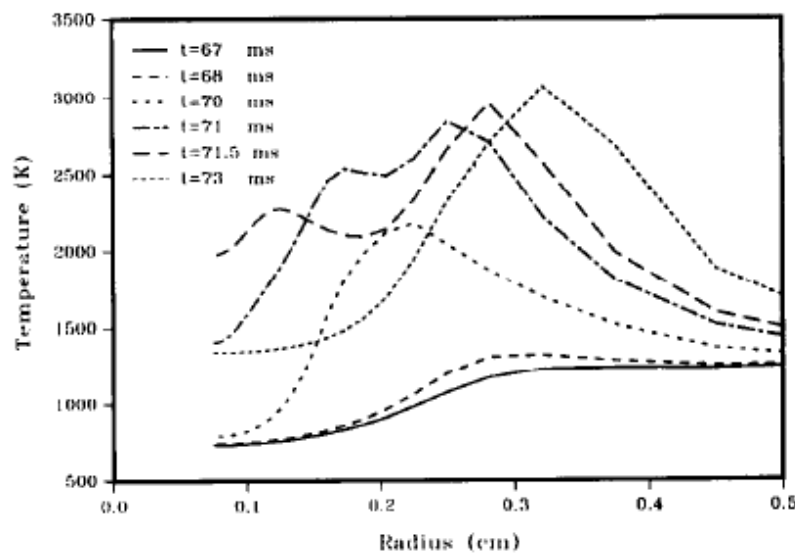


Figure 2-13 Development of flame profile over time predicted using cylindrical cloud model, from (Du, 1995)

While it is convenient in obtaining simplified results using a spherical cloud model, it is very difficult to simulate experimentally. The cylindrical cloud model is more useful for interpreting the experimental data for mono-sized stream of coal particles and can be done experimentally in an entrained flow reactor facility. From this model, the flame profile obtained in this study is illustrated in **Figure 2-13**, shown above, which presents the homogeneous ignition of coal particles at time $t=68ms$ (Du, 1995). Surprisingly, this

approach is not as widely used as spherical cloud approach in the ignition modeling although it can accurately predict homogeneous ignition time.

2.5 Impacts of mineral matters and solid additives on coal ignition

Other than ignition, ash-related slagging and fouling remain one of the primary technical challenge in the operation of pulverized coal boilers. These issues may drastically affect burner operation and downtime. Both slagging and fouling are defined as ash build-up in the heat transfer section during coal combustion with the former refers to the molten/semi-molten deposits in the radiant heat transfer section and the latter refers to the loosely-bonded deposits in the convective region in the boiler pass (Osborn, 1992). Slagging and fouling tendency of coal can be directly correlated to ash melting temperature, which is strongly dependent on coal ash composition (Bioenarea, 2012).

Perhaps, the most influential variable in triggering slagging and fouling problem is the AAEM species in coal. These ash-forming metal species are largely responsible for slagging and fouling in brown coal pc boiler (Brockway, 1991). For cleaner brown coal utilization, two methods were available to counter-act this issue; either by removal of ash-forming AAEM species through acid-washing (Wijaya, 2011b) or via injection of fuel additives for in-situ capture of the volatilized metal species (Lowe, 1993). The latter method is more practicable for application in the pulverized coal boiler as fuel additives can be directly injected with coal particle into the existing mill (Barnes, 2009). Silica-based sorbents, such as clay or kaolinite, was proposed as an efficient fuel additives to reduce slagging and fouling issue (Merrell, 1984). This approach was tested in several studies and was proven to remarkably decrease the ash deposition thickness (Lowe, 1993, Xiong, 2008). Additionally, these studies also reported the predominance effect of Na and K in fouling tendencies.

2.6 Summary

This chapter has provided a comprehensive literature study on coal ignition and combustion mechanism in oxy-fuel combustion. This also includes a mini review on the utilization of silica additives in pf boiler to minimize slagging and fouling problem. Based on this review, several research gaps that are relevant in brown coal combustion have been identified, listed below, which will be address throughout this research program.

- Firstly, Na, K species are abundant in brown coal and have been identified as the major cause of fouling problem in pc boiler. The addition of kaolinite has been proven to minimize slagging and fouling propensity. However, the ignition characteristic of coal + kaolinite has not been studied before.
- Secondly, coal ignition characteristics in O_2/CO_2 is well-established in the literature but most focused on combustion of high rank coal. Brown coal, with high moisture content, is likely to ignite differently from high rank coal. The effect of moisture may be significant as brown coal is only partially dried before being introduced to the furnace. This issue has not been addressed in the literature.
- In the case of low-rank coal combustion in oxy-fuel, the steam concentration is likely to increase drastically. To date, no research has ever been reported to study the coal ignition behavior under elevated steam concentration.
- Finally, most ignition studies investigate the ignition characteristic of single coal particle. While they may provide useful insight in understanding the fundamental ignition phenomena in O_2/CO_2 atmosphere, the particle-particle interactions in the practical coal combustors also exert major influences to coal ignition. Several studies have reported the ignition of dense particle stream in air. However, none has ever been performed in oxy-fuel atmosphere.

This page is intentionally left blank

Chapter 3

Research methodologies

This page is intentionally left blank

3. RESEARCH METHODOLOGIES

This chapter summarizes all the experimental facilities used throughout this research and their respective utilization method. Only the general operating procedures are presented here. The explicit details regarding the variation of the parameters depending on the experimental condition are given in the following relevant chapter. In addition, the modeling approach are also briefly discussed, with more details are to be included in the subsequent result chapters. The snapshot of all the experimental facilities employed in this study is given below.

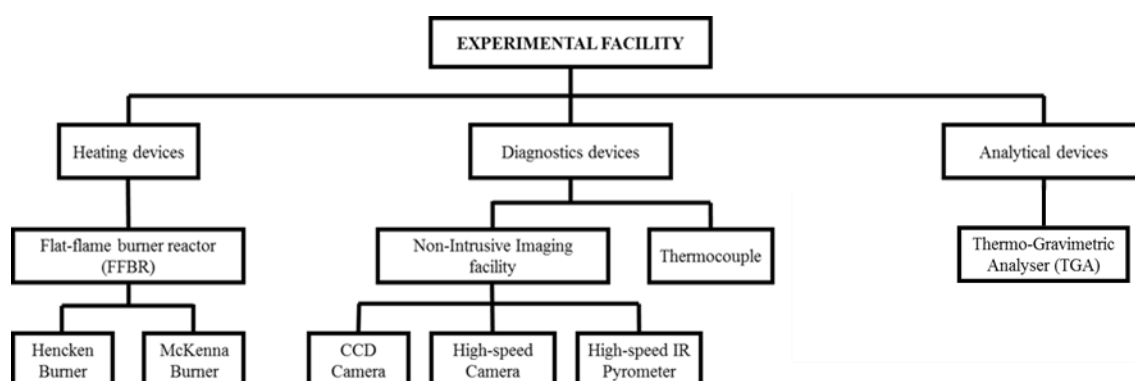


Figure 3-1 Snapshot of the facilities employed in this research

3.1. Heating devices

The flat flame burner reactor (FFBR) is the main heating device used for ignition experiments. The FFBR is designed as an entrained flow reactor (EFR), where coal particles are entrained in the hot gas mixtures as they flow through the reactor in a dense cloud. This laboratory-scale facility consists of moveable two-level bench (**figure 3-2**), where the burner is installed at the top-level and a piezo-electric feeder is located at the lower level (**figure 3-3**). Both devices are connected through a 1.0m long tube. At the top level, a tubular quartz reactor of 1.0m long with an inner diameter of 115mm is used to shield the atmosphere from the surrounding air. To minimize heat loss, the quartz reactor is mostly encapsulated with a 25mm insulation wool, except a 50mm x 300mm gap at the reactor base for the purpose of direct observation. The reactor is operated at the

atmospheric pressure and the combustion flue gas is discharged to the atmosphere through a filtered vacuum fan at the reactor exit. At the lower level, the piezo-electric feeder is insulated in a squared transparent case, to which a carrier gas is injected. The coal particles are then pneumatically conveyed to the burner via a carrier gas.



Figure 3-2 Full-view of FFBR facility



Figure 3-3 Piezoelectric coal feeding system located at the lower level bench

A mixture of gaseous fuels containing 80% ethylene (C_2H_4) and 20% Hydrogen (H_2) is burnt in the FFBR with an oxidizing agent to provide hot gas environment for coal combustion. The flat flame is achieved through the adjustment of the fuel/oxidizer flow rate (Bakali, 1998). Nitrogen is introduced through the burner as a shielding gas to protect the flat flame from the surrounding atmosphere. Two different types of flat flame burner are used in this research; non-premixed Hencken burner and premixed McKenna burner.

The general depiction of burner structure and configuration is detailed in the following section.

3.1.1. Hencken burner

Hencken burner, **figure 3-4**, is widely used and commercially available burner as diagnostic tools for H₂ flame research (Bertagnolli, 1998, Chai, 2007, Kulatilaka, 2004, Wooldridge, 2002). The burner is constructed from hundreds of hypodermic tube forming a 50mm x 50mm square honeycomb structure and installed in stainless steel housing. It is typically un-cooled and divided into a central flow and co-flow region. Within the central region, the liquid fuel is injected through the fuel tube and the oxidizer is fed into the alternating honeycomb channel surrounding the tubes. The fuel and oxidizer rapidly mix over the honeycomb structure and are burned, forming a flat flame atop. In the co-flow region of the honeycomb, a non-combustible gas is introduced as means to protect the flat flame. For the purpose of coal combustion study, a 3mm inner diameter feeding tube is integrated at the burner centre-line as the coal entry point through pneumatic conveying. This burner has main advantage to provide near-adiabatic flames over a wide range of equivalence ratio. However, it has shortcoming on the inability to support premixed flame due to flashback issue. In this thesis, this facility was used for experimental works in **Chapter 4, 5 and 6**.

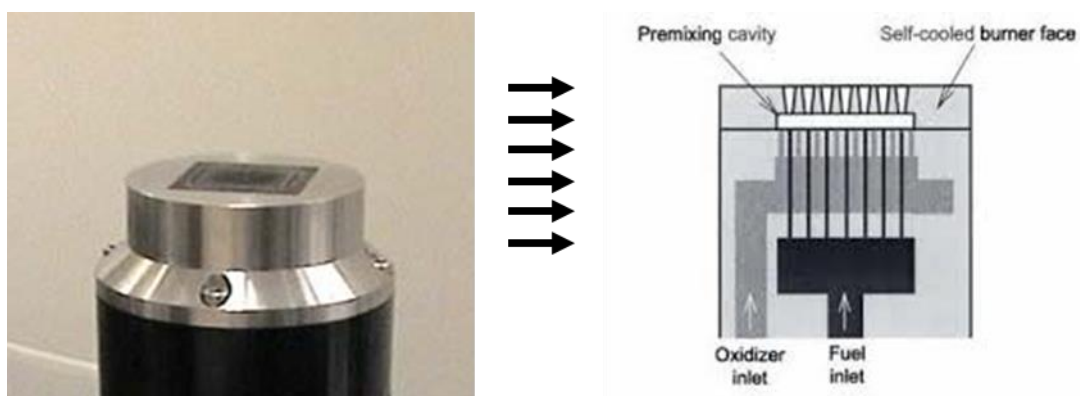


Figure 3-4 Hencken flat flame burner schematic, adapted from (Kastelis, 2008)

During these experiments, the burner was operated in atmospheric pressure. The flowrate of fuel and oxidizer were fixed 1slpm (*standard litre per minute*) and 10slpm, respectively. The primary gas flowrate was set at 0.7slpm, low enough to minimize the turbulent effect of gas and particle mixing at the early stage of coal combustion. This configuration produced a total flue gas flowrate of 11.7slpm after the flat flame and was maintained constant in all operating conditions investigated in these chapters. This was to prevent discrepancies in gas temperature in the reactor, which influentially affects coal ignition. The gas temperature was maintained at 1273K in every atmosphere investigated in this thesis. The flue gas composition described in the respective chapters, was the gas composition in the centre-line and obtained from equilibrium calculations.

3.1.2. McKenna burner

Another commercially available flat flame burner is McKenna burner, shown in **Figure 3.5**. It is commonly used to study the pollutants emitted from hydrocarbon fuels and to calibrate laser technology for optical diagnostics (Osswald, 2007, Prucker, 1994). The burner is made of a stainless steel outer which houses a porous, bronze, water-cooled, sintered matrix, which supports the generated flat flame. Slightly different from Hencken burner, the fuel/oxidizer is premixed in the chamber and evenly distributed throughout the sintered matrix prior to ignition. Also, the co-flow option that provide a shielding gas flow is designed only for non-combustible gases due to the lack of cooling provisions in the co-flow part of the burner plate. For this reason, the significant temperature/concentration gradient occurs towards the outer parts of the flame. Therefore, it has a major drawback in its application for absorption measurements and optical measurements that demand the use of atomic trace species. The issues described above is not subjects of concern in this research. Instead, the burner structure are modified by increasing the diameter of the coal entry tube located in the burner center-line for the purpose of research on the combustion of dense particle stream. In this thesis, this facility was used for the experimental works elaborated in **Chapter 7**.

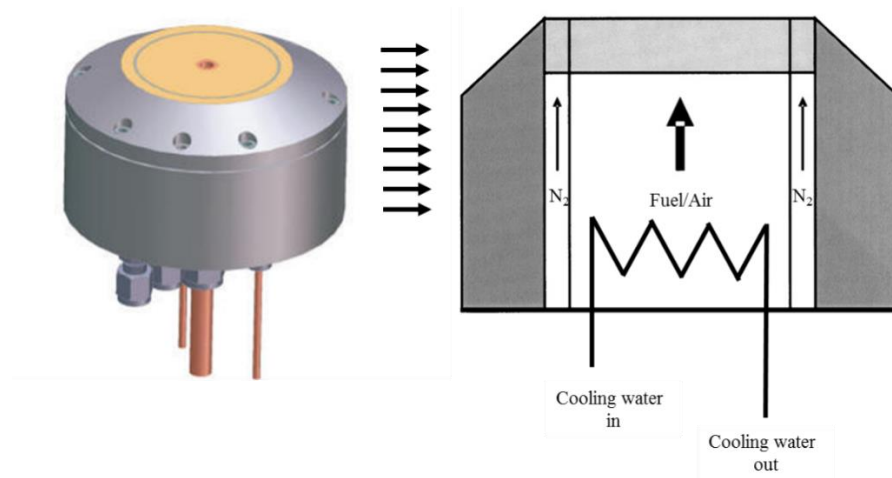


Figure 3-5 Schematic of McKenna flat flame burner

Principally, this facility operates in a similar way with the Hencken burner. However, the flowrate for fuel and oxidizer was increased to 1.6slpm and 20 slpm, respectively, while fixing the flow rate of the primary gas 0.7slpm similar to that used in Hencken burner facility. This is to provide enough gas in the environment to ensure that the feeding rate of coal has little disturbance on gas temperature that may affect ignition.

3.2. Diagnostic devices

Several diagnostics methods, including both non-intrusive and intrusive method, will be employed in this research to study coal ignition behaviour. The former refers to diagnostic approach without any intrusion to the combustion environment, using an imaging camera and a pyrometry technique. Conversely, in intrusive method, the diagnostic device is integrated to the furnace to capture the essential data, such as thermocouple.

3.2.1. Digital camera

A CCD digital camera, Nikon P7000, is used to capture images of burning coal particles. The camera settings and positioning are fixed to avoid interferences of background noise and camera focus. The camera is located 900mm away from the captured object. The exposure time is also fixed at 50ms. Captured images are processed and analysed using an

open-source image processing software, Image-J. Various data can be elucidated including coal ignition point, devolatilisation point, and char combustion length. An example of flame segmentation procedure is illustrated in **figure 3-6** (Published in: Prationo, W., Zhang, J., Cui, J., Wang, Y., Zhang, L., *Influence of Inherent Moisture on the Ignition and Combustion of Wet Victorian Brown Coal in Air-Firing and Oxy-Fuel Modes: Part 1: The Volatile Ignition and Flame Propagation*, Fuel Processing Technology, 2015, 138, pp 670-679). This information is generated through analysis of approximately 100 flame images. Coal ignition distance is obtained by an average value of pre-ignition length from a hundred images. The authors also use similar approach to measure devolatilisation and char combustion length. Consider that the measured length from the image is in pixel unit, the flat flame width at the burner base is also measured to calculate the conversion factor from pixel to mm unit. The real width of flat flame is measured before the start of any experiment. Therefore, real ignition length can be calculated using the equation shown below:

$$\text{Real length (mm)} = \frac{\text{Real flat flame width (pixel)}}{\text{Measured flat flame width (mm)}} * \text{Measured length (pixel)}$$

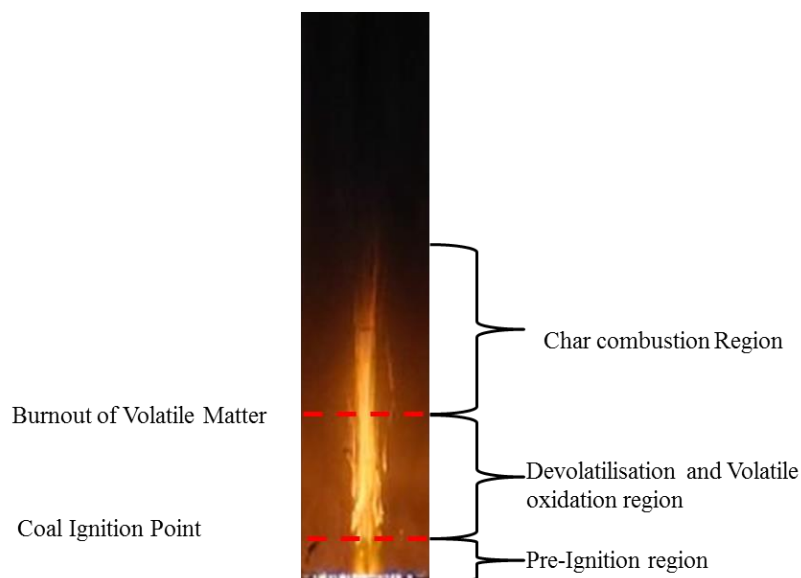


Figure 3-6 Combustion region segmentation based on flame structure

The images captured with the digital camera were used to calculate mainly coal flame length, which can be characterized into volatile oxidation and char oxidation length by analysis of approximately 100 images at each experimental case. The region of volatile oxidation, and char oxidation was pointed in **Figure 3**. As can be seen, the volatiles released from the coal particles burn after a certain distance which is called pre-ignition stage here. Such a stage is shown as a yellow blurred cloud with a very weak intensity reflecting the heat-up of particle and the release of volatile as well. Once being ignited, the released volatiles form a continuous fireball with the strongest intensity captured by the camera. The ignition point refers to the bottom boundary between pre-ignition and volatile oxidation stages. The luminous, thick flame following the ignition point and enveloping the cloud near the burner base signifies an intense release and homogeneous combustion of volatiles released from the coal pyrolysis, which in turn supplies heat feedback to ignite the char particles. The remaining length of the flame, with the less luminous region above the volatile oxidation regime, refers to char oxidation region. Similar analysis method has also been described elsewhere (Kim, 2010).

3.2.2. High-speed camera

A MotionPro Y3 high-speed camera mounted with a 25mm micro lens and an anti-blooming CMOS sensor was used to obtain monochrome photographs of coal combustion with short time interval. The camera focus is centered on the centre-line of the reactor where particle density is the highest. The capture speed is set at 1000 frames per second (fps) with lens exposure time of 997 μ s. It should be noted that no extra illumination is provided and the light emission captured in the images comes from the hot emission for coal particles and volatiles. The shutter speed is calibrated periodically via internal and external method. Internal method refers to the in-build calibration in the camera, whereas external method is conducted through measurement of a running electric counter with time resolution of 1ms. In this research, this device is used to measure the coal particle burning velocity. The measurement procedure was detailed elsewhere (Zhang, 2010a). This is vital to calculate coal ignition time from the ignition distance measured using a digital camera. Following that, the ignition time can be calculated as follow:

$$\text{Ignition time (ms)} = \frac{\text{Ignition distance (mm)}}{\text{Particle Velocity } (\frac{\text{mm}}{\text{ms}})}$$

3.2.3. High-speed infrared pyrometer

A high-speed infrared pyrometer from Kleiber-Gmbh (model: KS-740 LO) was installed next to the observation window along the quartz reactor on the FFBR. The pyrometer captures signal at the rate of 5MHz with the linear voltage output of 0-10 V which linearly correlate to particle temperature of 800-2300 °C. The pyrometer is calibrated periodically using a blackbody radiation source of pure copper as certified by National Institute for Standards and Technology (NIST). By comparing pyrometer measurement with melting point of pure copper, a correction factor was obtained. From here, the real temperature of can be calculated based on pyrometer signal. The detailed principle of pyrometer operation can be found in this reference (Khatami, 2011).

$$\text{Real Temperature (K)} = 1073 + (2573-1073) * 10^{-1} * \text{Measured Voltage (V)}$$

In this research, two wavelengths centering at 850nm and 1050nm are applied in the pyrometer for particle temperature measurement. These wavelengths are selected to avoid the adsorption band of a variety of species, including CO₂ (2.5-2.9μm and 4.6μm), H₂O (4.7μm) (Mollman, 2010), Na vapor (580 and 589.6nm) and K vapor (766.5 and 769.9nm) (Murphy, 2006, Saito, 1991). Nonetheless, particle temperature measured during the pyrolysis stage using these wavelengths is inaccurate due to the interference of volatile clouds. A wavelength of 4.0μm was suggested for more accurate measurement at this condition. Therefore, the particle temperature is measured at the later stage after coal pyrolysis has completed (Joutsenoja, 1997). Also, the emissivity of the pyrometer is adjusted to 0.8, based on reported study in literature for char particle temperature measurement (Baum, 1971).

3.2.4. Thermocouple

Thermocouple is one of the simplest techniques used to measure the gas temperature in the combustion environment. A complete understanding of the heat transfer mechanisms in the thermocouple bead is required to accurately derive the true gas temperature. The

procedure to calculate the radiation loss has been reviewed in the literature (Shaddix, 1999). In general, the energy balance around the thermocouple is a combination of conduction, convection, radiation as well as catalytically induced heating, as expressed with the equation (1) below.

$$Q_{cond} + Q_{conv} + Q_{rad} + Q_{cat} = \rho C_p V \frac{dT}{dt} \quad \dots \text{Equation (1)}$$

For the purpose of the thermocouple usage in combustion system to measure the local gas temperature, the main heat transfer mode to the thermocouple is driven by convection term. However, the other term, such as radiation is similarly important and has to be accounted for in order to accurately determine the true gas temperature. Both conduction and catalytic loss are difficult to be quantified in practice. Therefore, these terms were minimized when selecting the thermocouple. The type-K thermocouple wire used was coated with corrosive resistance stainless steel and designed sufficiently long, to minimize the conduction loss. The thermocouple energy balance in equation (1) is reduced into convective-radiative energy balance, and solved to obtain the local gas temperature in equation (2).

$$T_g = T_{tc} + \frac{\varepsilon_{tc} \sigma (T_{tc}^4 - T_w^4) d}{k Nu} \quad \dots \text{Equation (2)}$$

The loss from the thermocouple could be related to the values of the thermocouple emissivity, radiation from the surrounding (Furnace Wall), thermocouple diameter and the choice of the correlation used to calculate Nusselt's number. The fine-wire stainless-steel coated thermocouple used here is cylindrical with the diameter of 3mm. The emissivity of the type-K thermocouple was taken from data book, which is 0.9 for stainless steel (Cr-Ni) coating material (Haynes, 2014). The wall temperature of the furnace was 773K, based on the measurement with the thermocouple. For the cylindrical thermocouple with low Nusselt's number application, such as in combustion system, Collis and William's correlation is commonly used and shown in equation 3 (Collis, 1959). The comparison between the true reading from thermocouple and the radiation-corrected temperature was shown in Table 1.

$$Nu_d = 0.24 + 0.56Re_d^{0.45} \quad \dots \text{Equation (3)}$$

3.3. Analytical Device

A thermogravimetric analyser (TGA) series DTG-60H from Shimadzu is used to obtain char kinetic data for modeling investigation in this research. This model series able to simultaneously measures temperature and mass differences between inert reference, Al_2O_3 , and coal sample. The experiments are conducted either in air or CO_2 atmosphere, to obtain the respective char oxidation or char gasification kinetics. On the other hand, inert gas, either N_2 or Argon, is used to calculate coal devolatilisation kinetic. The typical curve obtained from the TGA analysis is shown below in **Figure 3.7** with brown, blue and red-colored line refer to mass-loss, DTG and temperature data over time, respectively. The pronounced decrease in mass loss is comprehended with increasing temperature, indicating reactions take place during coal conversion process. It should also be noted that DTG curve shows two peaks at different temperature, which can be directly correlated to heat released from coal combustion. The TGA experiment is done by loading 5-10mg of sample to the platinum crucible into the sample detector. The oxidizer flow rate is set to 100mL/min while the flowrate of inert gas is fixed at 30mL/min.

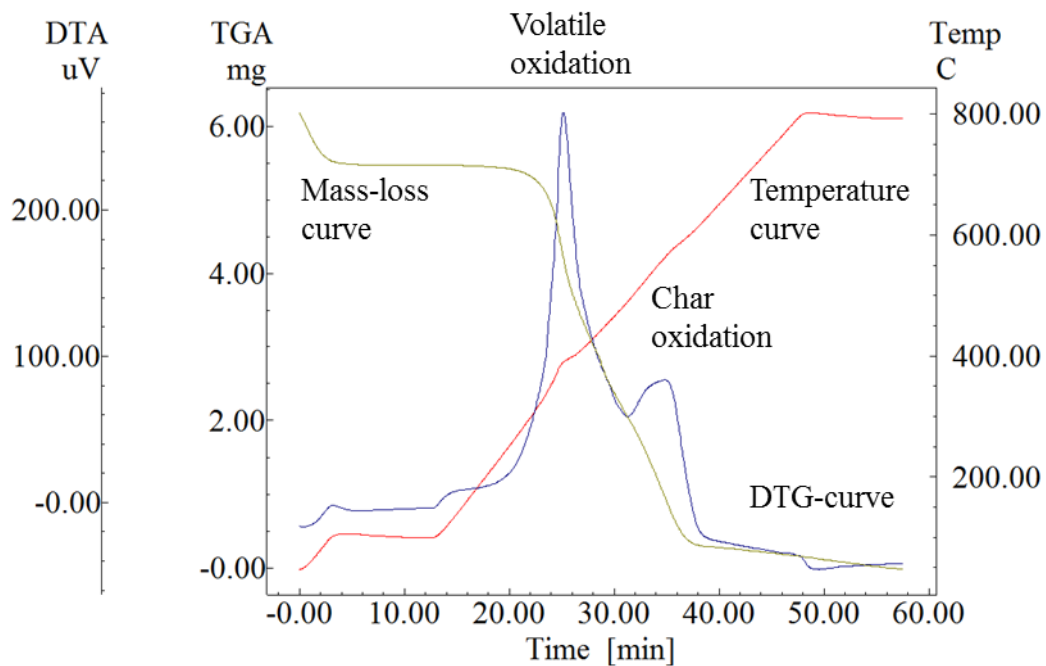
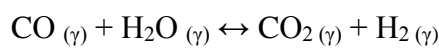
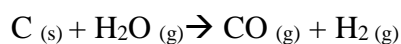


Figure 3-7 Typical curves obtained from TGA experiments in this research

3.4. Modeling approach

The modeling works in this thesis were conducted using MATLAB. The mathematical equation used in the MATLAB model was modified from the existing literature study. In the single particle study for wet brown coal, a 1-D coal combustion model was used to study the combustion behavior of wet coal. The sub-models used in the modeling works are as follows; McIntosh drying model for coal drying prediction, single kinetic rate Arrhenius model for coal devolatilisation, and multiple surface reaction single film model for char oxidation. Three char heterogeneous reactions, including char oxidation, char- CO_2 and char- H_2O gasification, were included for char combustion calculation. Volatile oxidation is insignificant in this model as this study focused on the ignition of dilute particle stream. This modified model has two purposes; to quantify the extent of moisture evaporation during initial coal drying process and to calculate the contribution of moisture to char-steam gasification reaction. Further details on the model are discussed in Chapter 5 and 6.

This thesis concludes with the investigation of the ignition of dense particle stream. Therefore, the above-mentioned model is not applicable under this condition. In this section, the transient cylindrical cloud group combustion model was used to predict the ignition behaviour of clusters of particle. This model was also written in MATLAB. As the conservation equations are typically hyperbolic differential equation, the time step used in the calculation was chosen carefully such that it did not affect the overall computational results. The series of differential equation was later solved using an explicit approach. A small modification was added to the entire model to account for the influence of steam on ignition. This further changes the total mass balance calculation and energy balance calculation in the initial model. Further details were described in Chapter 7 of this thesis. For the investigation of group particle ignition under oxy-fuel steam-enriched condition, the following reactions were added to the model:



Chapter 4

Effect of Clay and Minerals

This page is intentionally left blank

Monash University

Declaration for Thesis Chapter 4

Declaration by candidate

In the case of Chapter 4 the nature and extent of my contribution to the work was the following:

Nature of contribution	Extent of contribution (%)
Experimental, analysis and writing up	90%

The following co-authors contributed to the work. If co-authors are students at Monash University, the extent of their contribution in percentage terms must be stated:

Name	Nature of contribution	Extent of contribution (%) for student co-authors only
Hawra Ali Abdul Abbas	Experimental Works	10%
Lian Zhang		Supervisor

The undersigned hereby certify that the above declaration correctly reflects the nature and extent of the candidate's and co-authors' contributions to this work*.

**Candidate's
Signature**

	Date 22-09-2015
--	----------------------------

**Main
Supervisor's
Signature**

	Date 22-09-2015
--	----------------------------

*Note: Where the responsible author is not the candidate's main supervisor, the main supervisor should consult with the responsible author to agree on the respective contributions of the authors.

This page is intentionally left blank

4. INFLUENCE OF EXTERNAL CLAY AND INHERENT MINERALS ON LIGNITE OPTICAL IGNITION AND VOLATILE FLAME PROPAGATION IN AIR-FIRING AND OXY-FIRING

The influence of external clay additive and inherent minerals on the ignition of a Xinjiang lignite and its volatile flame propagation in air versus oxy-fuel combustion have been clarified in this paper, through the use of a flat-flame burner reactor (FFBR) coupled with *in-situ* optical diagnosis tools. The removal of HCl-soluble metals shifted coal devolatilisation towards higher temperatures in air and 21% O₂ in CO₂. The mixing of external clay with coal affected little on ignition time. It however enhanced the decomposition of volatiles, leading to a larger volatile cloud shielding on particle surface. The oxygen fraction in bulk gas is most influential. Increasing the oxygen fraction to 30% eliminated all the gaps between raw lignite, acid-washed lignite and the mixture of raw lignite and clay. The supporting information for this study has been published and attached in Appendix A.

4.1. Introduction

The ash-forming metals in coal, namely mineral matter, play a two-sided role during coal combustion. On the one hand, they are directly relevant to slagging and fouling that are two most crucial issues that negate the performance and efficiency of a coal-fired boiler (Barnes, 2009). On the other hand, they are capable of catalytically promoting coal oxidation rate, by acting as oxygen-shuttling agent for bulk oxygen activation (Gupta, 1999), or activating the surface stable oxides of coal organic portion during the early-stage of coal combustion (Wan, 2009). The impacts of mineral matter are profound for low-rank coal, such as sub-bituminous coal and lignite, as their ash-forming metals are generally dominated by alkali and alkaline earth metals that are highly catalytic for coal combustion, whilst also influential for severe slagging and fouling in a boiler.

To minimize/eliminate the slagging and fouling propensity of alkali and alkaline earth metals, the low-rank coal can be either prior treated by acid washing to remove the ash-forming metals, or by mixing with solid additive for the purpose of *in-situ* capture of alkali and alkaline earth metals in a boiler. For the former method, the resulting acid-

washed coal could be burnt in direct injection coal engine (DICE) or gas turbine to mitigate its carbon emission footprint on a step-change mode (Wijaya, 2011b). Our previous works have witnessed the simplicity of mobilising ash-forming metals from lignite, under the ambient conditions and using weak acids for an extremely short time (Wijaya, 2011a, Wijaya, 2012). Regarding the latter method for the mixing of additive with coal, it is more practicable for a pulverized-coal fired boiler, where the low-cost refractory minerals such as clay can be injected with coal particles together into the existing mill (Barnes, 2009, Raask, 1985, Vuthaluru, 1996). Prior to the deployment of either method in the industry, it is essential to clarify the changes on the combustion characteristics of lignite upon acid-washing and mixing with clay, as this is primarily important for the stability of an existing boiler.

To date, the literature research for acid-washed lignite was mainly focused on comparing the devolatilisation and burnout rates of raw coal, its acid-washed sample and those impregnated with different metals in thermo-gravimetric analyser (TGA) with extremely low-heating rates, or fixed-bed and fluidised-bed reactors where the volatiles released were quickly swept away from char particle surface by bulk gas (Tomita, 2004). Except the plenty of knowledge generated for coal burnout in the literature, there is still shortage of the essential information regarding the influence of ash-forming metals on particle ignition, flame propagation, tar formation and its *in-situ* oxidation. In a real combustion environment, the volatiles were released at a heating rate in the order of 10^5 K/s (Taniguchi, 2012), and the released volatiles also partly reside on char surface forming a cloud that affects the subsequent char ignition and oxidation steps (Chen, 1995).

The afore-mentioned facilities studies with low heating rates failed to address all of these aspects. Moreover, the addition of clay to coal can affect coal ignition by deactivating alkali and alkaline earth metals and/or catalytically promoting oxygen shuttling. These two roles could counterbalance one another, and hence, exert a complex effect on the ignition of coal particle.

In this study, a lignite rich in alkali and alkaline earth metals, its HCl-washed residue and the mixture of this coal with 3 wt% clay have been tested in a lab-scale FFBR (flat flame burner reactor) for their ignition, flame propagation and volatile cloud oxidation

properties. The FFBR used burns the mixture of hydrogen and ethylene to create a flat flame that can heat up coal particles at a rate of $\sim 10^5$ K/s, similar to that in the industrial boiler. It is coupled with various advanced optical instruments for *in-situ* diagnosis, including a high-resolution camera for flame observation, a high-speed camera for the observation of volatile release, its dynamic oxidation and distinction on particle surface, and particle velocity measurement. The results achieved were compared with and also interpreted by the data collected from TG-DTA (Thermo Gravimetric- Differential Thermal Analyzer). Apart from air-firing, the oxy-fuel combustion test in 21-31 vol% oxygen balanced by CO₂ has also been conducted. The coal sample selected is a lignite sample collected from Xinjiang Autonomous area, the data for which are practically non-existent due to the low exploration degree, although it contributes to approximately 40% of the whole Chinese coal reserves (Li, 2011).

4.2. Experimental

4.2.1. Coal properties

The coal used is Xinjiang lignite with a cut-off size of 105-153 μm , the proximate and ultimate properties of which are listed in **table 4.1**. The as-received coal has a relatively high content of moisture, whereas its ash-forming metals only account for 5 wt% in total. The concentrations of major ash-forming metals in raw coal and its sequential leaching residues are tabulated in **table 4.2**. Ca is the most prevalent metal within the raw coal, followed by Na, Fe, Al and Mg in a descending order. The concentration of Ca shows little change upon water washing. In contrast, it was dropped by nearly half upon ammonia acetate washing, suggestive of the abundance of ion-exchangeable Ca associated with oxygen-containing functional groups such as carboxylic acid in coal matrix. A further washing by HCl reduced the Ca concentration to approximately one tenth of its original quantity, indicating the abundance of oxide/carbonate grains. Another alkaline earth metal Mg shows the similar behavior upon sequential leaching, *i.e.* abundant ion-exchangeable cation and oxide/carbonate grains. In contrast, the two alkali metals behaved differently, of which Na is mainly partitioned between water-soluble and ammonia acetate-soluble fractions, whereas K had no change upon sequential leaching.

Regarding Fe, it was mainly eluted upon water washing, same as that observed for Victorian brown coal (Wijaya, 2011a). This is an indicator of the association of a portion of Fe with water-soluble hydrocarbons such as humic acid within coal matrix, forming an oxyhydroxide-like structure (Cook, 1987, Wijaya, 2011a). The ash-forming metal quantification and coal sequential leaching procedure are detailed in the supporting information (SI), shown in Appendix 1 in this thesis.

Table 4-1 Proximate analysis of Xinjiang lignite tested

<i>Proximate analysis</i>	
Fixed carbon, % <i>db</i>	64.20
Volatile matter, % <i>db</i>	30.77
Ash, % <i>db</i>	5.00
Moisture, % <i>ar</i>	19.10
<i>Ultimate analysis, %<i>db</i></i>	
C	74.5
H	2.90
N	0.42
S	0.37
O*	21.81

*by difference

Table 4-2 Properties of the ash-forming metals in the raw lignite and its sequential leaching residues, unit mg/kg

	Raw coal	Water-washed	AA-washed*	HA-washed [#]
Al	1568	2214	2284	2310
Ca	11294	11230	6393	1343
Fe	1643	703	952	615
K	60	69	59	54
Mg	1498	1677	871	328
Na	2175	796	127	71

*: AA – ammonia acetate (1M); #: HA – hydrochloric acid (HCl, 1 M).

4.2.2. Determination of coal devolatilisation, ignition and char oxidation by TG-DTA

A TGA has been employed to assess the reactivity of raw coal, acid-washed coal and coal mixed with clay samples. Maximum 10 mg of a sample was used for each run. Coal pyrolysis was carried out in argon grade 5.0 at four different heating rates from 10 K/min to 50 K/min. The argon flow rate was maintained at 100 mL/min in each case. Regarding the ignition and char oxidation rate, they were determined by replacing argon with air. The data interpretation procedure to extract the kinetic data (activation energy, E and pre-exponential factor, k) was detailed elsewhere (Harris, 2008).

4.2.3. Coal ignition and in-situ optical diagnosis

The coal combustion experiments and *in-situ* optical diagnosis were carried out in a lab-scale FFBR illustrated in **Figure 4.1**. The reactor was operated at atmospheric pressure and a flat flame Hencken diffusion burner was employed to provide a high temperature gas flow by burning the mixed liquid fuel of hydrogen (H_2) and ethylene (C_2H_4). The gas flow rate was adjusted to provide oxygen concentration of 21-31 vol% with N_2 or CO_2 as the balance, while holding the concentration of water vapor (generated by liquid fuel combustion) constant at 17.51 vol%. For simplification hereafter, the oxy-fuel conditions with the oxygen concentrations of 21%, 26% and 31% O_2 were referred as to oxy-21, oxy-26 and oxy-31, respectively.

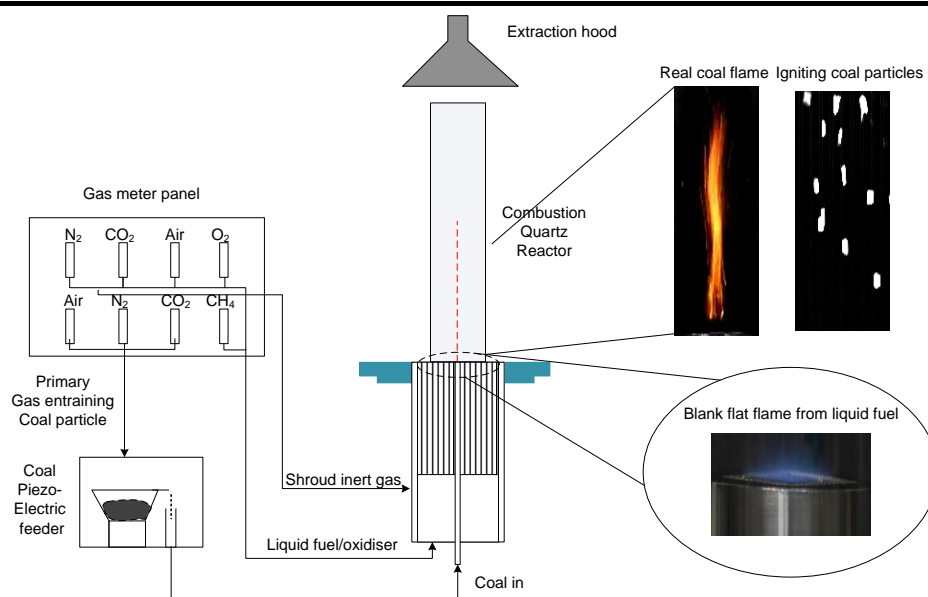


Figure 4-1 Schematics of the flat flame burner reactor used throughout this study

To minimize the turbulence effect of gas and particle mixing, the total gas flow rate was maintained at 11.7 L/min (STD). In all cases, the furnace/flue gas temperature was maintained at 1273 K at the flat flame burner base, see **Figure 4.1**, whilst a mean quartz wall temperature of 773 K was achieved due to heat loss. The pulverized fuel was fed with a piezoelectric feeder at 0.1 g/min and entrained by a carrier gas of 0.7 L/min (STD) into the reactor through the central tube of I.D. 1.5 mm in the Hencken burner. The combustion chamber is isolated with a 115 mm diameter cylindrical quartz tube reactor that is insulated by kaowool with a thickness of approximately 20 mm. A shroud inert gas of 1 L/min, either pure N₂ or CO₂, was injected at the outer ring of the burner to avoid the interference of surrounding air on the stability of flame.

Coal flame images were taken with a Nikon P7000 CCD camera. The images were processed to extract information regarding coal ignition distance, volatile oxidation duration and the duration of char combustion. The luminous, bright and thick flame segment next to coal ignition stage was assigned as a complete oxidation of volatiles, whereas the remaining tail of the flame with a rather weak luminosity was denoted as char combustion (Kim, 2010, Murphy, 2006). The measurement procedure has been detailed in **Section 3.2.1**. A MotionPro Y3 high speed camera from IDT coupled with micro-scale lens was employed to observe individual coal particles, including its velocity,

volatile cloud size and ignition time. The detailed method to calculate particle velocity has been previously described (Zhang, 2010a).

4.3. Results and discussion

4.3.1. Devolatilisation and char oxidation reactivity of coal samples

The lignite studied here possesses a large reactivity of devolatilisation and char oxidation. Its reactivity was summarised in **Table 4.3** and **Figure 4.2**, as the comparison with those published previously. For the devolatilisation rate in **Table 4.3** and **Figure 4.2(a)**, the raw lignite possesses a rate that is lower than the air-dried and ammonium acetate-washed Victorian brown coal, but it is certainly higher than raw Montana lignite, other Chinese lignite, and bituminous coals examined in the literature (Liu, 2004, Zhang, 2013). Upon HCl washing, coal devolatilisation rate was decreased to a level below the observations of Ubhayakar (Ubhayakar, 1977), and close to the bituminous coal results published by Kobayashi *et al* (Kobayashi, 1977). This echoes the loss of ash-forming metals including Ca, Fe, Mg and Na in **Table 4.2**, and supports the catalytic effect of these metals on coal volatile release. The pyrolysis of NaCl-loaded lignite in a fluidised-bed/fixed-bed reactor has witnessed an enhanced yield for the light species including formate, acetate and oxalate (Quyn, 2003). CaO has proven catalytic in cracking oxygen functional groups to carbon monoxide (Franklin, 1982). It was also proven reactive in promoting water-shift reaction for the pyrolysis of sewage sludge at 753 K (Folgueras, 2013). The removal of metals here is thus supposed to affect coal pyrolysis product distribution on an opposite manner, *i.e.* inhibiting the release of light hydrocarbons and deactivating hydrogen shuttling. By the use of TG-DTA for the pyrolysis of lignite and its demineralised samples, it has also been confirmed in the literature (Zou, 2007) that, the total weight loss of the demineralised sample was slightly lower than the raw coal. Such an observation is broadly consistent with our results for the HCl-washed Xinjiang lignite here.

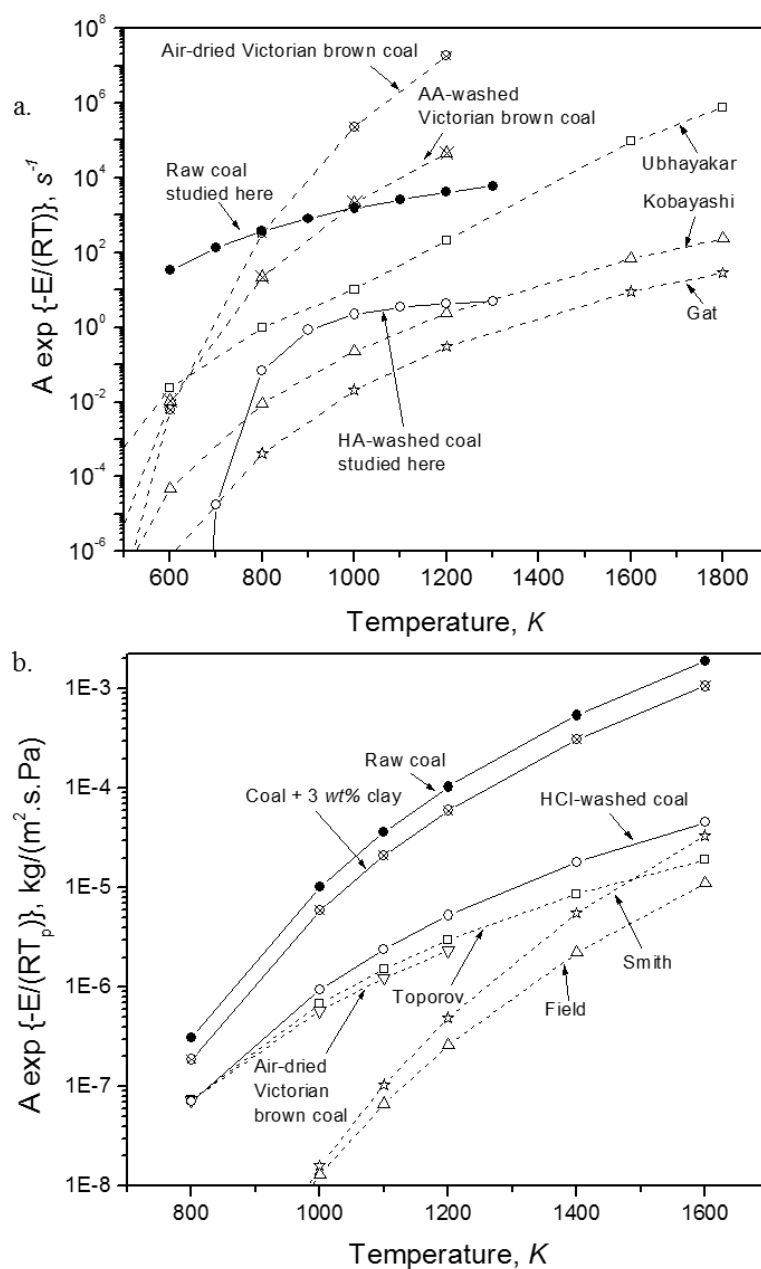


Figure 4-2 Comparison of measured kinetics of lignite and its acid-washed residues here and those reported in literatures (Kobayashi, 1977, Quyn, 2003, Ubhayakar, 1977, Zhang, 2013). Panels (a) and (b) are for devolatilisation and char oxidation, respectively.

Table 4-3 Activation energy (KJ/mol) and pre-factor (s-1) for raw coal, coal with 3 wt% clay and HA-washed coal (Xinjiang Coal as the test sample) and comparison with other coals (Copalakrishman, 1994, Morgan, 1986, Zhang, 2013)

	Activation Energy, KJ/mol	Pre-factor, s ⁻¹
<i>Devolatilisation</i>		
Raw coal	48	5.01E+05
Coal + 3 wt% clay	45	4.8E+05
HA-washed coal	14	6.58E+00
Raw Loy Yang brown coal	217	5.18E+16
Raw Montana lignite	58	8.0E+03
Acid-washed Montana	148	2.0E+08
Demineralised Shenfu sub-bituminous coal	164-227	4.4E+10 – 6.9E+12
Demineralised Huolingele lignite	82-212	1.4E+04 – 1.5E+13
<i>Air oxidation</i>		
Raw coal	116	4.33E+07
Coal+ 3 wt% clay	115	2.30E+07
HA-washed coal	86	1.10E+05
Beulah-Zap raw coal char(27	1.40E+08
Beulah-Zap demineralised coal char	36	3.30E+08

For the raw coal with and without clay, its oxidation reactivity at a given temperature in **Figure 2(b)** is 10-1000 times higher than the literature data. Removing the ash-forming metals by HCl washing dropped coal oxidation reactivity to a similar magnitude of order with bituminous coal. Here again, the ash-forming metals mentioned above are able to catalyse the ignition and oxidation of coal particles. **Figure A.5** in Appendix A further illustrates the DTA curves for the oxidation of raw coal, its ammonia acetate-washed residue, the residue after HCl washing and the mixture of coal with 3 wt% clay. Adding 3 wt% clay affected little on coal oxidation pattern. In contrast, the ammonia acetate washing caused a detectable right shift of the peak referring to coal ignition and maximum mass loss, which was further delayed to 873 K for the HCl-washed sample. Compared to ammonium acetate-soluble cations, the HCl-soluble species referring to discrete oxide mineral grains are clearly influential on char oxidation, which should be highly dispersed within coal matrix and hence possess an intimate with coal organic moieties. In addition, the oxidation of CaO-loaded coal char has confirmed that CaO is able to raise the char oxidation rate by up to 2700 times (Copalakrishnan, 1994).

4.3.2. High-resolution camera observation of flame characteristics in FFBR

The representative flame for the combustion of three coal samples are visualised in **Figure 4.3**. For the raw lignite, its combustion in air exhibits the brightest flame, in which the bottom segment in yellow color represents the initial step for coal drying and devolatilisation. The overall flame luminosity of raw coal was decreased profoundly by the use of oxy-21 in place of air. In the meanwhile the flame length and particularly length of the initial 'yellow' zone were enlarged noticeably, indicating the delay of coal ignition and the lift-up of its flame which is thus unstable in the oxy-21 mode. Increasing oxygen fraction in oxy-26 and oxy-31 brought the flame luminosity and length similar to that in the air case. The discrepancies observed between air and oxy-fuel cases here are broadly consistent with the literature observation (Davidson, 2010, Shaddix, 2003), which are mainly attributed to a larger specific heat capacity of CO₂ than N₂ that causes the delay on coal ignition as well as increases radiative heat flux from coal flame to the surrounding bulk gas.

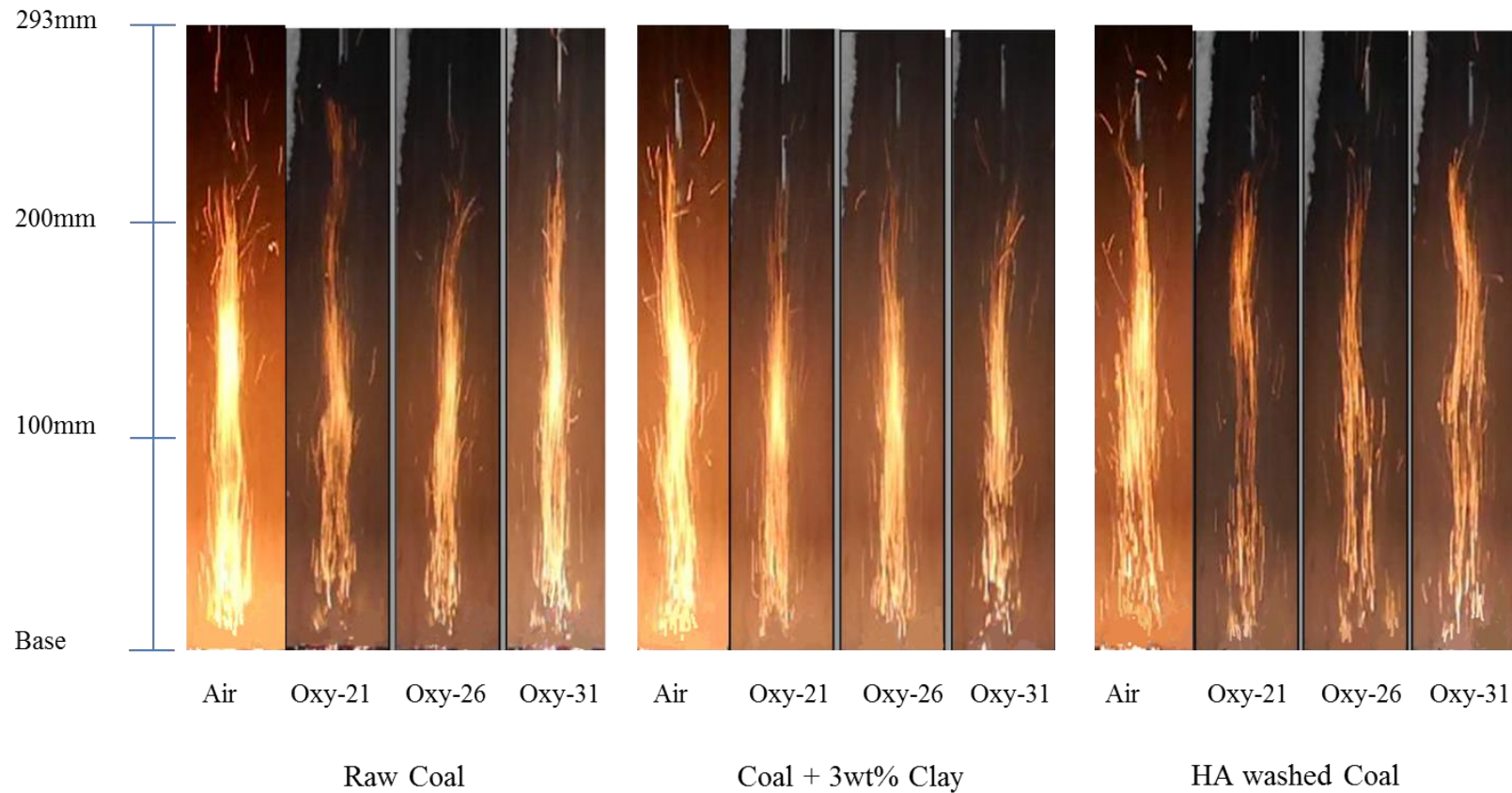


Figure 4-3 Representative flame patterns and flame lengths for raw coal, coal doped with 3 wt% clay and HA-washed coal in air versus oxy-fuel modes

HCl washing reduced coal air-firing flame intensity dramatically. In particular, the initial yellow zone for coal drying and devolatilisation was lifted up remarkably. In addition, the top bright section for char oxidation nearly disappeared, indicative of a significant delay on char particle ignition. In combination with the TGA observations in **Figure 4.2** above, this is clearly attributed to the loss of the HCl-soluble metals, which postpones both coal devolatilisation and char particle ignition. Substituting the oxidating gas to oxy-21 further worsened the HCl-washed coal flame intensity, which even lacks a clear ignition and oxidation stage for the volatiles. Increasing the oxygen fraction up to 31% in CO₂ was even in marginal favor of enhancing flame intensity of the acid-washed coal. The flame achieved in oxy-31 for acid-washed coal lignite is still less luminous than raw coal flame.

The use of clay as a fuel additive caused non-detectable change on coal volatile flame shape and intensity in air. However, for the oxy-21 case, the flame intensity of the top section referring to char oxidation zone was improved remarkably, when compared with the raw coal at the same experimental conditions. Increasing oxygen fraction in CO₂ gradually narrowed the gap between air and oxy-modes in regard to flame intensity. Such information was not detected in TGA, where both clay and coal particles remained still with little interaction. In other words, in a real coal-fired case where particles move rapidly, the influence of clay on coal oxidation is more obvious due to the intimate particle-to-particle interaction.

The coal ignition time was further measured and analysed statistically based on flame pictures, and summarised in **Figure 4.4**. For coal ignition duration in *panel (a)*, the raw coal showed a distance of 15 mm in air, which was enlarged to 20 mm on average in oxy-21, due to the larger specific heat capacity of CO₂ than N₂. A further increase in the oxygen fraction in CO₂ to 26% and 31% reduced raw coal ignition distance to 15 mm, substantiating the achievement of a similar ignition time with the air case. The HCl-washed coal showed a long ignition distance of ~25 mm in air. Its ignition distance was further increased to ~30 mm in oxy-21, and then reduced to a level close to raw coal in oxy-31. Adding clay to coal caused little change on coal ignition distance in air, but slightly reduced it in the oxy-21 case. More interestingly, by comparing the air and oxy-21 cases for coal mixed with 3% clay, one can see that, the difference of coal ignition

distance between these two cases was only 1.5 mm (16 mm in air vs 17.5 mm in oxy-21), compared to ~5 mm for raw coal (from 15 mm to 20 mm) and HCl-washed coal (from 22.5 mm to 27.5 mm). The use of clay clearly partly offset the negative effect of the large specific heat capacity of CO₂ in oxy-fuel cases.

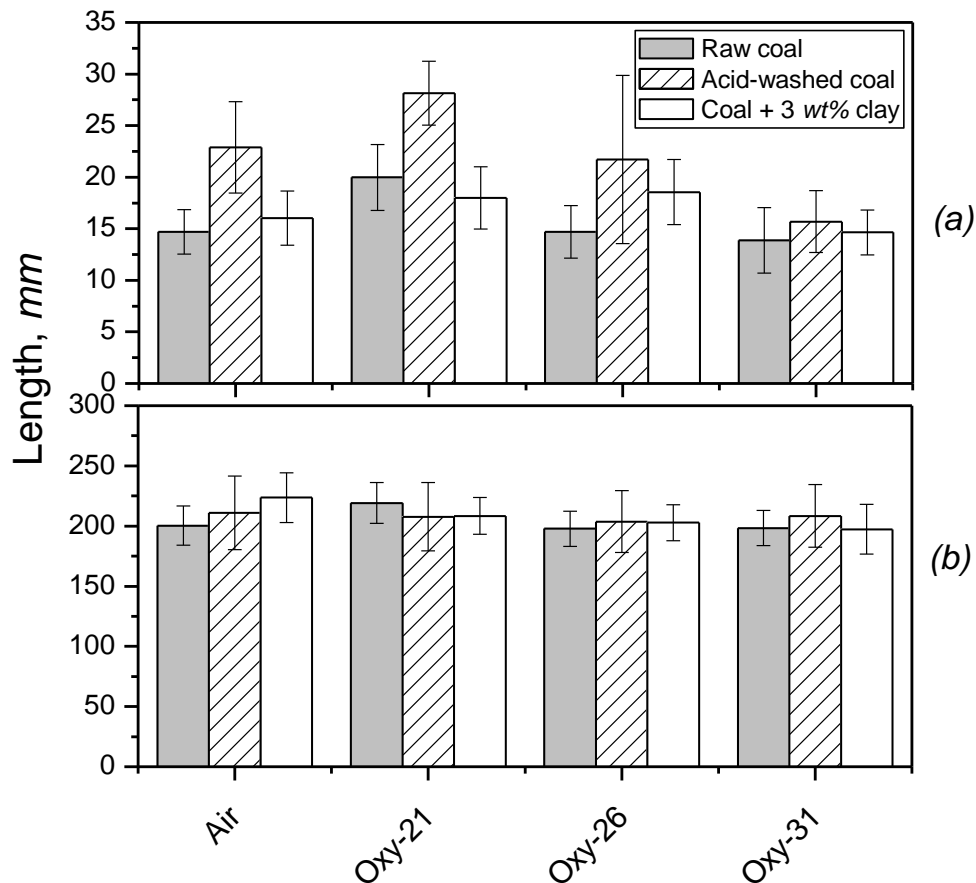


Figure 4-4 The distance for coal ignition (a) and oxidation (b) as a function of bulk gas composition for raw coal, acid-washed coal and coal added with 3 wt% clay

The total duration for the oxidation of coal volatiles and char in *panel (b)* showed less variation on bulk gas composition and the samples fed into the FFBR. This further suggests the primary importance of coal devolatilisation on its total burnout time. For a given bulk gas, the large similarity between raw coal and coal added with clay is expected, echoing the similar reactivity of these two samples confirmed by TGA. Regarding the HCl-washed coal, its oxidation duration is also rather comparable with that of raw coal,

which should be due to the use of excess air for coal oxidation in the FFBR here, as the TGA confirmation indicates a much slower reaction rate for the acid-washed coal.

4.3.3. High-speed camera observation of coal devolatilisation and ignition in FFBR

To clarify the transient phenomena occurring during the initial coal devolatilisation and ignition, the high-speed camera coupled with a micro-lens was further employed for photographing the first 5 cm distance from the FFBR burner base, at a shutter speed of 1000 frames per second and exposure time of 990 μ s for each frame. The typical photographs are visualised in **Figure 4.5**. **Figure 4.6** quantifies the size distribution of the observed bright spots. In each picture, the bright rod-like spots were assigned as igniting particles, the length of which refers to particle trajectory caused by its upward motion, whilst the width equals either the diameter of original coal particle or the diameter of volatile cloud envelope on particle surface. For the raw coal tested in air, the width of its bright spots vary broadly, with some being nearly round for an intense release of volatiles and their preferential residence and ignition on particle surface. The volatiles remaining on char surface are mainly viscous heavy hydrocarbons that are difficult to be swept away by bulk gas (Chen, 1995, Zhang, 2010b). **Figure 4.6(a)** confirmed a mean width of approximately 300 μ m for the volatile cloud formed in air, which is around four times of the original coal diameter. Interestingly, the substitution of oxy-21 for air yielded abundant thinner spots with a mean width of around 200 μ m, see **Figure 4.6(a)**. This is in agreement with **Figure 4.4(a)** for a slower ignition of raw coal in oxy-21, which in turn provided less heat feedback to its host coal particle to ensure a continuous release of the remaining volatiles out of coal matrix. Increasing oxygen fraction in CO₂ was in favor of the ignition of the initially released volatiles, which in turn promoted the release of the extra volatiles to form a larger and brighter igniting spot. However, these improvements are marginal, as the mean width for bright spots in the oxy-31 case is still smaller than the air-case.

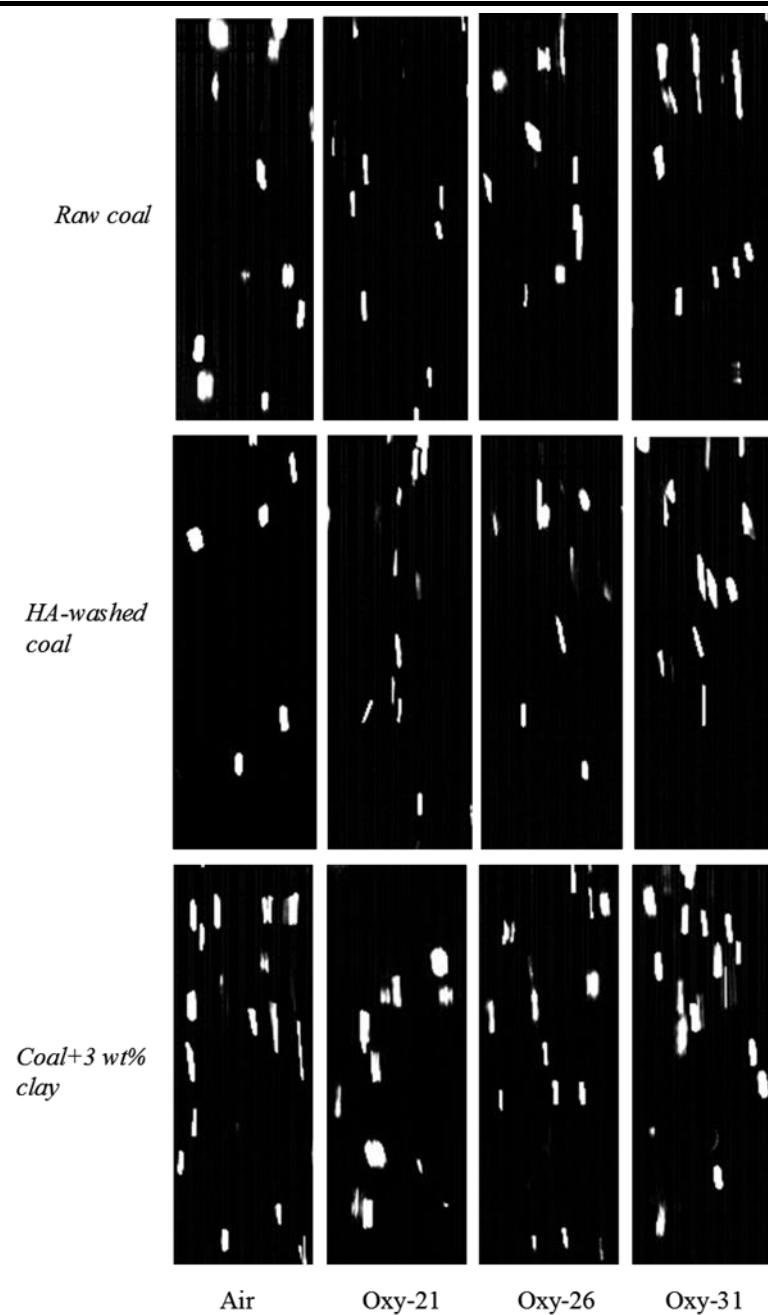


Figure 4-5 High-speed camera observations of the initial igniting particles for three cases at the height of 5 cm from burner base.

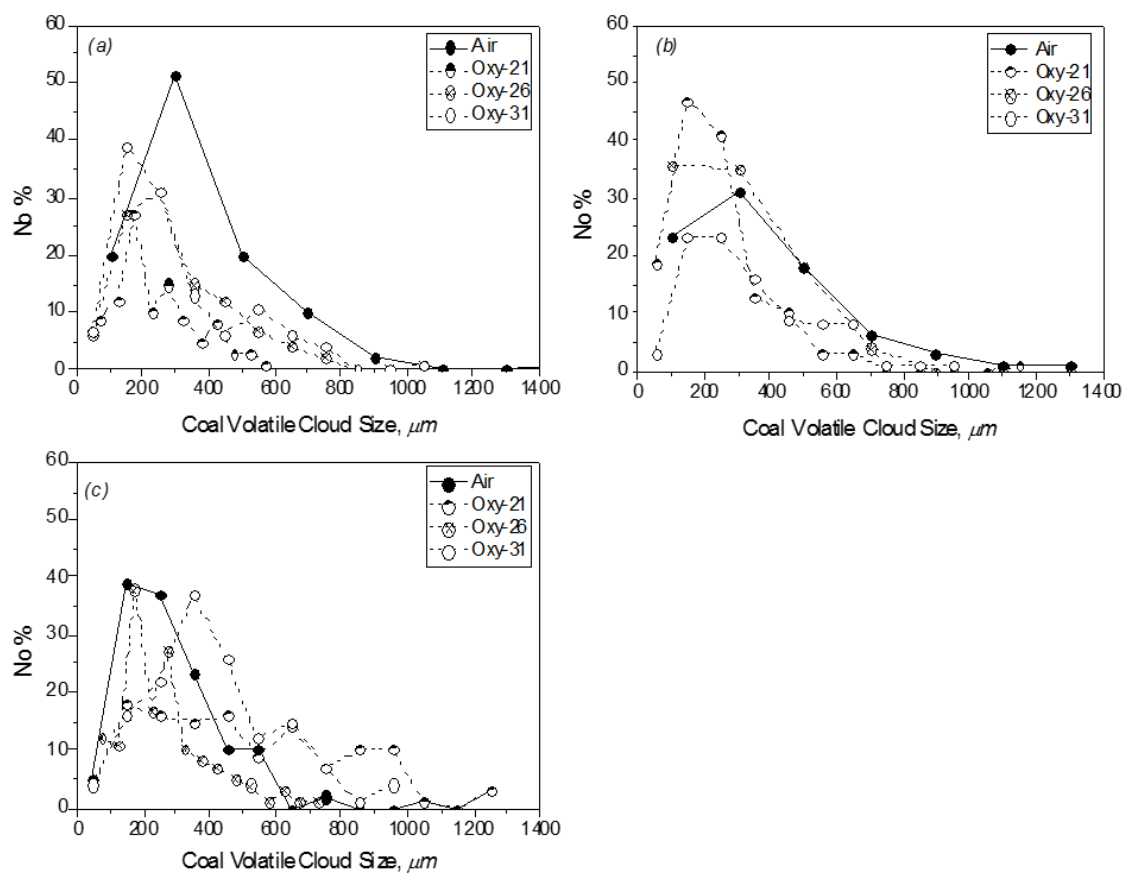


Figure 4-6 Igniting volatile cloud sizes as a function of bulk gas composition for three cases, raw coal (a), HCl-washed coal (b) and coal with 3 wt% clay (c). Measurement was done for the luminous spots observed at a height of 5 cm from burner base.

The acid-washing of coal caused little change on the mean width of bright spot (igniting particle) in the air case, although the igniting particle number density was reduced remarkably. Similar to the results achieved for raw coal, shifting air to oxy-21 for acid-washed coal reduced its igniting spot size dramatically. The mean size was reduced to less than 200 μm that is even close to the original coal size. This indicates that the devolatilisation of acid-washed coal has not been commissioned at the reactor distance of 15 mm. Increasing oxygen fraction in CO_2 to 31% improved coal volatile size to the same value as in the air case. Regarding the mixing of coal with clay, its effect on the change of igniting spot size is most influential. Although the majority of the igniting coal particles reside at the mean size of 200-300 μm in air, they were broadened to a wider range with a comparable fraction larger than 600 μm in the oxy-21 mode. Such an increase is a direct

evidence of the promoted coal devolatilisation by clay. This was not detected in the air case, suggesting a quick ignition of the fragmented light hydrocarbons in air. Increasing oxygen fraction in CO₂ improved the volatile oxidation rate for coal mixed with clay, which in turn decreased volatile cloud size. Its value at oxy-31 is even slightly smaller than the air case.

4.3.4. Burning particle velocity profiles in FFBR

Particle velocity profiles measured by high-speed camera are illustrated in **Figure 4.7**. Regardless of coal sample and bulk gas composition, the coal particle velocity was increased over the reactor path length and maximised at approximately 3.0 m/s at 120 mm, where char oxidation commenced. For the path lengths from 20 mm to 60 mm, the particle velocities variation of both raw coal and HCl-washed coal with bulk gas composition are very narrow and also fall within the error bar caused by the original coal particle size variation. In contrast, the addition of 3 wt% clay to coal broadened the discrepancy of particle velocity between different bulk gases. In particular, the gaps were maximised at 55 mm which corresponds to the top luminous section for the flame observed in **Figure 4.3**. The interference of clay particle velocity should not account for this phenomenon, as it remains invisible in the field of view of the camera where only the luminous particles are detectable.

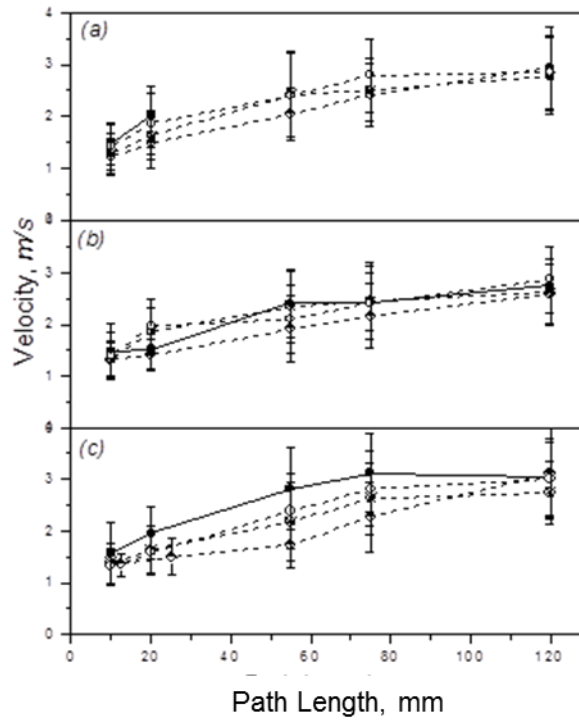


Figure 4-7 Particle velocity profiles in the early stage of coal combustion, as a function of bulk gas composition for three different cases, raw coal (a), HCl-washed coal (b) and coal mixed with 3 wt% clay (c)

4.4. General discussion

Combining the results in **Figures 4.4(a)** and **4.7**, the coal ignition time was deduced and plotted versus bulk gas composition in **Figure 4.8**. The raw coal exhibited an ignition time of approximately 8 ms in air, the magnitude of which is comparable to a high-volatile bituminous coal, Pittsburgh seam coal in a hotter gas of 1700 K (Shaddix, 2009). This further supports the high reactivity of the lignite tested here. Substituting oxy-21 for air postponed the ignition of raw coal to approximately 20 ms, which is more than twice compared to the air case. This echoes the larger specific heat capacity of CO₂ that is around 1.7 times of N₂. Increasing the volumetric specific heat capacity of bulk gas increases the auto-ignition time of a fuel linearly, as suggested by the adiabatic thermal explosion equation (4.1) below.

$$\tau_i = \frac{c_v(T_0/T_a)}{q_c Y_{F,0} A \exp(-T_a/T_0)} \quad (4.1)$$

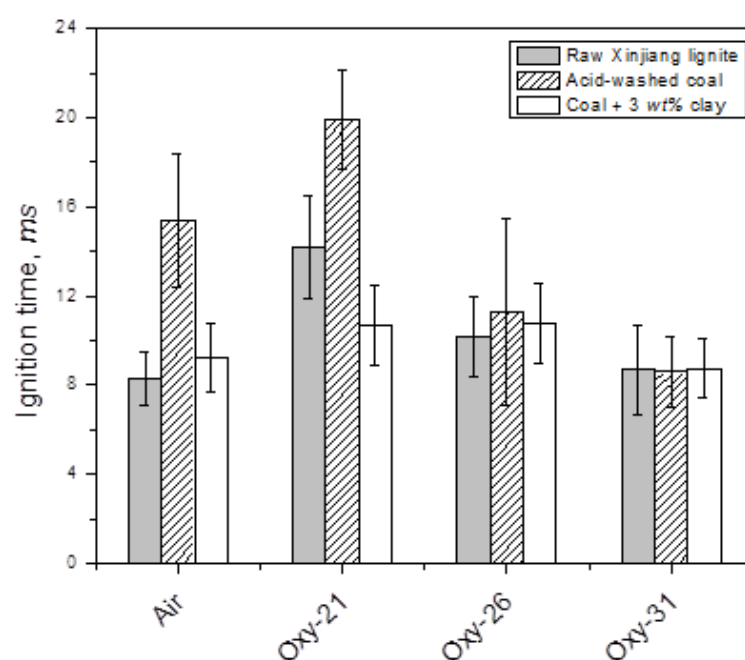


Figure 4-8 Coal ignition time (ms) as a function of bulk gas composition for three different cases, raw coal, acid-washed coal and coal mixed with 3 wt% clay

Increasing the oxygen fraction in CO_2 decreases the volumetric specific heat capacity of the overall bulk gas, but it also increases the reactivity of the fuel/oxidant mixture, $A \cdot \exp(-T_a/T_o)$. As a result, the gaps between three solid samples, raw coal, acid-washed coal and coal mixed with clay disappeared with the oxygen fraction increasing to 26% and above. Moreover, compared to raw coal and its acid-washed sample, the mixture of raw coal with clay showed a rather narrow discrepancy of ignition time between four different gases in **Figure 4.8**. The discrepancy between air and oxy-21 only accounts for approximately 1.5 ms, referring to 9.2 ms in air *versus* 10.7 ms in oxy-21. This can be attributed to the enhanced release of volatiles by the addition of clay to coal, as visualised in **Figures 4.5** and **4.6**. Such an improvement, referring local volatile mass fraction on coal particle, $Y_{F,0}$ in *equation 4.1*, clearly counterbalanced the negative effect of gas volumetric specific heat capacity. Since **Table 4.3** and **Figure 4.2** did not witness the catalytic influence of clay coal devolatilisation in TGA, the clay added here should promote the secondary cracking of the released primary hydrocarbons in coal particle vicinity, leading to the formation of more light moieties that can ignite readily. This is consistent with the literature that has confirmed the effect of clay in promoting the

secondary decomposition of coal tar (El-Rub, 2004). The clay was also proven reactive in promoting the activation of hydrogen transfer to coal and the reactions of de-alkyl and dehydrogenization (Liu, 2004).

Using the averaged volatile cloud sizes calculated based on **Figure 4.6** and equation(4.2)below for the quantification of volatile flame radius, one can determine the quantity of volatiles released on igniting particle surface. The equation (4.2) was derived from the literature (Howard, 1967), as follows:

$$r_s = \frac{d(\Delta V_v / V_0)}{dt} \left(\frac{w \cdot Y_v \cdot f_v \cdot R \cdot T}{3 \cdot D \cdot P \cdot \Delta p_0} \right) r_p^3 \quad (4.2)$$

Here the ignition temperature, T was derived from **Figure A.4** in Appendix A by comparing computational fluid dynamics (CFD) predicted particle temperature profile with the measured ignition distance results in **Figure 4.4(a)**, the ignition time dt in equation (4.2) was taken from **Figure 4.8**, and the symbol f_v was determined by the amount of oxygen needed for combustion of 1 g of heptane (treated as the main volatile species). **Figure 4.9** shows the calculated fractions of volatiles initially ignited on particle surface. Regardless of bulk gas composition, the initially ignited volatile percentage remains rather constantly at approximately 2 % of the total volatiles for the raw coal. The acid-washed coal has similar amount for its initially ignited volatiles in the air and oxy-21 cases, which was increased slightly to 2.5 wt% in oxy-26 and oxy-31. This insignificant increment is supposed to exert little effect on coal ignition, as the elution of the catalytic ash-forming metals decreased the reactivity (pre-factor) by $10^2 - 10^5$ folds. The increase on the volatile fractions by mixing of clay with coal is more pronounced, which was maximised at approximately 3.5 wt% in oxy-21 and gradually dropped to ~2.75 wt% in the oxy-31 case.

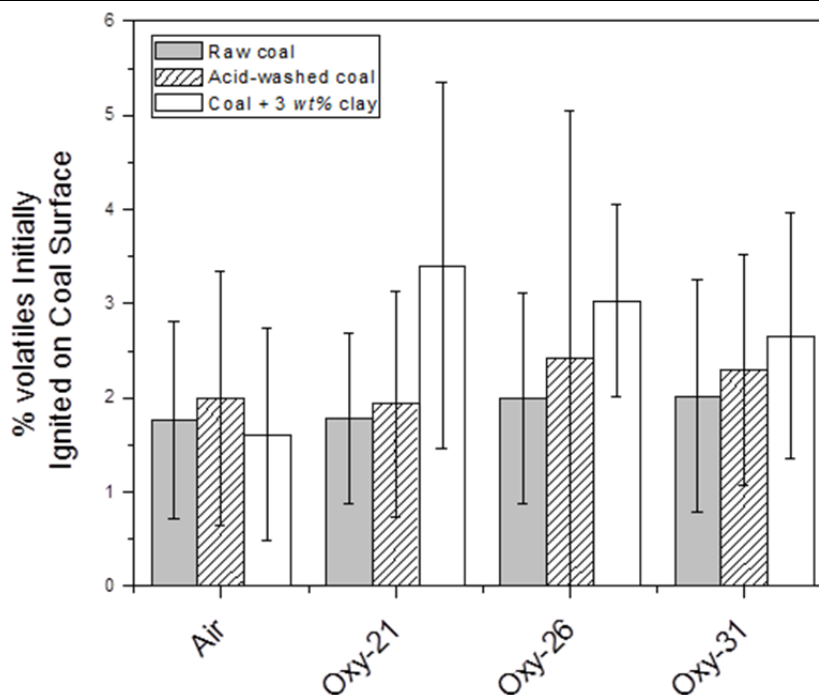


Figure 4-9 Calculated percentage of volatiles ignited initially on coal particle surface at the low temperatures

It remains intriguing to compare **Figure 4.9** with the results for tar formation from lignite pyrolysis in the literature. Although the same coal has not been examined for pyrolysis in the literature, study on a low-ash (~ 1.0 wt%-daf) Victorian brown coal has witnessed a yield of approximately 20 wt%-daf for the tar derived from the pyrolysis of raw coal at 773 K in either CO_2 or He, at a heating rate of 1000 K/s and a hold time of 10 s at the maximum temperature (Jamil, 2004). Loading NaCl or CaCl_2 by impregnation reduced tar yield to ~ 2.5 wt%-daf and 8.0 wt%, respectively, due to the enhanced catalysis of chlorides loaded onto coal (Quyn, 2003). The similar quantity of tar derived from *in-situ* photography of raw coal in this study supported the stronger catalytic effect of the inherent ash-forming metals in this coal. However, in contrast to the observation that the pre-acid washing of Victorian brown coal doubled its tar yield under the pyrolysis (Jamil, 2004), the results in **Figure 4.9** only witnessed a slight increase of tar yield by 0.5 wt% upon acid washing in the oxy-26 and oxy-31 cases. Clearly, the *in-situ* generated tar residing on char particle surfaces is easily cracked/consumed by a quick oxidation in the surrounding oxygen.

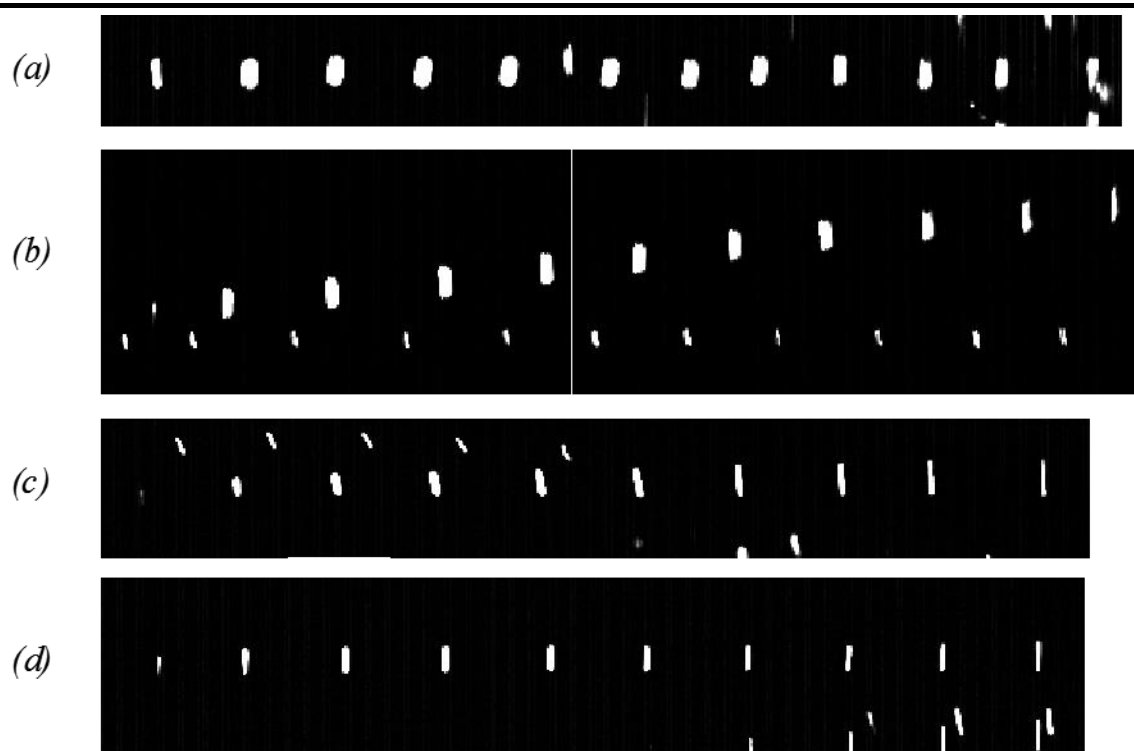


Figure 4-10 *Dynamic oxidation of the liquid volatiles on coal particle surface, at a shutter speed of 500 fps for the interval of 2 ms between two adjacent photographs. Series (a) ~ (d) are for raw coal in air, acid-washed coal in air, raw coal in oxy-21 and acid-washed coal in oxy-21, respectively. Measurements were taken from high speed camera images at 5 cm above the burner base.*

The dynamic release of volatile cloud (*i.e.* heavy hydrocarbons) and its oxidation rate on coal surface, referring to flame propagation velocity, were also traced by high-speed camera on a millisecond (*ms*) scale. The typical sequences are displayed in **Figure 4.10** in which the photographs were taken at an interval of 2 *ms*. For the case of raw coal in air, *sequence a*, the rod-like shape formed at the beginning of photographing refers to the volatiles released with a very thin layer (*i.e.* few amount), which was gradually enlarged to a near-round sphere signaling the enhanced release and accumulation of tarry volatile species on char surface. Subsequently, the volatile release was ceased from the eighth point, whilst it was solely consumed by oxidation on coal particle surface, leading to a gradual shrinking of the size of the igniting spot and the change of its shape back to rod with a thinner width referring to char particle. The duration of this process is the time for homogeneous oxidation of volatile cloud. The acid-washed coal in air (*sequence b*) possesses a relatively longer duration for its volatile cloud oxidation. The use of oxy-21

in place of air for the combustion of coal, either raw coal (*c*) or its acid-washed residue (*d*), increased the duration of this homogeneous process. Quantitative analysis of the volatile oxidation duration (*t*, *ms*) and volatile oxidation rate (*r*, *mg/s*) were statistically carried out by analyzing more than 100 igniting spots for each case, and summarised in **Figure 4.11**. Here, the volatile cloud oxidation rate was derived by

$$r = \frac{V_s w Y_V F_L}{t} \quad (4.3)$$

The F_L for the fraction of liquid tarry volatiles was taken from **Figure 4.9**, and the ignition delay *t* was taken from **Figure 4.8**. For all the cases examined here, the volatile cloud oxidation times fall in a wide range from ~ 17 *ms* to 36 *ms*, which is longer than a maximum duration of 12 *ms* (on average) confirmed by the imaging of Pittsburgh bituminous coal combustion by an ICCD camera (Shaddix, 2009), although the ignition delays of the coal samples tested here are rather comparable with the Pittsburgh coal. For raw coal sample, its volatile cloud oxidation in air lasted for approximately 17 *ms*, relative to ~ 19 *ms*, ~ 18 *ms* and ~ 16 *ms* for oxy-21, oxy-26 and oxy-31, respectively. The changes on it were smaller than the change on the respective ignition time in **Figure 4.4 (a)**. The addition of clay to raw coal affected little on the oxidation duration of volatile cloud except the oxy-21 case where the volatile oxidation duration was slightly reduced compared with raw coal. The acid-washing is more influential, enlarging the volatile cloud oxidation time (compared to raw coal) by around 4 *ms* for the three cases of air, oxy-26 and oxy-31, and even as larger as 14 *ms* in the oxy-21 case. Clearly, the ash-forming metals played a pivotal role in catalysing the oxidation of tarry volatile cloud, via acting as the oxygen-shuttling agent.

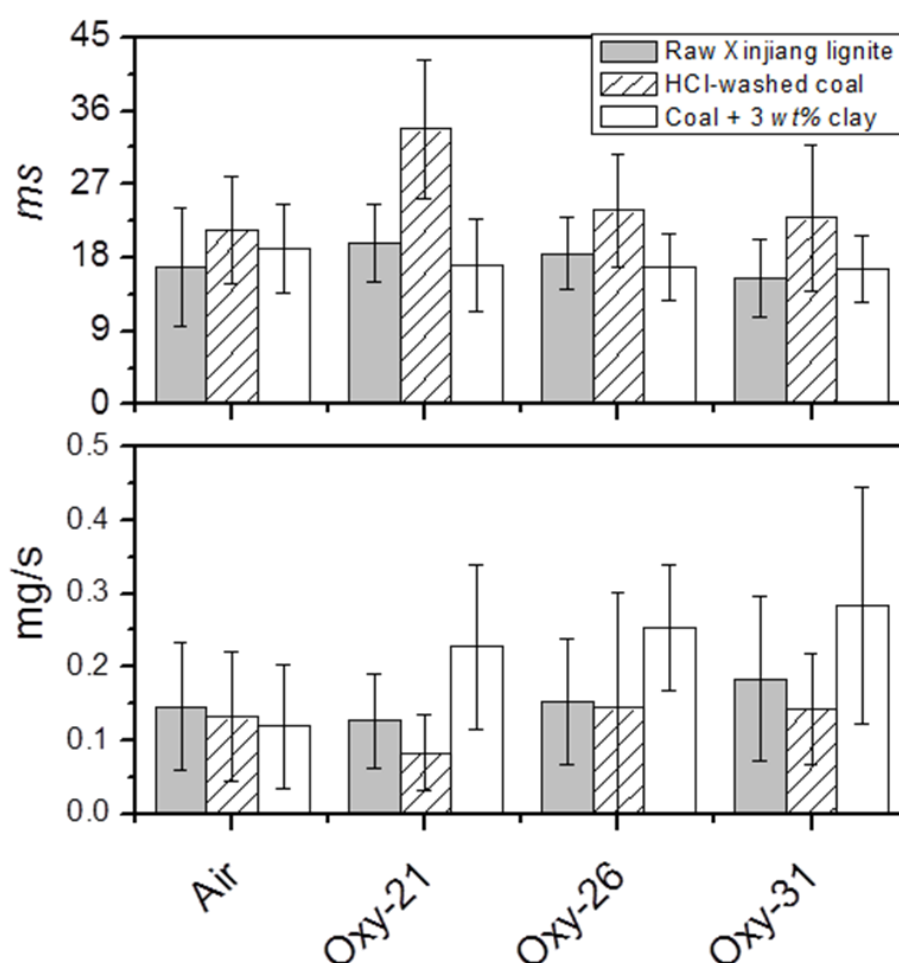


Figure 4-11 Liquid volatile combustion time (ms) on coal particle surface and its combustion rate (mg/s)

The volatile cloud oxidation rate derived from equation 4.3 demonstrates a slow oxidation rate for the volatile cloud on the acid-washed coal surface. Interestingly, the addition of clay promoted volatile cloud oxidation rate, although it affected little on the duration. This is due to the enhanced amount of the volatiles on coal particle surface, as discussed before. The extra tarry species were consumed at a same rate as those derived from raw coal pyrolysis. Same as that has been confirmed by ignition, the clay used should also be insignificant in promoting oxygen shuttling for the oxidation of volatiles. However, upon the mixing of coal with clay, the larger quantity of heat would be produced by volatile oxidation, which in turn increased char particle temperature and its oxidation rate, leading to a brighter top section for the flame observed in **Figure 4.3**. This is supported by the calculation results on the adiabatic particle temperature of volatile cloud (detailed in

Appendix A) in **Figure A.6** in appendix A. For the raw coal and acid-washed coal with an average amount of 2 wt% volatile cloud on its surface, its adiabatic particle temperature in air reaches approximately 1100 K, which is raised to ~1500 K when the clay is mixed with coal. The similar increment was confirmed in the oxy-21 case.

The oxidation rate of volatile cloud and its duration in **Figure 4.10 and 4.11** for raw coal and acid-washed coal can also be fitted by the TGA devolatilisation rate with the parameters in **Table 4.3**. Following a simple first-order reaction model for coal devolatilisation (detailed in Appendix A), **Figure 4.12** reveals the completion of raw coal devolatilisation in 20 ms and 24 ms for air and oxy-21 case, respectively. This is consistent with the corresponding values calculated in *figure 11*. The bottom panel in *figure 12* also indicates a maximum release rate of raw coal volatiles at around 7.5 ms and 11 ms for air and oxy-21, respectively. This is in good agreement with the photographic sequence for the two raw coal cases in *figure 10*. In contrast, the acid-washed coal, released maximum 0.4% of its volatiles in 40 ms in air or oxy-21 cases. Its volatile release/oxidation rate is also far slower than raw coal (see the bottom panel of *figure 12*). Here again, this was caused by loss of the catalytic metals in coal matrix. For the unreleased volatiles within char matrix, their oxidation should occur in parallel with the ignition and oxidation of the remaining char particle.

The oxidation rate measured here for the tarry species derived from lignite pyrolysis falls in the range of 0.1 – 0.3 mg/s, which is comparable to the wood volatile of approximately 0.25 mg/s (Bartle, 2009) in **Table 4.4**. This range is however far different from pure aliphatic liquid fuels and aromatic fuels (Tewarson, 1995) in **Table 4.4**, indicating the complexity for the components in volatile cloud. Moreover, by taking the surface area of volatile cloud (calculated by using its averaged diameter derived from **Figure 4.6**) into account, the volatile cloud oxidation rate can be further deduced to be $5.9 \times 10^{-3} - 1.48 \times 10^{-2} \text{ g/(cm}^2\text{.s)}$, which is significantly higher than the intrinsic reactivity of brown coal char of $10^{-8} - 10^{-4} \text{ g/(cm}^2\text{.s)}$ at 1000-1660 K (Smith, 1982). Clearly, the heat feedback from volatile cloud combustion is essential to promote char particle oxidation. The demineralisation of lignite reduced both the release and oxidation rates of volatile species, which thus mandates the use of an oxygen-enriched environment to ensure an efficient

combustion. The mixing of clay is beneficial in promoting volatile cracking and its oxidation rate under the oxygen-lean oxy-fuel conditions, although the benefit is marginal compared to the removal of inherent ash-forming metals from coal matrix.

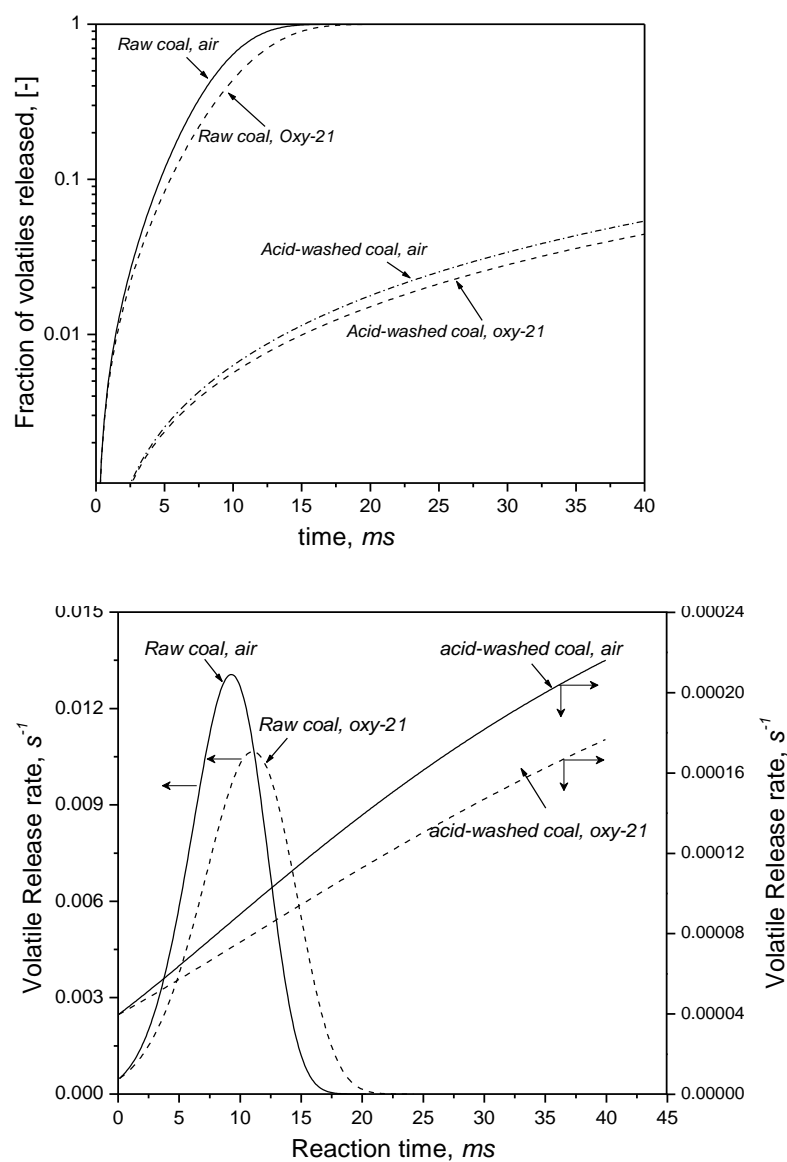


Figure 4-12 Predicted devolatilisation mass loss and rate of the raw coal and acid-washed coal in air and oxy-21 cases. The TGA data in table 3 were used for prediction based on first – order reaction.

Table 4-4 Combustion rate for liquid fuels in the literature (Smith, 1982, Tewarson, 1995)

	kg/(m ² .s)	mg/s
Polyethylene	0.026	0.044
Heavy fuel oil (2.6-23 m)	0.036	0.061
<i>n</i> -Heptane (1.2-10 m)	0.075	0.126
Benzene (0.75-6.0 m)	0.081	0.137
Diesel (2 mm)	-	1.000
<i>n</i> -dodecane (2 mm)	-	1.500
<i>n</i> -heptane (2 mm)	-	1.500
wood volatile	-	0.250

4.5. Conclusions

In this study, intensive experiment and discussion have been conducted on the ignition and flame properties of Xinjiang (China) lignite in air *versus* oxy-fuel combustion, and the influence of inherent ash-forming metals and external clay on its combustion properties. Through the use of a FFBR coupled with advanced optical diagnosis tools, the dynamic release of lignite volatile, formation, ignition and oxidation of volatile cloud, and flame propagation have been explored intensively. The major conclusions as follows have been achieved.

1. At a heating rate of approximately 10⁵ K/s in the FFBR, the ignition of the lignite tested was triggered by the homogeneous ignition of tarry volatile cloud on particle surface. The alkane species are supposed to dominate the first ignited volatile cloud with an auto-ignition temperature of approximately 500 – 600 K and an oxidation rate of 0.1-0.3 mg/s. Its fraction in the total volatile matter accounts for 2.0-3.5 wt%, depending on the existence of inherent ash-forming metals and external clay.
2. The removal of HCl-soluble metals shifted coal devolatilisation towards higher temperatures. The volatiles of acid-washed coal were released slowly. Its ignition time and oxidation duration were increased by nearly twice in air and oxy-21, compared with raw coal. The flame formed was lifted up (thus unstable) from the burner base.
3. The mixing of external clay with coal affected little on coal ignition onset in air and oxy-21, relative to coal alone. It enhanced the decomposition of volatiles, leading to a

larger volatile cloud shielding on coal particle surface that in turn enhanced coal flame, char particle temperature and burnout rate.

4. The oxygen fraction in bulk gas is most influential in coal ignition and oxidation rate. Increasing oxygen fraction to 30% in bulk gas eliminated all the gaps between raw lignite, its acid-washed sample and the mixture of lignite and clay.

4.6. Nomenclature

T	Particle temperature, K
T_{max}	The peak temperature in coal oxidation profile measured by TGA, K
T_0	Initial temperature of coal particle, K
T_a	Igniting coal particle temperature, K
C_v	Volumetric specific heat capacity of bulk gas,
$\Delta V/V_0$	Volatile release rate, [-]
Y_v	Mass fraction of volatiles in air-dried coal, [-]
R	Gas constant, $cm^3 atm/(mol.K)$
P	Gas pressure, atm
V_s	Single coal particle volume, m^3
F_L	Fraction of liquid tarry volatile cloud on particle surface, [-]
$Y_{F,0}$	Initial mass fraction of fuel, [-]
A	pre-factor for fuel ignition reactivity, s^{-1}
q_c	Combustion heat release per mass of fuel, KJ/g
r_s	volatile flame radius, m
f_v	The amount of oxygen needed to burn per gram of volatiles, [-]
r_p	Particle radius, cm
r_{cloud}	Volatile cloud oxidation rate, mg/s
t	time, s
w	Air-dried coal density, g/cm^3
β	Heating rate for particles in TGA, K/min
τ_i	auto-ignition time of a fuel,

This page is intentionally left blank

Chapter 5

Effect of Inherent Moisture on Volatile Ignition

This page is intentionally left blank

Monash University

Declaration for Thesis Chapter 5

Declaration by candidate

In the case of Chapter 5 the nature and extent of my contribution to the work was the following:

Nature of contribution	Extent of contribution (%)
Experimental, analysis and writing up	99%

The following co-authors contributed to the work. If co-authors are students at Monash University, the extent of their contribution in percentage terms must be stated:

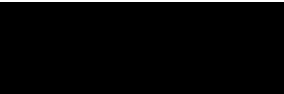
Name	Nature of contribution	Extent of contribution (%) for student co-authors only
Jian Zhang	Analysis	1%
Lian Zhang		Supervisor

The undersigned hereby certify that the above declaration correctly reflects the nature and extent of the candidate's and co-authors' contributions to this work*.

**Candidate's
Signature**

	Date 22-09-2015
--	----------------------------------

**Main
Supervisor's
Signature**

	Date 22-09-2015
---	----------------------------------

*Note: Where the responsible author is not the candidate's main supervisor, the main supervisor should consult with the responsible author to agree on the respective contributions of the authors.

This page is intentionally left blank

5. INFLUENCE OF INHERENT MOISTURE ON VOLATILE IGNITION AND FLAME PROPAGATION OF WET VICTORIAN BROWN COAL IN OXY-FUEL COMBUSTION

In this chapter, the influence of moisture on volatile ignition and flame propagation is investigated in a FFBR. This study for the first time reported the volatile ignition and oxidation for wet Victorian brown coal in both air-firing and oxy-fuel modes. Additionally, mathematical modelling using MATLAB was also performed to quantify the drying extent of brown coal.

5.1. Introduction

As a substitution for high-rank bituminous coal, low-rank coal has been receiving increased attention from the energy and mining sectors worldwide. Burning low-rank coal results in a high CO₂ emission rate compared to that of high-rank coal. In Victoria, Australia, the pulverised coal-fired power stations provide more than 85% of the electricity need in the whole State. Upon the restraint on CO₂ emission, there is an urgent need from the brown coal industry to deploy the next generation low emission technologies such as oxy-fuel combustion (Tomita, 2004). A common feature of brown coal is the presence of abundant inherent moisture within its carbonaceous matrix. An accurate understanding on the fate of brown coal moisture at high temperatures is pivotal for its burner/furnace design.

To date, the coal drying mechanism was simplified as the initial combustion step that was separated from and had little overlap with the following combustion sequences. This is the fundamental for wet coal combustion simulation in the commercial computational fluid dynamics (CFD) program, Fluent (2011, Kurose, 2001). The application of shrinking-core model to study the drying behaviour of Victorian brown coal in hot gas has been developed and verified (McIntosh, 1976a, McIntosh, 1976b). Once being vaporised, the moisture was merely considered as a form of external steam, creating steam-rich environment that is similar to wet flue gas recycle in the oxy-fuel mode (Hetch, 2011, Hu, 2011). In the previous lab-scale drop-tube furnace (DTF) study on wet coal combustion, the reduction on the temperature of burning wet coal particle has been witnessed, which was supposedly due to the contribution of steam gasification reaction

towards the char matrix, as opposed to the steam gasification from the ambient steam (Binner, 2011). In addition, a study on wet coal pyrolysis in drop-tube/fixed-bed furnace revealed the enhanced *in-situ* steam gasification on nascent char surface (Yip K., 2007). Following these observations, there are two types of moisture identified, one is external moisture that is released during the initial drying step and the other is internal moisture that preferentially remains firmly within coal matrix over a longer period of time. The use of a Curio-point pyrolyser further revealed the promoting effect of Sorbed water on the transformation of oxygen and hydrogen atoms into char, gaseous products CO and H₂, and liquid tar, probably via enhanced hydrolysis reactions (Hayashi, 1999). More interestingly, early work on coal-water slurry combustion revealed that, for an American lignite Beulah-water slurry droplet containing 60 wt% coal and in a size of 490-730 μm , its heating upon a Bunsen burner exhibited an initial temperature plateau at $\sim 200^\circ\text{C}$, rather than 100°C for the case of water evaporation from bituminous coal-water slurry (Yao, 1983). This was explained by a simultaneous moving of both water evaporation front and thermal front towards the centre of the droplet, as well as a violent devolatilisation of brown coal even at very low temperatures. The similar phenomenon was observed in another work for the combustion of wet Victorian brown coal (Loy Yang) in a fluidised bed reactor (Jung, 1980). At a hot air temperature of 770°C and an original coal size of 5.6-6.4 mm, approximately 40% of volatiles and 80% moisture (bulk and capillary waters) were released simultaneously in the first 15 s. The released water evaporation is continued, and the monolayer and/or multilayer water constitutes the most strongly held materials that are supposed to remain permanently in char particle. The authors confirmed a nearly constant total burnout time over a wide range of moisture content in coal, and even a faster burnout rate for the char from wet coal than from the nearly dried sample. This was hypothesised due to a greater porosity and/or a greater concentration of active sites of the wet coal char, rather than water-gasification reaction that was considered elsewhere (Matsuoka, 2009). Surprisingly, no research was continued further to prove these interesting but contradictory observations.

In this study, a flat flame burner reactor (FFBR) coupled with transparent quartz reactor and advanced *in-situ* optical diagnosis tools was employed to examine the combustion characteristics of wet Victorian brown coal in both air-firing and oxy-fuel modes. The flat

flame generated from the burning of gaseous fuel provided a rapid heating rate of $\sim 10^5$ C/s that is comparable to that in industrial-scale power plant. Moreover, high-speed camera with a maximum shutter speed of 5000 frames per second (*fps*) was used to track individual particles behaviour upon drying, devolatilisation, volatile cloud ignition and char particle motion (Zhang, 2010a, Binner, 2011, Zhang, 2010b). Apart from air-firing, the oxy-fuel condition was also employed to examine the combined impacts, if any, of CO₂ and steam on brown coal combustion characteristics. In order to further interpret the experimental results, a traditional one-dimensional single-film model with multiple surface reactions was applied and its results were compared with the collected experimental data. A joint effort of both experimental investigation and modelling study is expected to quantitatively clarify the role of moisture on the individual steps underpinning the combustion of brown coal in both air and O₂/CO₂ mixtures. This study has been split into two parts: part 1 for the study on volatile ignition and flame structure, and part 2 for char oxidation temperature profile.

5.2. Experimental facility

5.2.1. Fuel properties

The coal sample used was mined from Loy Yang open-cut seam in the Latrobe Valley, Australia. It is milled to a size fraction of 63-104 μm , similar to that used in the industrial power plant. The proximate and ultimate analysis of the brown coal is tabulated in **table 5.1**. The equilibrium moisture content in the coal is 12 *wt%*, termed as the air-dried coal sample in this paper. The air-dried coal sample was prepared by natural drying of the as-mined wet coal in ambient air and remained unchanged in the laboratory environment. The moisture remained should be attributed to the monolayer/multilayer moisture that binds atomically with the functional groups in coal matrix. For the wet coal samples, they were prepared by mixing the de-mineralised Milli-Q water to the air-dried coal, rather than drying the as-mined wet coal to a certain moisture level. The prepared wet coal samples were placed in a sealed bottle that was thoroughly mixed at the speed of 300 RPM in the rotator overnight. This is to ensure that the added water was fully adsorbed into coal matrix, and the porosity was identical for both the dried and wet coal samples. The current particle feeding system has a limited capability to supply wet coal with the

maximum moisture content of 30 wt%. Therefore, the wet coal samples with two moisture contents, 22 wt% and 30 wt%, were prepared and were identified as semi-dry and wet coal hereafter, respectively. For comparison purpose, the air-dried coal with 12 wt% equilibrated moisture is denoted as dry coal throughout this study.

Table 5-1 Properties of brown coal sample used in this study

Proximate Analysis (wt% dry-basis)	
Moisture content	12.0
Fixed carbon	47.1
Volatile matter	51.1
Ash	1.8
Ultimate Analysis (wt% dry-ash free)	
C	65.7
H	6.8
N	0.6
S	0.5
O (by-difference)	25.8

5.2.2. Non-premixed flat-flame burner reactor (FFBR)

The non-premixed Hencken flat-flame burner provides wide-range of flexibility on the gas temperature and the concentration of the O₂ at the post-flame based on the chosen flow rates of the fuel and oxidizer gases. The schematic of FFBR has been shown in **Figure 4.1** in the previous chapter. In this study, the fuel/oxidiser ratio was adjusted to provide post-flame oxygen concentration of 16-31 vol%, to study the effect of oxygen concentration in oxy fuel on wet coal combustion, whereas the steam concentration remained constant at 17.5 vol%. It is assumed that the concentration profile of the species gas (O₂, CO₂, H₂O and N₂) was uniform at the cross section. The burning of gaseous fuel lasted for at least 30 mins before coal was introduced into the reactor, to ensure a steady state temperature profile along the reactor height. The summary of the experimental conditions is given in **Table 5.2**. The concentration of the species gas in the reactor was calculated based on the stoichiometric reactions of gaseous fuel with oxygen assuming a complete combustion of ethylene/H₂ vapour. The chosen fuel/oxidizer flow rates provides

ambient temperature of 1200 K near the burner base, at the total gas flow rate of 11 slpm, regardless of the oxygen mole fraction. The gas temperature along the reactor height was measured using a type-K thermocouple and corrected for radiation loss (Shaddix, 1999). The calculation procedure to account for the radiation loss from the thermocouple is supplied in the Section A of the supporting documentation. **Figure 5.1** demonstrates a similar gas temperature profile along the reactor height for both O₂/N₂ and O₂/CO₂ mixtures under the blank condition (with no coal flowing). The gas temperature profiles are similar for all cases and therefore, have no effect on the coal ignition and combustion under different experimental cases.

Table 5-2 Summary of the experimental condition in this study

Gas Species	Gas composition (vol%)		
	Air	21% O ₂ /CO ₂	31% O ₂ /CO ₂
O ₂	21.03%	21.57%	31.54%
N ₂	44.04%	0.00%	0.00%
CO ₂	16.44%	59.92%	49.89%
H ₂ O	18.49%	18.50%	18.59%

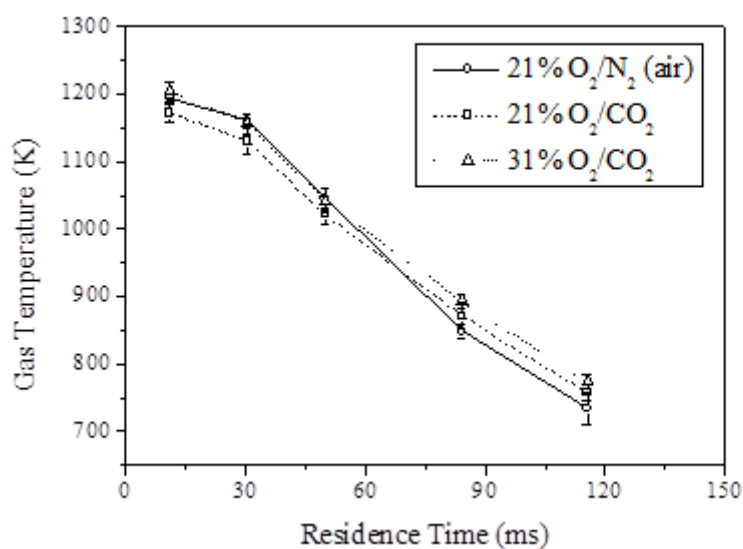


Figure 5-1 Centre-line gas temperature profile in air and 21%O₂/CO₂

5.2.3. Non-intrusive in- situ optical diagnostics facility

A P7000 Nikon CCD digital camera and a Motion Pro Y3 High-speed camera from IDT lens at a shutter speed of 1000 frames/s were employed for coal flame images acquisition. The high speed camera was also fitted with a 25mm micro - lens for high magnification images to capture fast-transient event that happens during the initial heating and combustion stage. The captured images were analysed using an open-source image processing software, Image-J, to obtain information regarding coal flame length, ignition point, burning particle size and particle velocity. The procedure to analyse data from CCD camera has been detailed in **Section 3.2.1**.

The trajectory and transformation of individual particles, including particle velocity, coal ignition point, and volatile cloud size, were tracked with a pre-calibrated high-speed camera. The images were taken at the first 1 cm, 5 cm and 10 cm above the burner base. The particles velocity was calculated by measuring the displacement of same individual particle between two adjacent frames, taking 1ms time interval between frames from the capture speed of 1000 fps. The detailed methods to calculate the particle velocity based on high-speed camera images have been described previously (Zhang, 2010a). The average particle velocity profile of the individual particle along the flame is given in **Figure 5.2**. The average particle velocity in oxy-fuel atmosphere is slightly lower as CO₂ has higher density than N₂. The rapid increase in the initial 5 cm of burner height is due to a rapid heating of individual coal particles that is caused by the mixing of cold carrier gas with surrounding hot gas. The particle speed reaches equilibrium with the surrounding gas as it travels along the reactor height.

The particle ignition point and volatile cloud size were measured from the high speed camera images, using Image-J. Compared with the images from digital camera, the high speed photography images provides more accurate representation of initial coal burning point that defines the particle ignition distance. The ignition point was measured from the burner base to the first point where the igniting bright spots were observed. The ignition time, volatile oxidation and char oxidation time were calculated by dividing measured lengths with the calculated particle velocity at their respective height. Note that, a low

particle feeding rate of $\sim 0.1\text{g/min}$ was used throughout this study to ensure the observation of single particles with minimal interference between one another.

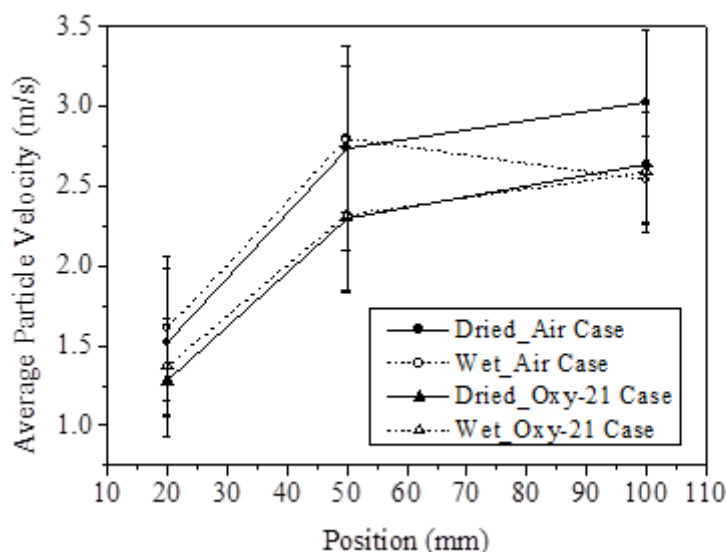


Figure 5-2 Calculated average particle velocity of dried and wet coal

5.3. Mathematical formulation

To interpret the experimentally observed coal particle ignition stage, a forward difference method and pseudo-code algorithm, as visualised in **Figure 5.3**, were employed to solve the sets of differential equations for particle heat-up, drying and devolatilization. The equations for these sub-steps are as follows:

Coal Drying: The receding wet-core dry-shell model from McIntosh (McIntosh, 1976a, McIntosh, 1976b) was used to calculate the coal drying time by equations (1) and (2). These equations below describe drying rate to be constant, which equals to the initial drying rate of non-shrinking water droplet. This expression has been accepted for the pulverized coal $<100\ \mu\text{m}$.

$$MC = MC_0(1 - nt) \quad \dots\text{Equation (1)}$$

Where MC and MC₀ are current moisture content coal and the initial moisture content within coal matrix, respectively, t is the drying time required to achieve current moisture content and n is an empirical constant expressed as:

$$n = \frac{6h(T_g - T_a)}{\frac{H_L \rho_{wc} [MC_0] d_p}{(1 + MC_0)}} \quad \dots \text{Equation (2)}$$

Where h = convective heat transfer coefficient, calculated based on a Nusselt number of 2 for pulverized coal combustion (Murphy, 2006), and the properties of gas mixtures were calculated based on the Wassiljewa's Equation with Maxon-Saxena formulation (Saxena, 1971), T_g = gas temperature, T_a = coal wet bulb temperature, H_L is the latent heat of vaporization, ρ_{wc} is density of wet coal and d is particle diameter. The wet-bulb temperature of hot gas, T_a is a function of ambient gas temperature and is set at 360 K for the hot gas temperature of 1200K in this study.

Coal Devolatilisation: The coal devolatilisation is modelled by a single kinetic rate model that assumes the rate of devolatilisation as first order (Baum, 1971), where the volatile release rate is proportional to the amount of volatile released and expressed as:

$$\frac{dV}{dt} = A_{devol} \exp\left(-\frac{E_{devol}}{RT}\right) [V^* - V] \quad \dots \text{Equation (3)}$$

Where V is the present mass of volatiles remaining and V^* is the initial volatile amount. The kinetic data for Arrhenius form of the equation was determined from thermogravimetric analyser. For Victorian brown coal studied here, the volatiles can be assumed to be composed of light hydrocarbon (Zhang, 2013), which is assumed as CH₄ in this study.

Coal Particle Heat-Up by Energy Balance: During the particle heat up stage, the particle absorbs heat from the hot gas as well as radiation heat from the furnace wall. The particle temperature was estimated using the following energy balance equation:

$$m_p c_p \frac{dT_p}{dt} = hA_p(T_\infty - T_p) + \varepsilon \sigma A_p(T_w^4 - T_p^4) + Q_{reaction} \dots \text{Equation (4)}$$

Where m_p is particle mass (kg), c_p is heat capacity of coal particle (kJ/kgK), h is convective heat transfer coefficient calculated assuming Nusselt number of 2. T_w is wall

temperature (773K), T_g is gas temperature measured with thermocouple, ε is particle emissivity (0.8) and σ is Stefan Boltzmann constant. Q_{reaction} refers to heat loss by vaporization and pyrolysis.

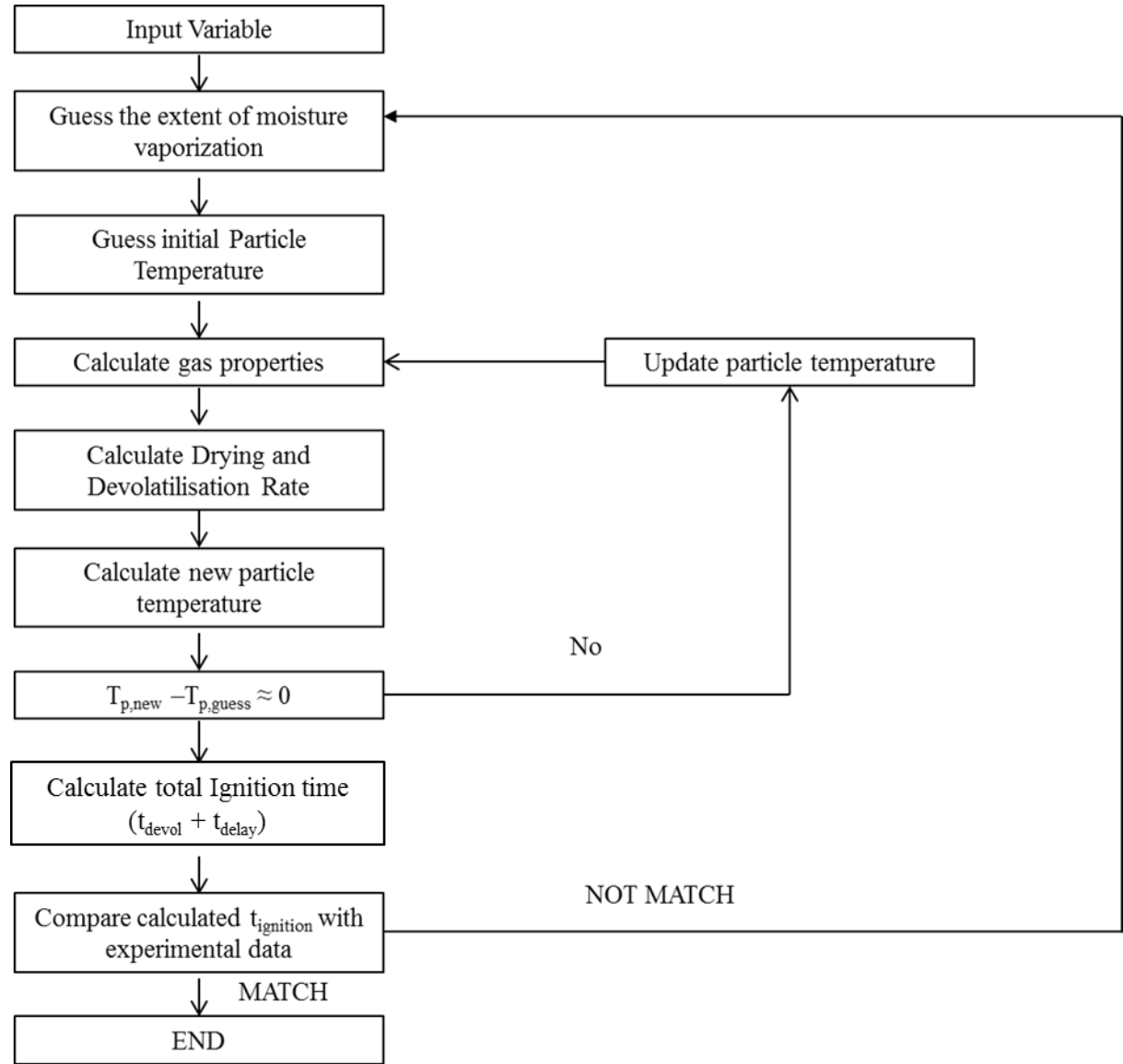


Figure 5-3 Calculation procedures to determine the extent of wet coal moisture evaporation

Regarding the ignition point for coal volatile combustion, it corresponds to the time required for particle to reach the stage where its volatile released has a local concentration equaling its flammability. In a numerical simulation approach, such a time includes the above-mentioned particle heat up, drying, and the release of volatiles. Once released, the volatiles are assumed to ignite instantaneously. **Figure 5.4** depicted the calculated mass

loss profile of the dried coal in air with the variation in its drying extent to demonstrate how the drying could affect the volatile release time, its mass loss derivative and local particle temperature. The mass loss derivative axis, on the right hand side, depicted the first order derivative of the weight loss over time. The turning point that defines the start of the devolatilization was defined from the sharp increase in the derivative graph at the time of ~ 10 ms, signifying the start of weight loss due to devolatilization. This point can be defined as the coal ignition time. The turning points in a mass loss- time plot in **Figure 5-4** at 10.2 ms, 11 ms and 12 ms were defined as the ignition time based on the drying extent of 30%, 65% and 85%, respectively. The particle temperature at the time of volatile release was found to be around 700 K.

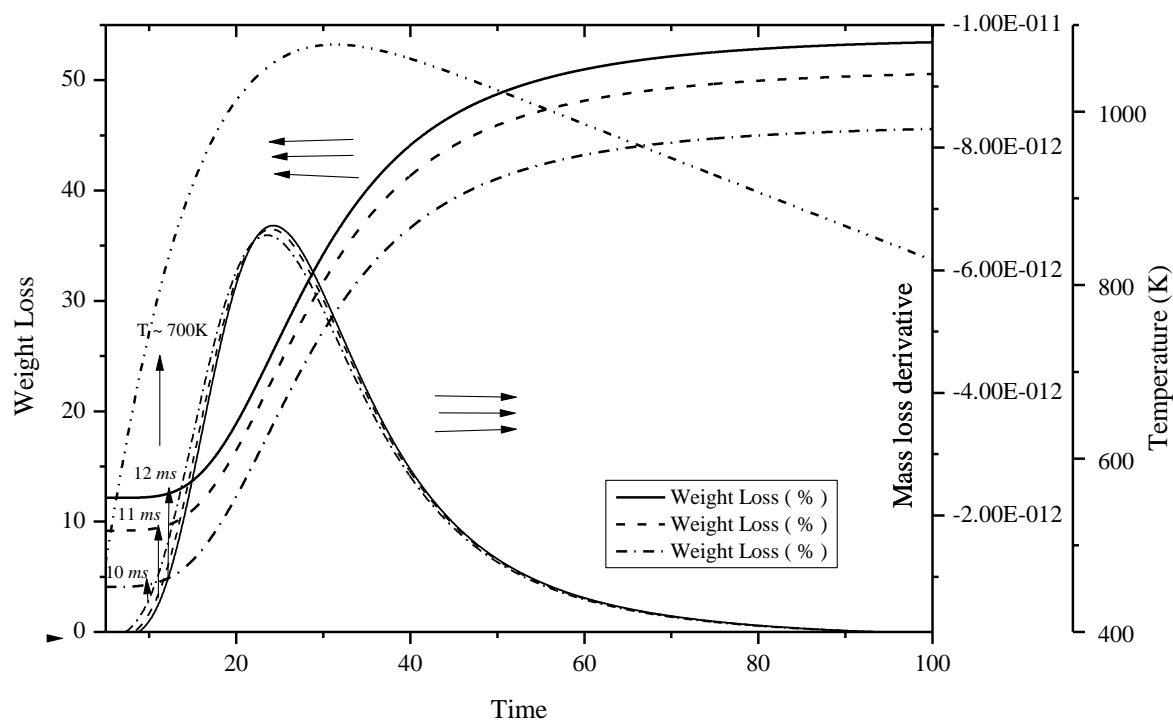


Figure 5-4 Method to determine the brown coal volatile release time with the variation of the drying extent to calculate the coal ignition time.

5.4. Results and discussion

5.4.1. Experimental observation on flame structure and ignition characteristics

The representative images for the combustion of all coal samples in air are visualised in **Figure 5.5(a)**, whereas in *panel (b)* are the axial gas temperatures measured for the three coal samples with different moisture content. As demonstrated in *panel (a)*, the flame from the combustion of dried coal has the highest intensity, whereas the boundary between different stages is vague. This is an indicator of the intense oxidation of dried Victorian brown coal due to its high reactivity, as has been confirmed previously (Zhang, 2010b). This is also in agreement with the precious brown coal ignition modeling studies where homogeneous ignition was found applicable for the fine brown coal particles (≤ 100 μm in diameter) immersed in 1000 K hot gas (Stevenson, 1973). The existence of moisture in coal matrix significantly changed the flame pattern. The semi-dried coal exhibits a clear boundary between its pre-ignition stage and volatile flame front. Such an ignition delay should be attributed to the evaporation of moisture within the coal particle. The flame observed also has a much weaker intensity than that observed for the dried coal. Regarding the wet coal with 30 *wt%* moisture within it, its flame formed is the weakest, and the bright flame for volatile oxidation observed for the other two coal samples was extinguished as well. *Panel (b)* reported the difference between the measured axial gas temperature in air for both blank case and the case with coal fed into the reactor. At the height of 50 *mm* closer to the coal ignition location, the measured gas temperature in the presence of wet coal combustion were ~ 150 K lower than the gas temperature measured in the presence of dried coal combustion. The observation here further strengthened the above observation that the volatile flammability was greatly reduced by the presence of the abundant moisture with the wet coal.

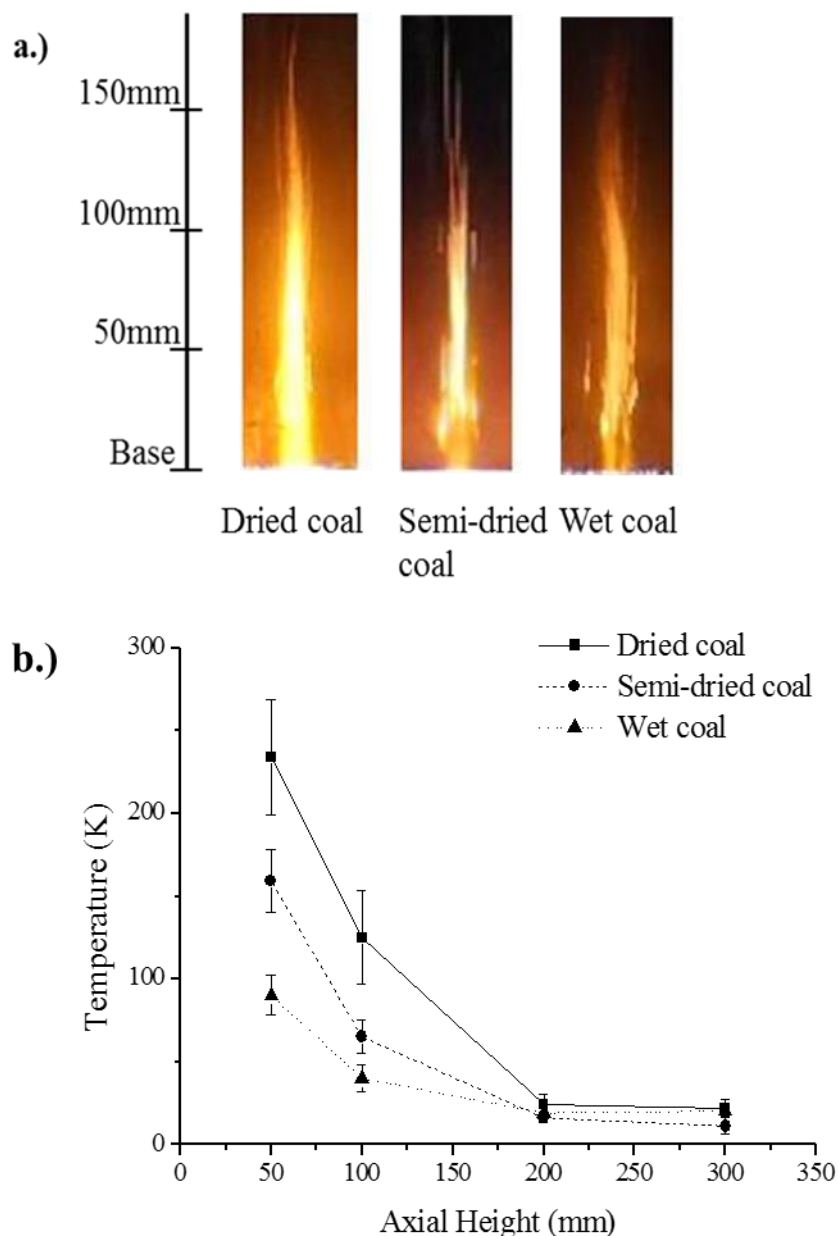


Figure 5-5 Combustion of dried coal, semi-dried coal and wet coal in air (21% O_2/N_2); Panel (a): flame structure; Panel (b): Measured axial gas temperature with coal burning in the reactor with relative to the blank gas temperature

Shifting the combustion atmosphere to oxy-fuel mode resulted in elongated coal flame with remarkable decrease in its intensity, irrespective of moisture content in coal. As demonstrated in **Figure 5.6(a)**, the flame formed for dried coal in 16% O_2 diluted by CO_2 exhibited the longest length, due to the large specific heat capacity of CO_2 (Shaddix, 2009), and a slower diffusion rate of O_2 in CO_2 -rich atmosphere. The combustion intensity was enhanced upon the increase of oxygen concentration in CO_2 . For the oxygen

concentration of 31 vol% in CO₂, the flame luminosity was found to even bear a stronger intensity than in air, which can be due to an enhanced rate for the heterogeneous oxidation of char particles. The similar results were observed for the combustion of semi-dried coal in oxy-fuel mode, whereas its flame intensity in each case is weaker than the dried coal under the same condition. The flame length is also longer than the dried coal, which is another strong indicator of a low combustion rate including ignition for semi-dried coal. For wet coal in panel (c), its particle ignition was unstable and even extinguished in the 16%O₂/CO₂. The flame was detached far from the burner base, substantiating the significant delay by the evaporation of added moisture prior to particle ignition. The flame stability was gradually improved by increasing the oxygen fraction to 31%. Nevertheless, the flame was still unstable and lifted up from the burner, the pattern of which also differs distinctively from both dried and semi-dried coals. **Figure 5.7** illustrated the gas temperature discrepancy between blank case and the combustion of a coal sample under the oxy-firing mode. Here again, the gas temperature was measured at the height of 50mm which is very close to particle ignition point. Similar to the trend reported in **Figure 5.6**, the gas temperature upon the wet coal combustion is the lowest in each oxygen concentration, which is only 20-40 K higher than the blank gas temperature. Apparently, the endothermic evaporation of coal moisture reduced both particle and gas temperatures significantly. Upon the increase of oxygen content in flue gas, the gas temperature discrepancy for dried coal was gradually narrowed down. This is due to an enhanced ignition that resulted in a quicker completion of dried coal particles. On the contrary, the upward trend for another two coals indicates that the increase in the oxidation rate of these two wet coals upon increasing oxygen content is rather marginal.

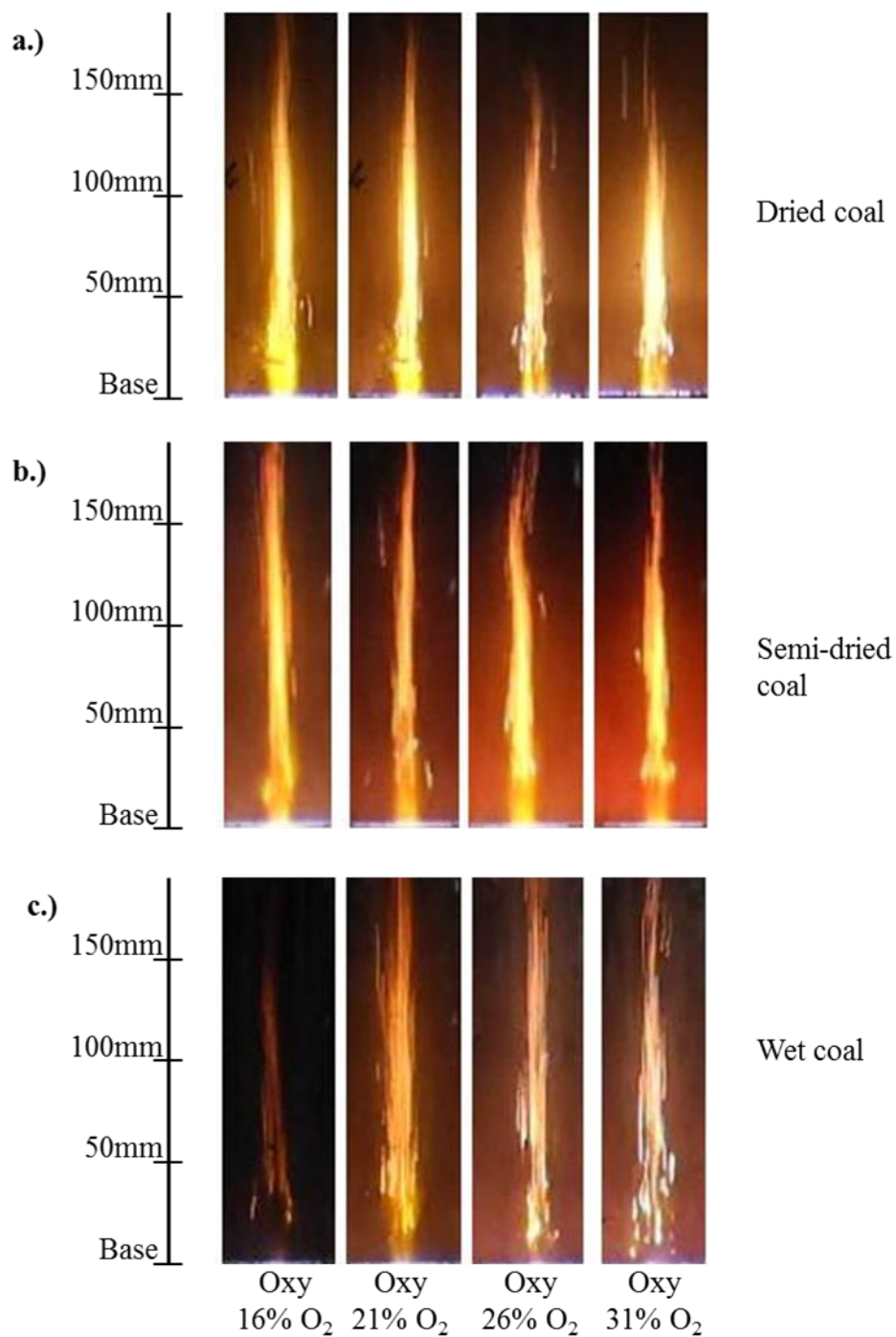


Figure 5-6 Representative images of the flame structure captured with digital camera in oxy-fuel combustion case for (a) dried coal, (b) semi-dried coal, and (c) wet coal

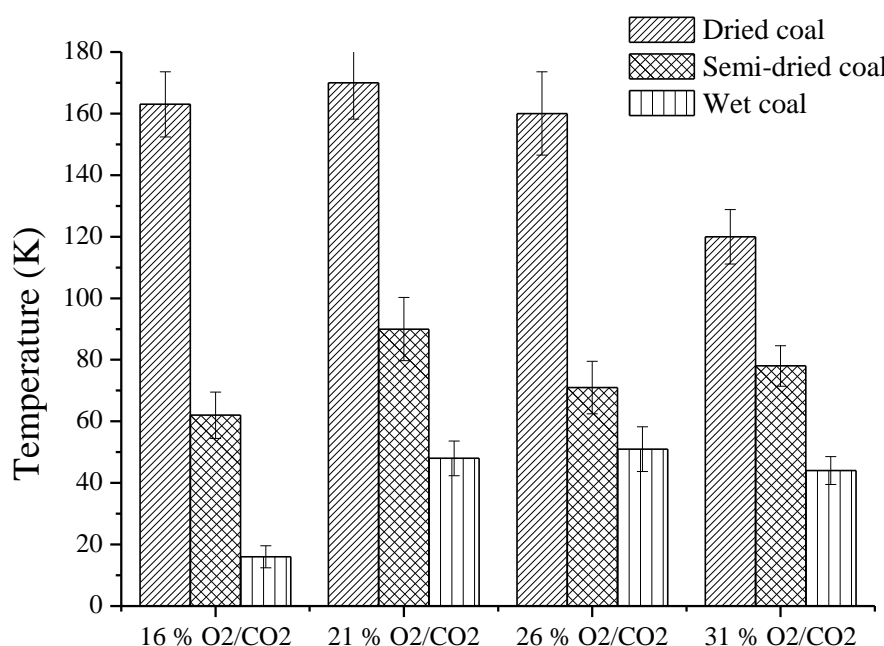


Figure 5-7 Difference between measured axial gas temperature with and without coal burning for dried and wet coal samples in oxy-fuel case

Following the classic theory of coal drying at which the coal drying is defined as the initial stage to be accomplished completely and separately prior to devolatilisation and ignition, the flame formed for wet coal should be identical with the dried coal in terms of flame intensity and shape, with the exception of an initial ignition delay to accommodate a short period for the evaporation of coal moisture. Moreover, the steam generated from the evaporation of coal moisture should be swept rapidly into bulk gas. Its interference to the subsequent volatile and char oxidation is thus negligible, as the maximum amount of steam derived from wet coal moisture evaporation accounts for only 0.03 g/min, based on a coal feeding rate of 0.1g/min of coal. This is equivalent to 0.04 slpm of extra steam contributed to flue gas which constitutes ~2-2.5slpm of steam derived from the gaseous fuel combustion. Therefore, the afore-mentioned phenomena observed in this study cannot be explained by the classic theory based on a consecutive sequence for individual steps. **Figure 5.8** depicts the durations of the three steps from particle ignition to volatile combustion and char oxidation, calculated based on the analysis of flame images obtained from CCD camera. For the ignition duration shown in *panel (a)*, the change is trivial upon the change from dried coal to wet coal in air-firing, which accounts for 2-4 ms. The

substitution of O_2/CO_2 mixtures for air further narrowed down and even diminished the discrepancy in the ignition between the three coal samples, irrespective of oxygen fraction in the bulk gas. This indicates an overweighing effect of CO_2 over the inherent moisture on coal ignition in the oxy-fuel mode. Regarding the duration of volatile combustion in *panel (b)*, although the discrepancy between three coal samples is negligible in air, an enlarged gap upon increasing the moisture content was confirmed for all the oxy-firing cases examined here. That is, the wet coal possessed the longest duration than its two counterparts in any oxygen fraction. The similar phenomenon was confirmed for the char oxidation stage shown in *panel (c)*. Apparently, the steam created from the evaporation of coal moisture partially or even fully resided in the vicinity of burning coal particle, which in turn exerted a remarkable impact on the oxidation duration of both volatiles and char particle.

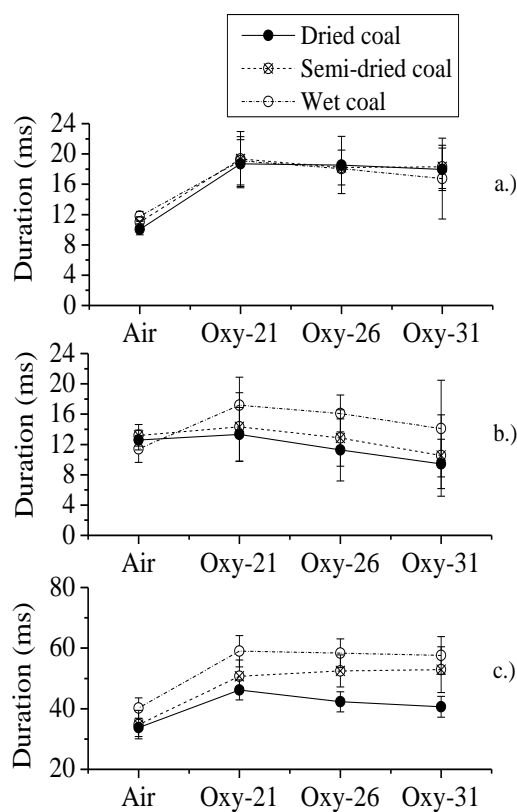


Figure 5-8 Comparison of the combustion time for all coal samples in all combustion cases, (a) ignition time, (b) volatile oxidation time, (c) char oxidation time

5.4.2. Comparison of experimental observations on coal ignition with modelling prediction

Back to **Figure 5.5**, the length of the yellowish segment in a flame refers to the initial flame front for coal volatile ignition, which is made up of moisture evaporation and volatile release. The high-speed camera observation was further conducted to accurately capture the ignition of coal particles (*i.e.*, bright spots in the field of view of a camera) so as to determine the distance and time for coal ignition. Subsequently, the results were compared with the modelling prediction to quantify the fraction of moisture evaporated prior to the ignition of coal particle.

Figure 5.9 demonstrates how the moisture evaporation extent affects the ignition time of a coal sample, according to the numerical approach. Irrespective of the initial moisture content, the ignition time of coal particle increases proportionally with the increase on the evaporation extent of moisture within it. This is due to the drying equations (1) and (2) used, which describes a linear relationship between the moisture evaporation rate and the required drying time. By matching the experimentally measured ignition time and the prediction curve for a coal sample, one can then quantify the moisture evaporation extent consequently. Figure 11 illustrates the matching results for the air-firing case, from which one can reveal the evaporation of approximately 30%, 20% and 10% for the moisture out of the dried coal, semi-dried and wet samples, respectively. These results substantiated an incomplete coal drying prior to particle ignition. In other words, the coal drying step and devolatilisation overlap significantly for the wet brown coal sample studied here. Such a conclusion is not surprising, which broadly agrees with the observations in the combustion of wet brown coal in fluidised bed reactor (Jung, 1980). In addition, the descending trend for the moisture evaporation extent from dried to wet coal indicates the encapsulation of the majority of the inherent moisture in the igniting wet coal particle. This can be explained by a slow motion of the moisture evaporation front towards the core of wet coal particle, due to less heat feedback generated from its igniting surface. Consequently, the unevaporated moisture residing inside coal particle has less opportunity to escape.

The substitution of CO_2 for N_2 to dilute oxygen is supposed to affect little on coal particle drying time, because the molar thermal conductivity of these two gases are identical. In equation 2, the thermal conductivity is the only property of a bulk gas affecting the moisture evaporation. A review paper on pulverized coal combustion (Chen, 2012) has also substantiated this statement. In this sense, the ignition delay upon shifting air to O_2/CO_2 in figure 7(a) is mainly caused by the large specific heat capacity of CO_2 and any other factors that are not related to coal drying step.

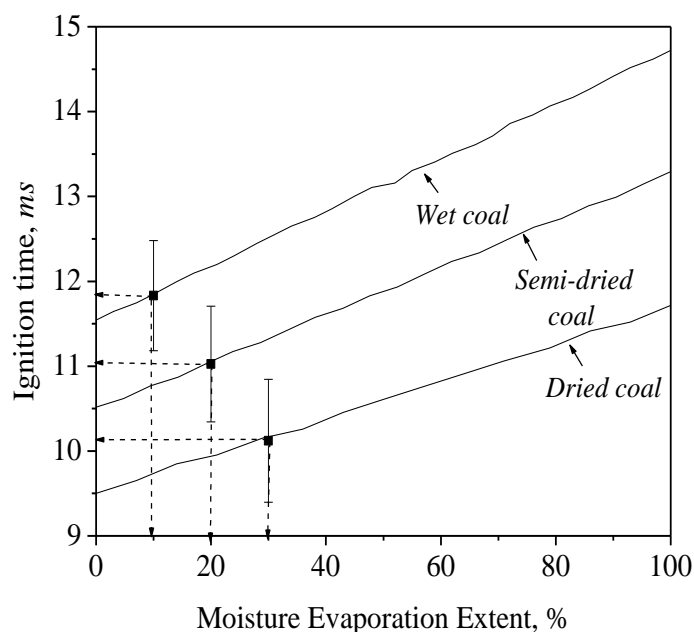


Figure 5-9 Effect of the extent of moisture evaporation on the ignition time of all three brown coal samples in air

Figure 5.10 plotted the measured ignition times for the oxy-fuel combustion of three coal samples, versus the predicted values. The drying time in O_2/CO_2 was fixed as the same as in air in the model. The dashed curve in each panels refer to the parity line for the match between measured and the respective prediction value. The air-firing results were also included as reference. Compared to the air-firing points falling on parity lines, the oxy-fuel results deviate remarkably from the parity lines. For a given O_2/CO_2 ratio, the prediction on wet coal is underestimated the most, whereas increasing the oxygen fraction in CO_2 narrowed down the discrepancy between prediction and the measurement. The ignition of dried and semi-dried coal in 31% O_2/CO_2 was predicted satisfactorily, as

indicated by the insignificant gap between the experimental points and the parity line. In contrast, the gap is still rather large for the wet coal ignition in 31% O_2 . Apparently, apart from the large specific heat capacity of CO_2 that has been incorporated into the model, there are a few of extra factors that negate the wet coal ignition under oxy-fuel mode. The first is the decreased flammability and ignition potential of volatiles on particle surface, due to the alteration of volatile composition and concentration through the dilution of CO_2 and steam. Secondly, the released steam has the potential to push the volatile flame front outwards away from particle surface, which in turn provides less heat feedback for the continuation of particle combustion. Thirdly, the possibility of the endothermic reaction resulting from char-steam gasification reaction on char surface reduces particle temperature. Another probable explanation is the different volatile oxidation mechanism in oxy-fuel mode, as this has already been clarified in the literature (Glarborg, 2008).

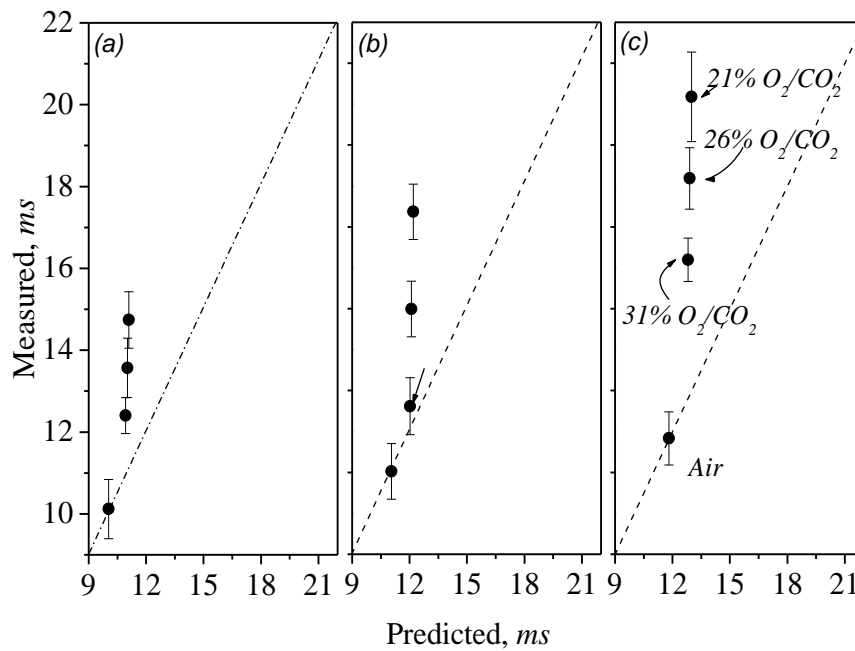


Figure 5-10 Experimental and prediction of ignition time for all combustion cases (a) dried coal, (b) semi-dried coal, (c) wet coal

5.4.3. Influence of moisture on coal volatile combustion

Figure 5.11 illustrates the dynamics of dried coal volatile ignition and the motion of igniting particle in air versus oxy-fuel mode with 21% and 31% O_2 balanced by CO_2 . In

the upper panel for the air case, the dried brown coal particles were confirmed to ignite quickly once passing the flat flame layer, emitting a strong radiative heat from its surface in the field of view of the high-speed camera. The appearance of large bright spots surrounding the igniting particles is a direct sign of the release and formation of volatile flame and its preferential residence at particle vicinity, same as that has been observed for the combustion of the same coal in the drop-tube furnace (Zhang, 2010b, Zhang, 2010a). A portion of the bright spots such as the one cycled in left hand of the dashed line also possess a long trace, which is the sign of a violent release and eruption of volatiles upon the provision of heat feedback from oxidation of the initial volatiles. The released volatiles were oxidised gradually, changing the solid particle from a circular shape at the start of volatile oxidation to a thin rod-like shape with weak radiation intensity, as demonstrated by the last spot falling on the right end of the dashed line. The change in the particle shape was attributed to the change in the particle velocity as well as the release extent of volatiles. The residence of volatiles on particle surface induced the formation of volatile cloud which possesses a circular shape and moves slowly due to the buoyance force, whereas the consumption of volatile cloud resulted in the exposure of solid char particle in the bulk gas, which moves fast in the field of view of the high-speed camera (Zhang, 2010a). Based on this analysis, the volatile oxidation of the traced particle in air was found to be accomplished in 5 *ms*.

With the substitution of air by 21% O₂/CO₂, the igniting coal spots were much thinner and less populated in number density, as shown in the middle panel in **Figure 5.11**. The ignition time for a luminous spot was also longer than 5 *ms*, as suggested by the little change on the shape of traced particle along the dashed line. The reasons for this can be attributed to the larger specific heat capacity of CO₂ than N₂ and the slower oxygen diffusion in CO₂. A slow ignition of the initially released volatiles induced the provision of less heat feedback to coal particle, and further reduced coal devolatilisation rate. By increasing the oxygen fraction from 21% to 31% in CO₂, more spherical spots surrounded by a thick volatile cloud layer were produced, demonstrating the enhancement on particle ignition and volatile oxidation in the oxygen-rich environment. The bottom panel in *figure 7* illustrated this phenomenon. Moreover, compared to the air case, the volatile cloud formed in 31% O₂/CO₂ is rather small. This is an indication that the volatile is consumed rapidly. A simultaneous oxidation of volatiles and char particles has been

reported for the combustion of Victorian brown coal in the oxygen-enriched environment (Shaddix, 2009).

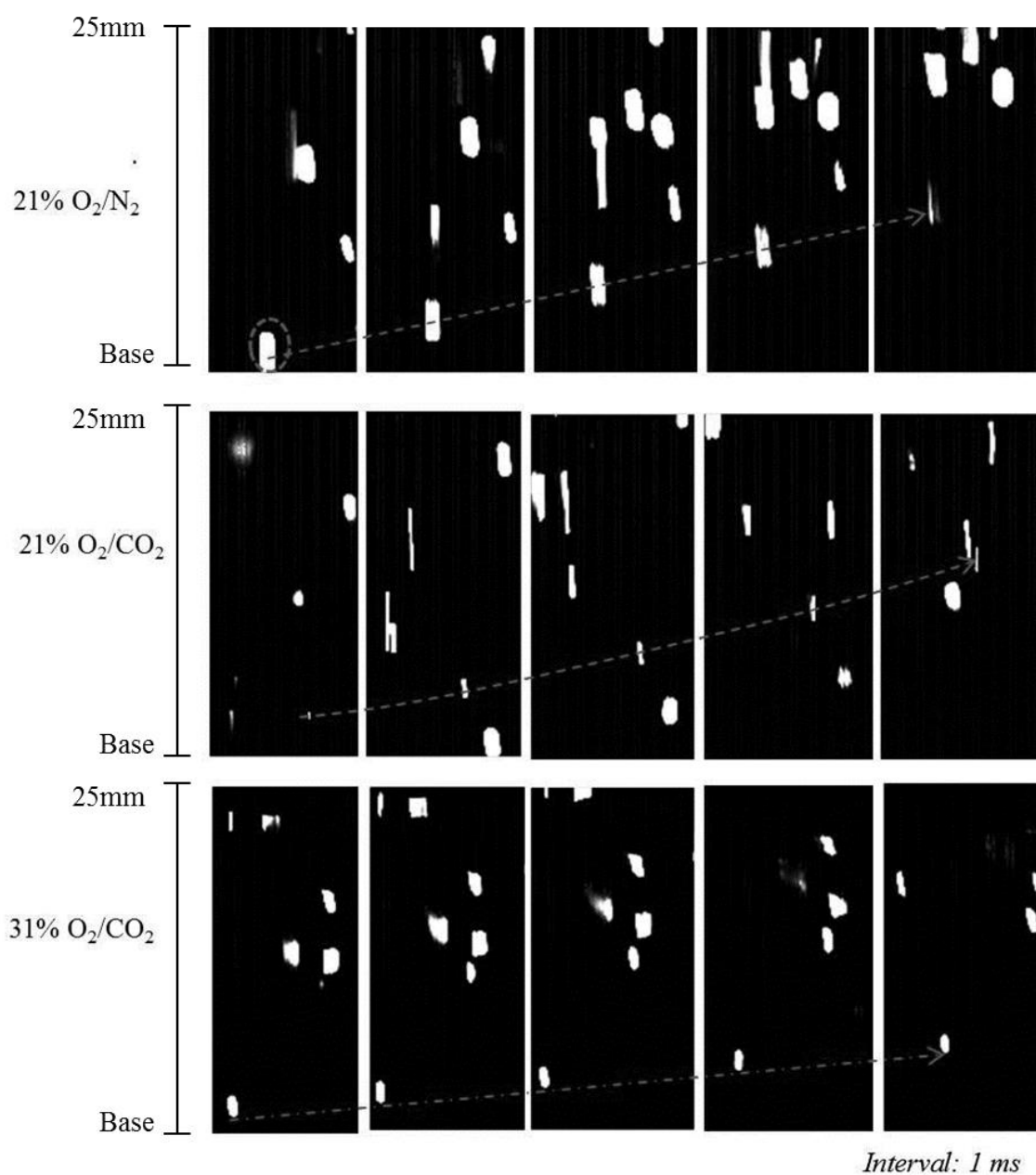


Figure 5-11 Representative images of dried coal captured near the burner base

The progress of wet coal ignition is even more intriguing, which is illustrated in **Figure 5.12**. For the reference air case, the igniting wet coal appears as a large spot with a long trace of volatile cloud compared to the dried coal. Such evidence strongly supports our hypothesis that moisture evaporation and volatile release overlap remarkably in the wet

coal case. It also proves the accuracy of the prediction results in **Figure 5.9**, where the majority of the moisture (~90%) is predicted to remain in wet coal matrix after ignition. The similar phenomenon was observed for the wet coal in 21% O₂/CO₂ shown in **Figure 5.12(b)**. Compared to air-firing case, a slow ignition and oxidation of volatile in 21% O₂/CO₂ induced a slow evaporation of inherent moisture as well. As a result, the majority of igniting particles are present as circular spots in the field of view of the camera, relative to the abundance of rod-like spots for dried coal in **Figure 5.11(b)**. The thick volatile cloud also remained on particle surface for a relatively long duration. Increasing oxygen fraction to 31% in CO₂ intensified the oxidation of volatile cloud, and therefore, enhanced the moisture evaporation rate as well. Consequently, the igniting particles are mostly present as rod-like shape with a larger width than those observed for dried coal in **Figure 5.11(c)**.

The statistical quantification results for the shape distribution of bright spots are further summarized in **Table 5.3**. The circular shape with a circularity range of 0.8-1.0 corresponds to the solid char particles that are enveloped fully in volatile cloud; the semi-circular shape in a range of 0.3-0.8 refers to the slight deviation caused by the volatile jet trace along the moving direction of an igniting particle, whereas the non-circular shape <0.3 corresponds to the rod-like moving char particles with fewer volatiles on the surface, undergoing heterogeneous oxidation on the surface. For the dried coal, shifting the bulk gas from air to 21% O₂/CO₂ increased the number percentage of the semi-circular spots for a long volatile jet on the surface. This reflects the ignition delay and slower volatiles oxidation in CO₂-rich atmosphere. Upon the increase of oxygen fraction to 31% in CO₂, the population of semi-circular spots was decreased whereas that of the circular shape was increased to the level close to the air case, as expected. Compared to the dried coal, the semi-dried and wet coal samples had a noticeable increase in the population of semi-circular spots, particularly under the oxy-fuel mode. This is also reasonable, as the coal volatile ignition and oxidation were delayed considerably under these cases, as visualised in **Figure 5.11** and **Figure 5.12**.

Table 5-3 Particle shape distribution in air, 21%O₂/CO₂ and 31%O₂/CO₂

Shape descriptions (Circularity range)	Air-dried coal			Semi-dried coal			Wet coal		
	Air	Oxy-21	Oxy-31	Air	Oxy-21	Oxy-31	Air	Oxy-21	Oxy-31
Circular (0.8-1.0)	40.54	31.74	37.93	38.80	25.74	25.43	38.85	35.87	34.94
Semi-circular (0.3-0.8)	58.25	65.91	61.92	58.87	70.84	73.69	58.45	63.04	64.75
Non circular (<0.3)	4.21	6.99	1.16	7.83	8.81	4.10	7.36	5.03	2.46

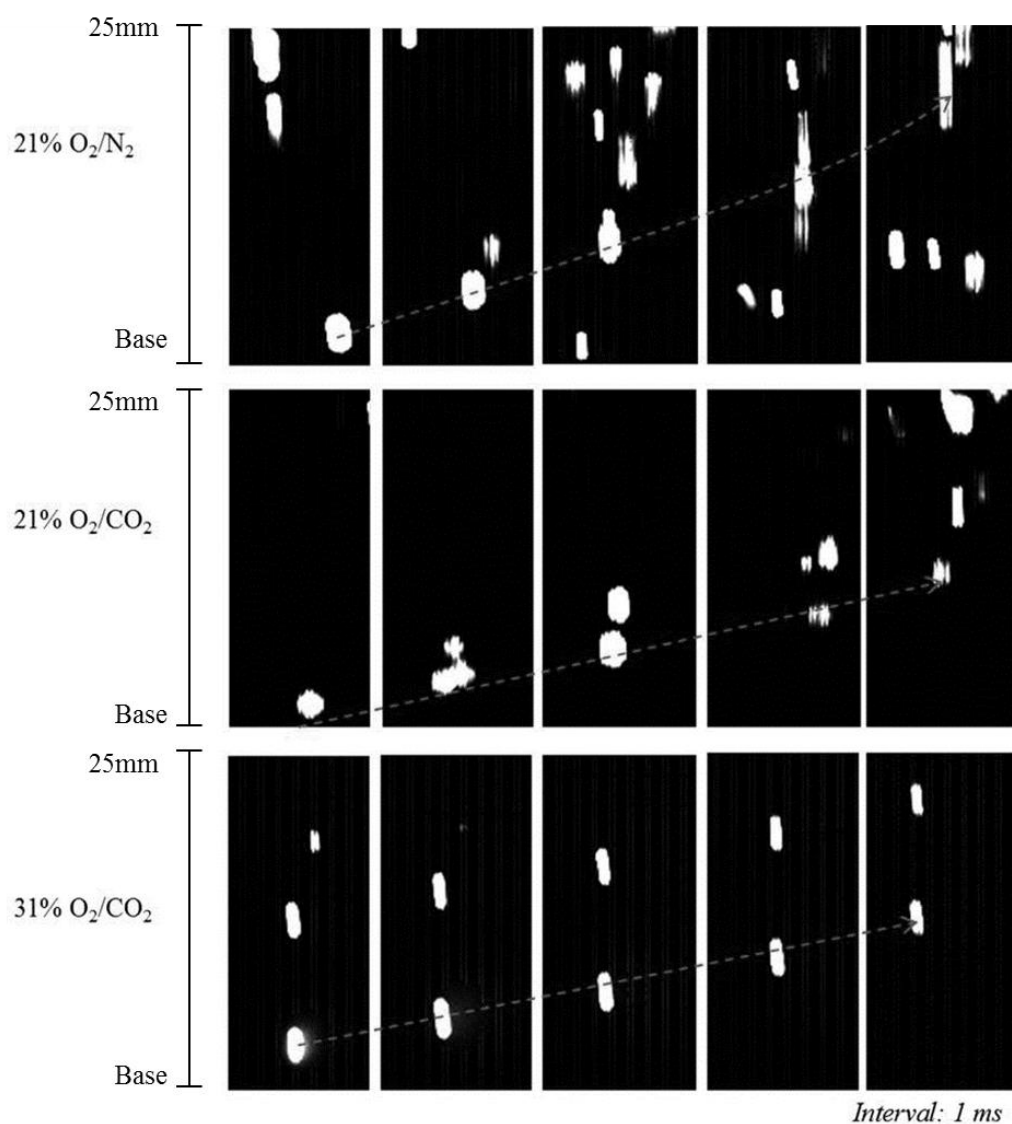


Figure 5-12 Representative images of wet coal captured near the burner base

Figure 5.13 summarized the measured size of volatile cloud and its distribution for all three coal samples in air and oxy-fuel modes. For each given bulk gas environment, one can see the enhanced volatile cloud size of semi-dried and wet coal in place of dried sample. In air, the mean volatile cloud size reached approximately 1400 μm for the dried coal sample, which was twenty times of the original coal size, showing the prevalence of volatiles on particle surface (Khatami, 2012b). This is reasonable as Victorian brown coal has abundant volatiles, which make it very reactive compared to other coals. The use of semi-dried and wet coal sample further increased the mean volatile cloud size to $\sim 1600 \mu m$, which echoes the co-existence of volatile and a portion of steam derived from coal moisture on particle vicinity. The substitution of 21% O_2/CO_2 for air reduced the volatile cloud size for all the three coal samples, reflecting the slow devolatilisation rate in this bulk gas. The interesting phenomenon was observed when increasing the O_2 content to 31% in CO_2 . All three samples exhibited similar cloud size. This is reasonable, as the drying time for 10% moisture only takes approximately 2 *ms* in a hot flue gas with a temperature of $\sim 1000^\circ C$, as confirmed by the drying model used in the literature (McIntosh, 1976a, McIntosh, 1976b). The violent oxidation of volatiles in 31% O_2 should feed a much faster heat back to the core of coal particle for eruption of moisture and volatiles remaining inside.

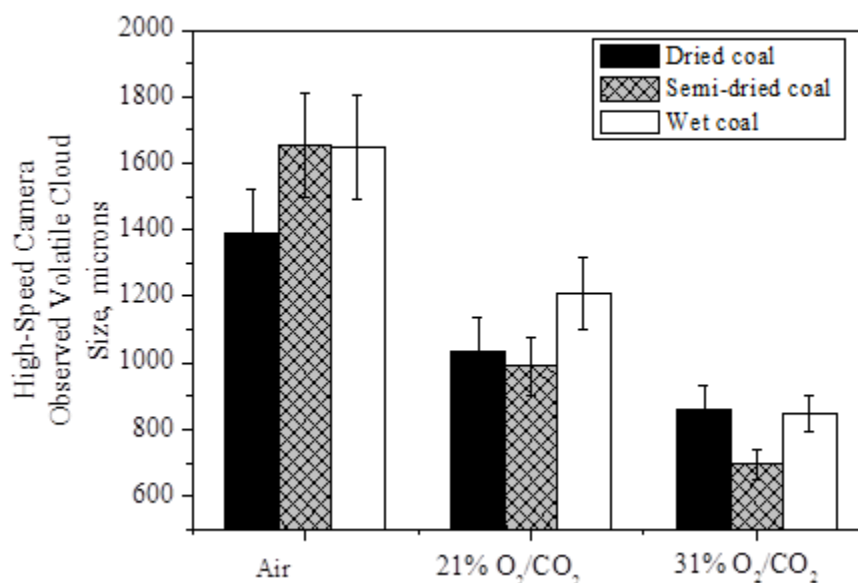


Figure 5-13 Measured volatiles cloud size for all coal samples in the axial centre line of the FFBR for three different bulk gases

5.5. Conclusion

For the first time, this paper has provided *in-situ* observations on the ignition and volatile flame propagation during the combustion of Victorian brown coal in both air-firing and oxy-fuel modes. The brown coal samples with moisture content of 12 - 30 wt% was burnt in a flat flame burner at a heating rate of $\sim 10^5$ K, with 16 – 31 vol% oxygen in the bulk gas. The major conclusions can be drawn as follows:

1. The evaporation of moisture for the drying of Victorian brown coal is incomplete prior to the particle ignition. The drying extent only accounts for 31%, 20% and 10% for the air-dried coal, semi-dry coal and wet coal, respectively. This is mainly due to a quick release and ignition of the volatiles on the dried coal particle surface. The remaining moisture was released with volatiles together, forming a thick cloud layer on particle surface.
2. The co-release of moisture and volatiles affected the composition and flammability of volatile compositions on particle surface. This played a combined role with the large specific heat capacity of CO₂ to significantly postpone the volatile ignition in oxy-fuel mode. For the wet coal with 30% moisture burning in 21% O₂ balanced by CO₂, its ignition delay reached around 10 ms, which is also far larger than the model

prediction due to a changed composition of volatile and mechanisms governing its ignition in CO₂. The percentage of O₂ in bulk gas has an overweighing influence than the negative effect of CO₂ and coal moisture. Increasing its fraction to 31% greatly narrowed the gap of coal volatile ignition time between air-firing and oxy-fuel mode.

3. The volatile cloud size of wet coal particles was significantly larger than the dried sample, due to the co-release of moisture and volatile together. Increasing the oxygen fraction to 31% in either N₂ or CO₂ eliminated the discrepancy of volatile oxidation duration between dry and wet coal samples, due to an intensified heating of coal particles in the oxygen-enriched environment

Chapter 6

Effect of Inherent Moisture on Char Steam Gasification

This page is intentionally left blank

Monash University

Declaration for Thesis Chapter 6

Declaration by candidate

In the case of Chapter 6 the nature and extent of my contribution to the work was the following:

Nature of contribution	Extent of contribution (%)
Experimental, analysis and writing up	99%

The following co-authors contributed to the work. If co-authors are students at Monash University, the extent of their contribution in percentage terms must be stated:

Name	Nature of contribution	Extent of contribution (%) for student co-authors only
Jian Zhang	Analysis	1%
Lian Zhang		Supervisor

The undersigned hereby certify that the above declaration correctly reflects the nature and extent of the candidate's and co-authors' contributions to this work*.

Candidate's Signature		Date 22-09-2015

Main Supervisor's Signature			Date 22-09-2015

*Note: Where the responsible author is not the candidate's main supervisor, the main supervisor should consult with the responsible author to agree on the respective contributions of the authors.

This page is intentionally left blank

6. INFLUENCE OF INHERENT MOISTURE ON CHAR-STEAM GASIFICATION RATE OF VICTORIAN BROWN COAL IN OXY-FUEL COMBUSTION

This chapter is a continuation from wet brown coal study from **Chapter 5**. In this section, the influence of steam on char-steam gasification reaction of brown coal was investigated via experimental and mathematical modelling. The extent of contribution from steam towards char-steam gasification reaction was determined by matching the theoretical calculated temperature with experimentally measured temperature.

6.1. Introduction

Oxy-fuel combustion is a promising low-emission technology that could be implemented in the short term to mitigate the carbon dioxide emitted from the stationary power plants. To date, most of the investigations mainly focused on the combustion on high-rank and bituminous coal (Khatami, 2012b, Molina, 2007, Murphy, 2006, Schiemann, 2009, Shaddix, 2009, Hu, 2011). The usage of Victorian brown coal, which is abundant in moisture (Allardice, 2004), in oxy-fuel mode generates abundant steam in the furnace, due to the recirculation of flue gas. Wall et al has pointed the necessity of the investigation of steam dilution in oxy-firing furnace (Wall, 2009). In the previous lab-scale drop-tube furnace (DTF) study on wet coal combustion, the reduction on the temperature of burning wet coal particle has been witnessed, which was supposed to due to the contribution of steam gasification reaction towards the char matrix as opposed to the steam gasification from the ambience steam (Binner, 2011). In contrast, another study on brown coal (~10%-60% moisture) in fluidised bed showed no change in the char oxidation regime with increasing moisture content, as the moisture has been completely dried prior to volatile release (Jung, 1980). A clear and generalised view on the oxy-firing of Victorian brown coal has not yet been reached.

Numerous approaches on the CFD modelling have also been done in oxy-fuel combustion (Al-Abbas, 2011, Al-Abbas, 2012b). The combustion behaviour has been successfully predicted from using the kinetic-diffusion single film model, but it neglected the effect of CO₂ and steam gasification reaction that may be significant in oxy-fuel atmosphere. Our previous modelling works has successfully utilised the multiple reaction model, including char - O₂, char - CO₂ and char - H₂O to predict the brown coal burning temperature profile in

drop-tube furnace (Zhang, 2013). One-dimensional modeling approach using SKIPPY (Surface Kinetics in Porous Particles) has also successfully clarified the effect of CO₂ and steam gasification reaction on the oxidation of bituminous coal char (Hetch, 2011, Hetch, 2012). These modeling approaches utilised traditional combustion model where coal is assumed to be completely dried prior to ignition and there is no overlapping effect of moisture after drying steps. Clearly, that is not the case for the oxy-firing of wet Victorian brown coal that has been observed in flat flame burner reactor (Pratono, 2015b) and in drop-tube furnace (Binner, 2011).

This paper is the second part of the study on wet Victorian brown coal combustion in flat flame burner reactor that employs a similar heating rate with the industrial boiler (Pratono, 2015b), which focuses to analyse the contribution of both char-CO₂ and char-H₂O gasification to the total char reaction rate based on fitting the measured particle temperature with the calculated value from mathematical modeling approach. Complementing to the first part focusing on the ignition and volatile oxidation, this paper aims to assess whether the inherent moisture affects char oxidation rate and char particle temperature through char-H₂O gasification reaction. As has been clarified in the first part, the inherent moisture is partially evaporated prior to volatile ignition. Consequently, the remaining moisture and volatiles are co-released as a thick could layer on char surface, which is supposed to increase the local steam partial pressure and hence trigger the char - steam gasification reaction. This is different from the previous studies where the external steam in flue gas was merely considered.

6.2. Experimental set-up

6.2.1. High-speed pyrometer for coal particle temperature measurement

The set-up of flat flame burner reactor (FFBR) and coal sample used for coal combustion have been detailed in **chapter 4 and chapter 5**, respectively. For char particle temperature measurement, a Kleiber-GmbH high-speed infrared pyrometer KS-740 LO was installed next to the observation window along the quartz reactor on the FFBR. The pyrometer captured signal at the rate of 5MHz with the linear voltage output of 0-10 V. It has the capability of measuring the surface temperature in the range of 800-2300 °C. The pyrometer operated at

the wavelength between $0.85 \mu\text{m}$ and $1.05\mu\text{m}$ to avoid the interference of the CO_2 and water vapour (Mollman, 2010), which are abundant in oxy-fuel atmosphere. The emissivity of the pyrometer was adjusted to be 0.8, based on suggestion from Baum (Baum, 1971). The data was captured using an oscilloscope and data acquisition instrument. The measurements were taken at the reactor height of 50 mm and 75 mm above the burner base. These two distances chosen refer to char oxidation stage with the first distance 50 mm for the simultaneous volatile and char oxidation and the second distance 75 mm for char oxidation alone.

6.3. Mathematical model

The modelling of single coal particle combustion here was modified based on the previous model described in the literature (Baum, 1971, Zhang, 2013). The code employed only focused on one-dimensional transient calculations. The gas mixture properties, including thermal conductivity, heat capacity, viscosity and density was calculated using the Wilke's Mixture rule and Maxon-Saxena formulation, corresponding to that in the statistical collision theory (Smith, 1980). This has been described in detail in Chapter 5.

6.3.1. Modelling approach

Coal particles undergo rapid heating once being introduced to the furnace. The heat transferred to particle is driven by the convection from hot gas and radiation from the surrounding volatile flame as well as radiation from the furnace wall, which has the potential to increase particle temperature in the magnitude of $\sim 10^5 \text{ K/s}$. The transient model of single spherical coal particle with a diameter d_p , immersed in the hot gas of temperature T_g , was used to simulate its combustion behaviour. The following sub-models were applied in sequence, drying model, devolatilisation model and finally char oxidation model. The former two have been detailed in **Chapter 5**, whereas the last one is detailed below.

Char Oxidation Model: The three heterogeneous char surface reactions, as listed in reaction (I) – (III) were assumed to occur with first-order global Arrhenius rates.





The rate of char burning is described using the multiple surface reactions kinetic - diffusion single - film approach, assuming that the above-listed multiple reactions occur in a frozen boundary layer at the particle surface with no gas - phase reactions. This model has been suggested to work well for the combustion of pulverised coal less than 100 μm in diameter (Mitchell, 1987). For the combustion of particles larger than 100 μm , Mitchell suggested that the conversion of CO to CO₂ in boundary layer could not be neglected (Mitchell, 1991). This has also been postulated by Law, where for droplets less than 100 μm in diameter, the characteristics diffusion time is negligible compared to characteristics chemical kinetic time (Law, 2006). In other words, the droplets less than 100 μm in diameter are too small to support the existence of gaseous flame. Therefore, it is safe to assume that the frozen boundary layer assumption can be used in this numerical study. The char combustion rate can be written as:

$$q = \frac{P_{O_2}}{\frac{1}{k_{c,o}} + \frac{1}{k_{d,o}}} + \frac{P_{CO_2}}{\frac{1}{k_{c,c}} + \frac{1}{k_{d,c}}} + \frac{P_{H_2O}}{\frac{1}{k_{c,s}} + \frac{1}{k_{d,s}}} \quad \dots \text{Equation (6.1)}$$

$$k_c = A \exp\left(-\frac{E}{RT}\right) \quad \dots \text{Equation (6.2)}$$

$$k_d = C_2 \frac{\left(\frac{T_p + T_\infty}{2}\right)^{0.75}}{d_p} \quad \dots \text{Equation (6.3)}$$

$$\frac{\partial d}{\partial t} = -\frac{2q}{\rho} \quad \dots \text{Equation (6.4)}$$

With k_c and k_d are chemical reaction rate coefficient and diffusion reaction rate coefficient, respectively. The chemical reaction rate coefficient is expressed in an Arrhenius form with A being the pre-exponential factor and E as the activation energy for reaction I - III. The kinetic parameters for reaction I - III are obtained from thermo-gravimetric analyser (TGA) measurement. For reaction I and II, the TGA experiments were conducted at different heating rate (10-50 K/min) for devolatilised char at both air and pure CO₂ (grade 5) atmosphere, which have proven accurate in our previous work (Zhang, 2013).

For the char-steam gasification reaction III, it is considered to include two reactions for wet coal combustion, one being induced by the external steam in bulk gas, and another one occurring within char matrix that is triggered by the internal moisture remaining ‘permanently’ after volatile ignition. The kinetic parameters for steam gasification were obtained from a steam - injected TGA at a heating rate of 40 K/min, with steam concentrations of 5%, 10% and 20% balanced by nitrogen. The resulting datasets were analysed using a Coats-Redfern method, shown in Equation 5, by assuming the reaction order of 1 for steam gasification (Coats, 1964).

$$\ln \frac{g(x)}{T^2} = \ln \frac{AR}{\beta E} - \frac{E}{RT} \quad \dots \text{Equation (6.5)}$$

With x is char conversion fraction, T is temperature (K), R is universal gas constant, β is heating rate, with A and E as the kinetic parameter for steam gasification. The variable $g(x)$ is the algebraic expressions of function of the common reaction mechanisms in solid-phase reactions. The assumption of the first order reaction yields the expression for $g(x) = -\ln(1-x)$. The kinetic parameters are calculated by plotting the graph of $\ln \frac{g(x)}{T^2}$ versus $1/T$, as shown in **Figure 6.1**. The rate constant of $3.6 \times 10^6 s^{-1}$ and activation energy of $206 kJ/mol$ were chosen for the Victorian brown coal studied here, as the steam concentration of 20% was comparable to the gas environment in the FFBR used here. The steam gasification kinetic rate used in this study is also comparable with other kinetics data of lignite steam gasification used in the literature and far more reactive compared to bituminous coal (Otto, 1979, Sandars, 1984, Ye, 1998), shown in **Figure 6.2**. In general, the steam gasification reaction turns significant with the reaction temperature exceeding 1000 K. The rate of carbon consumption from the gasification reactions was varied and its contribution to gasification was determined relative to the total carbon consumption rate from reaction 1 to 3.

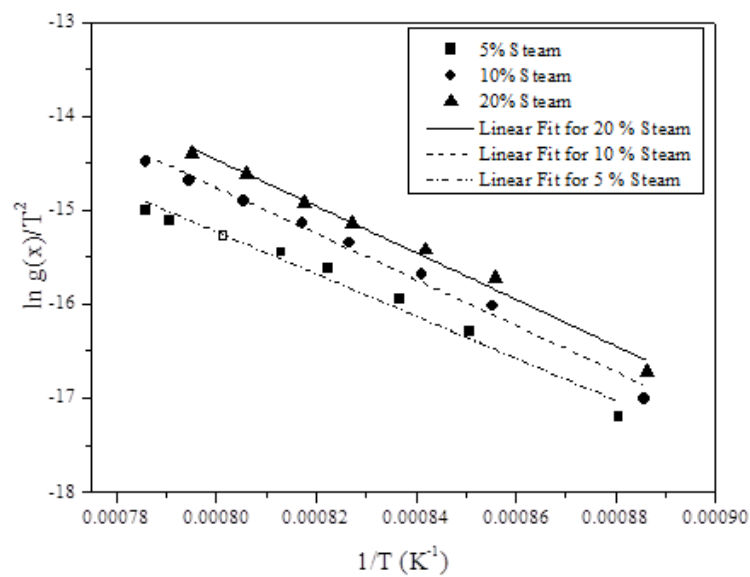


Figure 6-1 Linear plot of Coats-Redfern method for Loy Yang coal to determine the kinetic parameters for its char-steam gasification rate

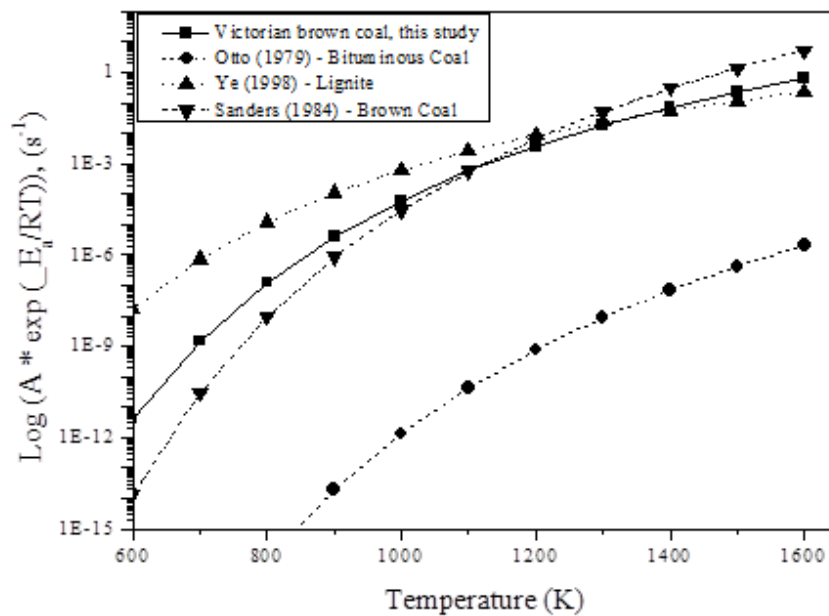


Figure 6-2 Comparison of measured gasification rate with other brown coals available in the literature (Otto, 1979, Sanders, 1984, Ye, 1998)

Particle Heat-up: The coal particle temperature profile in the furnace was calculated by an unsteady-state energy balance equation (6.6) shown below, considering both the heat transfer by radiation and convection from the surroundings.

$$m_p c_p \frac{dT_p}{dt} = hA_p(T_\infty - T_p) + \varepsilon \sigma A_p(T_w^4 - T_p^4) + H_{gen} \dots \text{Equation (6.6)}$$

Where m_p is the particle mass (kg), c_p is the heat capacity of coal particle (kJ/kg · K), h is the convective heat transfer coefficient calculated assuming Nusselt number of 2. T_w is the wall temperature (773 K), T_g is the gas temperature measured with thermocouple, ε is the particle emissivity (0.8) and σ is the Stefan Boltzmann constant.

The term H_{gen} is the total heat generated/released from the reaction I - IV. The heat generated from char oxidation reaction is calculated from the amount of CO/CO₂ produced. The ratio of CO₂/CO production at particle surface is calculated based on the coefficient suggested by Arthur et al (Arthur, 1951). At low temperature, little amount of CO₂ is produced at particle surface, while at higher temperature CO is the sole oxidation product and will react with O₂ to form CO₂ in the gas phase boundary layer.

6.3.2. Numerical calculation procedure

The series of differential equations to describe the transient change in particle temperature were programmed and solved numerically using MATLAB. The particle temperature and the char oxidation rate were calculated at any instantaneous time using Euler's method with increasing time step as shown in equation (7) below. The time step chosen was determined based on the trial and error method to ensure that the solution stabilizes. A pseudo-code algorithm has been developed to solve particle temperature history and is shown in **Figure 6.3**.

$$y(t + \Delta t) = y(t) + dt \times \frac{\partial y}{\partial t} \dots \text{Equation (6.7)}$$

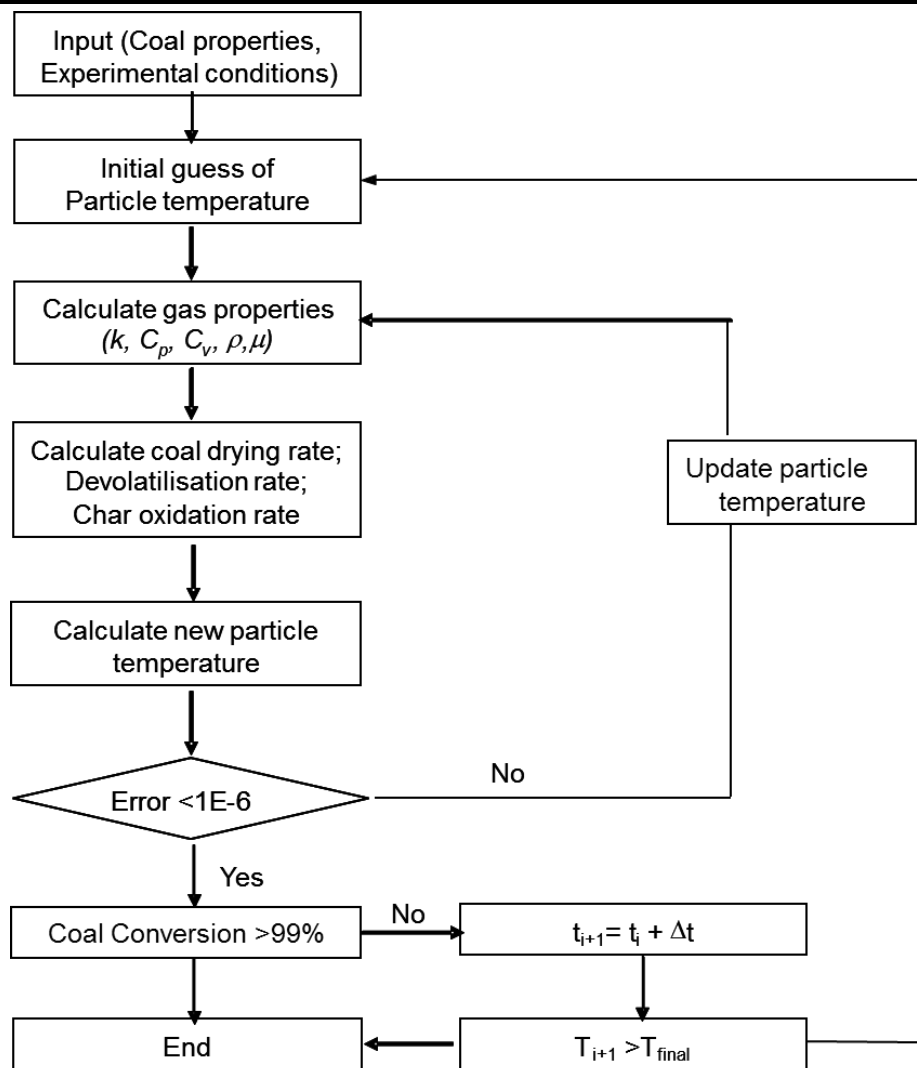


Figure 6-3 Schematic of the numerical procedure applied to determine the contribution of gasification reaction

6.4. Results and discussions

6.4.1. Influence of moisture and char-H₂O gasification on particle temperature in air-firing case

Figure 6.4 depicts the temperature profile for the burning coal particles in the air case. Irrespective of the original moisture content, most of the burning char particle temperature falls in the range of 1100 – 1250 K, which is approximately 100-200 K above the surrounding gas temperature at the respective location. This measurement is consistent with our previous study on the combustion of the same coal in drop – tube furnace (Binner, 2011,

Zhang, 2013), relative to the fact that the burning bituminous coal particle is usually 200-400 K hotter than the gas temperature (Murphy, 2006). The char temperature at the point further away from the burner should be lower, due to the lower surrounding gas temperature as well as the lower local char oxidation rate. For the dried coal sample, its temperature distribution at 50 mm has a peak at around 1120 K, with a considerable fraction settling at 1160 K and above. With the reactor distance extending to 75 mm, the peak was lowered ~1100 K and a sharp decrease in the fraction of particle hotter than 1160 K was also observed. The wet coal particle has a lower peak temperature than the dried coal at the same reactor distance. The peak is centered at 1100 K for both two distances, and less of hot particles above 1160 K have been observed. This is another direct sign of the ‘permanent’ residence of inherent moisture on char matrix, which negated both volatile oxidation and char consumption over a long duration.

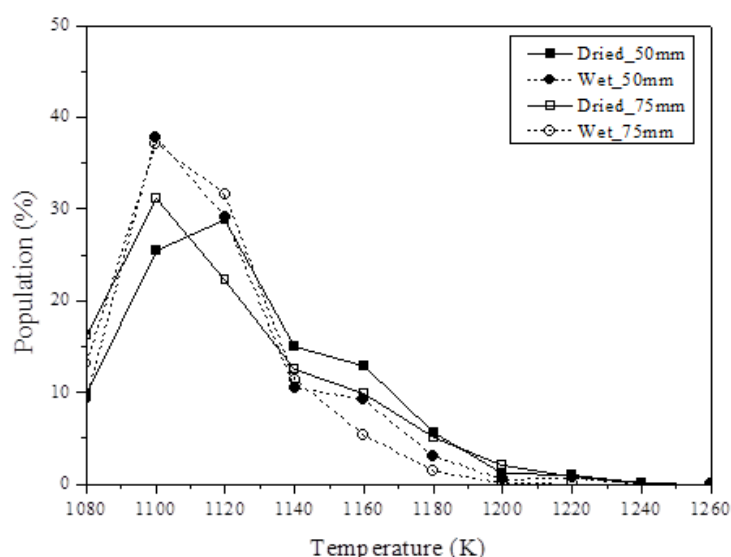


Figure 6-4 Distribution of measured char particle temperature of dried and wet coal in Air

Considering that the remaining moisture was released with volatiles together to form a thick cloud layer on char surface, it is hypothesised that such a thick cloud layer may increase the partial pressure of steam in char vicinity so as to enhance the char - steam gasification reaction consequently. The brown coal has been proven highly reactive for such a reaction from 1000 K onwards, as shown in **Figure 6.2**. Moreover, considering that a direct measurement on the partial pressure of steam derived from remaining moisture is implausible, we did not differentiate the two different steams during modelling. Instead, we simply varied

the partial pressure of steam in the model to reveal its influence on char particle temperature. The results are depicted in **Figure 6.5** for the combustion both dried and wet coal respectively in air. The distance of 75 mm was chosen here too avoid the interference of volatile combustion which is not fully finished at 50 mm. For both samples, the char particle temperature drops quickly upon increasing the extent of steam gasification reaction on char surface. The dried coal particle temperature could reach 1250 K upon the no contribution of char-steam gasification reaction, relative to 1000 K for the case that an extent of 67% occurring for such an endothermic reaction.

For the combustion of wet coal, its particle temperature without char - steam gasification reaches only 1175 K, which is around 80 K lower than the dried coal. This is due to the fact the existence of steam in volatile cloud reduces the heat to be released from its combustion, which in turn provides less heat feedback to the char particle. In **Figure 6.5**, the pyrometer data were added as rectangles with its width representing the variation of particle temperature. Clearly, one can conclude that the extent of steam gasification reaction reaches 14 - 17% (median 15.5%) for dried coal and 8 - 20% (median 14%) for wet coal, respectively. Considering that the median extent for such a reaction is very close for both dried and wet coal, it is safe to conclude that the extra moisture added in wet coal contributed little to char - steam gasification, although it co-exists with volatiles to form a thick cloud on char surface. In other words, the partial pressure of the extra steam in volatile cloud should be very low, thereby having no potential to trigger any extra reactions on char surface. This is reasonable as the coal feeding rate of 0.1 g/min creates only 0.04 l/min steam for the case of wet coal combustion, which is much lower than the 2.0 l/min steam created by the liquid fuel combustion. In addition, it is noteworthy that, the char - CO₂ gasification reaction was also included during the modelling for the air-firing case. It was however found insignificant with the contribution of less than ~1%. This is due to the low partial pressure of CO₂ (~15 vol%) and a low gas temperature in the reactor.

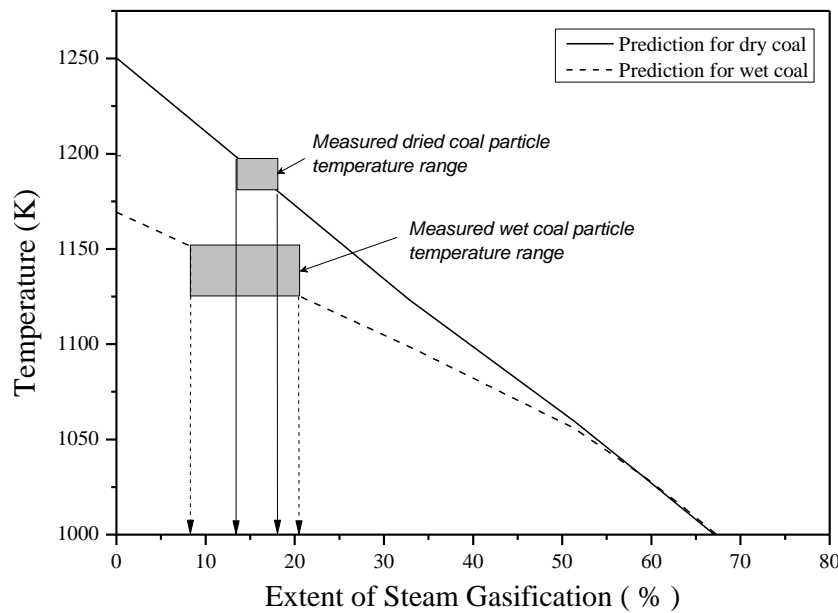


Figure 6-5 Method to determine the contribution of steam gasification reaction in air-firing case

6.4.2. Combined effect of char-H₂O and char-CO₂ gasification reaction in oxy-fuel mode

Figure 6.6(a) and 6.6(b) shows the measured burning char temperature profile at 50 mm and 75 mm in CO₂-rich atmosphere for oxy-21 and oxy-31, respectively. For dried coal in oxy-21 case, a noticeable fraction of hot particles with temperature above 1140 K appeared at the reactor height 75 mm, which opposite the trend observed in the air case where more hot particles are present at 50 mm. This is due to the delayed ignition in oxy-21 case which in turn shifted the char combustion stage to a later moment. On the other hand, the temperature distribution of wet coal was slightly higher at lower height of 50 mm. The similar phenomenon was confirmed for the wet coal particle temperature profile in oxy-21.

In oxy-31 case, as shown in **Figure 6.6(b)**, both dried and wet coal depicted a larger distribution of the hotter particles above 1140 K. Compared to the dried coal having a peak temperature of 1100 K at the reactor height of 50 mm, the wet coal even has more of the hot particles with the temperature beyond 1140 K. This is mainly due to a faster combustion of the dried coal which even occurred before 50 mm for a concurrent ignition and oxidation of

both its volatiles and char in the elevated oxygen concentration. With the reactor height increasing to 75 mm, the gap between two coal samples is narrowed, indicating that the combustion is close to the end.

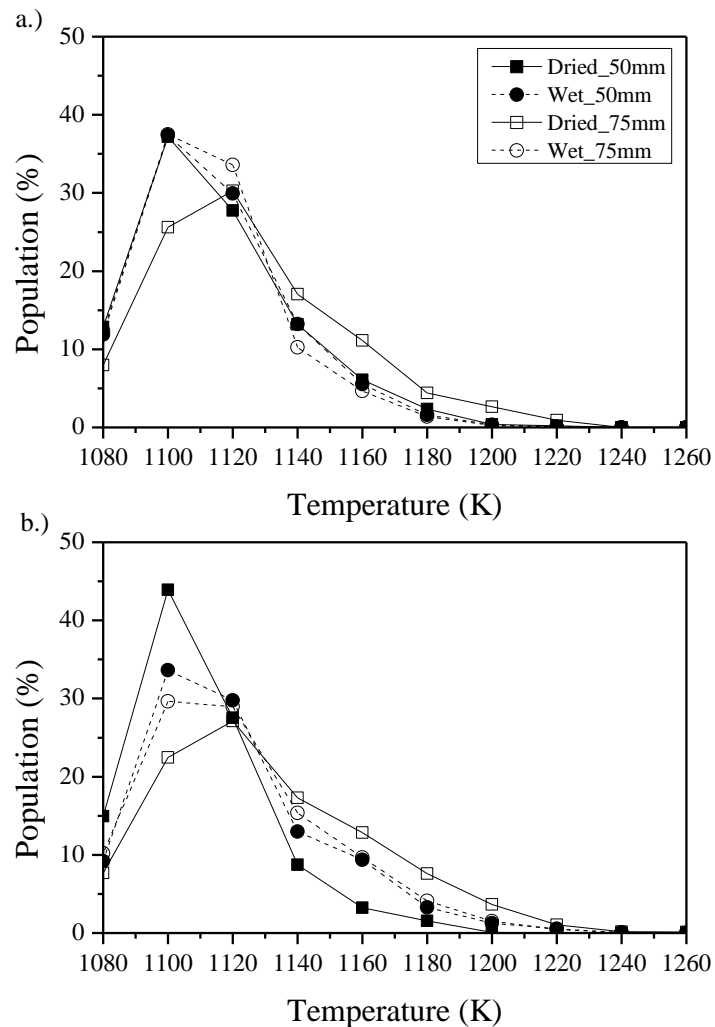


Figure 6-6 Measured pyrometer data for dried and wet brown coal at 50 mm and 75 mm height for (a) oxy-21 case and (b) oxy-31 case

Modeling work was conducted to compare with the pyrometer data so as to quantify the influence of the endothermic gasification reactions on particle temperature profile. Since the co-existence of CO_2 and steam in the oxy-firing mode, both char – CO_2 and char – steam gasification reactions could occur concurrently on char surface, which in turn reduce the char particle temperature significantly. Apparently, these two reactions could also affect each

other. To assess the significance of each gasification reaction, the modelling was first conducted by only considering the char – CO₂ gasification reaction. In other words, the char – steam reaction was switched off in the model. **Figure 6.7** demonstrates the predicted particle temperatures for both dried and wet coal samples burning in the three oxy-fuel cases, at the reactor height of 75 mm. The experimentally measured data were included for comparison. In addition, the numbers in parenthesis on the prediction bars refer to the extent of char – CO₂ gasification reaction that was determined by the reaction ratio of $r_{\text{char-CO}_2}$ to the overall reaction r . irrespective of the moisture content in coal, the contribution of char-CO₂ reaction was relatively low, reaching 2.6 - 2.89% and 6.17 - 7.68% for oxy - 21 and oxy - 31, respectively. This is much lower compared to ~20% observed for the bituminous coal at the oxygen concentration of 27% (Kim, 2014a). Again, this can be due to the very low flue gas temperature in the FFBR used throughout this study. Even by taking the char – CO₂ gasification reaction into account, the particle temperature is still over-predicted by the model. Apparently, the char – steam reaction is more influential. This could be the case, as char - steam gasification reaction reaches $3.66 \times 10^{-6} \text{ s}^{-1}$ at 1000 K, which is 1000 times higher than the char – CO₂ reaction at the same temperature range.

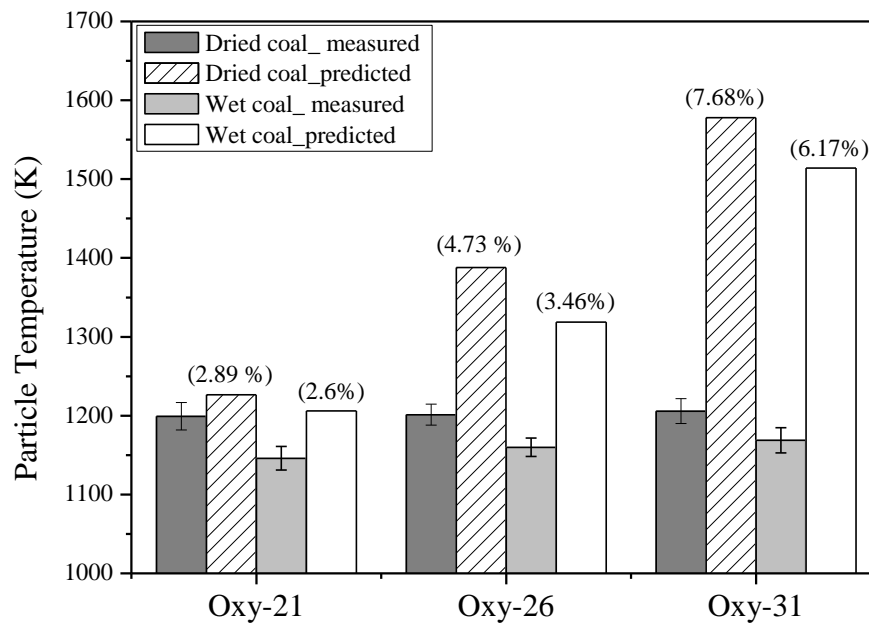


Figure 6-7 Predicted char particle temperature for dried coal and wet coal at 75mm at oxy-fuel combustion case with the consideration of char-CO₂ gasification reaction ONLY. The extent of char-CO₂ reaction is shown above the prediction bars in the figure.

Figure 6.8 demonstrates the contribution of char - CO₂ and char - steam reactions for the oxy-21 case. In the figure, the predicted particle temperature was plotted as a function of the total contribution of the two gasification reactions at the reaction height of 75 mm, and the pyrometer data were added in the places where they were matched satisfactorily by the prediction. From the match between the pyrometer data and prediction curve, the extent of each reaction on char surface was further calculated and plotted as pie chart next to the respective pyrometer point. For the combustion of dried coal in oxy-21, the total contribution of gasification reactions accounts for only 8%, with 5.53 % for char – steam reaction and 2.35% for char – CO₂ reaction. The extent of char – steam reaction is obviously low compared to that in the air case shown in **figure 6.5**, where the extent of char – steam reaction reaches 14 - 17% for the same coal. On the one hand, this should be attributed to the delayed ignition and oxidation of volatiles in the oxy – 21 case. The unreacted volatiles formed a thick cloud surrounding on char surface so as to enlarge the resistance against the external diffusion of oxygen towards char surface. On the other hand, a lower particle temperature caused by the heat sink of CO₂ was expected for the oxy-21 case, which was not

in favour of the endothermic gasification reaction, as explained earlier. For the wet coal combustion in 21% O₂ balanced by CO₂, the total contribution of ~18% from the two gasification reactions was observed, which was approximately 10% higher than that for the dried coal in the same bulk gas. In addition, the total gasification reaction contribution for wet coal in oxy-21 case is quite close to the air-firing case as shown in **figure 6.5**. Clearly, although the ignition delay and lower char particle temperature are also expected for the wet coal, the extra moisture within it increased the partial pressure of steam in the char particle vicinity. It thus enhanced the char - steam gasification reaction extent to a level that is comparable with the external steam in the bulk gas.

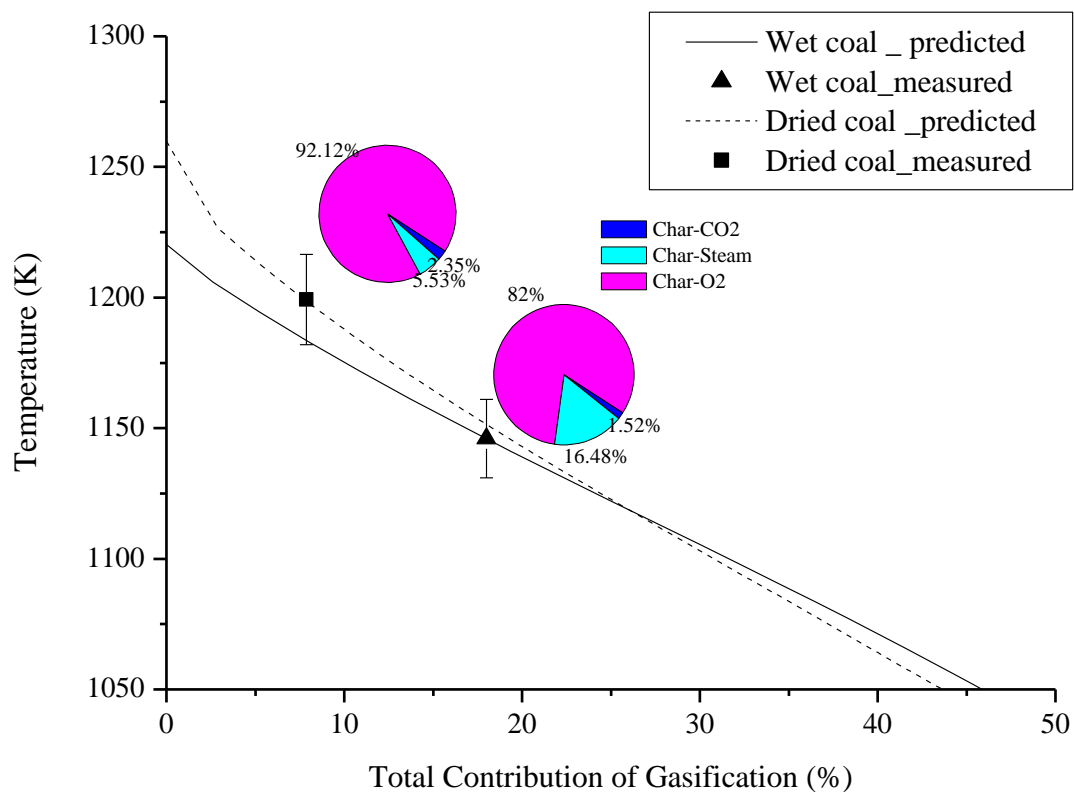


Figure 6-8 Contribution of char - CO₂ and char - steam gasification reactions for dried coal and wet coals in oxy-21 case

The contribution from two gasification reactions is more influential upon the rise of oxygen level to 26% and 31% balanced by CO₂. As illustrated in **Figure 6.9** for the oxy-26 case, the extent of char – steam gasification reaction was increased to 17.4 % and 22.2% for the dried and wet coal, respectively. This is attributed to the increase in the reaction rate for the

exothermic char – O₂ reaction which in turn improved the char particle temperature. Moreover, compared to a discrepancy of about 11% for the extent of char – steam reaction between the dried and wet coal in oxy-21 case, the gap was narrowed to about 4.8% for the oxy-26 case. Apparently, compared to the internal steam derived from inherent moisture, the external steam in bulk gas has a comparable and even larger role in triggering the char – steam gasification in the oxy-26 case. This should also be due to the enhanced char – O₂ reaction that led to a rapid release of the internal moisture out of char matrix. The CO₂ gasification is still insignificant in the oxy-26 case. This is because the char particle temperature is still fairly low, which, unless reaching 1600 K, has no potential to trigger the char – CO₂ gasification reaction for the Victorian brown coal studied here (Zhang, 2013).

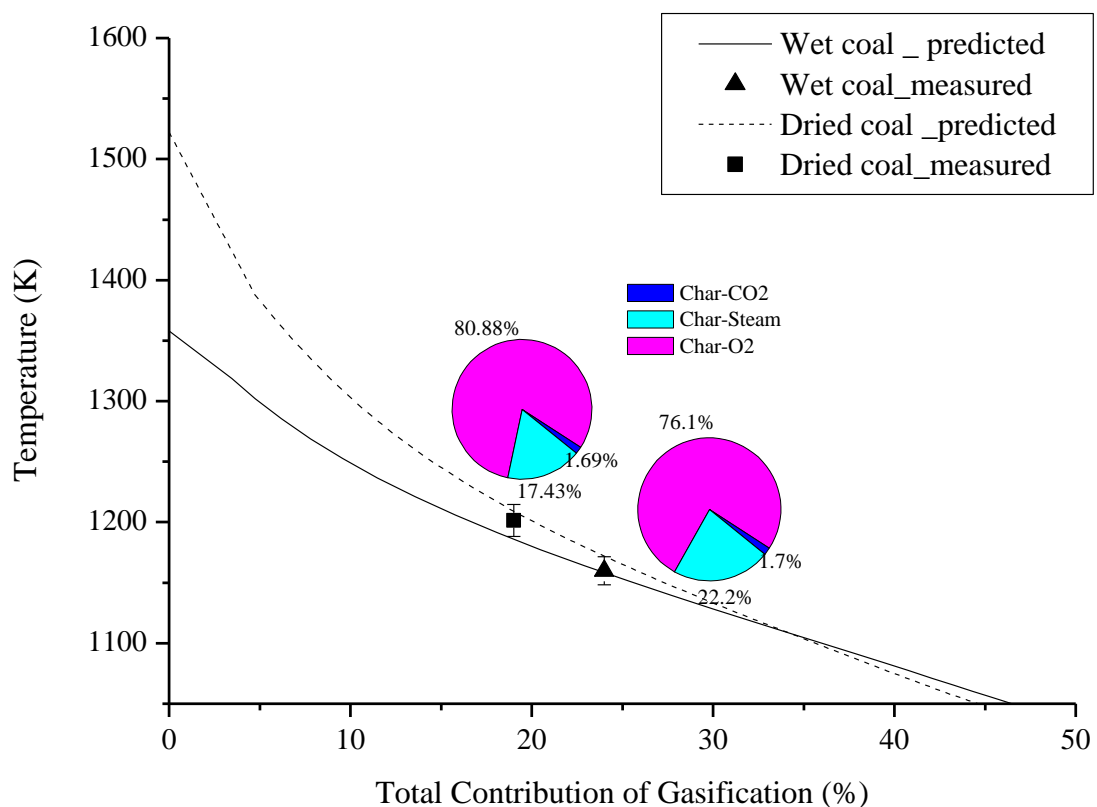


Figure 6-9 Contribution of char-CO₂ and char-steam gasification reaction for dried coal and wet coal in oxy-26 case

The enhanced char – steam gasification reaction was further confirmed in the oxy-31 case, where the char burnout rate due to the enhanced char – O₂ reaction is expected, as

substantiated in **Figure 6.10**. The extent of char – steam gasification reaction reaches 26.6% and 26.55% for the dried and wet coal sample, respectively. The gap between two coal samples is negligible, strongly supporting an insignificant role of the internal steam (derived from the inherent moisture in coal) on the combustion of wet coal in oxy-31 mode. The char – steam reaction was merely induced by the external steam in the reactor. To reiterate, this is due to a rapid release and escape of the inherent moisture from char surface. The high-speed camera imaging results in **Chapter 5** supports such a hypothesis.

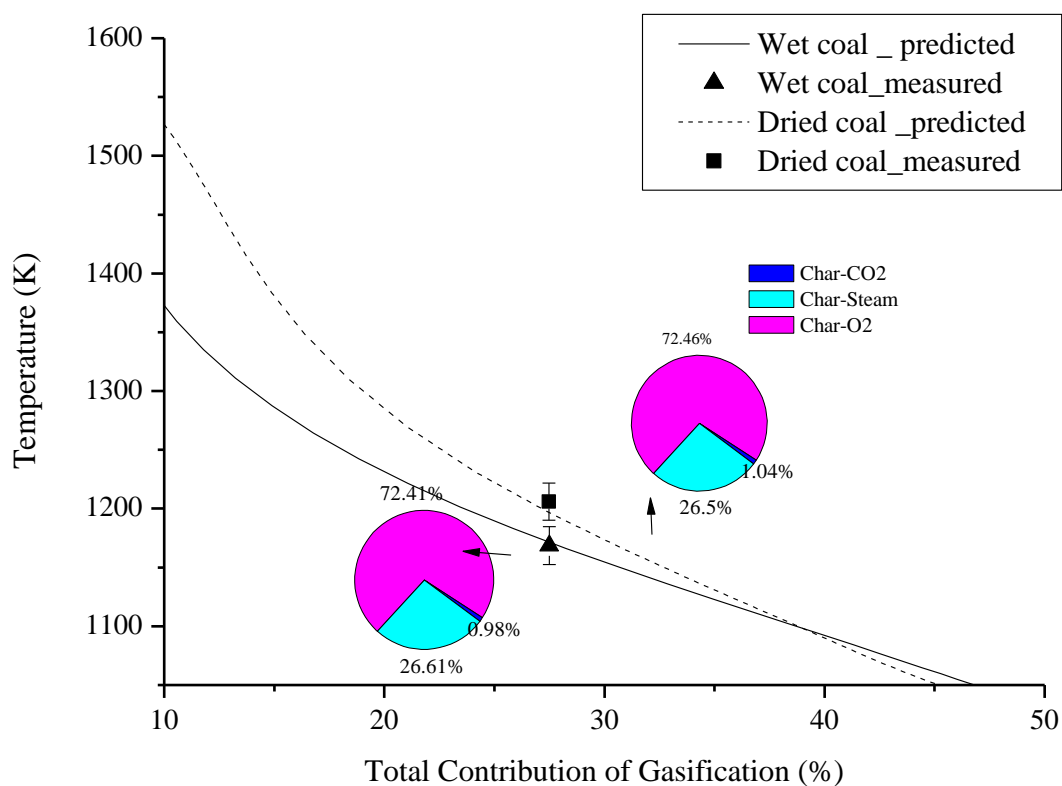


Figure 6-10 Contribution of char-CO₂ and char-steam gasification reaction for dried coal and wet coal in oxy-31 case

Table 6.1 depicts the summary on the contribution of char - CO₂ and char-steam reactions for both dried and wet coals in the oxy-fuel cases with the oxygen concentration increasing from 21% to 31% in CO₂ compared with some of the literature study related to bituminous coal. To reiterate, the contribution of char - CO₂ reaction here was approximately less than 3% in all cases, and no significant increment was observed with increasing oxygen concentration.

Such a value is low compared to the literature results, particularly due to the different rank of coal used. The char - CO₂ gasification accounted for ~15% for sub-bituminous and bituminous coal burnt at around 1500°C in lab-scaled combustor (Hetch, 2011, Kim, 2014a). The numerical study of wet recycle of bituminous coal in oxy-fuel combustion also presented the contribution of char - CO₂ and char -steam gasification as ~21% and 7.5% in the case of 24% O₂ balanced by CO₂(Hetch, 2012). The char – steam gasification reaction is more influential. For either dried or wet brown coal, its contribution increases upon increasing oxygen concentration in the bulk gas, reaching about 26% for both coal samples in the oxy-31 case. Such a value is obviously higher than that reported in the numerical study reported earlier for bituminous coal(Hetch, 2012). This is due to the abundance of alkali and alkaline earth metals in brown coal that can catalytically trigger the char – steam gasification from 1207 K onwards (Kajitani, 2010). In terms of the extent of char – steam gasification reaction, the discrepancy between dried and wet coal samples is certainly noteworthy. It is as broad as approximately 10% in the oxy - 21 case, and is gradually narrowed down to only 5% in oxy - 26 case and insignificant at the oxy-31 case. Such a discrepancy is mainly induced by the extra moisture in the wet coal, which formed a thick cloud on the char surface in the oxy - 21 case. The lowest oxidation of volatiles and char in the oxy-21 case caused a long duration of the evaporated steam in the char particle vicinity. Consequently, the char – steam reaction was triggered. Increasing the oxygen concentration in bulk gas enhanced the ignition and release of coal volatiles and inherent moisture, fewer of which resided on the char surface to trigger any extra gasification reaction. The similar phenomenon was confirmed for the air-firing of wet coal.

Table 6-1 Summary of the CO₂ and H₂O gasification reaction evaluated in this study compared with literature data (Hetch, 2011, Hetch, 2012, Kim, 2014)

Case Study	Coal Type	Facility	Temperature (K)	Gas Atmosphere	Particle Size (μm)	Contribution of Gasification (%)	
						CO ₂	H ₂ O
This Study	Dried brown coal	Flat flame burner	1100	21% O ₂ /CO ₂ – 18% H ₂ O	63-104	2.5	5.2
				31% O ₂ /CO ₂ – 18% H ₂ O		1	26
	Wet brown coal			21% O ₂ /CO ₂ – 18% H ₂ O		1.9	16.1
				31% O ₂ /CO ₂ – 18% H ₂ O		0.9	26.2
Hetch et al (2012)	Bituminous coal	SKIPPY 1-D program	1690	Dry recycle (14% H ₂ O)– 24% O ₂ /CO ₂	100	23.5	3.9
				Wet recycle (25% H ₂ O)– 24% O ₂ /CO ₂		21	7.4
Kim et al (2014)	Sub-bituminous coal	Flat flame burner	1700	21% O ₂ /CO ₂	75-106	15.3	-
				30% O ₂ /CO ₂		15.5	-

6.5. Conclusions

A Hencken flat-flame burner was used to study the combustion of wet Victorian brown coal in air-firing and oxy-fuel modes with 21 – 31 vol% oxygen in the bulk gas. The pyrometer was used to measure burning char particle temperature and compared with 1-D modelling considering all the surface reactions in char particle vicinity. The major conclusions can be drawn as follows:

1. Irrespective of the initial moisture content, the extent of char - steam gasification reaction was found to be ~15% in the air-firing case. Such a reaction was solely triggered by the external steam in the reactor, rather than the inherent moisture that has been fully released prior to char oxidation stage, having little interference on char consumption rate.
2. The combined effect of both char - CO₂ and char - H₂O gasification was significant in oxy-fuel combustion mode, especially for the wet coal. In the oxy-21 case, these two reactions have a total extent of around 8% and 18% on the burning char surface of dried coal and wet coal, respectively. The char - CO₂ gasification is insignificant, because the char particle temperature was very low. Increasing the oxygen percentage to 31% in CO₂ enhanced the extent of these two gasification reactions to reach 28% based on the mass of total carbon. Such an extent is comparable with the literature. However, the steam

gasification rate was far higher (~26% compared to ~10% in literature) substantiating the strong steam gasification reactivity of Victorian brown coal char.

3. The contribution of inherent moisture to char - steam gasification reaction is critical in the combustion of wet coal in the oxy-21 case, accounting for ~10 %. This is due to the long residence of the unevaporated steam as a thick cloud on the char surface. Increasing the oxygen concentration in CO₂ enhanced the char – O₂ reaction, the release of volatiles and inherent moisture, and hence, the char – steam reaction caused by the inherent moisture within coal matrix is minimised and eventually diminished in the oxy - 31 case.

Chapter 7

Effect of Steam on Ignition of Dense Particle Stream

This page is intentionally left blank

Monash University

Declaration for Thesis Chapter 7

Declaration by candidate

In the case of Chapter 7 the nature and extent of my contribution to the work was the following:

Nature of contribution	Extent of contribution (%)
Experimental, analysis and writing up	100%

The following co-authors contributed to the work. If co-authors are students at Monash University, the extent of their contribution in percentage terms must be stated:

Name	Nature of contribution	Extent of contribution (%) for student co-authors only
Lian Zhang		Supervisor

The undersigned hereby certify that the above declaration correctly reflects the nature and extent of the candidate's and co-authors' contributions to this work*.

**Candidate's
Signature**

	Date 22-09-2015
--	----------------------------------

**Main
Supervisor's
Signature**

		Date 22-09-2015
--	--	----------------------------------

*Note: Where the responsible author is not the candidate's main supervisor, the main supervisor should consult with the responsible author to agree on the respective contributions of the authors.

This page is intentionally left blank

7. INFLUENCE OF STEAM ON IGNITION OF VICTORIAN BROWN COAL PARTICLE STREAM IN OXY-FUEL COMBUSTION

This chapter presents the study on ignition of dense particle stream as an extension from the single particle ignition study from previous chapters. The ignition behaviour of brown coal particle stream in oxy-fuel combustion was examined. In addition, the impact of steam on ignition of dense particle stream was also thoroughly investigated.

7.1. Introduction

Coal is abundant and cheap compared to the other fossil fuels including natural gas and petroleum. It is also one of the most commonly used fossil fuel for the purpose of electric power generation in the world. Generally, black coal is burned in the coal-fired power plant for electricity generation from steam turbine. However, the continuing use of black coal as a major fuel source eventually leads to its depletion, which in turn increases the mining costs and coal price in the global trading market. On the other note, lignite or brown coal, is a cheap energy source and can be used as an alternative to black coal to produce electricity. However, it has a low heating value and burns less efficiently in coal-fired boiler than black coal, because of the existence of abundant moisture within its carbonaceous matrix (Li, 2004). Consequently, burning brown coal in a thermal power station tremendously increases carbon emission rate to the atmosphere.

Oxy-fuel combustion is one of the promising carbon capture and storage (CCS) technologies that can be directly retrofitted to the existing coal-fired power plants (Tomita, 2004). The feasibility of oxy-fuel combustion has been widely studied in the literature (Bejarano, 2008, Croiset, 2000, Kim, 2014b, Lei, 2014, Murphy, 2006, Riaza, 2014, Sarofim, 2007, Stivers, 2010). However, the centered focus of research was on black coal whilst the combustion characteristic of low-rank coal has not been studied intensively. Due to the presence of abundant inherent moisture, the combustion of brown coal yields a highly concentrated steam in the flue gas (Zhang, 2015). This condition is distinctive from that observed during black coal combustion and is expected to alter coal ignition and combustion property in the boiler.

The ignition delay in oxy-fuel combustion has been confirmed when a comparison was made with the ignition time in the conventional air-firing mode under an identical O₂ concentration (Hetch, 2011, Hetch, 2012, Kim, 2014a, Molina, 2007, Murphy, 2006, Shaddix, 2009, Zhang, 2013). This is due to the change on the gas properties and its temperature upon the substitution of CO₂ for N₂ (Law, 2006). CO₂ has a larger heat capacity of 57.83 kJ/mol than N₂, 34.18 kJ/mol at a gas temperature of 1400 K (Rathnam, 2009, Molina, 2007, Shaddix, 2009). On the other hand, the physiochemical properties of steam are different from that of N₂ and CO₂ (Riaza, 2011). At the elevated temperatures of 1000 -1500 K, the thermal conductivity of steam, 0.16 W/(m·K) is larger than that of N₂ and CO₂, 0.082 and 0.097 W/(m·K), respectively (Rathnam, 2009). Therefore, a high steam concentration encountered in the brown coal oxy-firing furnace is likely to increase the rate of particle heating. On the other hand, the heat capacity of steam, 45.93 kJ/mol, is lower than CO₂ but higher than that of N₂. Such a discrepancy may affect the particle ignition as well. Furthermore, steam is not an inert gas in the combustion, which participates a large number of elemental reactions through its chemical effects, thereby affecting coal particle ignition (Degges, 2010).

In a drop tube furnace heated to 1373 K, Riaza et al. observed a slightly higher ignition temperature, which referred to a delayed ignition, and increased CO concentration when the external steam was injected to the reactor (Riaza, 2011). The authors attributed the increased CO to the triggering of char-steam gasification reaction (Zhang, 2013). In contrast, in another independent study, a slightly better ignition was observed in O₂/H₂O atmosphere compared to that in O₂/N₂ atmosphere. The author suggested that the water-gas shift reaction was triggered to produce abundant H₂ that eventually hastened the ignition of coal volatiles (Lei, 2014, Zou, 2014).

It is also noteworthy that, most of the afore-mentioned studies were performed on the ignition of single particles or dilute particle stream. While these studies have provided deep understanding regarding the fundamentals of single coal ignition, the inter-particle interaction in the combustion of coal-dust is critical and is more relevant to the flame holding in the pulverized coal burner (Du, 1995). While experimental studies on ignition of coal particle stream have been performed in air (Liu, 2011), the ignition of coal stream in oxy-fuel

combustion received less attention. In particular, the effect of steam on the ignition of dense coal particle stream has never been studied before.

To investigate the issues addressed above, this paper aims to clarify the influence of steam on the ignition of dense particle stream under the steam-rich, oxy-fuel combustion conditions. For such a research, an entrained-flow reactor coupled with a flat-flame burner (FFBR) and non-intrusive *in-situ* diagnosis facilities was used to visualize the particle group ignition and its flame propagation. In addition, coal particle burning temperature was measured with a two-color infrared pyrometer. For validation purposes, the transient cylindrical cloud ignition model was modified and used to quantitatively confirm the role of steam, i.e. its participation on water gas - shift reaction and/or char-steam gasification reaction, and their effect on particle ignition and burnout. Apart from Victorian brown coal, two differently ranked coals, sub-bituminous and bituminous coals were also examined to reveal the effect of coal rank on its ignition in the steam-enriched oxy-fuel combustion environment.

7.2. Materials and Experimental Methodology

7.2.1. Fuel Properties

The Victorian brown coal tested here was collected from Loy Yang power station, labelled as Coal A. In addition, a sub-bituminous coal from Xinjiang, labelled as Coal B, and bituminous coal from Brisbane, Coal C, were tested to compare with the low-rank Victorian brown coal. The proximate analysis and ultimate analysis of the three coals are listed in **Table 7-1**. Each coal sample was air - dried, grounded and sieved to the size range of 63 - 104 microns prior to the combustion test. The moisture content in the dried coal reached equilibrium at 12 *wt%*.

Table 7-1 Proximate and Ultimate analysis of coal samples

Coal Type	Proximate Analysis (%db)			
	Moisture (%ar)	Ash	VM	Fixed Carbon
Coal A (VBC)	16.6	0.7	49.9	49.4
Coal B (XJC)	26.2	16.1	36.6	46.2
Coal C (BC)	5.8	23.9	16.9	57.9
	Ultimate Analysis (%daf)			
	C	H	N	S
Coal A (VBC)	70.2	4.7	0.52	0.35
Coal B (XJC)	62.5	3.4	0.73	0.83
Coal C (BC)	88.5	4.74	1.64	0.31

**VBC = Victorian brown coal, XJC = Xinjiang Coal, BC = Brisbane Coal*

7.2.2. Optical flat-flame McKenna burner experiments

Experiments were performed in an optical laminar McKenna flat flame burner reactor (FFBR), shown in **Figure 7-1**. The flat flame burner provides flexibility to generate different gas compositions via adjustment of fuel and oxidizer flow rates. The burner is constructed from a stainless steel outer which houses a porous bronze water-cooled sintered burner matrix. The fuel and oxidizer are premixed in the burner where the mixture of C_2H_4/H_2 was used as the gaseous fuel, and mixture of air/ CO_2/O_2 was introduced as the oxidizer. Coal particle was fed by a piezoelectric feeder and transported to the furnace through a 1-mm tube located at the burner centre-line. The particles were entrained using carrier gas with a volumetric flow rate of 0.7slpm (Standard litres per minute). A 115-mm diameter cylindrical quartz reactor was positioned on top of the burner to isolate combustion environment from surrounding air. To minimize the heat loss, the tubular reactor was insulated with a 25 mm - thick insulation wool except a small window of 10 x 30 cm² at the bottom of the reactor for the visual observation of coal flame. To simulate the wet flue - gas recirculation condition, external steam was injected tangentially through a silicone tube which was attached at 50-mm above the coal injection point. The external steam was generated via water evaporation, and was fed through a 30 cm long stainless steel tube that was heated to 473 K using a heating tape. With the experimental condition used in this study, the combustion of ethylene/hydrogen in flat flame produced a steam concentration of 13 vol% in the ambience, namely steam-lean combustion hereafter. The external steam was added to generate an elevated steam concentration of 26 vol% in the furnace, namely steam-rich combustion hereafter.

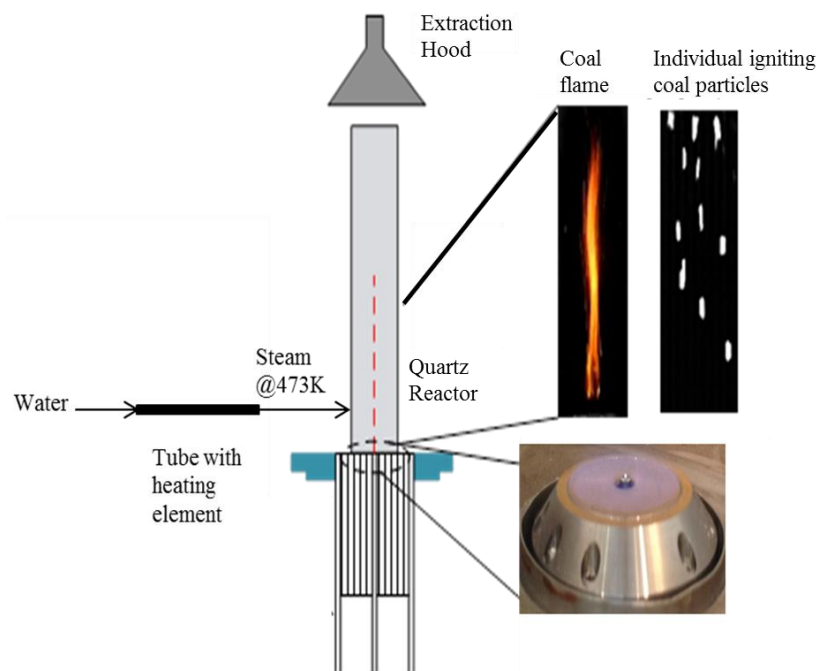


Figure 7-1 Schematic of Mckenna flat flame burner facility used in this study

The flat flame burner can be flexibly adjusted to suit the needs of the experiments. In this study, the total gas flow rate was kept constant at 22 *slpm* for all the experimental conditions tested. The gas temperature profile at the burner centre-line was measured using a B-type thermocouple, and corrected for the radiation loss (Shaddix, 1999). As illustrated in **Figure 7-2**, little or no variation was observed for the gas temperature measured between air-firing and oxy-fuel combustion with the oxygen concentrations of 21 *vol%* and 31 *vol%*. The temperature at the ignition zone near the burner base is approximately 1100 - 1200 K. A slight decrease in gas temperature was detected upon the injection of the external steam. This can be attributed to the mixing of low - temperature steam (473 K) with hot flue gas.

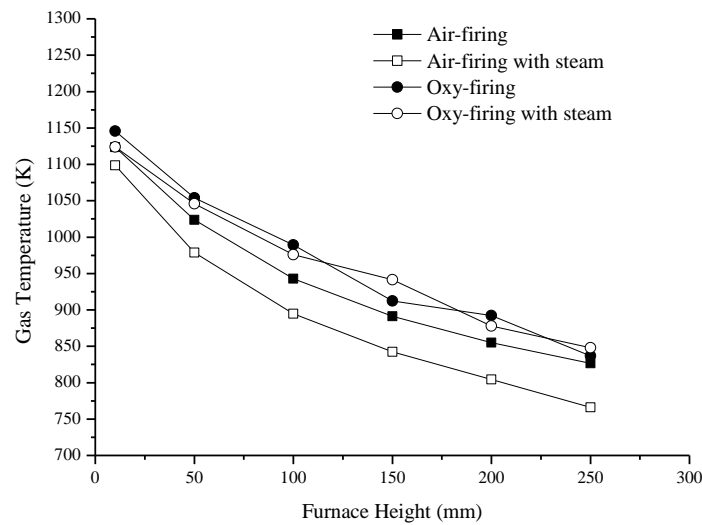


Figure 7-2 Centre-line gas temperature profile measured using the B-type thermocouple, corrected for radiation loss (Shaddix, 1999)

In this paper, the influence of particle loadings on ignition was evaluated by varying the coal feeding rate from 0.1g/min to 1g/min, referring to a particle number density range of 1×10^7 - 1×10^9 particles/m³ in the carrier gas. The oxygen concentration in the furnace is set to 21 – 31 vol% in both air-firing and oxy-fuel modes. The O₂/C molar ratio varies from 15 to 187 in this paper, corresponding to a fuel-lean region. Therefore, the differing ignition properties observed between different particle loadings (shown later) is mainly due to the inter-particle feedback interaction, rather than due to the change on the single burning char particle temperature.

7.2.3. Non-intrusive optical diagnosis facility

A digital camera, and high-speed infrared pyrometer was used to study ignition of particle stream in this study. The operational and analysis procedure has been discussed in depth in **Chapter 4, 5 and 6**. To convert the measured ignition point from digital camera to time-scale, high speed camera was used to capture the particle velocity near the burner base. The calculated particle velocity was 0.9m/s.

7.3. Modelling approach

7.3.1. Transient cylindrical cloud combustion model

The transient model was employed here to predict coal particle ignition time, by assuming that an initially cold cylindrical cloud formed by coal particles is suddenly immersed in a hot furnace. The ignition can be defined as either homogeneous ignition reflecting the point where the gas temperature rises rapidly or heterogeneous ignition at which point the solid particle temperature turns higher than the local gas. This has been detailed in **Chapter 3** of this thesis. To reiterate, the ignition criterion for both mechanisms is categorized as follows (Du, 1995). For the heterogeneous ignition, the particle temperature rises above the adjacent gas phase temperature, and hence, the particles transfer heat to the gas rather than gas transferring heat to the particles. In contrast, homogeneous ignition occurs when the gas temperature profile shows a peak at certain radial location. The ignition time was taken at which ignition mechanism occurs first in the transient ignition model.

The gas-phase conservation equations for mass, species and energy in the cylindrical cloud are given as:

Mass Conservation:

$$2\pi r \frac{\partial \rho}{\partial t} + \frac{\partial \dot{m}}{\partial r} = \dot{w}_m''' 2\pi r \quad \text{Equation (7.1)}$$

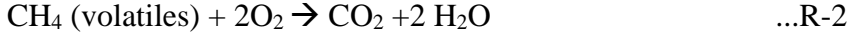
Species Conservation:

$$2\pi r \frac{\partial \rho Y_k}{\partial t} + \frac{\partial \dot{m} Y_k}{\partial r} - \frac{\partial}{\partial r} [2\pi r \rho D \frac{\partial Y_k}{\partial r}] = \dot{w}_k''' 2\pi r \quad \text{Equation (7.2)}$$

Energy Conservation:

$$2\pi r \frac{\partial \rho h_T}{\partial t} + \frac{\partial \dot{m} h_T}{\partial r} - \frac{\partial}{\partial r} [2\pi r \rho D \frac{\partial h_T}{\partial r}] = \dot{w}_h''' 2\pi r \quad \text{Equation (7.3)}$$

Where w_m , w_k and w_h are gas-phase sources for mass, species and enthalpy, respectively. In this paper, the following homogeneous reactions are considered to study the influence of steam on coal ignition.



The governing particle-phase equations for mass, density, diameter and temperature are described as:

$$\frac{dm_p}{dt} = \frac{dm_v}{dt} + \frac{dm_c}{dt} \quad \text{Equation (7.4)}$$

$$\frac{d\rho_p}{dt} = -\frac{6}{\pi d_p^3} \frac{dm_v}{dt} \quad \text{Equation (7.5)}$$

$$\frac{dd_p}{dt} = -\frac{2}{\pi \rho_p d_p^2} \frac{dm_c}{dt} \quad \text{Equation (7.6)}$$

$$m_p c_p \frac{dT_p}{dt} = h A_p (T_\infty - T_p) + \varepsilon \sigma A_p (T_w^4 - T_p^4) + h_c \frac{dm_c}{dt} - h_v \frac{dm_v}{dt} \quad \text{Equation (7.7)}$$

The kinetic for the pyrolysis reaction was modelled with the first order single rate kinetic Arrhenius model. This model has been used widely in the commercial CFD simulation and fundamental study (Badzioch, 1970, Zhang, 2013).

$$\frac{dm_v}{dt} = A_v \exp\left(-\frac{E_v}{RT}\right) [V^* - V] \quad \text{Equation (7.8)}$$

The heterogeneous carbon surface reactions were modelled using the kinetic-diffusion single film model for both carbon oxidation and carbon gasification reactions with CO_2 and steam as shown in equations (7.9-7.11):

$$\frac{dm_c}{dt} = \frac{P_{\text{O}_2}}{\frac{1}{k_{c,o}} + \frac{1}{k_{d,o}}} + \frac{P_{\text{CO}_2}}{\frac{1}{k_{c,c}} + \frac{1}{k_{d,c}}} + \frac{P_{\text{H}_2\text{O}}}{\frac{1}{k_{c,s}} + \frac{1}{k_{d,s}}} \quad \text{Equation (7.9)}$$

$$k_c = A \exp\left(-\frac{E}{RT}\right) \quad \text{Equation (7.10)}$$

$$k_d = \frac{4D_i M_c}{d_p R} \left(\frac{T_p + T_g}{2}\right)^{0.75} \quad \text{Equation (7.11)}$$

The kinetic parameters for brown coal devolatilisation, oxidation and gasification has been justified previously and used in this work (Zhang, 2013). The empirical devolatilisation model from Kobayashi was used to determine the fraction of each fraction released from coal devolatilisation (Kobayashi, 1977). The kinetic data for sub-bituminous and bituminous coal was cited from the literature (Hetch, 2012, Ye, 1998).

7.3.2. Numerical procedure

The series of partial differential equation were solved numerically using an explicit calculation procedure. The complete numerical procedure has been detailed in the literature (Du, 1995). The radius of the cylindrical cloud was taken at $R_c = 0.25\text{cm}$, measured from the experimental observation in the flat flame burner reactor. It should be noted that the model employed here is only to calculate the ignition time of coal particles in the cylindrical cloud. Therefore, the calculation stops once either a homogeneous or heterogeneous ignition time has been identified. For this simulation, the boundary and initial conditions used are as follow:

Boundary and initial condition:

Gas phase:

$$\begin{aligned} t = 0 \text{ and } r < R_c, Y_k &= Y_{k,0} & T &= T_{g,0} \\ t = 0 \text{ and } r > R_c, Y_k &= Y_{k,\infty} & T &= T_\infty \\ t > 0 \text{ and } r \rightarrow \infty, Y_k &= Y_{k,\infty} & T &= T_\infty \\ t > 0 \text{ and } r \rightarrow 0, & \text{symmetrical boundary condition} \end{aligned}$$

Solid phase:

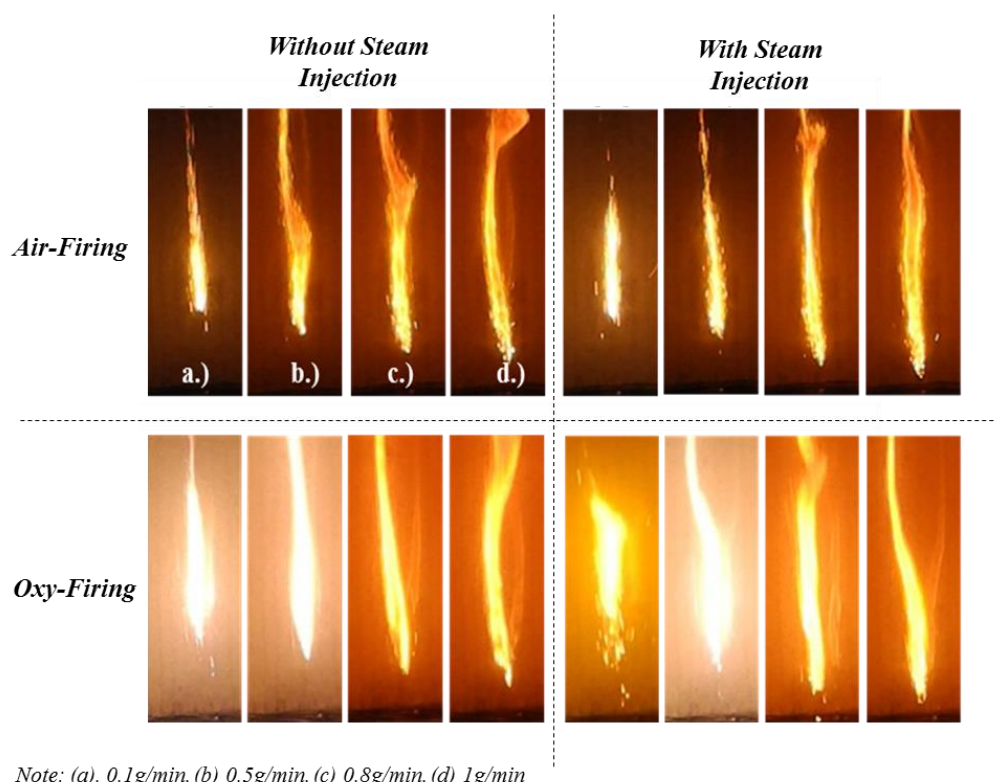
$$m_p = m_{p,0} \quad d_p = d_{p,0} \quad T_p = T_{p,0}$$

7.4. Experimental results and discussion

7.4.1. Effect of particle loading on brown coal ignition in both steam-lean and steam-rich contexts with 21% O_2

The typical photographs for the Victorian brown coal flame in 21vol% oxygen are shown in **Figure 7-3**. Based on the observations, the general combustion sequences can be concluded as follows: initially, upon reaching the devolatilisation temperature, coal particles release combustible volatiles until they reach the flammable limit which enables a homogeneous ignition of the volatiles. Subsequently, the volatiles burnt continuously to generate a large

fireball that is the brightest and most intense part in a flame, which subsequently initiate char ignition and oxidation. Lastly, char oxidation continues to form a yellow tail for the flame, which is accompanied by the decrease on particle temperature as the particles steadily approach furnace exit. The thick flame formed for the extensive homogeneous volatile oxidation is expected for high-volatile coal such as Victorian brown coal, in which the volatiles account for nearly half of the total coal on the dry mass basis.



Note: (a). 0.1g/min, (b) 0.5g/min, (c) 0.8g/min, (d) 1g/min

Figure 7-3 Photographs of brown coal burning in 21%O₂ in O₂/N₂ (top panel) and O₂/CO₂ (bottom panel).

For each series illustrated in **Figure 7-3**, the ignition time is shortened with increasing particle loading. This is because a high number particle density enhanced the inter-particle heat feedback. Such a trend has been confirmed previously (Liu, 2011). Based on the concept of particle number density, the minimum ignition time was reported at a particle number density of 4×10^9 particles/m³, calculated based on the cold flow feeding rate (Liu, 2011). Apart from coal loading, the gas environment (air vs oxy-fuel) and the presence of steam were also found to affect particle ignition time in **Figure 7-3**. To further quantitatively reveal these differences, the measured ignition point was converted to time - scale and shown in

Figure 7-4. Clearly, regardless of the steam injection, a delay of approximately 15 ms was observed at the lowest particle number density of $4 \times 10^7/\text{m}^3$, upon the shift of air-firing to the oxy-fuel mode. At a high number density of $4 \times 10^8/\text{m}^3$, this delay was slightly shortened to 10 ms by the enhanced heat feedback from the surrounding dense particles. Nevertheless, the trends observed here agree well with the reported literature results (Liu, 2011). The interesting point here is to clarify how the injected steam influences the ignition time, particularly at the high particle loading.

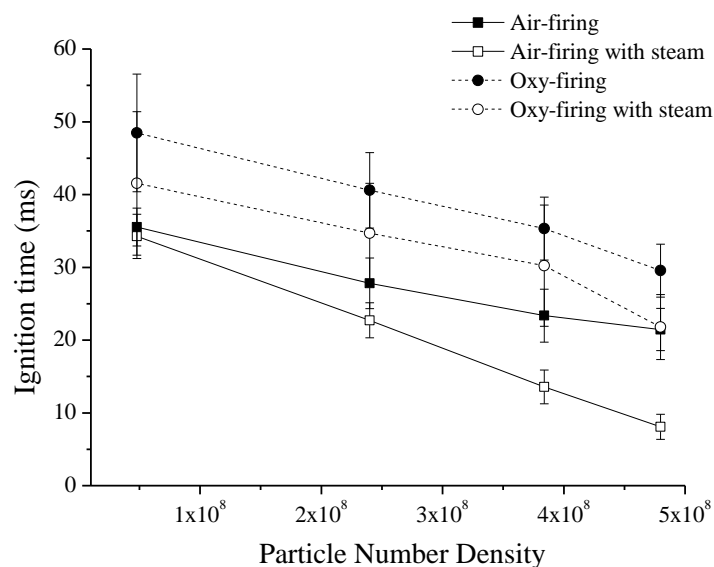


Figure 7-4 Ignition time of Victorian brown coal in air and oxy-fuel as the function of coal feeding rate in 21%O₂ without and with steam injection.

With the injection of steam, the coal ignition time in air-firing case was marginally decreased at the lowest particle number density of $4 \times 10^7/\text{m}^3$, corresponding to a coal feeding rate of 0.1g/min. Upon the increase of particle loading, one can clearly see that the coal ignition time was remarkably shortened upon the injection of the external steam. At the highest coal feeding rate of 1g/min, the coal particles were ignited in only 8 ms in the steam-rich air-firing case, compared to an ignition time of 22 ms with the steam-leach air-firing case. In other words, the injection of steam significantly hasten coal ignition by 14 ms at the high particle loading of 1g/min but slightly reduce coal ignition by only 1-2 ms at low particle loading. For the oxy-fuel combustion mode, the variation of particle ignition time upon steam injection is rather constant for all the particle loadings. That is, irrespective of coal particle loading, the

coal ignition time was shortened by 7-8 *ms* upon steam injection. Such a finding, however, is contradictory against the previously reported results (Riaza, 2011).

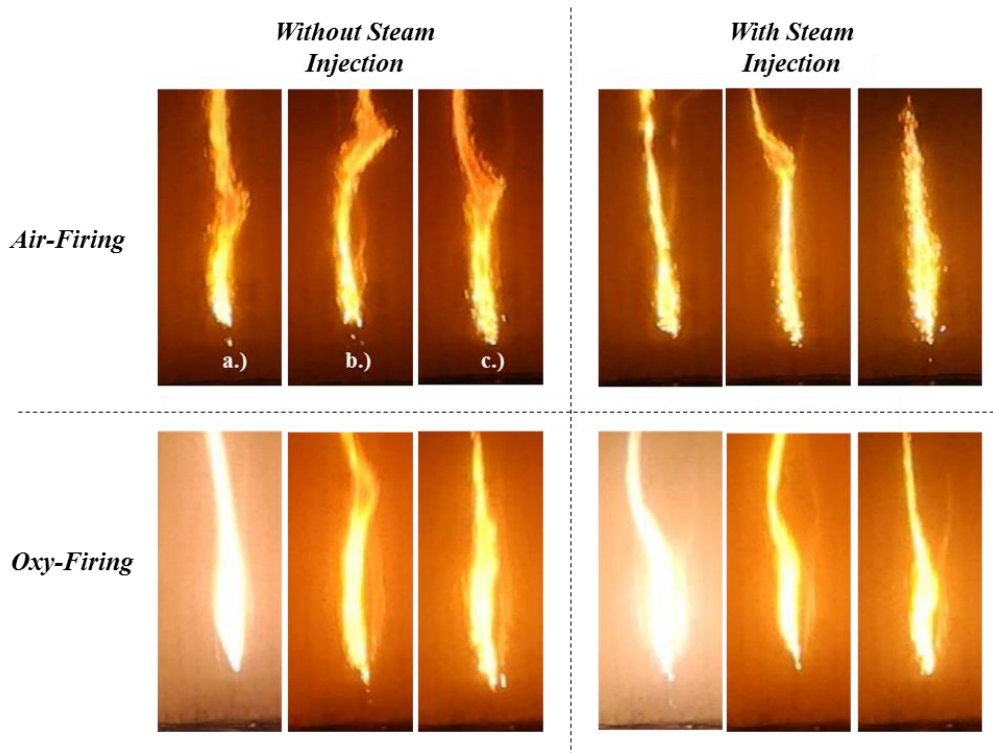
The injection of steam into the combustion chamber is supposed to exert three major influences on coal ignition. Firstly, the larger thermal capacity of H₂O compared to N₂ at elevated temperature is expected to postpone coal ignition (Law, 2006). Secondly, the heterogeneous char - steam gasification reaction may be triggered on the particle surface, which produces CO and H₂ that promote the local homogeneous gas - phase oxidation. Thirdly, the homogeneous water-gas shift reaction (R-3) of volatiles produces H₂ that can significantly reduce flammability limit of the local gaseous volatile mixture, thereby shortens the volatile homogeneous ignition time.

For the char-steam gasification and water-gas shift reactions, their potential and extent to occur are highly coal - specific. The former reaction would only be triggered when either the particle temperature is sufficiently high or the char is highly reactive. Low-rank brown coal generally has a high reactivity towards char-steam gasification even at low temperatures, due to the abundance of catalytic metals within it (Kajitani, 2010). On the other hand, the gas-phase water-gas shift reaction may be negligible if the local concentration of volatiles is sufficiently low, or the local temperature is sufficiently high since this reaction is unfavourable at high temperature (Mendes, 2010). Generally, it is expected that the char-steam gasification reaction occurs at the char oxidation regime. The extra production of CO and H₂ from this reaction will thus have minimal effect on the volatile ignition. In light of this, the role of water-gas shift reaction (R3) should be the major reaction that caused the decrease in coal ignition time in air-firing modes in **Figure 7.4**. The impact of this reaction in the air-firing mode is also highly dependent on the particle feeding rate.

For the lowest particle loading, the impact of water-gas shift reaction is marginal due to the small amount of volatiles generated from the devolatilisation of dilute coal particles stream. In contrast, at a high particle loading, the above – mentioned reaction can be significant as the amount of volatiles in the system increases substantially. Furthermore, volatiles composition in brown coal is mainly made up of light hydrocarbons such as CO and CH₄, in which the former serves as main reactant for water-gas shift reaction (Hayashi, 2004). As a result, the H₂ derived from reaction R-3 is abundant and is likely to decrease volatiles flammability in

the local gas mixtures. This explicates the reduced ignition time in steam-rich atmosphere. However, since the reverse reaction for R3 could occur in the CO₂-rich environment, its effect is marginal under the oxy-fuel combustion mode. The detailed discussion will be provided from the modeling perspective later.

7.4.2. Effect of oxygen concentration



Note: (a). 21%O₂, (b) 25% O₂, (c) 31% O₂

Figure 7-5 Photographs of brown coal ignition in air-firing mode (top panel) and oxy-firing mode (bottom panel). The coal feeding rate was fixed at 0.5g/min.

Figure 7.5 illustrates the ignition behavior of Victorian brown coal at various oxygen concentrations in both air-firing and oxy-firing modes. The coal feeding rate of 0.5g/min refers to a particle density of $2.4 \times 10^8/\text{m}^3$. Regardless of the oxygen concentration, brown coal exhibits a rapid ignition in both combustion modes. **Figure 7.6** shows the quantified ignition results as a function of O₂ concentration in both air-firing and oxy-firing modes. In the air-firing case with 21% O₂, the particles ignited by approximately 5ms quicker upon the injection of the external steam into the reactor. Upon the increase in the oxygen concentration in air, the effect of the external steam turns marginal and even negligible, as evident by the

overlapping of the ignition time for both steam-lean and steam-rich cases at 31% O₂ in air. Clearly, the influence of oxygen partial pressure to promote the ignition/oxidation is more pronounced than the external steam.

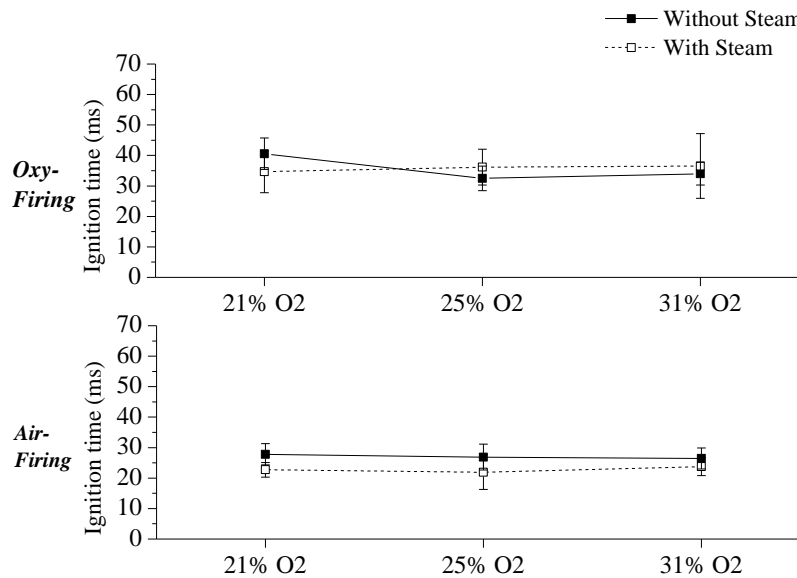


Figure 7-6 Measured brown coal ignition time at various oxygen concentration with fixed coal mass feeding rate of 0.5g/min

On the one hand, the increase in oxygen partial pressure is beneficial in increasing the oxidation rate for volatiles. On the other hand, the increase in the temperatures of igniting particle and its local surrounding gas are detrimental to the reaction R3 for water-gas shift reaction which is favored upon decreasing the temperature. The similar observation was confirmed for the oxy-fuel case. That is, the injection of external steam is effective in enhancing the ignition of coal particles at the low oxygen concentration. However, upon increasing the oxygen fraction to 25%, the ignition time of coal particles was even slightly increased upon the injection of external steam. This implies that the water-gas shift reaction (R-3) was inhibited. The injected steam (~ 473 K) may simply act as a heat sink that reduced the local gas temperature, thus increasing the particle ignition time.

7.4.3. Effect of coal rank

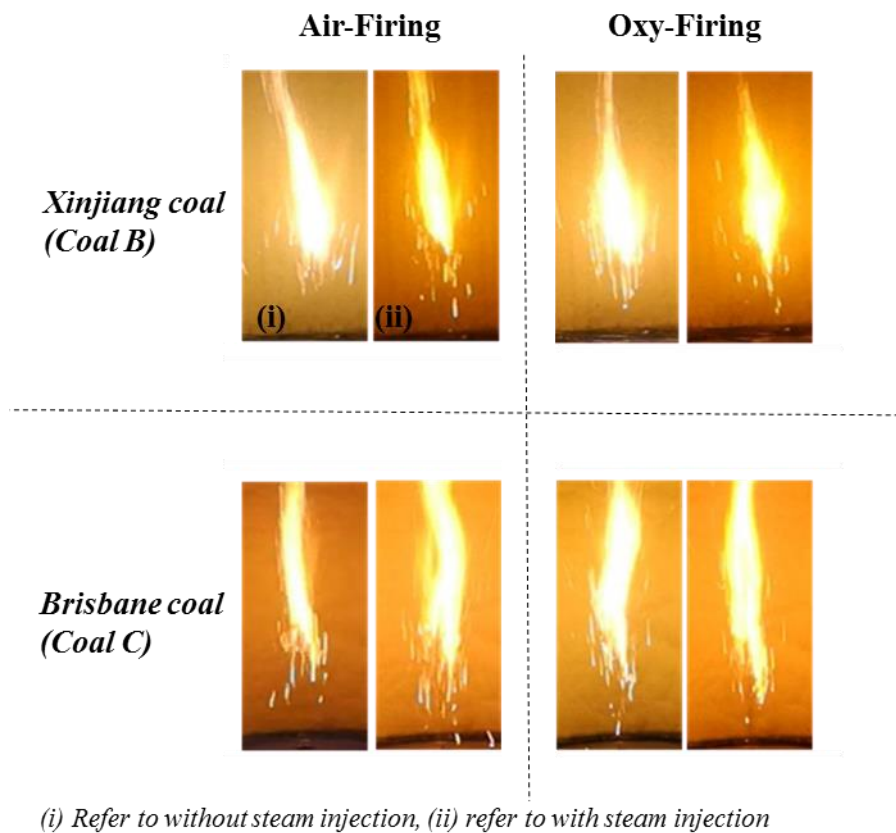


Figure 7-7 Images of XJC and BC burned in 21% oxygen, with fixed coal mass flow rate of 0.5g/min.

Figure 7.7(a) and **Figure 7.7(b)** further illustrates the flame images at a constant oxygen concentration of 21 vol% for Xinjiang sub-bituminous coal (Coal B) and Brisbane bituminous coal (Coal C), respectively. The coal feeding rate was fixed at 0.5 g/min. Clearly, both fuels exhibited different ignition properties from brown coal. For either coal sample, the volatile flame, representing the homogeneous volatile oxidation was much thicker and more intense than the brown coal flame shown in **Figures 7.3** and **7.5**. This is due to the abundance of heavy hydrocarbons such as tar in the high-rank coal volatiles (Chen, 1992). These heavy hydrocarbons, once released, prefer to reside and ignite on coal particle surface. This explains the existence of individual igniting particles at the flame front.

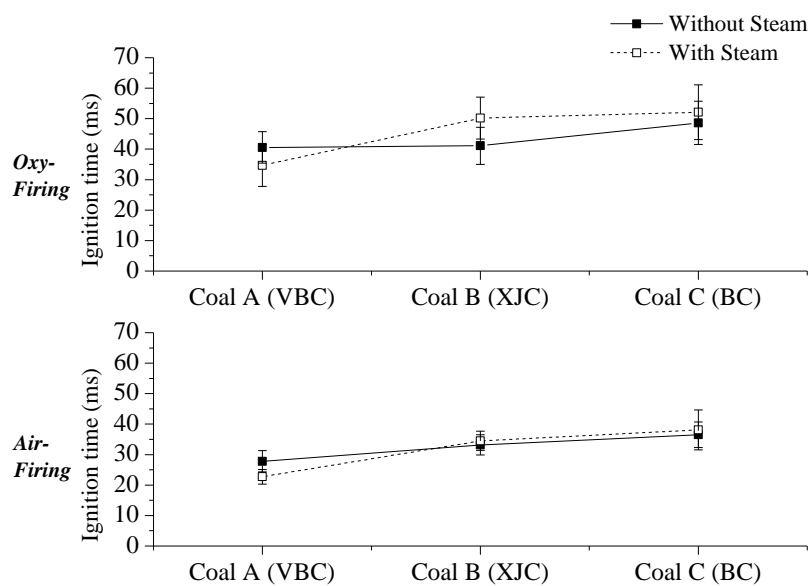


Figure 7-8 Quantitative measurements of the ignition time for all coals at a fixed coal loading rate of 0.5 g/min in all cases. (Data for Coal A was replicated from Figure 7.4)

Figure 7.8 provides the quantitative measurements of the ignition time for both coals with respect to the combustion mode as shown in **Figure 7.7**. The ignition results for brown coal at the same mass feeding rate was also included for comparison. Clearly, irrespective of gas environment, brown coal ignition is the quickest amongst the three coals. In the steam-injection case, steam expedited the ignition of brown coal, but exerted insignificant influence on the ignition of Xinjiang sub-bituminous coal (Coal B) and Brisbane coal (Coal C). Instead, the ignition of these coals was slightly delayed. This delay is even more pronounced in the oxy-firing mode. Clearly, the heat sink effect of the external steam is more pronounced for these two high-rank coals.

7.5. Experimental results validation using transient ignition model

The results from the refined transient model are present here to quantitatively clarify the effect (both physical and chemical effects) of steam on coal particle ignition. **Figure 7.9** demonstrates the comparison between the model predicted ignition time and the respective value measured for Victorian brown coal, as a function of particle number density in the steam – rich environment with 21 vol% O₂. To clarify the importance of the water-gas-shift reaction (R3), two simulation scenarios were considered here, one including this reaction and

another one without it. As evident in Figure 9, the predicted ignition time, with reaction R-3 included, approximated the experimental data much better. The model has also successfully confirmed the delay in the ignition time under oxy-fuel conditions, where the heat sink effect of both CO_2 and H_2O are far more pronounced than the chemical effect of steam for the reaction R3.

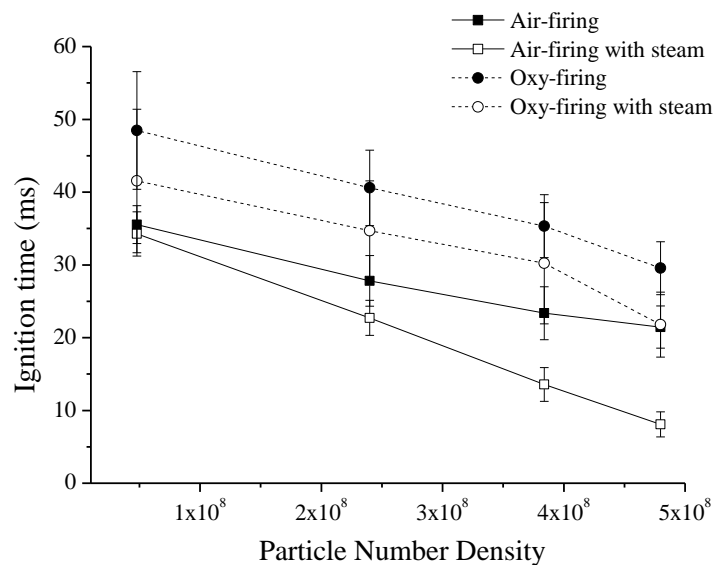


Figure 7-9 Comparison between calculated ignition time and experimental ignition time in the steam injection case with 21vol% O_2 for Victorian brown coal. Note that R-3 refers to water-gas shift reaction

Figure 7.10 depicts the predicted ignition time in the steam - rich environment with the variation of the O_2 concentration under both air-firing and oxy-firing modes. The model further confirmed the importance of the water-gas shift reaction on coal particle ignition under the air-firing mode, whereas such a reaction is insignificant for the oxy-fuel mode, since the prediction results from the model without including the water-gas shift reaction R3 indeed fall into the standard error bars related to the experimental measurement. Instead, the model including such a reaction slightly underestimated the ignition time. In addition, it was found that the refined model did not agree very well with experimental data observed in 25 vol% and 31 vol% O_2 under both combustion modes. This is probably due to the failure in the model to account for the dynamic movement of volatile reaction sheet. By using the same model for spherical cloud, Ye has also reached the similar conclusion in calculating the ignition time of Hulunbel Lignite in 15% O_2 at 1500 K (Ye, 2014).

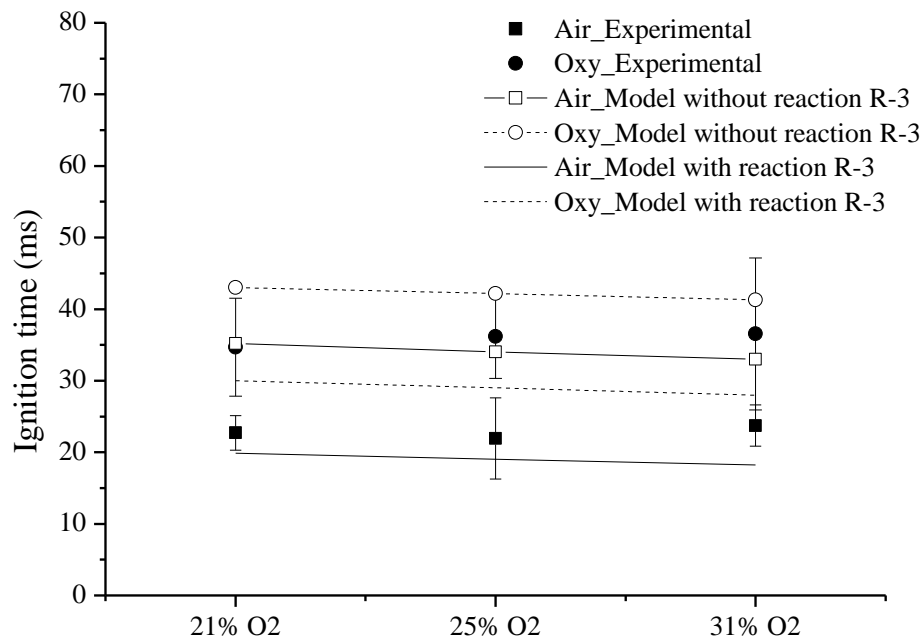


Figure 7-10 Comparison between calculated and experimental brown coal ignition time at varied oxygen concentration in steam-injection case

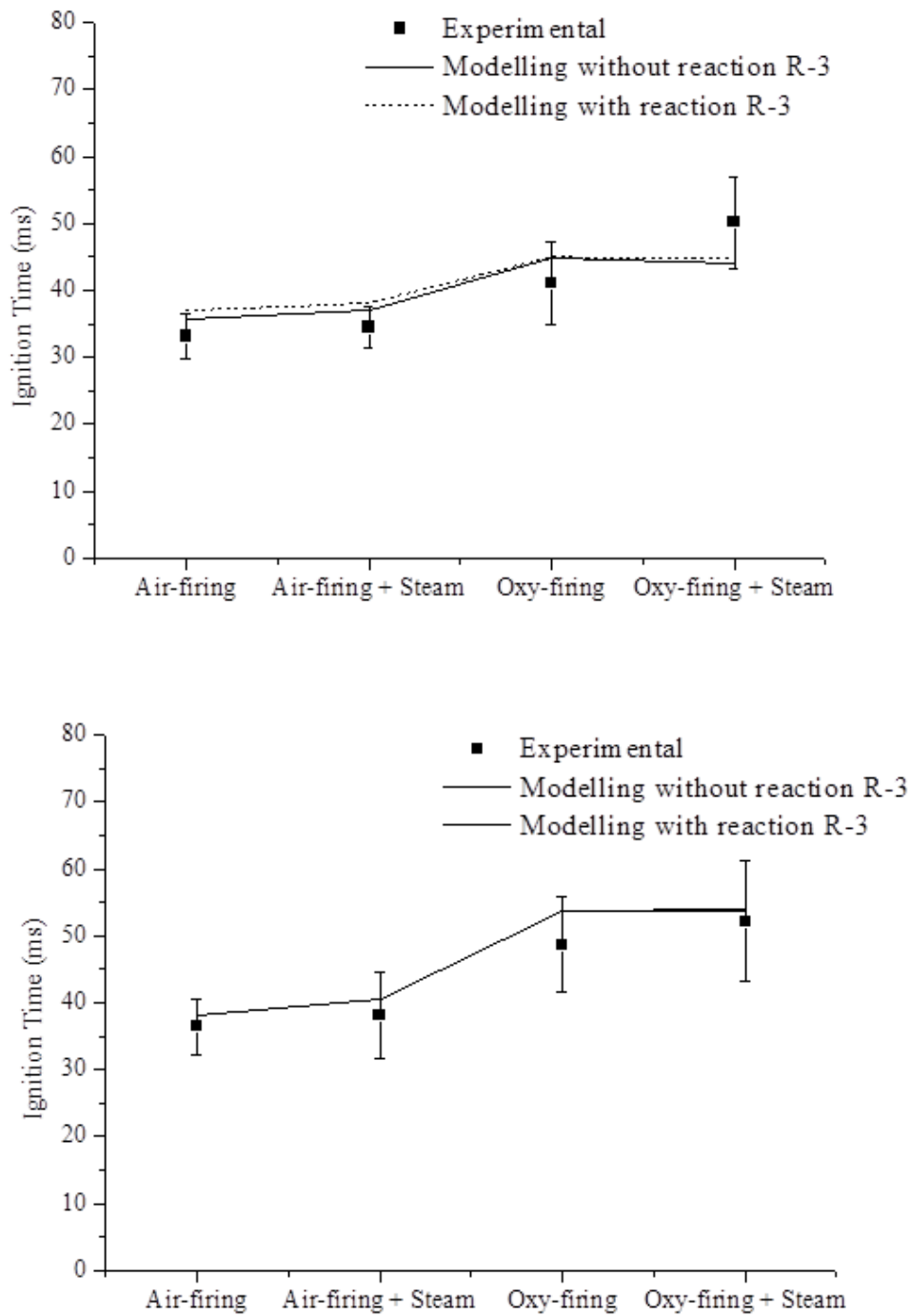


Figure 7-11 Ignition modelling case studies for higher rank coals for (top panel) sub-bituminous coal and (bottom panel) bituminous coal. Two modelling approach were used, with and without the inclusion of water-gas shift reaction, R-3

Figure 7.11 demonstrates the modelling results for both sub-bituminous coal (Coal B) and bituminous coal (Coal C). Two modelling approaches were also considered here, modelling without water-gas shift reaction (R-3) in the model, and modelling with consideration of this reaction. For both sub-bituminous and bituminous coals, the difference between the two modelling approaches was insignificant. Instead, a slight delay in coal ignition was observed when water-gas shift reaction was included in the simulation. As the shift reaction is exothermic in nature, incorporating this reaction in the model should increase the local gas temperature and therefore, accelerate coal ignition, rather than delaying ignition as observed in **Figure 7.11**. To reiterate, the main reagent for shift reaction, CO is short from the devolatilisation of high - rank coal (Kobayashi, 1977). Secondly, the water-gas shift reaction is reversible and dominantly controlled by the temperature (Mendes, 2010). The conversion extent of reagent CO to product H₂ is lowered significantly at high temperatures. As these conditions are not in favour for water gas shift reaction in high-rank coal, it is unlikely that water-gas shift reaction will be influential during combustion of high rank coal.

Figure 7.12 demonstrates the pyrometer-measured particle temperatures for the three coals at a distance of 65 mm above the flat flame in 21%O₂. For the steam-lean air-firing cases, brown coal exhibits the lowest temperature, followed by Coal B and Coal C in an ascending sequence. This is due to the abundance of gaseous volatile components in brown coal, which escaped quickly from coal particle surface and burnt mainly in the gas phase. Adding the external steam however increased the brown coal particle temperature remarkably, contradicting the decrease on the particle temperature for the other two coals. This is a strong evidence on the promotion effect of steam on the ignition of brown coal via its participation in the water-gas shift reaction R3. In contrast, the heat sink effect is more influential for the other two coals. The similar trends were observed for the oxy-fuel combustion cases.

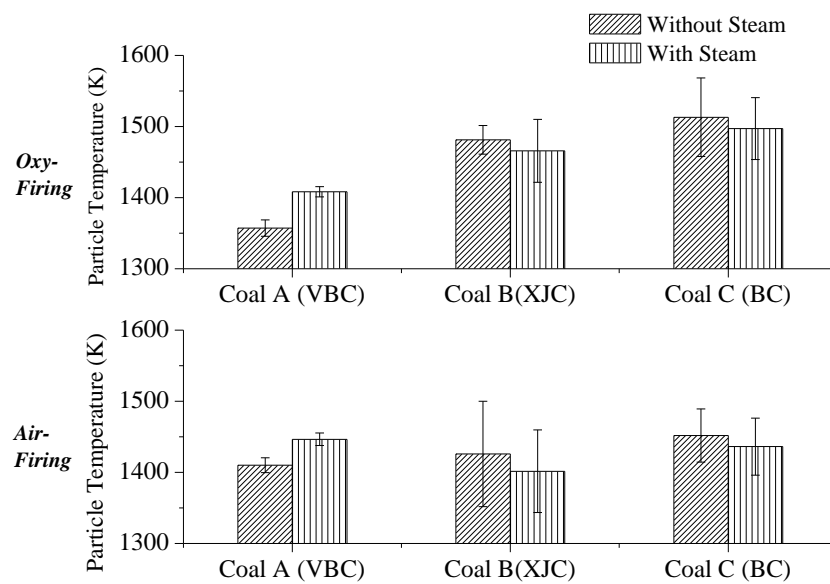


Figure 7-12 Measured particle temperature in 21% oxygen at 65 mm above the burner base. Coal feeding rate was fixed at 0.5g/min.

In addition to the homogeneous water-gas shift reaction, the external steam in flue gas is also supposed to trigger the heterogeneous char-steam gasification reaction during the char oxidation stage. As has been suggested by our previous works (Pratono, 2015a) and those reported in the literature (Hetch, 2012, Lei, 2014), the char - steam gasification reaction can take place together with char - CO₂ gasification reaction under the oxy-firing mode. In light of this, the char conversion stage was further modelled through the use of a single particle combustion model that was previously developed (Pratono, 2015a). By matching the particle temperature data in **Figure 7.12**, the contribution of char-steam gasification reaction can be determined through varying the extent of char - steam gasification reaction in the model.

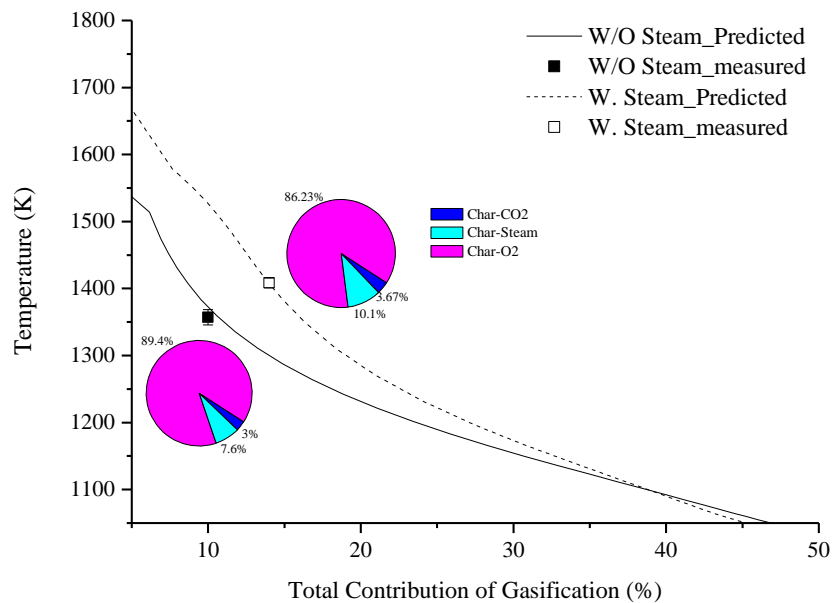


Figure 7-13 Method to determine the contribution of char gasification reaction towards total char consumption rate. An example of the simulation was shown here with brown coal as the test subject.

Figure 7.13 demonstrates the contribution of char –steam gasification reaction for Victorian brown coal under the oxy-firing condition with 21% O₂. In the steam-lean case, the char – CO₂ reaction and char – steam reaction contributed 3% and 7.9% to the overall char burnout, respectively. Upon the injection of external steam, the extents of these two reactions were increased to 3.6% and 10.17%, respectively. Using the similar approach, the contribution of char gasification for the other two coals was also calculated. **Figure 7.14** illustrates the results for all the three coals under the oxy-firing condition with 21% O₂. The contribution of char gasification (both char - CO₂ and char - H₂O) for brown coal is obvious, as discussed before. However, it only reached 9% for the sub-bituminous coal (Coal B), irrespective of steam injection. This reaction is even insignificant for the bituminous coal (Coal C), reaching only 5% in non-steam injection and 6% in steam-injection case for the measured particle temperature of 1450 K and 1437 K, respectively. For both coal B and coal C, it is clear that the injection of extra steam has a trivial role in triggering char-steam gasification reaction. This should be mainly due to the low furnace temperature used in this study. Clearly, brown coal has the highest reactivity in terms of steam-gasification reaction of all three coals. This can be partly explained by the difference in mineral composition between coals of different

ranks. The mineral matter in low-rank coal is generally dominated by alkaline and alkali earth metal species which are highly catalytic towards gasification (Franklin, 1982, Kajitani, 2010, Raask, 1985). In other words, the existence of steam is most beneficial for Victorian brown coal studied here, fastening its ignition as well as improving its char burnout rate.

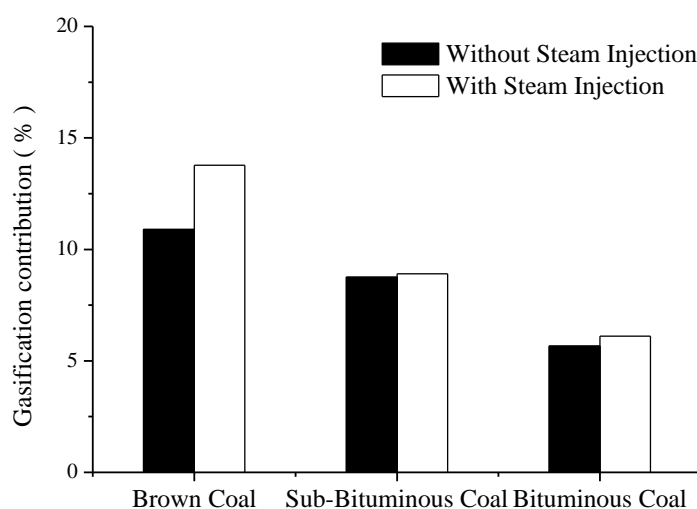


Figure 7-14 Contribution of char gasification to char-consumption rate at 21% oxygen concentration in oxy-firing mode. The calculation was done by comparison of measured particle temperature with the theoretically predicted particle temperature.

7.6. Conclusions

In this work, the ignition behaviour of Victorian brown coal in steam-rich environment has been examined via both experimental investigation and modelling approach. The *in-situ* diagnosis of brown coal flame were conducted for a range of particle feeding rate, 21 - 31% oxygen in both N₂ and CO₂ diluents, comparison between Victorian brown coal and two high-rank coals, and the injection of external steam (26 vol%) to mimic the wet flue gas recycle in an oxy-firing furnace. The major conclusions achieved are as follows:

- At a high particle loading, brown coal particles ignited quickly upon the injection of external steam. The external steam triggered both water-gas shift reaction and char-steam gasification reaction. The former reaction generated abundant H₂ which accelerated the homogeneous ignition and improved the flammability of brown coal volatiles, while the latter improved char burnout rate.

- The refined transient ignition model results agreed well with the measured coal ignition data, proving the influence of water-gas shift reaction on the ignition of Victorian brown coal. On the contrary, the sub-bituminous and bituminous coal showed an even larger ignition delay with the injection of external steam. This is due to the lack of CO in the volatiles generated from the pyrolysis of high-rank sub-bituminous and bituminous coal. Therefore, the impact of water-gas shift reaction for these coals was insignificant. Instead, the heat sink of steam is more pronounced for these two high - rank coals.
- With the injection of external steam, brown coal experienced an enhancement in its char-steam gasification reaction at a low furnace temperature of ~1200 K examined here, while it has minimal effect for sub-bituminous coal and bituminous coal. This indicates the high reactivity of Victorian brown coal towards char - steam gasification due to the catalytic effect of its mineral matters.

This page is intentionally left blank

Chapter 8

Conclusions and Recommendations for Future Research

This page is intentionally left blank

8. CONCLUSIONS AND RECOMMENDATIONS

This chapter provides summaries and major conclusions that are derived from the findings in this thesis, linking their practicality to the industry sector. Some recommendations for future research directions are also included in the closing section.

8.1. Conclusions

A comprehensive set of experiments and modeling studies were conducted to examine the ignition characteristics of brown coal in air-firing and oxy-firing mode; focusing on the issues associated with the unique properties of Victorian brown coal, such as AAEM species and its solid additives, impact of inherent moisture content in wet brown coal and the influence of steam. A bench-scale entrained flow reactor (EFR) with flat flame burner was integrated with an advanced in-situ diagnostic facility for ignition research. The major conclusions from each study are further highlighted below.

8.1.1. Influence of external clay and AAEM species on ignition

In this study, the impact of clay and AAEM ash-forming metal species during ignition were examined. A 1M Hydrochloric-Acid (HCl) was used to leach the majority of the AAEM species in coal matrix, such as Ca, Mg and Na. Removal of HCl-soluble metals significantly reduced flame stability and delayed coal ignition by two order of magnitude in air-firing and oxy-firing mode with 21% O₂. On the other hand, the addition of external clay to raw coal, from 1wt% to 3wt%, negligibly affected coal ignition, indicating its practicality in coal power stations. Also, an improvement in volatile decomposition rate was observed with an injection of clay, which in turn enhanced the flame intensity and char burnout rate. In the oxy-firing mode, an oxygen concentration of 30% was found to eliminate the discrepancies between the ignition time of raw coal and demineralised coal.

8.1.2. Influence of moisture on volatile flame propagation

Following the study on AAEM species, this research then breached out to focus on the moisture in brown coal and its implication on coal ignition. Brown coal samples with differing moisture content from 12% (air-dried coal) to 30% (wet coal) were prepared by

addition of demineralised water to the air-dried brown coal. Through experimental observations, the delayed ignition of wet coal particles was confirmed in both air-firing and oxy-firing mode. It was also concluded that the moisture released from wet coal exerted an effect on the subsequent coal devolatilisation and char combustion stage rather than solely influenced coal drying and ignition. From the modeling perspective, the theoretical model indicated incomplete moisture evaporation prior to coal ignition. This accounted for 31% evaporation extent in air-dried coal and 10% in wet coal. The remaining moisture was co-released with the volatiles during devolatilisation and significantly altered volatile flammability and composition at the particle surface. This suggested that two different types of moisture exist in brown coal matrix; external moisture and internal moisture. The external moisture is fully evaporated during coal drying while the inherent moisture is released together with volatiles due to its strong binding with the brown coal carbonaceous matrix. In oxy-fuel mode, increasing the oxygen molar fraction to 31% was found sufficient to reduce the gap of ignition time and volatile flame size between air-dried coal and wet coal.

8.1.3. Influence of moisture on char gasification reaction

Succeeding the results achieved in Section 8.1.2, the impact of remaining inherent moisture on char combustion stages was clarified through calculating the contribution of char-steam gasification reaction. The extent of influence was determined by matching the experimentally measured char particle temperature with the theoretically calculated temperature for each coal sample. In the air-firing case, the inherent moisture was insignificant towards its contribution to the char-steam gasification, which was approximately 15% for each coal and was triggered solely by external steam in the reactor. This suggested the complete release of moisture during pyrolysis before the start of char oxidation during air combustion. On the other hand, the inherent moisture in wet coal was significant due to the co-influence of both char-CO₂ and char-steam gasification reaction in oxy-firing mode (21% O₂). This improved the total gasification extent, from 8% in air-dried coal to 18% in wet coal. The extra 10% contribution in wet coal was due to the long residence of the un-evaporated steam as a thick cloud on the particle surface. Also, the differences between air-dried coal and wet coal were negligible when O₂ concentration was increased to 31%. Both samples exhibited gasification extent of

28% in this condition, to which steam and inherent moisture contributed approximately 26% of the gasification rate.

8.1.4. Influence of external steam on combustion of dense cloud

To finalise this research and determine its applicability on a larger-scale basis, the ignition of dense coal particle stream, instead of dilute particle stream, was examined under the typical wet-recycle atmosphere in oxy-fuel combustion (26% H₂O). Apart from the combustion of brown coal, the ignition attribute of high rank coal, i.e sub-bituminous and bituminous coal, was also investigated. For brown coal burned in steam-enriched condition, the ignition of dense particle stream was significantly accelerated by 15ms in air-firing and 10ms in oxy-firing mode with 21%O₂, in comparison with the ignition of dilute particle stream. On the other hand, increasing the oxygen concentration from 21% to 31% is insignificant in terms of the ignition for dense particle stream under the steam-enriched combustion condition. Under the similar condition, the ignition of the two high-rank coals was slightly delayed rather than being enhanced, contradicting to that observed in brown coal. From the modeling approach, the water-gas shift reaction, $\text{CO}_{(\text{g})} + \text{H}_2\text{O}_{(\text{g})} \rightarrow \text{CO}_{2(\text{g})} + \text{H}_{2(\text{g})}$, was found influential in hastening the ignition of brown coal as brown coal volatiles are majorly constituted from light hydrocarbon, such as CO. Using the modelling approach as inferred in Section 8.1.3, the contribution of external steam towards char gasification was also calculated. Upon the injection of external steam, the extent of char-steam reaction of brown coal increased by 3%, whereas no improvement was found on sub-bituminous and bituminous coal.

8.2. Practical implications

Some of the findings reported in this thesis can be directly applied in the existing industry sector. Firstly, the unchangeable ignition characteristic upon the injection of clay allows its utilisation in current power plant without burner retrofitting for the purpose of minimising slagging and fouling in the boiler. Secondly, blends of high rank and low-rank coal has been adopted as primary fuels in power stations to reduce electricity generation cost and increase coal availability. Brown coal is proposed as a suitable material for blends due to its low ash and sulphur content. From this research, an oxygen concentration of 30% in oxy-fuel combustion is suggested to achieve a stable heat transfer performance in the boiler and also

improves the ignition of brown coal to that similar in air-firing case. Therefore, brown coal can be used in the blending combustion furnace with minimum cost associated with burner retrofitting. Finally, the wet coal combustion modeling approach developed in this thesis can be applied to improve the accuracy for the prediction of wet coal combustion calculation.

8.3. Recommendation for future research

This study was set out to establish an understanding of the impacts of AAEM and moisture in brown coal on ignition under oxy-fuel combustion mode. Some recommendations are recommended by the author for future investigations.

1. The study on AAEM was focused on the ignition of dilute particle streams. However, most practical combustors implement the combustion of dense particle. It is suggested that additional ignition experiments are performed with the stoichiometric O/C ratio of 1.2, similar to that of the practical furnace. Also, different types of sorbents should be considered as an alternative to clay.
2. The modelling work completed in this thesis was based on hand-written code in MATLAB using 1-dimensional (1D) modelling approach. It will be advantageous if this approach can be extended and implemented into commercial simulation software, such as ANSYS Fluent.
3. The contribution of inherent moisture to char-steam gasification was calculated from the modelling study. This result can be further verified experimentally by the sampling of wet coal char at different locations throughout the furnace to derive its steam gasification kinetics.
4. Extension of the current single-film model char oxidation study by implementation of moving flame-front volatile combustion (MFFVC) model to clarify the role of moisture during volatile combustion.
5. In the wet recycle study, the additional steam was injected tangentially at the side of the furnace. As coal ignition is highly affected by burner aerodynamics, change in steam injection position is likely to produce different ignition characteristic to that shown in this thesis. For future experiments, the author proposes the injection of preheated steam together with the liquid fuel/oxidiser in the flat flame burner to further assess the role of steam on ignition.

6. The water-gas shift reaction has been identified as an influential reaction for wet recycle combustion through theoretical modelling study. The modelling works conducted in Section 8.1.4 can be extended for application in the commercial CFD software. Also, a high-speed thermal imaging camera can be used to further verify the production of H_2 from the water-gas shift reaction.

This page is intentionally left blank

REFERENCES

- ABDUL-GANI, Z. F. 2011. *Ignition behaviour of individual pulverized coal particles in air and oxy-fuel environments*. PhD, The University of Newcastle.
- ABRAHAM, B., ASBURY, J., LYNCH, E., TEOTIA, A. 1982. Coal-Oxygen Process provides Carbon Dioxide for Enhanced Recovery. *Oil Gas Journal*, 80, 68-70.
- ABS. 2011. *Carbon Emissions in Victoria* [Online]. Australia Bureau of Statistics. Available: <http://www.abs.gov.au/ausstats/abs@.nsf/Lookup/by+Subject/1367.0~2011~Main+Features~Carbon+Emissions~3.39> [Accessed 15 August 2015].
- AHN, D. H., GIBBS, B.M., HO, K.H., KIM, J.J. 2001. Gasification kinetics of an Indonesian sub-bituminous coal-char with CO₂ at elevated pressure. *Fuel*, 80, 1651-1658.
- AL-ABBAS, A. H., NASER, J. 2012a. Numerical study of one air-fired and two oxy-fuel combustion cases of propane in a 100 kW furnace. *Energy and Fuels*, 26, 952-967.
- AL-ABBAS, A. H., NASER, J., DODDS, D. 2011. CFD modelling of air-fired and oxy-combustion of lignite in a 100kW furnace. *Fuel*, 90.
- AL-ABBAS, A. H., NASER, J., DODDS, D. 2012b. CFD modelling of air-fired and oxy-fuel combustion in a large-scale furnace at Loy Yang A brown coal power station. *Fuel*, 102.
- AL-MAKHADMEH, L., MAIER, J., SCHEFFKNECHT, G. 2009. Coal pyrolysis and char combustion under oxy-fuel condition. *The 34th international technical conference on coal utilization & fuel systems*. Clearwater, FL.
- ALLARDICE, D. J., CHAFFEE, A. L., JACKSON, R.W., MARSHALL, M. 2004. Water in brown coal and its Removal. In: LI, C. Z. (ed.) *Advances in the science of Victorian brown coal*. Elsevier.
- ALVAREZ, L., GHAREBAGHI, M., POURKASHANIAN, M., WILLIAMS, A., RIAZA, J., PEVIDA, C., PIS, J.J., RUBIERA, F. 2011. CFD modelling of oxy-coal combustion in an entrained flow reactor. *Fuel processing Technology*, 92, 1489-1497.
- ANDERSEN, J., RASMUSSEN, C.L., GISELSSON T., GLARBORG, P. 2009. Global combustion mechanism for use in CFD modelling under Oxy-Fuel conditions. *Energy and Fuels*, 23.
- ANDERSSON, K., BIRKESTAD, H., MAKSINEN, P., JOHNSON, F., STRÖMBERG, L., LYNGBERG, A. 2003a. An 865 MWe lignite-fired power plant with CO₂ capture — a technical feasibility study. *Greenhouse Gas Control Technology*.

REFERENCES

- ANDERSSSEN, K., JOHNSON, F., STORMBERG, L. 2003b. Large scale CO₂ capture — applying the concept of O₂/CO₂ combustion to commercial process data. *VGB Powertech*, 83, 29-33.
- ANDERSSSEN, K., MAKINEN, P. 2002. *Process evaluation of CO₂ free combustion in an O₂/CO₂ power plant*. Master of Science, Chalmers University of Technology.
- ANDERSSON, K., JOHANSSON, R., HJARTSTAM, S., JOHNSON, F., LECKNER, B. 2008a. Radiation intensity of lignite-fired oxy-fuel flames. *Experimental Thermal and Fluid Science*, 33, 67-76.
- ANDERSSON, K., JOHANSSON, R., JOHNSON, F., LECKNER, B. 2008b. Radiation intensity of propane-fired oxy-fuel flames: implications for soot formation. *Energy and Fuels*, 22, 1535-1541.
- ANDERSSON, K., JOHNSON, F. 2007. Flame and radiation characteristics of gas-fired O₂/CO₂ combustion. *Fuel*, 86, 656-668.
- ANHEDEN, M., BURCHHARDT, U., ECKE, H., FABER, R., JIDINGER, O., GIERING, R., KASS, H., LYSK, S., RAMSTRÖM, E. AND YAN, J. 2011. Overview of operational experience and results from test activities in Vattenfall's 30 MWth oxyfuel pilot plant in Schwarze Pumpe. *Energy Procedia*, 4, 941-950.
- ANNAMALAI, K., RAMALINGAM, S.C. 1987. Group combustion of char/carbon particles. *Combustion and Flame*, 70, 307-332.
- ANNAMALAI, K., RAMALINGAM, S.C., DAHDAH, T., CHI, D. 1988. Group combustion of a cylindrical cloud of char/carbon particles. *Journal of Heat Transfer*, 110, 190-200.
- ANSYS, I. 2011. Ansys Fluent Theory Guide. In: ANSYS, I. (ed.). Canonsburg, PA.
- ARTHUR, J. R. 1951. Reactions between carbon and oxygen. *Transac Farad Soc*, 47, 164-78.
- AYLING, A. B., SMITH, I.W. 1972. Measured Temperatures of Burning Pulverized-Fuel Particles, and the Nature of the Primary Reaction Product. *Combustion and Flame*, 18, 173-184.
- BABCOCK, W. 1978. *Steam, Its generation and use*, 39th Ed., New York, USA.
- BADZIOCH, S., HAWKSLEY, P.G.W. 1970. Kinetics of thermal decomposition of pulverized coal particles. *Ind Eng Chem Process Des Develop*, 9, 521-530.
- BAKALI, A. E., DELFAU, J.L., VOVELLE, C. 1998. Experimental Study of 1 Atmosphere, Rich, Premixed n-heptane and iso-octane Flames. *Combustion Science and Technology*, 140, 69-91.
- BARNES, I. 2009. Slagging and fouling in coal-fired boiler. London, UK: IEA Clean Coal Centre.

REFERENCES

- BARTLE, K. D., FITZPATRICK, E.M., JONES, J.M., KUBACKI, M.L., PLANT, R., POURKASHANIAN, M., ROSS, A.B., WILLIAMS, A. 2009. The combustion of droplets of liquid fuels and biomass particles. *4th European Combustion Meeting*. Vienna, Austria.
- BARTON, C. M., GLOE, C.S., HOLDGARE, G.R. 1993. Latrobe Valley, Victoria, Australia: A world class brown coal deposit. *International Journal of Coal Geology*, 23, 193-213.
- BAUKAL, C. E. 1998. Oxygen-enhanced Combustion. Boca Raton, FL: CRC Press.
- BAUM, M. M., STREET, P.J 1971. Predicting the combustion behaviour of coal particles. *Combust Sci Technol*, 3, 231-243.
- BAYARSAIKHAN, B., SONOYAMA, N., HOSOKAI, S., SHIMADA, T., HAYASHI, J., LI, C.Z., CHIBA, T. 2006. Inhibition of Steam Gasification of Char by Volatiles in a Fluidized Bed under Continuous Feeding of a Brown Coal. *Fuel*, 85, 340-349.
- BEASSE, G., CLAIRE, B-W, DAEDEN, S., GRANADOS, L., LOCKWOOD, F., MORESCHINI, P., RIVIERE, M. 2013. Callide Oxyfuel Project Results from the CPU. *Oxyfuel Combustion Conference 3*. Ponferrada, Spain.
- BEER, J. M., CHIGIER, N.A. 1972. *Combustion Aerodynamics*, London, Applied Science Publishers.
- BEJARANO, P. A., LEVENDES, Y.A. 2008. Single coal particle combustion in O₂/N₂ and O₂/CO₂ environments. *Combustion and Flame*, 153, 270-287.
- BERTAGNOLLI, K. E., LUCHT, R.P., BUI-PHAF, M.N. 1998. Atomic hydrogen concentration profile measurements in stagnation-flow diamond forming flames using three-photon excitation laser-induced fluorescence. *Journal of Applied Physics*, 83.
- BINNER, E., ZHANG, L., LI, C.,Z., BHATTACHARYA, S., 2011. In-situ observation of the combustion of air-dried and wet Victorian brown coal. *Proc Combust Inst*, 33, 1739-1746.
- BIOENAREA. 2012. *The Bioenergy System Planners Handbook - BISYPLAN* [Online]. Available: <http://bisoplan.bioenarea.eu/Handbook-intro.html> [Accessed 2 Sep 2015].
- BIRKESTAD, H. 2002. *Separation and compression of CO₂ in an O₂/CO₂-fired power plant*. Master of Science, Chalmers University of Technology.
- BLACK, S., SZUHANSKI, J., PRANZITELLI, A., MA, L., STANGER, P.J., INGHAM, D.B., POURKASHANIAN, M. 2013. Effects of firing coal and biomass under oxy-fuel conditions in a power plant boiler using CFD modelling. *Fuel*, 113, 780-786.
- BORREGO, A. G., ALVAREZ, D. 2007. Comparison of chars obtained under oxy-fuel and conventional pulverized coal combustion atmospheres. *Energy and Fuels*, 21, 3171-3179.

REFERENCES

- BRIX, J., JENSEN, P.A., JENSEN, A.D. 2010. Coal devolatilization and char conversion under suspension fired conditions in O₂/N₂ and O₂/CO₂ atmospheres. *Fuel*, 89, 3373-3380.
- BROCKWAY, D. J., OTTREY, A.L., HIGGINS, R.S. 1991. Inorganic constituent. In: DURIE, R. A. (ed.) *The science of Victorian Brown Coal*. Oxford: Butterworth-Heinemann.
- BUHRE, B. J. P., ELLIOT, L.K., SHENG, C.D., GUPTA, R.P., WALL, T.F. 2005. Oxy-fuel combustion technology for coal-fired power generation. *Progress in Energy and Combustion Science*, 31, 283-307.
- CEN, K., YAO, Q., CAO, X., ZHAO, X., HUANG, Z., ZHOU, J. 1997. *Theory and application of combustion, flow, heat transfer and gasification of coal slurry*, Hangzhou, Zhejiang University Press.
- CHAI, N., KULATILAKA, W.D., NAIK, S.V., LAURENDREAU, N.M, LUCHT, R.P., KUEHNER, J.P., KATTA, V.R., GORD, J.R 2007. Nitric oxide concentration measurements in atmospheric pressure flames using electronic-resonance-enhanced coherent anti-Stokes Raman scattering. *Applied Physics B-lasers and optics*, 88, 141-150.
- CHEN, C., WANG, J., LIU, W., ZHANG, S., YIN, J., LUO, G., YAO, H. 2013. Effect of pyrolysis conditions on the char gasification with mixtures of CO₂ and H₂O. *Proceedings of the Combustion Institute*, 34, 2453-2460.
- CHEN, C. J., NIKSA, S. 1992. Coal devolatilization during rapid transient heating. 1. Primary devolatilization. *Energy and Fuels*, 6, 254-264.
- CHEN, J. C., TANIGUCHI, M., ITO, K. 1995. Observation of laser ignition and combustion of pulverized coal. *Fuel*, 74, 323-330.
- CHEN, L., YONG, S.Z., GHONLEM, A.F. 2012. Oxy-fuel combustion of pulverized coal: Characterization, fundamentals, stabilization and CFD modelling. *Prog Energy Combust Sci*, 38, 156-214.
- CHEN, L., ZENG, C., GUO, X., MAO, Y., ZHANG, Y., ZHANG, X., LI, W., LONG, Y., ZHU, H., EITENEER, B., ZAMANSKY, V. 2010. Gas evolution kinetics of two coal samples during rapid pyrolysis. *Fuel processing Technology*, 91, 848-852.
- CHIU, H. H., LIU, F.M. 1977. Group Combustion of Liquid Droplets. *Combustion Science and Technology*, 17, 127-142.
- CHUI, E. H., DOUGLAS, M.A., TAN, Y. 2003. Modeling of oxy-fuel combustion for a western Canadian sub-bituminous coal. *Fuel*, 82, 1201-1210.
- COATS, A. W., REDFERN, J.P. 1964. Kinetic parameters from thermogravimetric data. *Nature*, 201, 68-9.

REFERENCES

- COLLIS, D. C., AND WILLIAMS, M.J. 1959. Two-dimensional convection from heated wire at low Reynolds Number. *J Fluid Mechs*, 6, 357-384.
- COOK, P. S., CASHION, J.D. 1987. Mossbauer study of iron exchanged into brown coal. *Fuel*, 66, 661-668.
- COPALAKRISHMAN, R., FULLWOOD, M.J., BARTHOLOMEW, C.H. 1994. Catalysis of char oxidation by calcium minerals: Effects of calcium compound chemistry on intrinsic reactivity of doped Spherocharb and Zap chars. *Energy and Fuels*, 8, 984-989.
- COSTA, M., GODOY, S., LOCKWOOD, F.C., ZHOU, J. 1994. Initial stages of the devolatilisation of pulverized-coal in turbulent jet. *Combustion and Flame*, 96, 150-162.
- CRISTINA, G.-T., JIMENEZ, S., BALLESTER, J. 2012. Gasification of a pulverized sub-bituminous coal in CO₂ at atmospheric pressure in an entrained flow reactor. *Combustion and Flame*, 159, 385-395.
- CROISET, E., THAMBIMUTHU, K.V. 2001. NO_x and SO₂ emissions from O₂/CO₂ recycle coal combustion. *Fuel*, 80, 2117-2121.
- CROISET, E., THAMBIMUTHU, K.V., PALMER, A. 2000. Coal combustion in O₂/CO₂ mixtures compared with air. *The Canadian Journal of Chemical Engineering*, 78, 402-407.
- DAI, B., WU, X., DE GIROLAMO, A., ZHANG, L. 2015. Inhibition of lignite ash slagging and fouling upon the use of a silica-based additive in an industrial pulverised coal-fired boiler. Part 1. Changes on the properties of ash deposits along the furnace. *Fuel*, 139, 720-732.
- DAVIDSON, R. M., SANTOS, S. 2010. Oxyfuel combustion of pulverised coal London, UK: IEA Clean Coal Centre.
- DAVISON, J. 2007. Performance and costs of power plants with capture and storage of CO₂. *Energy*, 32, 1163-1176.
- DEGGES, M. J., BOYER, E.J., KUO, K.K., BASINI, L. 2010. Influence of steam on the flammability limits of premixed natural gas/oxygen/steam mixtures. *Chemical Engineering Journal*, 165, 633-638.
- DILLON, D. J., WHITE, V. ALLAM, R.J., WALL, R.A., GIBSON, J. 2005. Oxy-combustion processes for CO₂ capture from power plant. IEA greenhouse gas R&D research and development program.
- DU, X., GOPALAKRISHNAN, C., ANNAMALAI, K. 1995. Ignition and combustion of coal particle streams. *Fuel*, 74, 487-494.
- DUAN, L., ZHAO, C., ZHOU, W., QU, C., CHEN, X. 2009. Investigation on Coal Pyrolysis in CO₂ Atmosphere. *Energy and Fuels*, 23, 3826-3830.

REFERENCES

- EDGE, P., GHAREBAGHI, M., IRONS, R., PORTER, R., PORTER, R.T.J., POURKASHANIAN, M., SMITH, D., STEPHENSON, P., WILLIAMS, A. 2011. Combustion modelling opportunities and challenges for oxy-coal carbon capture technology. *Chemical Engineering Research and Design*, 89.
- EIA, U. S. 2010. International Energy Outlook 2010. Washington, DC 20585: U.S Energy Information Administration.
- EL-RUB, Z. A., BRAMER, E.A., BREM, G. 2004. Evaluation of catalysts for tar-elimination in biomass gasification processes. *Industrial & Engineering Chemistry Research*, 43, 6911-6919.
- ESSENHEIGH, R. H., MISRA, M.K., SHAW, D.W. 1989. Ignition of Coal Particles: A Review. *Combustion and Flame*, 44, 3-30.
- FEI, H., HU, S., XIANG, J., SUN, L., FU, P., CHEN, G. 2011. Study on coal chars combustion under O₂/CO₂ atmosphere with fractal random pore model. *Fuel*, 90, 441-448.
- FIELD, M. A. 1969. Rate of combustion of size graded fractions of char from a low-rank coal between 1200K and 2000K. *Combustion and Flame*, 13, 237-252.
- FLETCHER, T. H., BARFUSS, D., PUGMIRE, R.J. 2015. Modeling Light Gas and Tar Yields from Pyrolysis of Green River Oil Shale Demineralized Kerogen Using the Chemical Percolation Devolatilization Model. *Energy and Fuels*, 29, 4921-4926.
- FOLGUERAS, M. B., ALONSO, M., DIAZ, R.M. 2013. Influence of sewage sludge treatment on pyrolysis and combustion of dry sludge. *Energy*, 2013, 426-435.
- FRANKLIN, H. D., PETER, W.A., HOWARD, J.B. 1982. Mineral matter effects on the rapid pyrolysis and hydropyrolysis of a bituminous coal. 1. Effects on yield of char, tar and light gaseous Volatiles. *Fuel*, 61, 155-160.
- GALE, T. K., WENDT, O.L. 2002. High-temperature interactions between multiple-metals and kaolinite. *Combustion and Flame*, 131, 299-307.
- GEIER, M., SHADDIX, C.R., DAVIS, K.A., SHIM, H.S. 2012. On the use of single-film models to describe the oxy-fuel combustion of pulverized coal char. *Applied Energy*, 93, 675-679.
- GIBBINS-MATHAM, J., KANDIYOTI, R. 1988. Coal pyrolysis yields from fast and slow heating in a wire-mesh apparatus with a gas sweep. *Energy and Fuels*, 2, 505-511.
- GLARBORG, P., BENTZEN, L.L.B. 2008. Chemical effects of a high CO₂ concentration in Oxy-fuel combustion of methane. *Energy Fuels*, 22, 291-6.
- GLOBAL_CCS_INSTITUTE 2012. Global Status of CCS: 2012. Canberra, ACT, Australia.

REFERENCES

- GORDON, C. 2006. Ash management in coal-fired power plant. London, UK: IEA Clean Coal Centre.
- GRANT, D. M., PUGMIRE, R.J., FLETCHER, T.H., KERSTEIN, A.R. 1989. Chemical percolation model of coal devolatilization using percolation lattice statistics. *Energy and Fuels*, 3, 175-186.
- GSSCI 2009. Strategic Analysis of the Global Status of Carbon Capture and Storage, Report 2: Economic Assessment of Carbon Capture and storage technologies. Canberra, Australia: Global CCS Institute.
- GUAN, Q. L., BI, D.P., XUAN, W.W., ZHANG, J.S. 2015. Kinetic model of hydropyrolysis based on the CPD model. 152.
- GUPTA, R. P., GURURAJAN, V.S., LUCAS, J., WALL, T.F. 1990. Ignition temperature of pulverised coal paricles: Experimental techniques and coal related influences. *Combustion and Flame*, 79, 333-339.
- GUPTA, R. P., WALL, T.F. 1985. The optical properties of fly ash in coal fired furnaces. *Combustion and Flame*, 61, 145-151.
- GUPTA, R. P., WALL, T.F., BAXTER, L. 1999. *Impact of Mineral Impurities in Solid Fuel Combustion*, New York, Kluwer Academic/Plenum.
- GURURAJAN, V. S., WALL, T.F., GUPTA, R.P., TRUELOVE, J.S. 1990. Mechanisms for the Ignition of Pulverized Coal Particles. *Combustion and Flame*, 81, 119-132.
- HACKETT, L. 2015. *Helping to Seed a CCS Industry: The White Rose CCS Project* [Online]. Available: <http://cornerstonemag.net/helping-to-seed-a-ccs-industry-the-white-rose-ccs-project/> [Accessed 31 August 2015].
- HARRIS, A., ZHONG, Z. 2008. Non-isothermal thermogravimetric analysis of plywood wastes under N₂, CO₂ and O₂ atmosphere. *Asia Pacific Journal of Chemical Engineering*, 3, 474-480.
- HASEGAWA, T. 2013. Development of semiclosed cycle gas turbine for oxy-fuel IGCC power generation. In: BENINI, E. (ed.) *Progress in Gas Turbing Performance*. InTech.
- HAYASHI, J., MIURA, K. 2004. Pyrolysis of Victorian brown coal. In: LI, C. Z. (ed.) *Advances in the Science of Victorian Brown Coal*. Elsevier.
- HAYASHI, J., NORINAGA, K., YAMASHITA, T., CHIBA, T. 1999. Effect of sorbed water on conversion of coal by rapid pyrolysis. *Energy Fuels*, 13, 611-6.
- HAYNES, W. M. 2014. *CRC Handbook of Chemistry and Physics 94th Edition*, CRC Press.

REFERENCES

-
- HETCH, E. S., SHADDIX, C.R., GEIER, M., MOLINA, A., HAYNES, B.S. 2012. Effect of CO₂ and steam gasification reactions on the oxy-combustion of pulverized coal char. *Combust Flame*, 159, 3437-3447.
- HETCH, E. S., SHADDIX, C.R., MOLINA, A., HAYNES, B.S. 2011. Effect of CO₂ gasification reactions on oxy-combustion of pulverized coal char. *Proc Combust Inst*, 33, 1699-1706.
- HJARTSTAM, S., ANDERSSON, K., JOHNSON, F., LECKNER, B. 2009. Combustion characteristics of lignite-fired oxy-fuel flames. *Fuel*, 88, 2216-2224.
- HORN, F. L., STEINBERG, M., 1982. Control of Carbon Dioxide Emissions from a Power Plant (and use in Enhanced Oil Recovery). *Fuel*, 61, 415-422.
- HOWARD, J. B., ESSENHEIGH, R.H. 1967. Mechanism of solid-particle combustion with simultaneous gas-phase volatiles combustion. *Proc Combust Inst*, 11.
- HU, S., ZENG, D., SAYRE, A.N., SARV, H. 2011. Effect of Moisture on Char burnout during warm-recycle oxy-fuel combustion. Babcock & Wilcox power generation group.
- HUO, W., ZHOU, Z., CHEN, X., DAI, Z., YU, G. 2014a. Study on CO₂ gasification reactivity and physical characteristics of biomass, petroleum coke and coal chars. *Biosource Technology*, 159, 143-149.
- HUO, W., ZHOU, Z., WANG, F., WANG, Y., YU, G. 2014b. Experimental study of pore diffusion effect on char gasification with CO₂ and steam. *Fuel*, 131, 59-65.
- IEO 2011. International Energy Outlook 2011. U.S. Department of Energy.
- IPCC 2005. IPCC Special Report on Carbon Dioxide Capture and Storage. . In: WORKING GROUP III OF THE INTERGOVERNMENTAL PANEL ON CLIMATE CHANGE [METZ, B., O. DAVIDSON, H. C. DE CONNICK, M. LOOS, AND L. A. MEYER] (ed.). Cambridge, United Kingdom and New York, NY, USA.
- JAMIL, K., HAYASHI, J.-I., LI, C.Z. 2004. Pyrolysis of a Victorian brown coal and gasification of nascent char in CO₂ atmosphere in a wire mesh reactor. *Fuel*, 83, 833-843.
- JIANG, H., RADOVIC, L.R. 1991. A transient kinetic studies of char gasification in carbon dioxide and oxygen. *Energy and Fuels*, 5, 68-74.
- JONES, W. P., LINDSTEDT, R.P. 1988. Global reaction schemes for hydrocarbon combustion. *Combustion and Flame*, 73, 233-249.
- JOUTSENOJA, T., STENBERG, J., HERBERG, R., AHO, M. 1997. Pyrometric measurement of the temperature and size of individual combusting fuel particles. *Applied Optics*, 36, 1525-1535.

REFERENCES

- JOVANOVIC, R., MILEWSKA, A., SWIATKOWSKI, B., GOANTA, A., SPLIETHOFF, H. 2011. Numerical investigation of influence of homogeneous/heterogeneous ignition/combustion mechanisms on ignition point position during pulverized coal combustion in oxygen enriched and recycled flue gas atmosphere. *International journal of mass transfer*, 54, 921-931.
- JUNG, K., STANMORE, B.,R. 1980. Fluidised bed combustion of wet brown coal. *Fuel*, 59, 74-80.
- KAJITANI, S., TAY, H.L., ZHANG, S., LI, C.Z. 2010. Kinetics of steam gasification of brown coal and volatile-char interactions. In: BIGGS, M. J. (ed.) *Chemeca*. Adelaide, SA: ICMS Pty Ltd.
- KANNICHE, M., GROS-BONNIVARD, R., JAUD, P., VALLE-MARCOS, J., AMANN, J., -M., BOUALLOU, C. 2010. Pre-combustion, post-combustion and oxy-combustion in thermal power plant for CO₂ capture. *Applied Thermal Engineering*, 30, 53-62.
- KHARE, S. P., WALL, T.F., FARIDA, A.Z., LIU, Y., MOGHTADERI, B., GUPTA, R.P. 2008. Factors influencing the ignition of flames from air-fired swirl pf burners retrofitted to oxy-fuel. *Fuel*, 87, 1042-1049.
- KHATAMI, R., LEVENDIS, Y.A. 2011. On the deduction of single coal particle combustion temperature from three-color optical pyrometry. *Combustion and Flame*, 158, 1822-1836.
- KHATAMI, R., STIVERS, C., JOSHI, K., LEVENDIS, Y.A., SAROFIM, A.F. 2012a. Combustion behavior of single particles from three different coal ranks and from sugar cane bagasse in O₂/N₂ and O₂/CO₂ atmospheres. *Combustion and Flame*, 159, 1253-1271.
- KHATAMI, R., STIVERS, C., LEVENDIS, Y.A. 2012b. Ignition characteristics of single coal particles from three different ranks in O₂/N₂ and O₂/CO₂ atmospheres. *Combust Flame*, 159, 3554-68.
- KIGA, T., TAKANO, S., KIMURA, N., OMATA, K., OKAWA, M., MORI, T., KATO, M. 1997. Characteristics of pulverized-coal combustion in the system of oxygen/recycled flue gas combustion. *Energy Conversion and Management*, 38, S129-S134.
- KIM, D., CHOI, S., SHADDIX, C.R., GEIER, M. 2014a. Effect of CO₂ gasification reaction on char particle combustion in oxy-fuel conditions. *Fuel*, 120, 130-140.
- KIM, J. D., KIM, G.B., CHANG, Y.J., SONG, J.H., JEON, C.H. 2010. Examination of flame length for burning pulverized coal in laminar flow reactor. *Jour Mech Sci Technol*, 24, 2567-2575.
- KIM, R. G., LI, D., JEON, C.H. 2014b. Experimental investigation of ignition behavior for coal rank using a flat flame burner at a high heating rate. *Experimental Thermal and Fluid Science*, 54, 212-218.

REFERENCES

- KIMURA, N., OMATA, K., KIGA, T., TAKANO, S., SHIKISIMA, S. 1995. The characteristics of pulverized coal combustion in O₂/CO₂ mixtures for CO₂ recovery. *Energy Conversion and Management*, 36, 805-808.
- KOBAYASHI, H., HOWARD, J.B., SAROFIM, A.F. 1977. Coal devolatilization at high temperatures. *Symposium International on Combustion*, 16, 411-425.
- KOMAROVA, E., GUHL, S., MEYER, B. 2015. Brown coal char CO₂-gasification kinetics with respect to the char structure. Part I: Char structure development. *Fuel*, 152, 38-47.
- KOSMINSKI, A., ROSS, D.P., AGNEW, J.B. 2006. Reactions between sodium and kaolin during gasification of a low-rank coal. *Fuel processing Technology*, 87, 1051-1062.
- KULATILAKA, W. D., LUCHT, R. P., HANNA, S. F., KATTA, V. R. 2004. Two-color, two-photon laserinduced polarization spectrometry (LIPS) measurements of atomic hydrogen in nearadiabatic, atmospheric hydrogen/air flames. *Combustion and Flame*, 137, 523-537.
- KUROSE, R., TSUJI, H., MAKINO, H. 2001. Effect of moisture in coal on pulverized coal combustion characteristics. *Fuel*, 80, 1457-65.
- LAW, C. K. 2006. Combustion Physics. Cambridge: Cambridge University Press.
- LEI, C., ZOU, C. , LIU, Y., ZHOU, K., HAN, Q., ZHENG, C 2014. Numerical and experimental studies on the ignition of pulverized coal in O₂/H₂O atmospheres. *Fuel*, 139, 198-205.
- LI, C. Z. 2004. Advance in the science of Victorian brown coal. Elsevier.
- LI, J., QUEROL, X., ZHUANG, X., FONT, O. 2011. Comparative study of coal qualities from three large coal basins in Xinjiang, Northwest China. *31st meeting of the Spanish Mineralogy Society (SEM)*. Barcelona, Spain: Spanish Mineralogy Society.
- LI, Q., ZHAO, C., CHEN, X., WU, W., LI, Y. 2009. Comparison of pulverized coal combustion in air and in O₂/CO₂ mixtures by thermo-gravimetric analysis. *Journal of Analytical and Applied Physics*, 85, 521-528.
- LI, X. C., RATHNAM, R.K., YU, J.L., WANG, Q., WALL, T.F., MEESRI, C. 2010. Pyrolysis and Combustion Characteristics of an Indonesian Low-Rank Coal under O₂/N₂ and O₂/CO₂ Conditions. *Energy and Fuels*, 24, 160-164.
- LIU, H. 2009. Combustion of coal chars in O₂/CO₂ and O₂/N₂ mixtures: a comparative study with non-isothermal thermogravimetric analyzer (TGA) tests. *Energy and Fuels*, 23, 4278-4285.
- LIU, H., ZAILANI, R., GIBBS, B.M. 2005a. Comparison of Pulverized Coal Combustion in Air and in Mixture of O₂/CO₂. *Fuel*, 84.

REFERENCES

- LIU, H., ZAILANI, R., GIBBS, B.M. 2005b. Pulverized Coal Combustion in Air and in O₂/CO₂ mixtures with NO_x Recycle. *Fuel*, 84, 2109-2115.
- LIU, L., CAO, Y., LIU, Q.C. 2015. Kinetics studies and structure characteristics of coal char under pressurized CO₂ gasification conditions. *Fuel*, 146, 103-110.
- LIU, M. Q., LIU, J.Z., YU, Y.J., WANG, Z.H., ZHOU, J.H., CEN, K.F. 2012. Investigation of Lignite Combustion Characteristics with Thermal Analysis. *Advanced Materials Research*, 614-615, 25-30.
- LIU, Q., HU, H., ZHOU, Q., ZHU, S., CHEN, G. 2004. Effect of inorganic matter on reactivity and kinetics of coal pyrolysis. *Fuel*, 83, 713-718.
- LIU, Y., GEIER, M., MOLINA, A., SHADDIX, C. 2011. Pulverized coal stream ignition delay under conventional and oxy-fuel combustion conditions. *International Journal of Greenhouse Gas Control*, 5S, S36-S46.
- LOCKWOOD, F. C., MAHMUD, T., YEHIA, M.A. 1998. Simulation of pulverised coal test furnace performance. *Fuel*, 77, 1329-1337.
- LOWE, A. J., MCCAFFREY, D.J.A., RICHARDS, D.G. 1993. An investigation into the effectiveness of fireside fuel additives. *Fuel processing Technology*, 36, 47-53.
- LUCAS, J. A., WALL, T.F. 1994. Volatile matter release, particle/cloud ignition, and combustion of near-stoichiometric suspensions of pulverized coal. *Twenty-fifth Symposium (International) on Combustion*. The Combustion Institute.
- MAFFEI, T., KHATAMI, R., PIERUCCI, S., FARAVELLI, T., RANZI, E., LEVENDIS, Y.A. 2013. Experimental and modeling study of single coal particle combustion in O₂/N₂ and Oxy-fuel (O₂/CO₂) atmospheres. *Combustion and Flame*, 160, 2559-2572.
- MARIN, O., CHATEL-PELAGE, F., PERRIN, N., CHEN, S., LU, Q., ROSTAM-ABADI, M. 2003. Economic analysis of oxygen-fired coal boiler. *28th international conference on coal utilisation & fuel systems*. Clearwater, FL.
- MATSUOKA, K., KAJIWARA, D., KURAMOTO, K., SHARMA, A., SUZUKI, Y. 2009. Factor affecting steam gasification rate of low rank coal in a pressurized fluidized bed. *Fuel Process Technol*, 90, 895-900.
- MATSUOKA, K., MA, Z.X., AKIHO, H., ZHANG, Z.G., TOMITA, A. 2003. High-pressure coal pyrolysis in a drop tube furnace. *Energy and Fuels*, 17, 984-990.
- MCDONALD, D. K., ESTOPINAL, M., MUALIM, H. 2012. FutureGen 2.0: Where are we now? *Clearwater Clean Coal Conference*. Clearwater, Florida, U.S.A.
- MCDONALD, D. K., FLYNN, T.J., DEVAULT, D.J., VARAGANI, R., LEVESQUE, S., CASTOR, W. 2008. 30 MW_t Clean Environment Development of Oxy-Coal Combustion Test Program. *The 33rd International Technical Conference on Coal Utilization and Fuel System*. Clearwater, Florida.

REFERENCES

- MCINTOSH, M., J. 1976a. Mathematical model of drying in a brown coal mill system. 1. Formulation of model. *Fuel*, 55, 47-52.
- MCINTOSH, M., J. 1976b. Mathematical model of drying in a brown coal mill system. 2. Testing of model. *Fuel*, 55, 53-8.
- MCLEAN, W. J., HARDESTY, D.R., POHL, J.H. 1981. Direct observations of devolatilizing pulverized coal particles in a combustion environment. *Symposium International on Combustion*, 18.
- MENDES, D., MENDES, A., MADEIRA, L.M., IULIANELLI, A., SOUSA, J.M., BASILE, A. 2010. The water-gas shift reaction: from conventional catalytic system to Pd-based membrane reactors-a review. *Asia Pacific Journal of Chemical Engineering*, 5, 111-137.
- MERRELL, G. A. 1984. *Method of conditioning fireside fouling deposits using large particle size amorphous silica*
- MITCHELL, R. E. 1987. Experimentally determined overall burning rates of coal chars. *Combust Sci Technol*, 53, 165-86.
- MITCHELL, R. E., KEE, R.J., GLARBORG, P., COLTRIN, M.E., 1991. The effect of CO conversion on the boundary layers surrounding pulverized coal-char particles. *Proc Combust Inst*, 23, 1169-76.
- MITCHELL, R. E., MA, L., KIM, B.J. 2007. On the burning behavior of pulverized coal chars. *Combustion and Flame*, 151, 426-436.
- MOLINA, A., HECHT, E.S., SHADDIX, C.R. 2009. Ignition of a group of coal particles in oxyfuel combustion with CO₂ recirculation. *Proceedings of AIChE Conference*, 31, 1905-1912.
- MOLINA, A., SHADDIX, C., 2007. Ignition and devolatilisation of pulverized bituminous coal particles during oxygen/carbon dioxide coal combustion. *Proceedings of the Combustion Institute*, 31, 1905-1912.
- MOLLMAN, K. P., PINNO, F., VOLLMER, M. 2010. Two-Color or Ratio Thermal Imaging - Potentials and Limits. *FLIR Technical Series*. FLIR.
- MORGAN, M., JEKINS, R.G. 1986. Pyrolysis of a lignite in an entrained flow reactor: 1. Effect of cations on total weight loss. *Fuel*, 65, 757-768.
- MURPHY, J. J., SHADDIX, C.R. 2006. Combustion kinetics of coal chars in oxygen-enriched environments. *Combust Flame*, 144, 710-729.
- NIKSA, S. 1994. FLASHCHAIN Theory for rapid coal devolatilisation kinetics. 4. Predicting ultimate yields from ultimate analysis alone. *Energy and Fuels*, 8, 659.

REFERENCES

-
- NOZAKI, T., TAKANO, S., KIGA, T. 1996. Analysis of the Flame Formed during Oxidation of Pulverized Coal by an O₂-CO₂ Mixture. *Energy*, 22, 199-205.
- NSAKALA, N. Y., MARION, J., BOZZUTO, C., LILJEDAHL, G., PALKES, M., VOGEL, D., ET AL 2001. Engineering feasibility of CO₂ capture on an existing us coal-fired power plant. *First national conference on carbon sequestration*. Washington DC.
- NUSSELT, W. Z. 1924. VDI. 68, 124.
- OKAWA, M., KIMURA, N., KIGA, T., TAKANO, S., ARAI, K., KATO, M. 1997. Trial design for a CO₂ recovery power plant by burning pulverized coal in O₂/CO₂. *Energy Conservation Management*, 38 (Suppl.), S123-S127.
- OSBORN, G. A. 1992. Review of sulphur and chlorine retention in coal-fired boiler deposits. *Fuel*, 71, 131-142.
- OSSWALD, P., STRUCKMEIR, U., KASPER, T., KOHSEHOINGHAUS, K., WANG, J., COOL, T.A., HANSEN, N., WESTMORELAND, P.R. 2007. Isomer-Specific Fuel Destruction Pathways in Rich Flames of Methyl Acetate and Ethyl Formate and Consequences for the Combustion Chemistry of Esters. *Journal of Physical Chemistry*, 111, 4093-4101.
- OTTO, K. L., B., AND SHELEF, M., 1979. Catalysis of Carbon-Steam gasification by Ash Components from Two lignites. *Fuel*, 58, 85-91.
- PATEL, M. M., DANA, T.G., YOUNG B.C. 1988. Combustion rates of lignite char by TGA. *Fuel*, 67, 165-169.
- PAYNE, R., CHEN, S.L., WOLSKY, A.M., RICHTER, W.F. 1988. CO₂ Recovery via Coal Combustion in Mixtures of Oxygen and Recycled Flue Gas. *Combustion Science and Technology*, 67, 1-16.
- PONZIO, A., SENTHOORSELVAN, S., YANG, W., BLASIAK, W., ERIKSSON, O 2008. Ignition of single coal particles in high-temperature oxidizers with various oxygen concentrations. *Fuel*, 87, 1489-1497.
- PRATIONO, W., ZHANG, J., ABBAS, H.A.A., WU, X., CHEN, X.D., ZHANG, L. 2014. Influence of External Clay and Inherent Minerals on Lignite Optical Ignition and Volatile Flame Propagation in Air-Firing and Oxy-Firing. *Industrial & Engineering Chemistry Research*, 53, 2594-2604.
- PRATIONO, W., ZHANG, J., CUI, J., WANG, Y., ZHANG, L. 2015a. Clarifying the influence of moisture on the ignition and combustion of wet Victorian brown coal in air-firing and oxy-fuel modes: Part 2: Contribution of gasification reaction to char oxidation rate. *Fuel Processing Technology*.
- PRATIONO, W., ZHANG, J., CUI, J., WANG, Y., ZHANG, L. 2015b. Influence of Inherent Moisture on the Ignition and Combustion of Wet Victorian Brown Coal in Air-Firing

REFERENCES

- and Oxy-Fuel Modes: Part 1: Volatile Ignition and Flame Propagation. *Fuel Process Technol.*
- PRUCKER, S., MEIER, W., STRICKER, W. 1994. A flat flame burner as calibration source for combustion research-temperatures and species concentrations of premixed H₂/air flames. *Review of Scientific Instruments*, 65, 2908-2911.
- QIAO, Y., ZHANG, L., BINNER, E., XU, M., LI, C.Z. 2010. An investigation of the causes of the difference in coal particle ignition temperature between combustion in air and in O₂/CO₂. *Fuel*, 89, 3381-3387.
- QUYN, D. M., WU, H., HAYASHI, J.I., LI, C.Z. 2003. Volatilisation and catalytic effects of alkali and alkaline earth metallic species during the pyrolysis and gasification of Victorian brown coal. Part IV. Catalytic effect of NaCl and ion-exchangeable Na in coal on char reactivity. *Fuel*, 82, 587-593.
- RAASK, E. 1985. Mineral impurities in coal combustion , behaviour , problem and remedial measures. Washington, DC: Hemisphere Publishing Corporation.
- RATHNAM, R. K., ELLIOTT, L.K., WALL, T.F., LIU, Y., MOGHTADERI, B. 2009. Differences in reactivity of pulverized coal in air (O₂/N₂) and oxy-fuel(O₂/CO₂) conditions. *Fuel Process Technol*, 90, 797-802.
- REHFELDT, S., KUHR, C., EHMANN, M., BERGINS, C., SCHEFFKNECHT, G., MAIER, J. 2009. Basic experiments and CFD calculations of air and oxyfuel firing of lignite and bituminous coals in 0.5 and 1MW scale combustion test facilities. 34th *International Technical Conference on Clean coal and fuel systems*. Clearwater, FL.
- RIAZA, J., ALVAREZ, L., GIL, M., V., PEVIDA, C., PIS, J., J., RUBERIA, F. 2011. Effect of oxy-fuel combustion with steam addition on coal ignition and burnout in an entrained flow reactor. *Energy*, 36, 5314-5319.
- RIAZA, J., KHATAMI, R., LEVENDIS, Y.A., ALVAREZ, L., GIL, M.V., PEVIDA, C., RUBIERA, F., PIS, J.J. 2014. Single particle ignition and combustion of anthracite, semi-anthracite and bituminous coals in air and simulated oxy-fuel conditions. *Combustion and Flame*, 161, 1096-1108.
- ROBERTS, D. G., HARRIS, D.J. 2000. Char Gasification with O₂, CO₂, and H₂O: Effects of Pressure on Intrinsic Reaction Kinetics. *Energy and Fuels*, 14, 483-489.
- ROBERTS, D. G., HARRIS, D.J. 2014. Char Gasification Kinetics in Mixtures of CO₂ and H₂O: The Role of Partial Pressure in Determining the Extent of Competitive Inhibition. *Energy and Fuels*, 28, 7643-7648.
- RUIZ, M., ANNAMALAI, K., DAHDAH, T. 1990. An experimental study on group ignition of coal particle streams. In: GROSSHANDLER, W. L., SEMERJIAN, H.G. (ed.) *Heat and mass transfer in fires and combustion systems*. Dallas, Texas: The American society of chemical engineers.

REFERENCES

-
- SAITO, M., SADAKATA, M., SATO, M., SOUTOME, T., MURATA, H., OHNO, Y. 1991. Combustion rates of pulverized coal particles in high-temperature/high-oxygen concentration atmosphere. *Combustion and Flame*, 87, 1-12.
- SANDARS, G. A., JONES, C.K.S. Study of the gasification of various Victorian brown coals by the non-isothermal thermo-gravimetric measurement. Proc Aust Coal Science Conf, 1984 Churchill, Victoria. 98-105.
- SANTOS, S., HAINES, M. 2005. Oxy-fuel combustion application for coal-fired power plant. Cottbus, Germany: IEA Greenhouse Gas R&D Programme.
- SAROFIM, A. F. 2007. Oxy-fuel combustion: Progress and remaining issues. *2nd workshop on International Oxy-combustion research network*. Windsor, CT, USA.
- SAXENA, S. C. 1971. Transport properties of gases and gaseous mixtures at high temperatures. *High Temp Sci*, 3, 168-88.
- SCHEFFKNECHT, G., LEEMA, A-M, SCHNELL, U., MAIER, J. 2011. Oxy-fuel Coal Combustion- A Review of the Current State-of-the-Art. *International Journal of Greenhouse Gas Control*, 5S, S16-S35.
- SCHIEHMANN, M., SCHERER, V., WIRTZ, S. 2009. Optical coal particle temperature measurements under oxy-fuel conditions: Measurement methodology and initial results. *Chemical Engineering Technology*, 32, 2000-2004.
- SERIO, M. A., HAMBLIN, D.G., MARKHAM, J.R., SOLOMON, P.R. 1987. Kinetics of volatile product evolution in coal pyrolysis: experiment and theory. *Energy and Fuels*, 1, 138-152.
- SGV. 2015. *Victoria's Earth Resources: Coal* [Online]. Victoria State Government. Available: <http://www.energyandresources.vic.gov.au/earth-resources/victorias-earth-resources/coal> [Accessed 15 August 2015].
- SHADDIX, C., MOLINA, A. 2009. Particle imaging of ignition and devolatilisation of pulverized coal during oxy-fuel combustion. *Proc Combust Inst*, 32, 2091-2098.
- SHADDIX, C., MOLINA, A. 2011. Ignition, flame stability, and char combustion in oxy-fuel combustion. In: ZHENG, L. (ed.) *Oxy-fuel combustion for power generation and carbon dioxide (CO₂) capture*. Cambridge, UK: Woodhead Publishing Limited.
- SHADDIX, C., MURPHY, J.J. 2003. Coal char combustion reactivity in oxy-fuel applications. *20th Pittsburgh Coal Conference*. Pittsburgh, PA.
- SHADDIX, C. R. 1999. Correcting thermocouple measurements for radiation loss: A critical review. *33rd National Heat Transfer Conference* Albuquerque, NM: American Society of chemical Engineer.

REFERENCES

- SHAH, K., ELLIOTT, L., SPORL, R., BELO, L., WALL, T.F. 2014. Coal quality impacts and gas quality control in oxy-fuel technology for carbon capture and storage – cost impacts and coal value. Australia: The University of Newcastle.
- SHAN, J. 2011. Oxy-Coal Burner Design for Utility Boilers. In: ZHENG, L. (ed.) *Oxy-Fuel Combustion for Power Generation and Carbon Dioxide (CO₂) Capture*. Cambridge, UK: Woodhead Publishing Limited.
- SINGH, D., CROISSET, E., DOUGLAS, P.L., DOUGLAS, M.A. 2003. Techno-economic study of CO₂ capture from an existing coal-fired power plant: MEA scrubbing Vs. O₂/CO₂ recycle combustion. *Energy Conservation Management*, 44, 3073-3091.
- SIVATHANU, Y. R., FAETH, G.M. 1990. Generalized state relationships for scalar properties in non-premixed hydrocarbons/air flames. *Combustion and Flame*, 82, 211-230.
- SMITH, I. W. 1971. Kinetics of combustion of size-graded pulverized fuels in the temperature range 1200-2270K. *Combust Flame*, 17, 303-14.
- SMITH, I. W. 1982. The combustion rates of coal chars: a review. *Nineteenth Symposium (International) on Combustion/The Combustion Institute*, 1045-1065.
- SMITH, J. P., SMOOT, D.L. 1980. One-dimensional model for pulverized-coal combustion and gasification. *Combust Sci Technol*, 23, 17-31.
- SMOOT, L. D. 1984. Modelling of coal-combustion process. *Progress in Energy and Combustion Science*, 10, 229-267.
- SOLOMON, P. R., FLETCHER, T.H 1994. Impact of coal pyrolysis on Combustion. *Symposium International on Combustion*, 25, 463-474.
- SOLOMON, P. R., FLETCHER, T.H., PUGMIRE, R.J. 1993. Progress in coal pyrolysis. *Fuel*, 72, 587-597.
- STARK, A. K., BATES, R.B., ZHAO, Z.L., GHONIEM, A.F. 2015. Prediction and Validation of Major Gas and Tar Species from a Reactor Network Model of Air-Blown Fluidized Bed Biomass Gasification. *Energy and Fuels*, 29, 2437-2452.
- STEVENSON, A. J., THOMAS, R.G., EVAN, D.G. 1973. Modelling the ignition of brown-coal particles. *Fuel*, 52, 281-287.
- STIVERS, C., LEVENDIS, Y.A. 2010. Ignition of single coal particles in O₂/N₂/CO₂ atmospheres. *The 35th international technical conference on clean coal & fuel systems*. Clearwater, FL.
- STURGEON, D. W., CAMERON, E.D., FITZGERALD, F.D. 2009. Demonstration of an oxyfuel combustion system. *Energy Procedia*, 1, 471-478.

REFERENCES

- TANIGUCHI, M. 2012. Fundamental experiments of coal ignition for engineering design of coal power plants. In: RASUL, M. (ed.) *Thermal Power Plants*. Rijeka, Croatia: Intech.
- TANIGUCHI, M., OKAZAKI, H., KOBAYASHI, H., AZAHATA, S., MIYADERA, H., MUTO, H., TSUMURA, T. 2001. Pyrolysis and ignition characteristics of pulverized coal particles. *Transactions of the ASME*, 123, 32-38.
- TEWARSON, A. 1995. *SFPE Handbook of Fire protection engineering*, 2nd ed., Quincy, MA, National Fire Protection Association.
- THIMSEN, D., WHEELDON, J., DILLON, D. 2011. Economic comparison of oxy-coal carbon dioxide (CO₂) capture and storage (CCS) with pre- and post-combustion CCS. In: ZHENG, L. (ed.) *Oxy-fuel combustion for power generation and carbon dioxide (CO₂) capture*. Cambridge, UK: Woodhead Publishing Limited.
- TIMOTHY, L. D., SAROFIM, A.F., BEER, J.M. 1982. Characteristic of single particle coal combustion *Nineteenth Symposium (International) on Combustion/The Combustion Institute*, 1123-1130.
- TOFTEGAARD, M. B., BRIK, J., JENSEN, P.A., GLARBORG, P., JENSEN, A.D. 2010. Oxy-fuel combustion of solid fuels. *Progress in Energy and Combustion Science*, 36, 581-625.
- TOGNOTTI, L., LONGWELL, J.P., SAROFIM, A.F. 1990. The products of the high temperature oxidation of a single char particle in an electrodynamic balance. *Proceedings of the Combustion Institute*, 23, 1207-1213.
- TOGNOTTI, L., MALOTTI, A., PETARCA, L., ZANELLI, S. 1985. Measurement of Ignition Temperature of Coal Particles Using a Thermogravimetric Technique. *Combustion Science and Technology*, 44, 15-28.
- TOMITA, A., OHTSUKA, Y. 2004. Gasification and combustion of brown coal. In: ZHU, L. C. (ed.) *Advances in the Science of Victorian Brown Coal*. Oxford: Elsevier Ltd.
- TSUJI, H. 2003. High temperature air combustion: from energy conservation to pollution reduction. Boca Raton, FL: CRC Press.
- URNS, S. R. 2000. *An introduction to combustion: concepts and applications*, 2nd ed, Boston, McGraw-Hill.
- UBHAYAKAR, S. K., STICKLER, D.B., VON ROSENBERG, C.W., GANNON, R.E. 1977. Rapid devolatilization of pulverized coal in hot combustion gases. *Symposium International on Combustion*, 16, 427-436.
- VARAGANI, R. K., CHÂTEL-PÉLAGE, F., PRANDA, P., ROSTAM-ABADI, M., LU, Y., BOSE, A.C. 2005. Performance simulation and cost assessment of oxy-combustion

REFERENCES

- process for CO₂ capture from coal-fired power plants. *The fourth annual conference on carbon sequestration*. Alexandria, VA.
- VARHEGYI, G., TILL, F. 1999. Comparison of temperature-Programmed char combustion in CO₂-O₂ and Ar-O₂ mixtures at elevated pressure. *13*.
- VUTHALURU, H. B., DOMAZETIS, G., WALL, T.F., VLEESKENS, J.M. 1996. Reducing fly ash deposition by pretreatment of brown coal: Effect of aluminum on ash character. *Fuel processing Technology*, 46, 117-132.
- WALL, T., ET AL. 2009. An overview on oxyfuel coal combustion- State of the art research and technology development. *Chemical Engineering Research and Design*, 87, 1003-1016.
- WALL, T., F. 2007. Combustion processes for carbon capture. *Proceedings of the Combustion Institute*, 31, 31-47.
- WALL, T., STANGER, R., SANTOS, S. 2011. Demonstrations of coal-fired oxy-fuel technology for carbon capture and storage and issues with commercial deployment. *International Journal of Greenhouse Gas Control*, 5, S5-S15.
- WALL, T. F., GUPTA, R.P., GURURAJAN, V.S., ZHANG, D.K. 1991. The ignition of coal particles. *Fuel*, 70.
- WALL, T. F., STEWART, I.M. 1973. The measurement and prediction of solids- and soot-absorption coefficients in the flame region of an industrial P.F. chamber. *Symposium International on Combustion*, 14, 689-697.
- WAN, S., CHEN, W.-Y., SHI, G. 2009. Roles of Mineral Matters in the early stage of Coal Combustion. *Energy Fuels*, 23, 710-718.
- WANG, C. S., BERRY, G.G., CHANG, K.C., WOLSKY, A.M 1988. Combustion of Pulverized Coal using Waste Carbon Dioxide and Oxygen. *Combustion and Flame*, 72, 301-310.
- WESTBROOK, C. K., DRYER, F.L. 1981. Chemical kinetics and modeling of combustion processes. *Symposium International on Combustion*, 18, 749-767.
- WESTBROOK, C. K., DRYER, F.L. 1984. Chemical kinetic modeling of hydrocarbon combustion. *Progress in Energy and Combustion Science*, 10, 1-57.
- WHITE, V., FOGASH, K. 2009. Purification of Oxyfuel-Derived CO₂: Current Developments and Future Plans. *1st IEA Oxy-Fuel Combustion Conference*. Cottbus, Germany.
- WHITE, V., WRIGHT, A., TAPPE, S., YAN, J. 2013. The Air Products Vattenfall Oxyfuel CO₂ Compression and Purification Pilot Plant at Schwarze Pumpe. *Energy Procedia*, 37, 1490-1499.

REFERENCES

- WIJAYA, N., CHOO, T.K., ZHANG, L. 2011a. Generation of ultra clean coal from Victorian brown coal - Sequential and single leaching at room temperature to elucidate the elution of individual inorganic elements. *Fuel processing Technology*, 92, 2127-2137.
- WIJAYA, N., CHOO, T.K., ZHANG, L. 2012. Generation of ultra clean coal from Victorian brown coal: Effect of hydrothermal treatment and particle size on coal demineralization and the extraction kinetic of individual metal. *Energy and Fuels*, 26, 5028-5035.
- WIJAYA, N., ZHANG, L. 2011b. A critical review of coal demineralization and its implication on understanding the speciation of organically bound metals and submicrometer mineral grains in coal. *Energy and Fuels*, 25, 1-16.
- WILLIAMS, A., BACKREEDY, R., HABIB, R., JONES, J.M., POURKASHANIAN, M. 2002. Modelling coal combustion: the current position. *Fuel*, 81, 605-618.
- WOOLDRIDGE, M. S., TOREK, P.V., DONOVAN, M.T., HALL, D.L., MILLER, T.A. 2002. An Experimental Investigation of Gas-Phase Combustion Synthesis of SiO₂ Nanoparticles Using a MultiElement Diffusion Flame Burner. *Combustion and Flame*, 131, 98-109.
- WU, Z. 2005. Fundamentals of pulverised coal combustion. IEA Clean coal centre.
- XIONG, S. J., BURVALL, J., ORBERG, H., KALEN, G., THYREL, M., OHMAN, M., BOSTROM, D. 2008. Slagging Characteristics during Combustion of Corn Stovers with and without Kaolin and Calcite. *Energy and Fuels*, 22, 3465-3470.
- YAMADA, T., ISHII, T., TAKAFUJI, M., ISO, Y. 2010. Study Results in Demonstration Operation of Oxyfuel Combustion Boiler for CO₂ Capture. *Engineering Review*, 43, 47-54.
- YAO, S., C., LIU, L. 1983. Behaviour of the suspended coal-water slurry droplet in combustion environment. *Combust Flame*, 51, 335-45.
- YE, D. P., AGNEW, J.B., ZHANG, D.K. 1998. Gasification of a South Australian low rank coal with carbon dioxide and steam: kinetics and reactivity studies. *Fuel*, 77, 1209-1219.
- YE, Y., LI, S., LI, G., WU, N., YAO, Q. 2014. The transition of heterogeneous-homogeneous ignitions of dispersed coal particle streams. *Combust Flame*, 161, 1458-1468.
- YIP K., W., H., ZHANG, D.K. 2007. Effect of inherent moisture in Collie coal during pyrolysis due to in-situ steam gasification. *Energy Fuels*, 21, 2883-91.
- YOUNG, B. C., NIKSA, S., 1988. Combustion Rates for Selected Low-Rank Coals. *Fuel*, 67, 155-164.

REFERENCES

- YU, J., ZHANG, M.C. 2009. Mass transfer coefficients for the combustion of a char particle in O_2/CO_2 . *Energy & Fuels*, 23, 5717-5724.
- YUZBASI, N. S., SELCUK, N. 2011. Air and oxy-fuel combustion characteristics of biomass/lignite blends in TGA-FTIR. *Fuel Processing Technology*, 92, 1101-1108.
- ZHANG, J., DAI, B., MENG, Y., WU, X., ZHANG, J., ZHANG, X., NINOMIYA, Y., ZHANG, Z., ZHANG, L. 2015. Pilot-scale experimental and CFD modeling investigations of oxy-fuel combustion of Victorian brown coal. *Fuel*, 144, 111-120.
- ZHANG, J., PRATIONO, W., ZHANG, L., ZHANG, Z.X. 2013. Computational Fluid Dynamics modelling on the air-firing and oxy-fuel combustion of dried Victorian brown coal. *Energy Fuels*, 27, 4258-4269.
- ZHANG, L. 2014. Pilot-scale oxy-fuel combustion of Victorian brown coal. Canberra, AU: ANLEC R&D and Brown coal Innovation Australia (BCIA).
- ZHANG, L., BINNER, E., QIAO, Y., LI, C.Z., 2010a. High-speed camera observation of coal combustion in air and O_2/CO_2 mixtures and measurement of burning coal particle velocity. *Energy Fuels*, 24, 29-37.
- ZHANG, L., BINNER, E., QIAO, Y., LI, C.Z., 2010b. In situ diagnostics of Victorian brown coal combustion in O_2/N_2 and O_2/CO_2 mixtures in drop-tube furnace. *Fuel*, 89, 2703-12.
- ZHAO, Y. H., KIM, H.Y., SOON, S.Y. 2007. Transient group combustion of the pulverized coal particles in spherical cloud. *Fuel*, 86, 1102-1111.
- ZHENG, L. 2011. Overview of Oxy-Fuel Combustion Technology for Carbon Dioxide (CO_2) capture. In: ZHENG, L. (ed.) *Oxy-Fuel Combustion for Power Generation and Carbon Dioxide (CO_2) capture*. Cambridge, UK: Woodhead Publishing Limited.
- ZOU, C., LEI, C., ZHENG, C. 2014. Numerical research on the homogeneous/heterogeneous ignition process of pulverized coal in oxy-fuel combustion. *Int Jour Heat Mass*, 73, 207-216.
- ZOU, X., YAO, J., YANG, X., SONG, W., LIN, W. 2007. Catalytic effects of metal chlorides on the pyrolysis of lignite. *Energy and Fuels*, 21, 619-624.

APPENDIX A

Supporting Information for Chapter 4
(Published as Supplementary
Information for journal paper written
based on results in chapter 4)

This page is intentionally left blank

1 ICP-OES quantification and coal sequential leaching

Quantification of the major ash-forming metals within this coal and its sequential leaching residues were conducted by inductively coupled plasma optical emission spectroscopy (ICP-OES, Perkin Elmer 7000 DV). The standardised methods for ICP-OES analysis were summarised elsewhere¹. The sequential leaching was conducted by using Milli-Q water, ammonia acetate (1 M), and hydrochloric acid (1 M) in sequence, removing the water-soluble species, ion-exchangeable cations and discrete mineral grains of oxide, carbonates and sulfate, respectively². Each leaching was conducted by a magnetic stirrer, under the conditions of room temperature, liquid to solid ratio of 10, and 2 hrs.

2. Coal ignition in the FFBR

A mixture of C_2H_4/H_2 is used as the fuel for the flat flame burner. The Oxygen and Carbon dioxide gas were chosen as the oxidizer for oxy-fuel conditions and the air and oxygen were the oxidizer for air conditions. The gas flow rate is adjusted carefully to provide the gas compositions of 21% O_2 under N_2 and CO_2 diluted conditions with 15% H_2O level. The total gas flow rate is fixed at 11slpm for all cases. The pulverized coal is fed with a piezoelectric feeder at fixed feeding rate of 0.1g/min and entrained with the diluting gas at very low flow of 0.7slpm. This is to prevent the thermal shielding effect during combustion due to the cold gas flow. The furnace temperature is fixed at 1173K for all cases. The gas temperature is measured using R-type thermocouple corrected for radiation losses³. The furnace is allowed to start up for thirty minutes for heating up process before starting the experiments. The furnace temperature profile for 21% oxygen

in both air and oxy-fuel mode is shown in Figure S1. The gas compositions in the FFBR are summarised in table S1.

Table S1 Gas compositions from C₂H₄/H₂ combustion

Case name	Air_21	Oxy_16	Oxy_21	Oxy_26	Oxy_31
O ₂	21.03%	16.64%	21.57%	26.54%	31.54%
N ₂	44.04%	0.00%	0.00%	0.00%	0.00%
CO ₂	16.44%	64.90%	59.92%	54.92%	49.89%
H ₂ O	18.49%	18.46%	18.50%	18.55%	18.59%

Gas Temperature Profiles

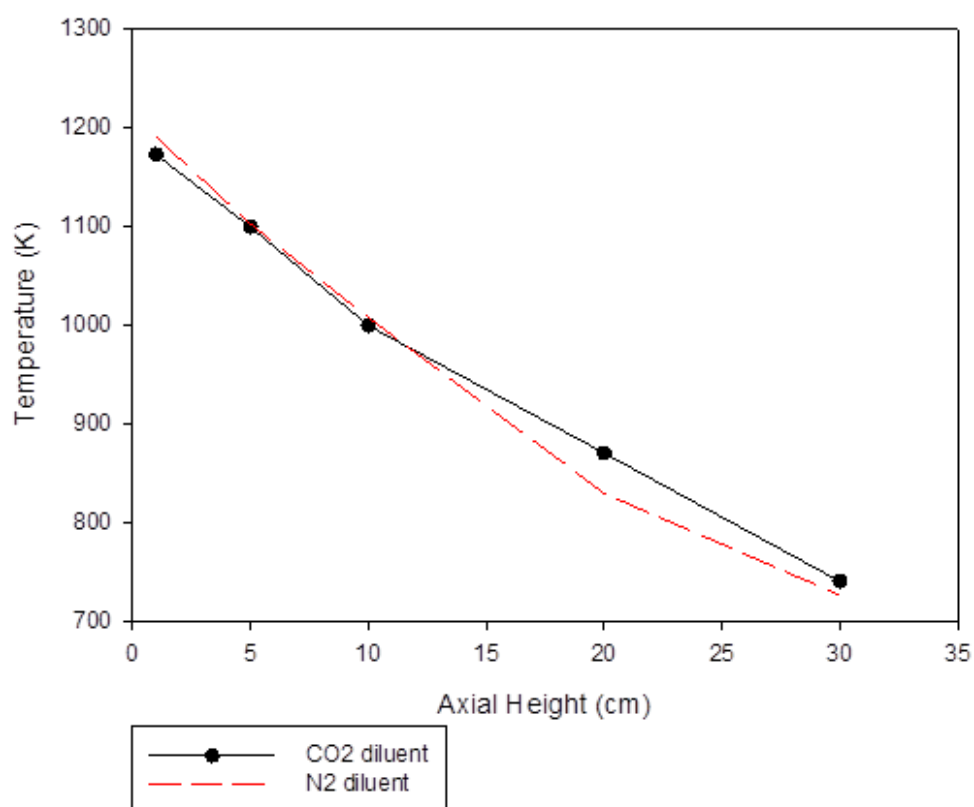


Figure S1 Blank gas temperature profile along reactor axis

3. Image processing to clarify coal ignition and oxidation

The images of coal flame were taken using a Nikon P7000 digital camera. More than 100 images were taken at each operating conditions for statistic analysis. The average length of coal flame was determined via digital image processing software, ImageJ. The measurements were taken from the burner base ($h = 0$) up to the edge of flame ($h = L$). There are three different regions that can be identified in coal flame pattern, initial drying/devolatilization, volatile combustion and char oxidation, as demonstrated in **figure S2**. These regions are identified and supported with the images obtained from the high speed camera observation. The combustion intensity is also characterized by means of flame luminosity and flame pattern. Total coal burning time can also be quantified by characterization of flame length and compared with the numerical calculations to predict the combustion efficiency.

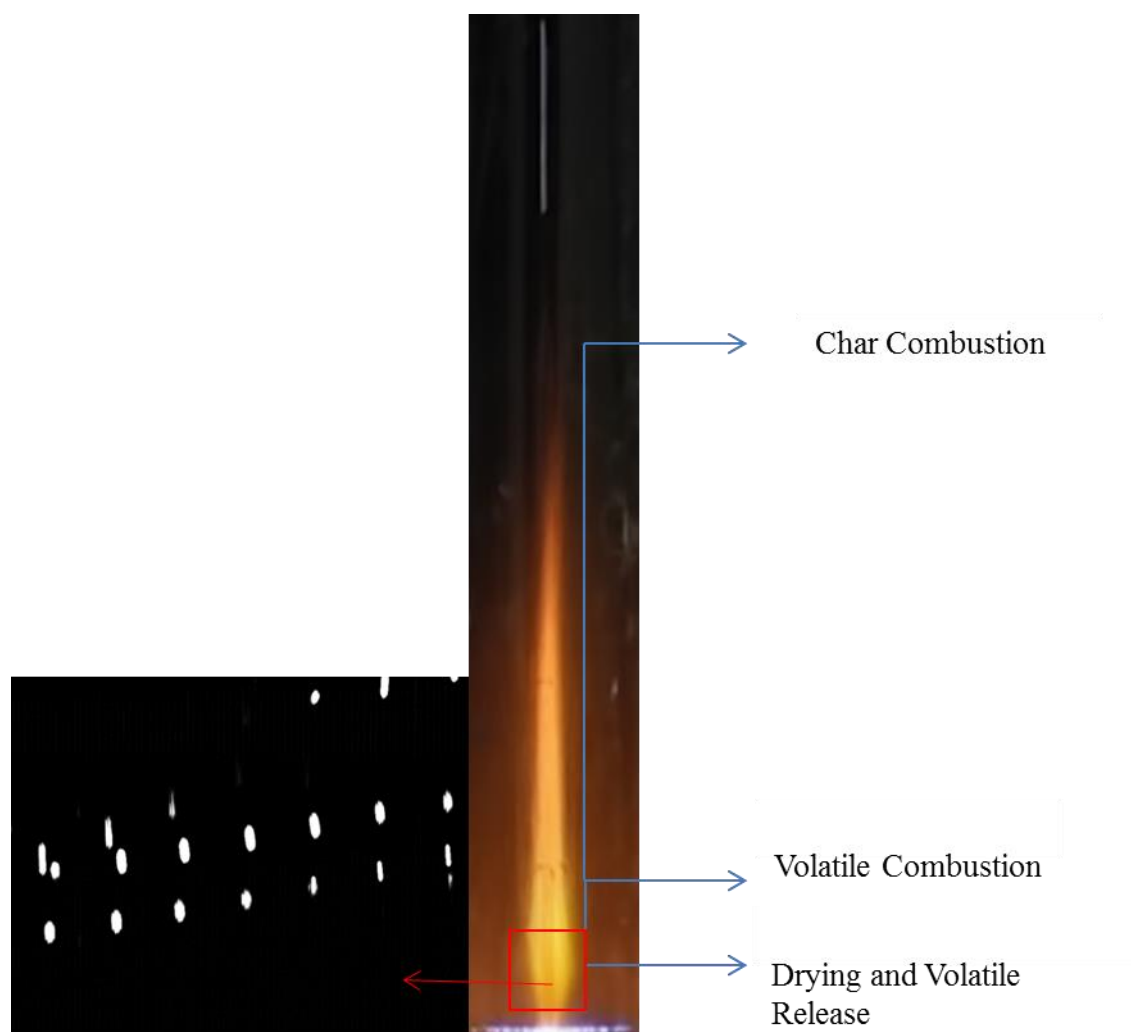


Figure S2 Sample Image of burning raw coal in air

4. High Speed Camera Facility for Single particle imaging

A MotionPro Y3 high speed camera equipped with microscopic lens is employed to visualize the burning behaviour of single coal particle. The camera is set to capture 1000 frames per seconds (fps) corresponding to an exposure time of $997 \mu s$. Note that, None of external light source has been used during the high-speed camera photographing, because the flat flame formed by liquid fuel provided sufficient heat to light up the un-reacted coal particles close to the burner base. For the ignited coal particles, their brightness was strong enough for photographing.

More than 1000 photos were taken (as a form of video) and statistically analysed by ImageJ to determine the average particle velocity profile in the reactor. The analysis method is shown in *figure S3*.

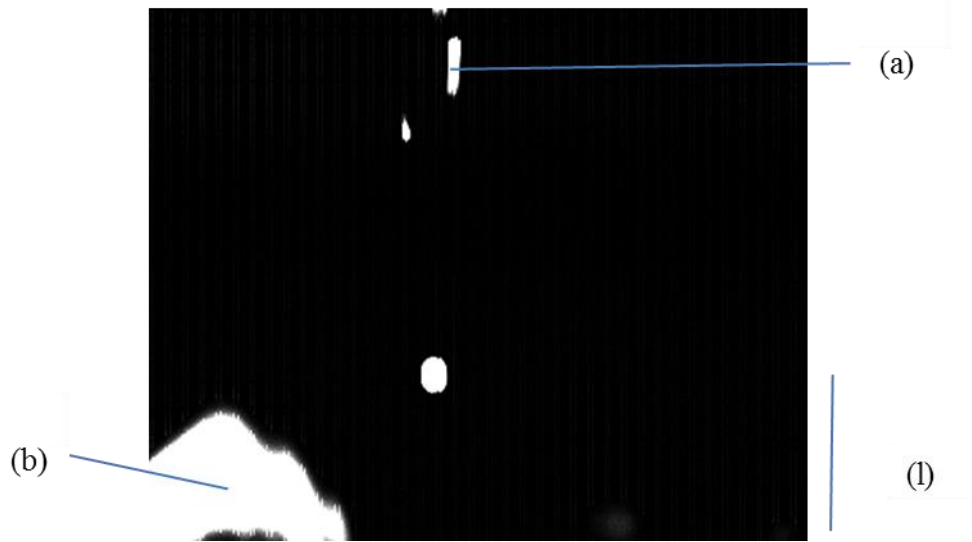


Figure S3 Sample images obtained using high speed camera for combustion of coal in air, taken at position of 50 mm from burner base

The elongated particle length (*Point a*) corresponds to the velocity of particle travelling at that particular point. *Point (b)* is the flame of the burning ethylene/hydrogen fuel. The particle velocity is calculated by:

$$PV = \frac{\text{Length of the travelling particle}}{\text{exposure time (997}\mu\text{s)}} \quad (8)$$

5. CFD modeling for the initial non-reactive particle heat-up stage

To supplement the experimental observations, the commercial CFD software, Ansys FLUENT 13.0 has been employed to predict coal particle velocity and oxidation time in the FFBR. The FFBR geometry was established by using GAMBIT 2.4.6 preprocessor to create the grids. The structural hexahedral cells with a total number of 56,000 were

created. The sub-models chosen for coal combustion are the same as that we had used for the modeling of coal combustion in drop-tube furnace⁴. Regarding the clay mixed with coal, it mainly consists of 56 wt% SiO₂, 18% Al₂O₃, and 10% CaO, with a cut-off size bin of 0~38 μm . In the CFD model, the clay was set as a separate ‘inert’ stream with the physical properties as: density $\rho = 2160 \text{ kg/m}^3$, specific heat capacity $C_p = 1381 \text{ J/(kg.k)}$, thermal conductivity $k = 0.15 \sim 1.8 \text{ W/(m.K)}$, emissivity $\varepsilon = 0.75$, and thermophoretic coefficient determined by Tablot-diffusion method that is also the default method in the FLUENT package. Given that the thermal conductivity of clay varies broadly and the other properties are rather constant⁵, for each case two modeling runs were conducted by using two extremities of the thermal conductivity of clay.

The initial particle temperature profile, prior to its ignition, is shown as solid curves in figure S4 below. The dashed lines in each panel were used to interpret the particle temperature prior to its ignition. For each dashed line, its x-axis value referring to the path length for coal ignition shown in figure 4 in the manuscript.

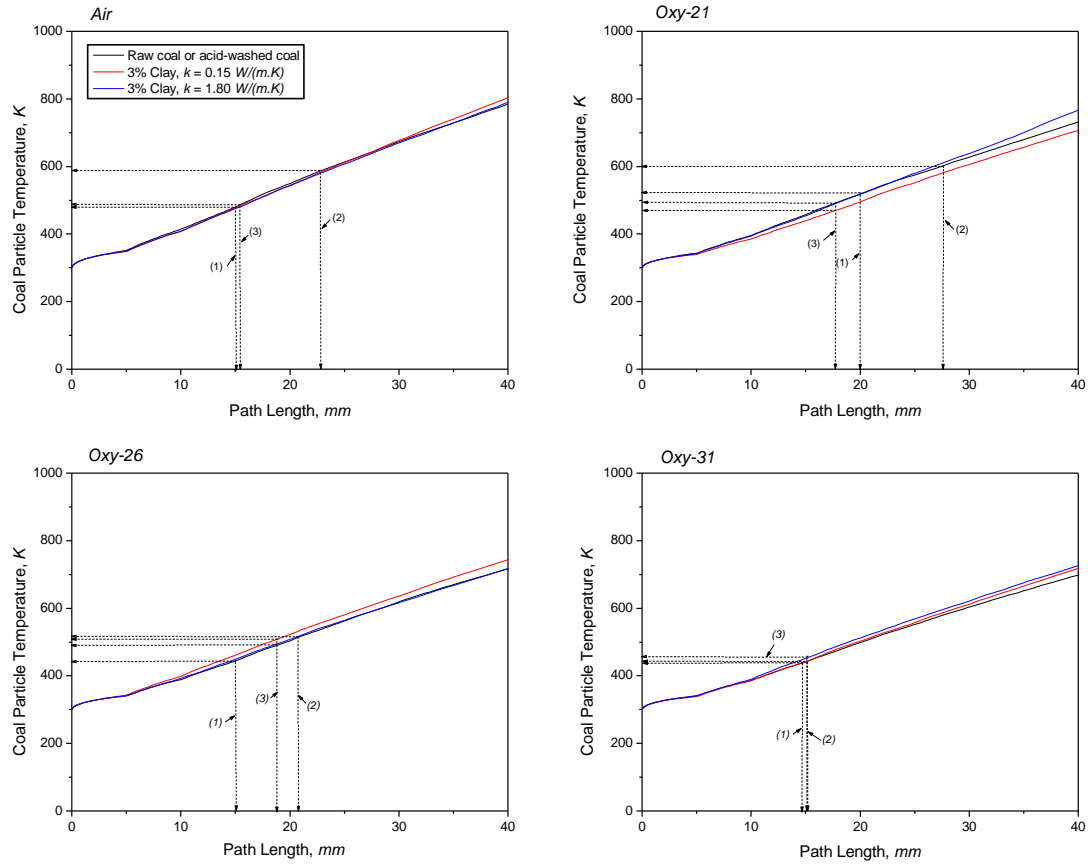


Figure S4 The initial heat-up process for non-reactive coal particle and the way to determine the particle temperature when it is being ignited

6. Calculation of the adiabatic temperature for igniting coal particle

This was done by assuming the volatile cloud as hexane (C_6H_{14}) and its combustion occurs at the stoichiometric ratio to oxygen on its flame front on particle surface. For a single coal particle when its volatile cloud (hexane) is burning, its solid mass was determined by using the average diameter ($83 \mu\text{m}$) and a particle density of 800 kg/m^3 . The particle was simplified as non-reactive C(s) , which merely adsorbs the heat feedback

from the endothermic oxidation of volatile cloud on its surface. The fraction of volatile cloud was determined by figure 12 in the manuscript. The oxygen fraction was determined according to the stoichiometric ratio by the oxidation equation. The balance gas, N₂ or CO₂, was determined according to its volumetric ratio to oxygen in the bulk gas.

The module “heat and material balances” in HSC Chemistry 7.1 was employed for the calculation. The input includes above volatile cloud and its temperature sets at the initial coal ignition temperature in figure 9 in the manuscript, whereas the bulk gas (O₂, N₂) temperature was set at 1000°C, according to figure S1. Its output includes the oxidation products of the hexane oxidation, CO_{2(g)} and H₂O_(g). Energy loss was assumed as zero, all the heat released from hexane oxidation was used to heat up char particle, C_(s) and the gas products. The calculated results are shown in figure S7 next page.

7. Coal devolatilisation rate using the E and pre-factor parameters derived from TGA data

The calculation was conducted based on the first order reaction rate for coal devolatilisation in the equation of $dx/dt = A \exp \{-E/(RT)\} (1-x)$, where x refers to the released fraction of volatiles, t time, A pre-factor, E activation energy, and T particle temperature. The particle temperature T at a certain time t was calculation by linear interpretation between the two ends, the initial temperature for coal to ignite in figure 11 and the adiabatic temperature predicted in figure S6. The above equation for coal devolatilisation was solved by assuming a fixed step 0.01 *ms* for time increment dt .

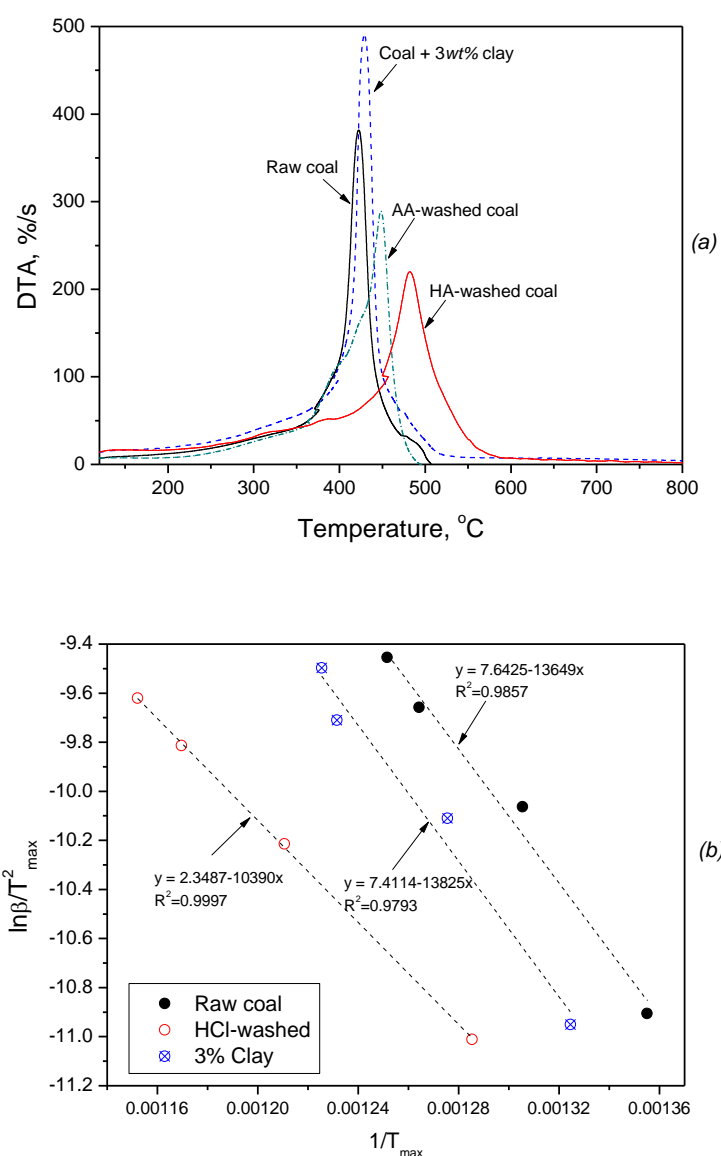


Figure S5 Heterogeneous ignition temperatures for raw coal, coal with clay, acid-washed coals measured by TGA. Panels (a) and (b) are for the measurement at the heating rate of 10°C/min and $\ln \beta / T^2 - 1/T_{\max}$ relationships for three cases, respectively.

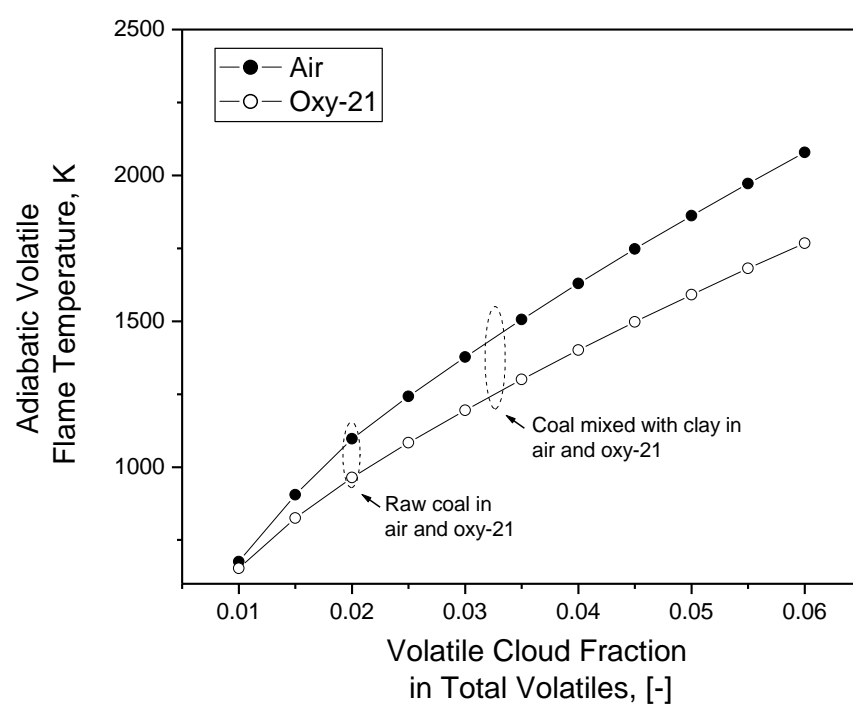


Figure S6 Adiabatic particle temperatures in the period of volatile cloud oxidation

References

- (1) Low F, Zhang L, Microwave digestion for the quantification of inorganic elements in coal and coal ash using ICP-OES, *Talanta***2012**,*101*, 346-52.
- (2) Wijaya N, Choo TK, Zhang L, Generation of ultra-clean fuel from Victorian brown coal - sequential and single leaching at room temperature to elucidate the elution of individual inorganic elements, *Fuel Process Technol***2011**, 92(11), 2127-37.
- (3) Shaddix, CR, Correcting Temperature Measurement for Radiation Loss, in *Proceedings of the 33rd National Heat Transfer Conference*, Albuquerque, NM, **1999**.
- (4) Zhang J, Prationo W, Zhang L, Zhang Z, Computational Fluid Dynamics Modeling on the Air-Firing and Oxy-fuel Combustion of Dried Victorian Brown Coal, *Energy Fuels***2013**, 27, 4258-69.
- (5) http://www.engineeringtoolbox.com/thermal-conductivity-d_429.html
- (6) Harris A, Zhong Z, Non-isothermal thermogravimetric analysis of plywood wastes under N₂, CO₂ and O₂ atmospheres, *Asia-Pacific J Chem Eng***2008**, 3, 473-80.

This page is intentionally left blank

APPENDIX B

Published First-Author Papers Included
in the Main Body of Thesis

This page is intentionally left blank

Influence of External Clay and Inherent Minerals on Lignite Optical Ignition and Volatile Flame Propagation in Air-Firing and Oxy-Firing

Wirhan Pratiomo,[†] Jian Zhang,[†] Hawra Ali Abdul Abbas,[†] Xiaojiang Wu,^{†,‡} Xiaodong Chen,[†] and Lian Zhang^{†,*}

[†]Department of Chemical Engineering, Monash University, Clayton Campus, GPO Box 36, Wellington Road, Victoria 3800, Australia

[‡]Shanghai Boiler Works Co. Ltd., 250 Huaning Road, Minhang, Shanghai 200245 China

Supporting Information

ABSTRACT: The influence of external clay additive and inherent minerals on the ignition of a Xinjiang lignite and its volatile flame propagation in air versus oxy-fuel combustion have been clarified in this work, through the use of a flat flame burner reactor (FFBR) coupled with in-situ optical diagnosis tools. As has been confirmed, ignition of the lignite studied in this paper was initiated by homogeneous oxidation of a tarry volatile cloud. The removal of HCl-soluble metals shifted coal devolatilization toward higher temperatures in air and 21% O₂ in CO₂. The mixing of external clay with coal had little effect on the ignition time. However, it enhanced the decomposition of volatiles, leading to a larger volatile cloud shielding on the particle surface. The oxygen fraction in the bulk gas was found to be most influential. Increasing the oxygen fraction to 30% eliminated all of the discrepancies between raw lignite, acid-washed lignite, and a mixture of raw lignite and clay.

1. INTRODUCTION

The ash-forming metals in coal, namely, mineral matter, play a dual role during coal combustion. On one hand, they are directly relevant to slagging and fouling, which are the two most crucial issues that negate the performance and efficiency of coal-fired boilers.¹ On the other hand, they are capable of catalytically promoting coal oxidation, by acting as oxygen-shuttling agents for bulk oxygen activation² or activating the stable surface oxides of the organic portion of coal during the early stage of coal combustion.³ The impacts of mineral matter are profound for low rank coal, such as sub-bituminous coal and lignite, as their ash-forming metals are generally dominated by alkali and alkaline earth metals that are highly catalytic for coal combustion but also influential for severe slagging and fouling in boilers.

To minimize/eliminate the slagging and fouling propensity of alkali and alkaline earth metals, low-rank coal can be either treated first by acid washing to remove the ash-forming metals or by mixing with a solid additive for the purpose of in situ capture of alkali and alkaline earth metals in a boiler. For the former method, the resulting acid-washed coal can be burned in a direct-injection coal engine (DICE) or gas turbine to mitigate its carbon emission footprint on a step-change mode.⁴ Our previous works have demonstrated the simplicity of mobilizing ash-forming metals from lignite under ambient conditions and using weak acids for an extremely short time.^{5,6} Regarding the latter method for the mixing of additives with coal, this approach is more practicable for pulverized-coal-fired boilers, where low-cost refractory minerals such as clay can be injected together with coal particles into the existing mill.^{1,7,8} Prior to the deployment of either method in industry, it is essential to clarify the changes in the combustion characteristics of lignite upon acid-washing and mixing with clay, as this is primarily important for the stability of an existing boiler.

To date, the research on acid-washed lignite reported in the literature has mainly focused on comparing the devolatilization and burnout rates of raw coal, acid-washed coal, and coal impregnated with different metals by thermogravimetric analysis (TGA) at extremely low heating rates or in fixed- and fluidized-bed reactors where the volatiles released are quickly swept away from the char particle surface by bulk gas.⁹ Despite the abundance of knowledge on coal burnout in the literature, there is still a shortage of essential information regarding the influence of ash-forming metals on particle ignition, flame propagation, tar formation, and in situ tar oxidation. In a real combustion environment, the volatiles are released at a heating rate on the order of 10⁵ K/s,¹⁰ and the released volatiles also partly reside on the char surface, forming a cloud that affects subsequent char ignition and oxidation steps.¹¹

The aforementioned studies with low heating rates failed to address all of these aspects. Moreover, the addition of clay to coal can affect coal ignition by deactivating alkali and alkaline earth metals and/or catalytically promoting oxygen shuttling. These two roles could counterbalance one another and, hence, exert a complex effect on the ignition of coal particles.

In this study, a lignite rich in alkali and alkaline earth metals, its HCl-washed residue, and a mixture of this coal with 3 wt % clay have been tested in a laboratory-scale flat flame burner reactor (FFBR) for their ignition, flame propagation, and volatile cloud oxidation properties. The FFBR used burns a mixture of hydrogen and ethylene to create a flat flame that can heat coal particles at a rate of ~10⁵ K/s, similar to the rate found in industrial boilers. It is coupled with various advanced

Received: August 8, 2013

Revised: December 30, 2013

Accepted: January 16, 2014

Published: January 16, 2014

optical instruments for in situ diagnosis, including a high-resolution camera for flame observation and a high-speed camera for observation of the release, dynamic oxidation, and distinction of volatiles on the particle surface and particle velocity measurements. The measured results were compared with and also interpreted by data collected from thermogravimetry-differential thermal analysis (TG-DTA). In addition to air-firing, an oxy-fuel combustion test in 21–31 vol % oxygen with CO₂ balance was also conducted, where the steam concentration is kept constant at 17.5 vol %. The coal sample selected is a lignite sample collected from Xinjiang Autonomous Area, the data for which are practically nonexistent because of the low exploration degree, even though such coal contributes approximately 40% of the overall Chinese coal reserves.¹²

2. EXPERIMENTAL SECTION

2.1. Coal Properties. The coal used is Xinjiang lignite with a cutoff size of 105–153 μm , the proximate and ultimate properties of which are listed in Table 1. The as-received coal

Table 1. Proximate Properties of the Xinjiang Lignite Tested

Proximate Analysis	
fixed carbon (% db)	64.20
volatile matter (% db)	30.77
ash (% db)	5.00
moisture (% ar)	19.10
Ultimate Analysis (% db)	
C	74.5
H	2.90
N	0.42
S	0.37
O*	21.81

*By difference.

has a relatively high content of moisture, whereas its ash-forming metals account for only 5 wt % in total. The concentrations of major ash-forming metals in the raw coal and its sequential leaching residues are reported in Table 2. Ca is

Table 2. Properties of Ash-Forming Metals in the Raw Lignite and Its Sequential Leaching Residues (mg/kg)

	raw coal	water-washed	AA-washed ^a	HA-washed ^b
Al	1568	2214	2284	2310
Ca	11294	11230	6393	1343
Fe	1643	703	952	615
K	60	69	59	54
Mg	1498	1677	871	328
Na	2175	796	127	71

^aAA = ammonia acetate (1 M). ^bHA = hydrochloric acid (HCl, 1 M).

the most prevalent metal within the raw coal, followed by Na, Fe, Al, and Mg in descending order. The concentration of Ca showed little change upon water washing. In contrast, it dropped by nearly half of its initial amount upon ammonia acetate washing, suggesting an abundance of ion-exchangeable Ca associated with oxygen-containing functional groups such as carboxylic acid groups in the coal matrix. A further washing by HCl reduced the Ca concentration to approximately one-tenth of its original quantity, indicating the abundance of oxide/carbonate grains. Another alkaline earth metal, Mg, showed similar behavior upon sequential leaching, namely, abundant

ion-exchangeable cation and oxide/carbonate grains. In contrast, the two alkali metals behaved differently, with Na being mainly partitioned between water-soluble and ammonia acetate-soluble fractions, whereas K had no change upon sequential leaching. Fe was mainly eluted upon water washing, as was also observed for Victorian brown coal.⁵ This is an indicator of the association of a portion of Fe with water-soluble hydrocarbons such as humic acid within the coal matrix, forming an oxyhydroxide-like structure.^{5,13} The ash-forming metal quantification and coal sequential leaching procedure are detailed in the Supporting Information (SI).

2.2. Determination of Coal Devolatilization, Ignition, and Char Oxidation by TG-DTA. TGA was employed to assess the reactivity of raw coal, acid-washed coal, and coal mixed with clay. At most 10 mg of sample was used for each run. Coal pyrolysis was carried out in argon grade 5.0 at four different heating rates from 10 to 50 K/min. The argon flow rate was maintained at 100 mL/min in each case. The ignition and char oxidation rates were determined by replacing argon with air. The data interpretation procedure to extract the kinetic data (activation energy, E , and pre-exponential factor, k) was detailed elsewhere.¹⁴

2.3. Coal Ignition and in Situ Optical Diagnosis. The coal combustion experiments and in situ optical diagnosis were carried out in the laboratory-scale FFBR illustrated in Figure 1. The reactor was operated at atmospheric pressure, and a flat-flame Hencken diffusion burner was employed to provide a high-temperature gas flow by burning a mixed liquid fuel of hydrogen (H₂) and ethylene (C₂H₄). The gas flow rate was adjusted to provide an oxygen concentration of 21–31 vol % with N₂ or CO₂ as the balance, while holding the concentration of water vapor (generated by liquid fuel combustion) constant at 17.51 vol %. For simplification hereafter, the oxy-fuel conditions with the oxygen concentrations of 21%, 26%, and 31% are referred as to oxy-21, oxy-26, and oxy-31, respectively.

To minimize the turbulence effect of gas and particle mixing, the total gas flow rate was maintained constant at 11.7 L/min (STD). In all cases, the furnace/flue gas temperature was maintained at 1273 K at the flat-flame burner base (see Figure 1), whereas a mean quartz wall temperature of 773 K was achieved due to heat loss. The pulverized fuel was fed with a piezoelectric feeder at 0.1 g/min and entrained by a carrier gas of 0.7 L/min (STD) into the reactor through a central tube of 1.5-mm i.d. in the Hencken burner. The combustion chamber was isolated with a 115-mm-diameter cylindrical quartz tube reactor insulated by Kaowool with a thickness of approximately 25 mm. A shroud inert gas of 1 L/min, either pure N₂ or CO₂, was injected at the outer ring of the burner to avoid interference of surrounding air in the stability of the flame.

Coal flame images were taken with a Nikon P7000 CCD camera. The images were processed to extract information regarding coal ignition distance, volatile oxidation distance, and duration of char combustion. The ignition distance is defined from the burner base to the point where the flame is visually observed. This distance is usually yellowish in color, showing the release of the volatiles prior to the initial ignition stage. The luminous, bright, and thick flame segment next to the coal ignition stage signified complete oxidation of volatiles, whereas the remaining tail of the flame with rather weak luminosity was denoted as char combustion.^{15,16} The quantitative method for three combustion stages is further detailed in Figure S2 of the SI. A MotionPro Y3 high-speed camera from IDT coupled with microscope lens was employed to analyze individual burning

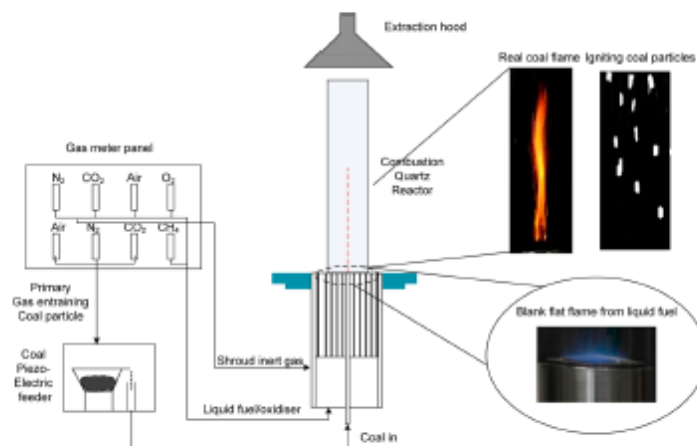


Figure 1. Schematic of the flat-flame burner reactor used throughout this study.

particles, including their velocities, volatile cloud sizes, and ignition times. The detailed method for calculating particle velocities has been previously described¹⁷ and is also detailed in Figure S3 of the SI.

3. RESULTS AND DISCUSSION

3.1. Devolatilization and Char Oxidation Reactivities of Coal Samples. The lignite studied in this work had high reactivity toward devolatilization and char oxidation. Its reactivity is summarized in Table 3 and Figure 2, in a comparison with previously published results. For the devolatilization rate in Table 3 and Figure 2a, the raw lignite has a devolatilization rate that was lower than those of air-dried and ammonium acetate-washed Victorian brown coal but

Table 3. Activation Energy (kJ/mol) and Prefactor (s^{-1}) for Raw Coal, Coal Mixed with 3 wt % Clay, and HCl-Washed Coal^a) and Comparison with Other Coals

	activation energy (kJ/mol)	prefactor (s^{-1})
Devolatilization		
raw coal	132	1.48×10^{16}
coal + 3 wt % clay	45	4.8×10^{16}
HCl-washed coal	59	1.08×10^{13}
raw Loy Yang brown coal ¹⁹	217	5.18×10^{16}
raw Montana lignite ¹⁷	58	8.0×10^{16}
acid-washed Montana ¹⁷	148	2.0×10^{16}
devolatilized Shenda sub-bituminous coal ²⁴	164–227	4.4×10^{10} – 6.9×10^{12}
devolatilized Haulongde lignite ²⁴	82–212	1.4×10^{16} – 1.5×10^{13}
Air Oxidation		
raw coal	116	4.33×10^{17}
coal + 3 wt % clay	115	2.30×10^{17}
HCl-washed coal	86	1.10×10^{13}
Beckli-Zap raw coal char ²⁴	27	1.40×10^{18}
Beckli-Zap devolatilized coal char ²⁴	36	3.30×10^{18}

^aXinjiang coal as the test sample.

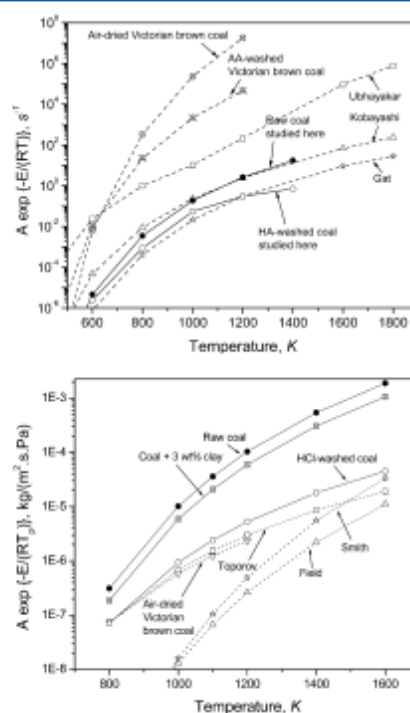


Figure 2. Comparison of the kinetics of lignite and its acid-washed residues measured here and reported in refs 19–22: (a) devolatilization and (b) char oxidation.

certainly higher than those of raw Montana lignites, other Chinese lignites, and bituminous coals examined in the

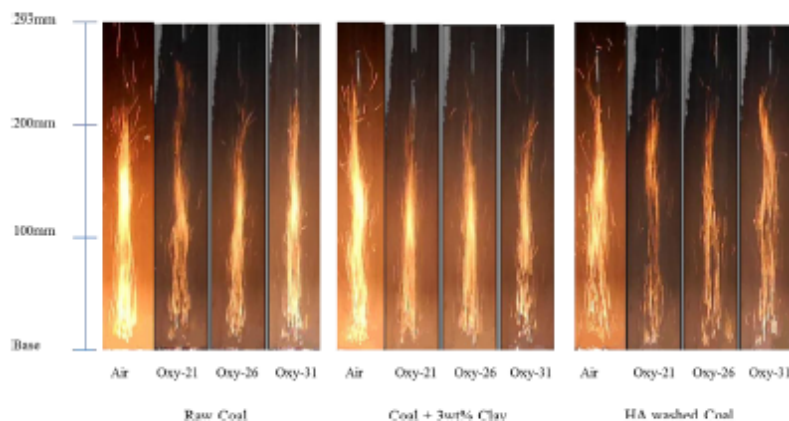


Figure 3. Representative flame patterns and flame lengths for raw coal, coal doped with 3 wt % clay, and HA-washed coal in air versus oxy-fuel modes.

literature.^{18,19} Upon HCl washing, the coal devolatilization rate was decreased to a level close to the observations on bituminous coals published by Ubhayakar et al.²⁰ and Kobayashi et al.²¹ This echoes the loss of ash-forming metals including Ca, Fe, Mg, and Na in Table 2 and supports the catalytic effect of these metals on coal volatiles release. The pyrolysis of NaCl-loaded lignite in a fluidized-bed/fixed-bed reactor exhibited an enhanced yield for light species including formate, acetate, and oxalate.²² CaO has been demonstrated to be catalytic in cracking oxygen functional groups to carbon monoxide.²³ It has also been shown to be reactive in promoting the water-gas shift reaction for the pyrolysis of sewage sludge at 753 K.²⁴ The removal of metals here is thus supposed to affect the coal pyrolysis product distribution in an opposite manner, namely, inhibiting the release of light hydrocarbons and deactivating hydrogen shuttling. By the use of TG-DTA for the pyrolysis of lignite and its demineralized samples, it has also been confirmed in the literature²⁵ that the total weight loss of the demineralized sample was slightly lower than that of the raw coal. Such an observation is broadly consistent with our results for HCl-washed Xinjiang lignite here.

For the raw coal with and without clay, the oxidation reactivity at a given temperature in Figure 2b is 10–1000 times higher than the literature data. Removing the ash-forming metals by HCl washing decreased the coal oxidation reactivity to an order of magnitude similar to that of bituminous coal. Here again, the ash-forming metals mentioned above are able to catalyze the ignition and oxidation of coal particles. Figure S5 (SI) further illustrates the DTA curves for the oxidation of raw coal, its ammonia acetate-washed residue, the residue after HCl washing, and a mixture of coal with 3 wt % clay. Adding 3 wt % clay slightly affected the coal oxidation pattern. In contrast, the ammonia acetate washing caused a detectable rightward shift of the peak referring to coal ignition and maximum mass loss, which was further delayed to 873 K for the HCl-washed sample. Compared to ammonium acetate-soluble cations, the HCl-soluble species referring to discrete oxide mineral grains, which should be highly dispersed within the coal matrix and hence have intimate contact with coal organic moieties, are clearly influential in char oxidation. In addition, the oxidation of

CaO-loaded coal char confirmed that CaO is able to raise the char oxidation rate by a factor of up to 2700.²⁶

3.2. High-Resolution Camera Observation of Flame Characteristics in an FFBR. The representative flames for the combustion of three coal samples are visualized in Figure 3. For the raw lignite, its combustion in air exhibits the brightest flame, in which the bottom segment in yellow color represents the initial step for coal drying and devolatilization. The overall flame luminosity of raw coal was decreased profoundly upon the use of oxy-21 in place of air. At the same time, the flame length and particularly the length of the initial yellow zone were noticeably enlarged, indicating the delay of coal ignition and the lifting of its flame, which is thus unstable in oxy-21 mode. Increasing the oxygen fraction in oxy-26 and oxy-31 restored the flame luminosity and length to values similar to those observed in the air case. The discrepancies observed between the air and oxy-fuel cases here are broadly consistent with the literature observations,^{27,28} which are mainly attributed to a larger specific heat capacity of CO₂ than N₂ that causes the delay in coal ignition and increases the radiative heat flux from the coal flame to the surrounding bulk gas.

HCl washing reduced the coal air-firing flame intensity dramatically. In particular, the initial yellow zone for coal drying and devolatilization was lifted significantly. In addition, the top bright section for char oxidation nearly disappeared, indicating a significant delay in char particle ignition. In combination with the TGA observations in Figure 2, this result is clearly attributed to the loss of HCl-soluble metals, which postpones both coal devolatilization and char particle ignition. Changing the oxidizing gas to oxy-21 further worsened the HCl-washed coal flame intensity, which even lacked a clear ignition and oxidation stage for the volatiles. Increasing the oxygen fraction to 31% in CO₂ marginally enhanced the flame intensity of the acid-washed coal. However, the flame achieved in oxy-31 for acid-washed coal lignite was still less luminous than the raw coal flame.

The use of clay as a fuel additive caused nondetectable changes in the coal volatile flame shape and intensity in air. However, for the oxy-21 case, the flame intensity of the top section referring to the char oxidation zone was markedly

improved when compared with that for the raw coal under the same experimental conditions. Increasing the oxygen fraction in CO_2 gradually narrowed the gap between air and oxy modes in regard to flame intensity. Such information was not detected by TGA, where both the clay and coal particles remained still with little interaction. In other words, in a real coal-fired case, where particles move rapidly, the influence of clay on coal oxidation is more obvious because of the intimate particle-to-particle interactions.

The coal ignition time was further measured and analyzed statistically based on flame pictures, as summarized in Figure 4.

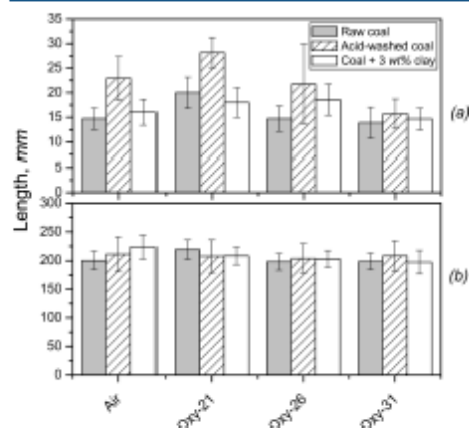


Figure 4. Distances for (a) coal ignition and (b) oxidation as a function of bulk gas composition for raw coal, acid-washed coal, and coal mixed with 3 wt % clay.

For coal ignition distance in panel a, the raw coal showed a distance of 15 mm in air, which was enlarged to 20 mm on average in oxy-21, because of the larger specific heat capacity of CO_2 compared to N_2 . Further increases in the oxygen fraction in CO_2 to 26% and 31% reduced the raw coal ignition distance to 15 mm, substantiating the achievement of a similar ignition time with the air case. The HCl-washed coal showed a long ignition distance of ~25 mm in air. Its ignition distance was further increased to ~30 mm in oxy-21 and then reduced to a level close to that of raw coal in oxy-31. Adding clay to coal caused little change in the coal ignition distance in air but slightly reduced it in the oxy-21 case. More interestingly, by comparing the air and oxy-21 cases for coal mixed with 3% clay, one can see that the difference in coal ignition distance between these two cases was only 1.5 mm (16 mm in air vs 17.5 mm in oxy-21) compared to ~5 mm for raw coal (from 15 to 20 mm) and HCl-washed coal (from 22.5 to 27.5 mm). The use of clay partly offset the negative effect of the large specific heat capacity of CO_2 in the oxy-fuel cases.

The total distance for the oxidation of coal volatiles and char in panel b showed less variation with bulk gas composition and the samples fed into the FFBR. This further suggests the primary importance of coal devolatilization on its total burnout time. For a given bulk gas, a large similarity between raw coal and coal mixed with clay is expected, echoing the similar reactivity of these two samples confirmed by TGA. Regarding

the HCl-washed coal, its oxidation duration was also rather comparable to that of raw coal, which should be because of the use of excess air for coal oxidation in the FFBR here, as the TGA confirmation indicated a much lower reaction rate for the acid-washed coal.

3.3. High-Speed Camera Observation of Coal Devolatilization and Ignition in an FFBR. To clarify the transient phenomena occurring during the initial coal devolatilization and ignition, a high-speed camera coupled with a microlens was further employed to photograph the first 5-cm distance from the FFBR burner base, at a shutter speed of 1000 frames per second and an exposure time of 990 μs for each frame. Typical photographs are presented in Figure 5. Figure 6 quantifies the



Figure 5. High-speed camera observations of the initial ignition of particles for three cases at a height of 5 cm from the burner base.

size distribution of the observed bright spots. In each picture, the bright rodlike spots were assigned as igniting particles, the length of which refers to the particle trajectory caused by its upward motion, whereas the width equals either the diameter of the original coal particle or the diameter of the volatile cloud envelope on the particle surface. For the raw coal tested in air, the width of the bright spots varied broadly, with some being nearly round for an intense release of volatiles and their

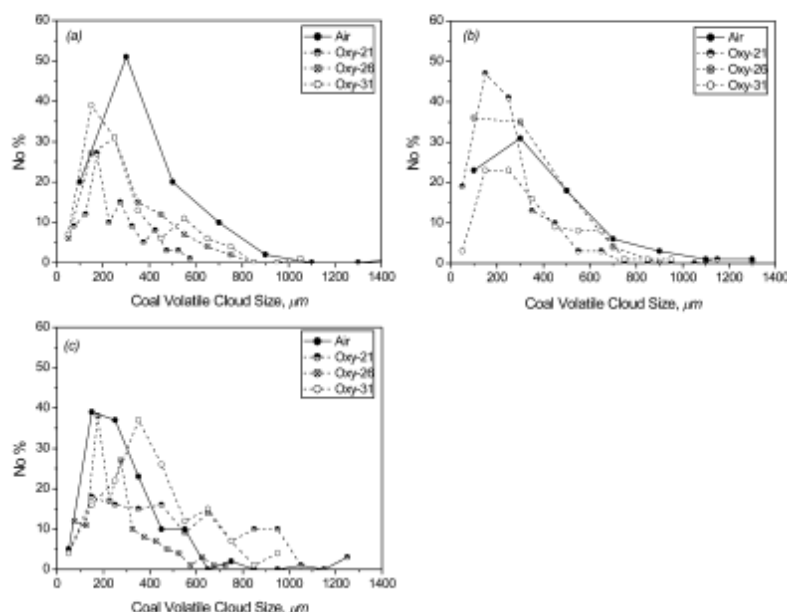


Figure 6. Igniting volatile cloud sizes as a function of bulk gas composition for three cases: (a) raw coal, (b) HCl-washed coal, and (c) coal mixed with 3 wt % clay. Measurements were done for the luminous spots observed at a height of 5 cm from the burner base.

preferential residence and ignition on particle surface. The volatiles remaining on the char surface are mainly viscous heavy hydrocarbons that are difficult to be swept away by bulk gas.^{11,29} Figure 6a confirmed a mean width of approximately 300 μm for the volatile cloud formed in air, which is around 4 times the size of the original coal particle diameter. Interestingly, the substitution of oxy-21 for air yielded abundant thinner spots with a mean width of around 200 μm; see Figure 6a. This is in agreement with Figure 4a for the slower ignition of raw coal in oxy-21, which, in turn, provided less heat feedback to its host coal particle to ensure a continuous release of the remaining volatiles from the coal matrix. Increasing the oxygen fraction in CO₂ favored the ignition of the initially released volatiles, which, in turn, promoted the release of extra volatiles to form a larger and brighter igniting spot. However, these improvements were marginal, as the mean width for bright spots in the oxy-31 case was still smaller than that in the air case.

The acid-washing of coal caused little change in the mean width of the bright spot (igniting particle) in the air case, although the igniting particle number density was remarkably reduced. Similarly to the results achieved for raw coal, changing air to oxy-21 for the acid-washed coal dramatically reduced its igniting spot size. The mean size was reduced to less than 200 μm, which is even close to the original coal size. This indicates that the devolatilization of acid-washed coal did not occur at a reactor distance of 15 mm. Increasing the oxygen fraction in CO₂ to 31% improved the coal volatile size to the same value as in the air case. The effect of the mixing of coal with clay on the change in igniting spot size was most influential. Although the majority of the igniting coal particles resided at the mean size of

200–300 μm in air, the particle sizes were broadened to a wider range with a comparable fraction larger than 600 μm in the oxy-21 mode. Such an increase is direct evidence of the promotion of coal devolatilization by clay. This was not detected in the air case, suggesting a quick ignition of the fragmented light hydrocarbons in air. Increasing the oxygen fraction in CO₂ improved the volatile oxidation rate for coal mixed with clay, which, in turn, decreased volatile cloud size. Its value at oxy-31 was even slightly smaller than in the air case.

3.4. Burning Particle Velocity Profiles in an FFBR

Particle velocity profiles measured by high-speed camera are illustrated in Figure 7. Regardless of the coal sample and bulk gas composition, the coal particle velocity increased over the reactor path length and maximized at approximately 3.0 m/s at 120 mm, where char oxidation commenced. For path lengths from 20 to 60 mm, the variations in the particle velocities of both raw coal and HCl-washed coal with bulk gas composition were very narrow and also fell within the error bars caused by the variations in the original coal particle size. In contrast, the addition of 3 wt % clay to coal broadened the discrepancy in particle velocity between different bulk gases. In particular, the gaps were maximized at 55 mm, which corresponds to the top luminous section for the flame observed in Figure 3. The interference of the clay particle velocity cannot account for this phenomenon, as the clay remains invisible in the field of view of the camera where only the luminous particles are detectable.

4. GENERAL DISCUSSION

Combining the results in Figures 4a and 7, the coal ignition time was deduced and is plotted versus bulk gas composition in Figure 8. The raw coal exhibited an ignition time of

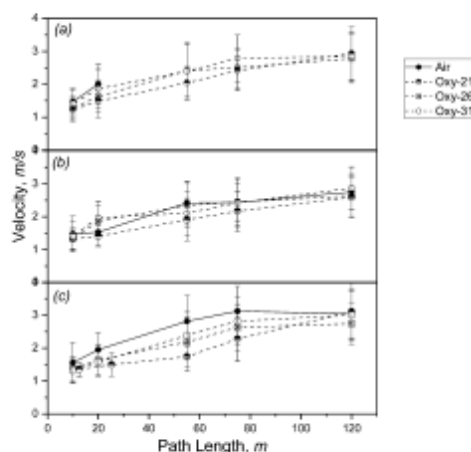


Figure 7. Particle velocity profiles in the early stage of coal combustion as a function of bulk gas composition for three different cases: (a) raw coal, (b) HCl-washed coal, and (c) coal mixed with 3 wt % clay.

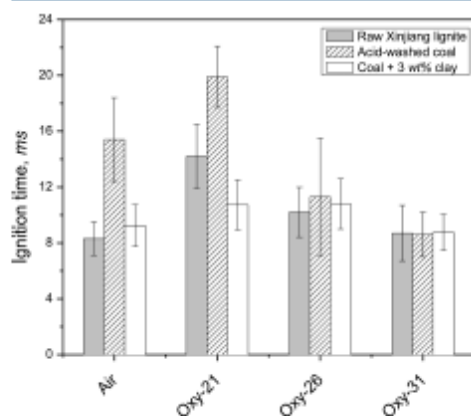


Figure 8. Coal ignition time (ms) as a function of bulk gas composition for three different cases: raw coal, acid-washed coal, and coal mixed with 3 wt % clay.

approximately 8 ms in air, the magnitude of which is comparable to that of a high-volatile bituminous Pittsburgh seam coal in a hotter gas of 1700 K.³⁰ This further supports the high reactivity of the lignite tested here. Substituting oxy-21 for air postponed the ignition of raw coal to approximately 20 ms, which is more than twice the value obtained in the air case. This echoes the larger specific heat capacity of CO₂, which is around 1.7 times that of N₂. Increasing the volumetric specific heat capacity of the bulk gas increases the autoignition time of a fuel linearly, as suggested by the adiabatic thermal explosion equation

$$\tau_i = \frac{c_p(T_0/T_i)}{q_c Y_{F,0} A \exp(-T_i/T_0)} \quad (1)$$

Increasing the oxygen fraction in CO₂ decreases the volumetric specific heat capacity of the overall bulk gas, but it also increases the reactivity of the fuel/oxidant mixture, $A \exp(-T_i/T_0)$. As a result, the gaps between the three solid samples, namely, raw coal, acid-washed coal, and coal mixed with clay, disappeared when the oxygen fraction increased to 26% and above. Moreover, compared to raw coal and its acid-washed sample, the mixture of raw coal with clay showed a rather narrow discrepancy in ignition times between four different gases in Figure 8. The discrepancy between air and oxy-21 accounts for only approximately 1.5 ms, referring to 9.2 ms in air versus 10.7 ms in oxy-21. This can be attributed to the enhanced release of volatiles upon the addition of clay to coal, as visualized in Figures 5 and 6. Such an improvement, referring to the local volatile mass fraction on coal particle, $Y_{F,0}$ in eq 1, clearly counterbalanced the negative effect of the gas volumetric specific heat capacity. Because Table 3 and Figure 2 did not evidence the catalytic influence of clay coal devolatilization in TGA, the clay added here should promote the secondary cracking of the released primary hydrocarbons in the vicinity of coal particles, leading to the formation of more light moieties that can readily ignite. This is consistent with the literature, which has confirmed the effect of clay in promoting the secondary decomposition of coal tar.³¹ The clay was also found to be reactive in promoting the activation of hydrogen transfer to coal and the reactions of dealkylation and dehydrogenation.¹⁸

Using the average volatile cloud sizes calculated based on Figure 6 and eq 2 below for the quantification of volatile flame radius, one can determine the quantity of volatiles released on igniting particle surface. Equation 2 was derived from the literature³² as follows

$$r_s = \frac{d(\Delta V_s/V_0) \left(w Y_{F,0} R T \right)}{3 D P \Delta p_0} \left(\frac{1}{\rho} \right)^3 \quad (2)$$

In this equation, the ignition temperature, T , was derived from Figure S4 (SI) by comparing the particle temperature profile predicted by computational fluid dynamics (CFD) with the measured ignition distance results in Figure 4a, the ignition time dt in eq 2 was taken from Figure 8, and the symbol f_v was determined by the amount of oxygen needed for the combustion of 1 g of heptane (treated as the main volatile species). Figure 9 shows the calculated fractions of volatiles initially ignited on the particle surface. Regardless of the bulk gas composition, the initially ignited volatile percentage remained rather constantly at approximately 29% of the total volatiles for the raw coal. The acid-washed coal had similar amounts for its initially ignited volatiles in the air and oxy-21 cases, which increased slightly to 2.5 wt % in oxy-26 and oxy-31. This insignificant increment is assumed to have little effect on coal ignition, as the elution of the catalytic ash-forming metals decreased the reactivity (prefactor) by 10^2 – 10^5 -fold. The increase in the volatile fractions upon mixing clay with coal was more pronounced; it was maximized at approximately 3.5 wt % in oxy-21 and gradually dropped to ~2.75 wt % in the oxy-31 case.

It remains intriguing to compare Figure 9 with the results for tar formation from lignite pyrolysis in the literature. Although the same coal has not been examined for pyrolysis in the

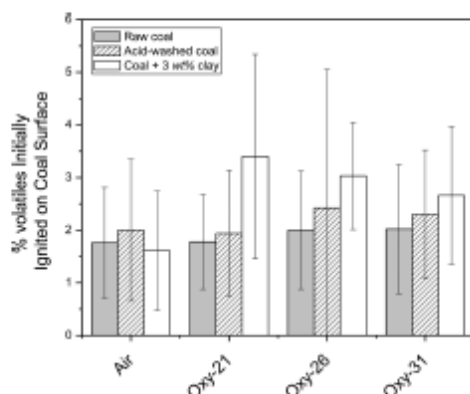


Figure 9. Calculated percentages of volatiles ignited initially on the coal particle surface at low temperatures.

literature, a study of a low-ash (~ 1.0 wt %, daf) Victorian brown coal reported a yield of approximately 20 wt % (daf) for the tar derived from the pyrolysis of raw coal at 773 K in either CO_2 or He at a heating rate of 1000 K/s and a hold time of 10 s at the maximum temperature.³³ Loading NaCl or CaCl_2 by impregnation reduced the tar yield to ~ 2.5 and 8.0 wt % (daf), respectively, because of the enhanced catalysis of chlorides loaded onto the coal.²² The similar quantity of tar derived from in situ photography of raw coal in this study supported the stronger catalytic effect of the inherent ash-forming metals in this coal. However, in contrast to the observation that the acid prewashing of Victorian brown coal doubled its tar yield under the pyrolysis,³³ the results in Figure 9 indicated only a slight increase of tar yield by 0.5 wt % upon acid washing in the oxy-26 and oxy-31 cases. Clearly, the in situ generated tar residing on the char particle surfaces is easily cracked/consumed by the rapid oxidation in the surrounding oxygen.

The dynamic release of a volatile cloud (i.e., heavy hydrocarbons) and its oxidation rate on the coal surface, referring to flame propagation velocity, were also traced by high-speed camera on a millisecond time scale. The typical sequences are displayed in Figure 10, in which the photographs were taken at intervals of 2 ms. For the case of raw coal in air, sequence a, the rodlike shape formed at the beginning of the photographs refers to the volatiles released with a very thin layer (i.e., small amount), which gradually enlarged to a nearly round sphere signaling the enhanced release and accumulation of tarry volatile species on char surface. Subsequently, the volatile release ceased from the eighth point, as the volatile cloud was solely consumed by oxidation on the coal particle surface, leading to a gradual shrinking of the size of the igniting spot and a change of its shape back to a rod with a thinner width referring to the char particle. The duration of this process is the time for homogeneous oxidation of the volatile cloud. The acid-washed coal in air (sequence b) had a relatively longer duration for its volatile cloud oxidation. The use of oxy-21 in place of air for the combustion of coal, either raw coal (sequence c) or its acid-washed residue (sequence d), increased the duration of this homogeneous process. Quantitative analysis of the volatile oxidation duration (t , ms) and volatile oxidation rate (r , mg/s) was carried out statistically by analyzing more

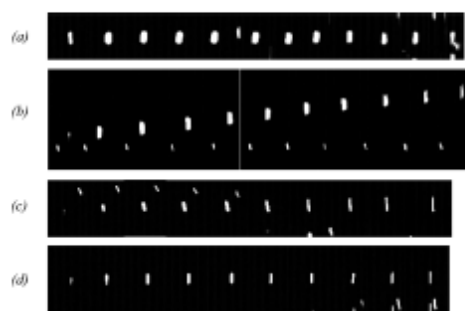


Figure 10. Dynamic oxidation of liquid volatiles on the coal particle surface at a shutter speed of 500 fps for the interval of 2 ms between two adjacent photographs: (a) raw coal in air, (b) acid-washed coal in air, (c) raw coal in oxy-21, and (d) acid-washed coal in oxy-21. Measurements were taken from high-speed camera images at 5 cm above the burner base.

than 100 igniting spots for each case, as summarized in Figure 11. Here, the volatile cloud oxidation rate was determined as

$$r = \frac{V_0 Y_V F_1}{t} \quad (3)$$

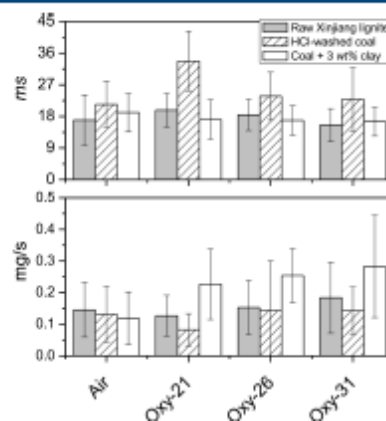


Figure 11. Liquid volatile combustion time (ms) on the coal particle surface and its combustion rate (mg/s).

The value of F_1 for the fraction of liquid tarry volatiles was taken from Figure 9, and the ignition delay t was taken from Figure 8. For all of the cases examined here, the volatile cloud oxidation times fell in a wide range from ~ 17 to 36 ms, which is longer than the maximum duration of 12 ms (on average) confirmed by the imaging of Pittsburgh bituminous coal combustion with an intensified charge-coupled device (ICCD) camera,³⁰ although the ignition delays of the coal samples tested here were rather comparable to those of the Pittsburgh coal. For the raw coal sample, the volatile cloud oxidation in air lasted for approximately 17 ms, compared to ~ 19 , ~ 18 , and ~ 16 ms for oxy-21, oxy-26, and oxy-31, respectively. These

changes were smaller than the changes in the respective ignition time in Figure 4a. The addition of clay to raw coal affected the oxidation duration of the volatile cloud only slightly, except in the oxy-21 case, where the volatile oxidation duration was slightly reduced compared with that of raw coal. The acid washing was more influential, increasing the volatile cloud oxidation time (compared to that of raw coal) by around 4 ms for the three cases of air, oxy-26, and oxy-31, and even as much as 14 ms in the oxy-21 case. Clearly, the ash-forming metals play a pivotal role in catalyzing the oxidation of the tarry volatile cloud, by acting as the oxygen-shuttling agent.

The volatile cloud oxidation rate derived from eq 3 demonstrates a low oxidation rate for the volatile cloud on the acid-washed coal surface. Interestingly, the addition of clay promoted the volatile cloud oxidation rate, although it affected the duration only slightly. This is due to the enhanced amount of volatiles on the coal particle surface, as discussed before. The extra tarry species were consumed at the same rate as those derived from raw coal pyrolysis. As confirmed by ignition, the clay used should also be insignificant in promoting oxygen shuttling for the oxidation of volatiles. However, upon the mixing of coal with clay, a larger quantity of heat would be produced by volatile oxidation, which, in turn, would increase the char particle temperature and oxidation rate, leading to a brighter top section for the flame observed in Figure 3. This is supported by the calculation results on the adiabatic particle temperature of volatile cloud detailed in Figure S6 (SI). For the raw coal and the acid-washed coal with an average amount of 2 wt % volatile cloud on its surface, the adiabatic particle temperature in air reached approximately 1100 K, which was raised to ~1500 K when clay was mixed with the coal. A similar increment was confirmed in the oxy-21 case.

The oxidation rate of the volatile cloud and its duration in Figures 10 and 11 for raw coal and acid-washed coal can also be fitted by the TGA devolatilization rate with the parameters in Table 3. Following a simple first-order reaction model for coal devolatilization (detailed in the SI), Figure 12 reveals the completion of raw coal devolatilization in 20 and 24 ms for the air and oxy-21 cases, respectively. This is consistent with the corresponding values calculated in Figure 11. The bottom panel in Figure 12 also indicates a maximum release rate of raw coal volatiles at around 7.5 and 11 ms for air and oxy-21, respectively. This is in good agreement with the photographic sequence for the two raw coal cases in Figure 10. In contrast, the acid-washed coal released a maximum of 0.4% of its volatiles in 40 ms in the air and oxy-21 cases. Its volatile release/oxidation rate was also far lower than that of raw coal (see the bottom panel of Figure 12). Here again, this was caused by the loss of the catalytic metals in coal matrix. For the unreleased volatiles within the char matrix, their oxidation should occur in parallel with the ignition and oxidation of the remaining char particle.

The oxidation rate measured here for the tarry species derived from lignite pyrolysis falls in the range of 0.1–0.3 mg/s, which is comparable to the wood volatile oxidation rate of approximately 0.25 mg/s³⁴ in Table 4. This range, however, is far different from that of pure aliphatic liquid fuels and aromatic fuels³⁵ in Table 4, indicating the complexity of the components in the volatile cloud. Moreover, by taking the surface area of the volatile cloud (calculated using the averaged diameter derived from Figure 6) into account, the volatile cloud oxidation rate can be further deduced to range from 5.9×10^{-3} to 1.48×10^{-2} g/(cm² s), which is significantly higher than the intrinsic

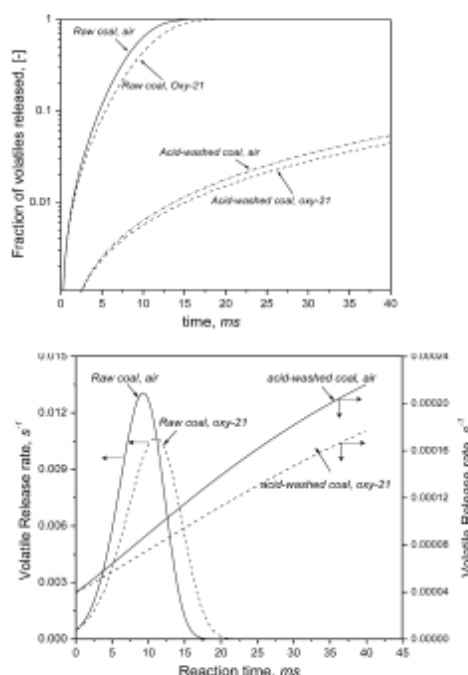


Figure 12. Predicted devolatilization mass loss and rate for raw coal and acid-washed coal in air and oxy-21. The TGA data in Table 3 were used for predictions based on a first-order reaction.

Table 4. Combustion Rates for Liquid Fuels in the Literature

	kg/(m ² s)	mg/s
polyethylene ³³	0.026	0.044
heavy fuel oil (2.6–23 m) ³³	0.036	0.061
n-heptane (1.2–10 m) ³³	0.075	0.126
benzene (0.75–6.0 m) ³³	0.081	0.137
diesel (2 mm) ³⁶		1.000
n-dodecane (2 mm) ³⁶		1.500
n-heptane (2 mm) ³³		1.500
wood volatile ³⁴		0.250

reactivity of brown coal char of 10^{-3} – 10^{-4} g/(cm² s) at 1000–1660 K.³⁶ Clearly, the heat feedback from volatile cloud combustion is essential to promote char particle oxidation. The demineralization of lignite reduced both the release and oxidation rates of volatile species, which thus mandates the use of an oxygen-enriched environment to ensure efficient combustion. The mixing of clay is beneficial in promoting volatile cracking and oxidation under the oxygen-lean oxy-fuel conditions, although the benefit is marginal compared to the removal of inherent ash-forming metals from the coal matrix.

5. CONCLUSIONS

In this study, intensive experiments have been conducted on the ignition and flame properties of Xinjiang (China) lignite in air versus oxy-fuel combustion and the influence of inherent

ash-forming metals and external clay on its combustion properties. Through the use of an FFBR coupled with advanced optical diagnosis tools, the dynamic release of lignite volatiles; the formation, ignition, and oxidation of the volatile cloud; and flame propagation have been explored intensively. The major conclusions as follows have been achieved:

(1) At a heating rate of approximately 10^5 K/s in the FFBR, the ignition of the lignite tested was triggered by the homogeneous ignition of the tarry volatile cloud on the particle surface. Alkane species are assumed to dominate the first ignited volatile cloud with an autoignition temperature of approximately 500–600 K and an oxidation rate of 0.1–0.3 mg/s. Its fraction in the total volatile matter accounts for 2.0–3.5 wt %, depending on the presence of inherent ash-forming metals and external clay.

(2) The removal of HCl-soluble metals shifted coal devolatilization toward higher temperatures. The volatiles of acid-washed coal were released slowly. The ignition time and oxidation duration were increased by nearly a factor of 2 in air and oxy-21, compared with raw coal. The flame formed was lifted from the burner base and thus unstable.

(3) The mixing of external clay with coal affected the coal ignition onset in air and oxy-21 conditions only minimally relative to that of coal alone. It enhanced the decomposition of volatiles, leading to a larger volatile cloud shielding the coal particle surface that, in turn, enhanced the coal flame, char particle temperature, and burnout rate.

(4) The oxygen fraction in the bulk gas is most influential on the coal ignition and oxidation rate. Increasing the oxygen fraction to 30% in the bulk gas eliminated all gaps between raw lignite, its acid-washed sample, and a mixture of lignite and clay.

■ ASSOCIATED CONTENT

Supporting Information

Blank gas temperature profile, procedures for coal particle heating profile, CFD modeling, and adiabatic particle temperature and coal devolatilization rate calculations. This material is available free of charge via the Internet at <http://pubs.acs.org>.

■ AUTHOR INFORMATION

Corresponding Author

Notes

The authors declare no competing financial interest.

■ ACKNOWLEDGMENTS

The authors are grateful for support from the Australian Research Council (FT01009909), Australian National Low Emission Coal (ANLEC) R&D, and Brown Coal Innovation Australia (BCIA). X.W. is supported by an Australian Academy of Technological Engineering Science (ATSE) Joint Co-ordination Grant (JCG) 2013-14 for long-term visiting to Monash University. He also thanks National Natural Science Foundation of China (NSFC 50906055 NS 51276212) for the support of a portion of the work. We also thank Hubei Yihua Group Co. Ltd., Yichang City, Hubei, China, for providing lignite coal and clay samples.

■ NOMENCLATURE

A = prefactor for fuel ignition reactivity, s^{-1}
 C_v = volumetric specific heat capacity of bulk gas

F_L = fraction of liquid tarry volatile cloud on particle surface
 f_v = amount of oxygen needed to burn per gram of volatiles
 P = gas pressure, atm
 q_c = combustion heat release per mass of fuel, kJ/g
 R = gas constant, $cm^3 \text{ atm}/(\text{mol K})$
 r_{doad} = volatile cloud oxidation rate, mg/s
 r_p = particle radius, cm
 r_v = volatile flame radius, m
 t = time, s
 T = particle temperature, K
 T_0 = initial temperature of coal particle, K
 T_a = igniting coal particle temperature, K
 T_{max} = peak temperature in coal oxidation profile measured by TGA, K
 V_s = volume of a single coal particle, m^3
 w = density of air-dried coal, g/cm^3
 Y_v = mass fraction of volatiles in air-dried coal
 Y_{sp} = initial mass fraction of fuel
 β = heating rate for particles in TGA, K/min
 $\Delta V/V_0$ = volatiles release rate
 τ_i = autoignition time of fuel i , s

■ REFERENCES

- (1) Barnes, I. *Slagging and Fouling in Coal-Fired Boilers*; IEA Clean Coal Centre: London, Apr 2009.
- (2) Gupta, R. P.; Wall, T. F.; Baxter, L., Eds. *Impact of Mineral Impurities in Solid Fuel Combustion*; Kluwer Academic/Plenum Publishers: New York, 1999.
- (3) Wai, S.; Chen, W.-Y.; Shi, G. Roles of mineral matters in the early stage of coal combustion. *Energy Fuels* 2009, 23, 710–718.
- (4) Wijaya, N.; Zhang, L. A critical review of coal demineralization and its implication on understanding the speciation of organically bound metals and submicrometer mineral grains in coal. *Energy Fuels* 2011, 25, 1–16.
- (5) Wijaya, N.; Choo, T. K.; Zhang, L. Generation of ultra-clean coal from Victorian brown coal—Sequential and single leaching at room temperature to elucidate the duration of individual inorganic elements. *Fuel Process. Technol.* 2011, 92, 2127–2137.
- (6) Wijaya, N.; Choo, T. K.; Zhang, L. Generation of ultra-clean coal from Victorian brown coal: Effect of hydrothermal treatment and particle size on coal demineralization and the extraction kinetic of individual metals. *Energy Fuels* 2012, 26, 5028–5035.
- (7) Rasek, E., Ed. *Mineral Impurities in Coal Combustion, Behavior, Problems and Remedial Measures*; Hemisphere Publishing Corporation: Washington, DC, 1985; pp 283–310.
- (8) Vuřaluru, H. B.; Domazetis, G.; Wall, T. F.; Vleskens, J. M. Reducing fly ash deposition by pretreatment of brown coal: Effect of aluminum on ash character. *Fuel Process. Technol.* 1996, 46, 117–132.
- (9) Tomita, A.; Ohtsuka, Y. Gasification and Combustion of Brown Coal. In *Advances in the Science of Victorian Brown Coal*; Li, C.-Z., Ed.; Elsevier: , 2004; Chapter 5, pp 223–285.
- (10) Taniguchi, M. Fundamental experiments of coal ignition for engineering design of coal power plants. In *Thermal Power Plants*; Rasul, M., Ed.; InTech: Rijeka, Croatia, 2012; Chapter 4, pp 65–89.
- (11) Chen, J. C.; Taniguchi, M.; Ito, K. Observation of laser ignition and combustion of pulverized coals. *Fuel* 1995, 74, 323–330.
- (12) Li, J.; Querol, X.; Zhuang, X.; Font, O. Comparative Study of Coal Qualities from Three Large Coal Basins in Xinjiang, Northwest China. In *31st Meeting of the Spanish Mineralogical Society (SEM)*; Spanish Mineralogical Society: Barcelona, Spain, 2011; pp 121–122.
- (13) Cook, P. S.; Cashion, J. D. Mössbauer study of iron exchanged into brown coal. *Fuel* 1987, 66, 661–8.
- (14) Harris, A.; Zhong, Z. Non-isothermal thermogravimetric analysis of plywood wastes under N_2 , CO_2 and O_2 atmosphere. *Asia-Pac. J. Chem. Eng.* 2008, 3, 473–80.

- (15) Kim, J. D.; Kim, G. B.; Chang, Y. J.; Song, J. H.; Jeon, C. H. Examination of flame length for burning pulverized coal in laminar flow reactor. *J. Mech. Sci. Technol.* **2010**, *24*, 2567–75.
- (16) Murphy, J. J.; Shaddix, C. R. Combustion kinetics of coal chars in oxygen-enriched environments. *Combust. Flame* **2006**, *144*, 710–29.
- (17) Zhang, L.; Binner, E.; Qiao, Y.; Li, C.-Z. High-speed camera observation of coal combustion in air and O₂/CO₂ mixtures and measurement of burning coal particle velocity. *Energy Fuels* **2010**, *24*, 29–37.
- (18) Liu, Q.; Hu, H.; Zhou, Q.; Zhu, S.; Chen, G. Effect of inorganic matter on reactivity and kinetics of coal pyrolysis. *Fuel* **2004**, *83*, 713–8.
- (19) Zhang, J.; Pratiño, W.; Zhang, L.; Zhang, Z. Computational fluid dynamics modeling on the air-firing and oxy-fuel combustion of Dried Victorian brown coal. *Energy Fuels* **2013**, *27*, 4258–69.
- (20) Ubhayakar, S. K.; Stickle, D. B.; Von Rosenberg, C. W.; Gannon, R. E. Rapid devolatilization of pulverized coal in hot combustion gas. *Symp. (Int.) Combust., Proc.* **1976**, *16*, 427–436.
- (21) Kobayashi, H.; Howard, J. B.; Sarofim, A. F. Coal devolatilization at high temperatures. *Symp. (Int.) Combust., Proc.* **1976**, *16*, 411–425.
- (22) Qynn, D. M.; Wu, H.; Hayashi, J. I.; Li, C. Z. Volatilization and catalytic effects of alkali and alkaline earth metallic species during the pyrolysis and gasification of Victorian brown coal. Part IV. Catalytic effects of NaCl and ion-exchangeable Na in coal on char reactivity. *Fuel* **2003**, *82*, 587–93.
- (23) Franklin, H. D.; Peter, W. A.; Howard, J. B. Mineral matter effects on the rapid pyrolysis and hydropyrolysis of a bituminous coal. 1. Effects on yields of char, tar and light gaseous volatiles. *Fuel* **1982**, *61*, 155–60.
- (24) Folguera, M. B.; Alonso, M.; Diaz, R. M. Influence of sewage sludge treatment on pyrolysis and combustion of dry sludge. *Energy* **2013**, *55*, 426–35.
- (25) Zou, X.; Yao, J.; Yang, X.; Song, W.; Lin, W. Catalytic effects of metal chlorides on the pyrolysis of lignite. *Energy Fuels* **2007**, *21*, 619–24.
- (26) Copalakis, R.; Fullwood, M. J.; Bartholomew, C. H. Catalysis of char oxidation by calcium minerals: Effects of calcium compound chemistry on intrinsic reactivity of doped Spherochar and Zap chars. *Energy Fuels* **1994**, *8*, 984–9.
- (27) Davidson, R. M.; Santos, S. *Oxyfuel Combustion of Pulverized Coal*; IEA Clean Coal Centre: London, Jun 2010.
- (28) Shaddix, C.; Murphy, J. J. Coal char combustion reactivity in oxy-fuel applications. Presented at the 20th Pittsburgh Coal Conference, Pittsburgh, PA, Sep 15–19, 2003.
- (29) Zhang, L.; Binner, E.; Qiao, Y.; Li, C.-Z. In situ diagnostics of Victorian brown coal combustion in O₂/N₂ and O₂/CO₂ mixtures in drop-tube furnace. *Fuel* **2010**, *89*, 2703–12.
- (30) Shaddix, C. R.; Molina, A. Particle imaging of ignition and devolatilization of pulverized coal during oxy-fuel combustion. *Proc. Combust. Inst.* **2009**, *32*, 2098–8.
- (31) B-rub, Z. A.; Bramer, E. A.; Brem, G. Evaluation of catalysts for tar elimination in biomass gasification processes. *Ind. Eng. Chem. Res.* **2004**, *43*, 6911–19.
- (32) Howard, J. B.; Essenhigh, R. H. Mechanisms of Solid Particle Combustion with Simultaneous Gas-Phase Volatiles Combustion. *Symp. (Int.) Combust., Proc.* **1967**, *11*, 399–408.
- (33) Jamil, K.; Hayashi, J.-I.; Li, C.-Z. Pyrolysis of a Victorian brown coal and gasification of nascent char in CO₂ atmosphere in a wire-mesh reactor. *Fuel* **2004**, *83*, 833–43.
- (34) Barde, K. D.; Fitzpatrick, E. M.; Jones, J. M.; Kubacki, M. L.; Plant, R.; Pourkashanian, M.; Ross, A. B.; Williams, A. The combustion of droplets of liquid fuels and biomass particles. Presented at the 4th European Combustion Meeting, Vienna, Austria, Apr 14–17, 2009. Available at <http://www.cwprp.leu.ac.uk/hartford/~ernesto/S2013/MMEES/Papers/ENERGY/5Biomass/Barde2009-LiquidFuelBiomassCombustion.pdf>.
- (35) Tewarson, A. *SFPE Handbook of Fire Protection Engineering*, 2nd ed.; National Fire Protection Association: Quincy, MA, 1995.
- (36) Smith, I. W. The combustion rates of coal chars: A review. *Symp. (Int.) Combust., Proc.* **1982**, *19*, 1045–1065.
- (37) Morgan, M.; Jenkins, R. G. Pyrolysis of a lignite in an entrained flow reactor: 1. Effect of cations on total weight loss. *Fuel* **1986**, *65*, 757–68.

This page is intentionally left blank



Research article

Influence of inherent moisture on the ignition and combustion of wet Victorian brown coal in air-firing and oxy-fuel modes: Part 1: The volatile ignition and flame propagation

Wirhan Pratiño^a, Jian Zhang^a, Jianfang Cui^b, Yatao Wang^b, Lian Zhang^{a,*}^a Department of Chemical Engineering, Monash University, Clayton, Victoria 3800, Australia^b Coal Chemical R&D Center of Kailuan Group, South No. 3 Road, Seaport Economic Development Zone, Tangshan, Hebei Province 063611, China

ARTICLE INFO

Article history:

Received 20 May 2015

Received in revised form 6 July 2015

Accepted 8 July 2015

Available online xxxxx

Keywords:

Oxy-fuel combustion

Wet Victorian brown coal

Inherent moisture

ABSTRACT

This study for the first time reported the volatile ignition and oxidation for wet Victorian brown coal in both air-firing and oxy-fuel modes. The aim is to quantitatively understand the evaporation of inherent moisture and its overlapping with the subsequent volatile ignition and oxidation steps during pulverised coal combustion. A wet Victorian brown coal sample with the moisture content up to 30 wt% and a size range of 63–104 µm has been tested. Its ignition, volatile flame propagation and char oxidation have been diagnosed optically in a laboratory-scale flat-flame burner reactor (FFBR) coupled with a high-speed camera. 1-D modelling was also conducted to predict coal ignition based on the classic coal drying theory and coal devolatilisation rate. As has been confirmed, the release of moisture on the initial drying stage is incomplete prior to the subsequent volatile ignition. The fraction of moisture released upon drying only accounted for 10% of its original amount in wet brown coal prior to ignition. This is due to a firm residence of the moisture within coal capillaries, and a rapid heat feedback from hot gas to the dried particle surface that was ignited instantaneously prior to the release of the remaining moisture. The unevaporated moisture was observed to be released with the volatiles together to form a thick cloud layer in the vicinity of the coal particle, thereby enlarging the sizes of the volatile flame remarkably, which are approximately twice the size of the dried coal flame. However, the intensity of the wet coal flame was much weaker than dried coal, due to the dilution effect of the inherent moisture on the volatile cloud. In the oxy-fuel combustion mode, the inherent moisture interrelated with CO₂, a tri-atomic gas with a larger specific heat capacity than N₂, to significantly delay the ignition of the wet coal particle and its flame intensity and propagation velocity.

© 2015 Elsevier B.V. All rights reserved.

1. Introduction

As a substitution for high-rank bituminous coal, low-rank coal has been receiving increased attention from the energy and mining sectors worldwide. Burning low-rank coal results in a high CO₂ emission rate compared to that of high-rank coal. In Victoria, Australia, the pulverised coal-fired power stations provide more than 85% of the electricity need in the whole State. Upon the restraint on CO₂ emission, there is an urgent need from the brown coal industry to deploy the next generation low emission technologies such as oxy-fuel combustion [1]. A common feature of brown coal is the presence of abundant inherent moisture within its carbonaceous matrix. An accurate understanding on the fate of brown coal moisture at high temperatures is pivotal for its burner/furnace design.

To date, the coal drying mechanism was simplified as the initial combustion step that was separated from and had little overlapping with

the following combustion sequences. This is fundamental for wet coal combustion simulation in the commercial computational fluid dynamics (CFD) program, Fluent [2,3]. The application of a shrinking-core model to study the drying behaviour of Victorian brown coal in hot gas has been developed and verified [4,5]. Once being vaporised, the moisture was merely considered as a form of external steam, creating a steam-rich environment that is similar to wet flue gas recycle in the oxy-fuel mode [6,7]. In our previous lab-scale drop-tube furnace (DTF) study on wet coal combustion, the reduction on the temperature of a burning wet coal particle has been witnessed, which was supposedly due to the contribution of steam gasification reaction towards the char matrix, as opposed to the steam gasification from the ambient steam [8]. In addition, a study on wet coal pyrolysis in a drop-tube/fixed-bed furnace revealed the enhanced in-situ steam gasification on the nascent char surface [9]. Following these observations, there are two types of moisture identified, one is external moisture that is released during the initial drying step and the other is internal moisture that preferentially remains firmly within the coal matrix over a longer period of time. The use of a Curie-point pyrolyser further revealed the promoting

<http://dx.doi.org/10.1016/j.fuproc.2015.07.008>
0378-3820/© 2015 Elsevier B.V. All rights reserved.

Please cite this article as: W. Pratiño, et al., Influence of inherent moisture on the ignition and combustion of wet Victorian brown coal in air-firing and oxy-fuel modes: Part 1, Fuel Processing Technology (2015), <http://dx.doi.org/10.1016/j.fuproc.2015.07.008>

effect of sorbed water on the transformation of oxygen and hydrogen atoms into char, gaseous products CO and H₂, and liquid tar, probably via enhanced hydrolysis reactions [10]. More interestingly, early work on coal–water slurry combustion revealed that, for an American lignite Beulah–water slurry droplet containing 60 wt.% coal and in a size of 490–730 µm, its heating upon a Bunsen burner exhibited an initial temperature plateau at ~473 K, rather than 373 K for the case of water evaporation from bituminous coal–water slurry [11]. This was explained by a simultaneous moving of both water evaporation front and thermal front towards the centre of the droplet, as well as a violent devolatilisation of brown coal even at very low temperatures. A similar phenomenon was observed in another work for the combustion of wet Victorian brown coal (Loy Yang) in a fluidised bed reactor [12]. At a hot air temperature of 1043 K and an original coal size of 5.6–6.4 mm, approximately 40% of volatiles and 80% moisture (bulk and capillary waters) were released simultaneously in the first 15 s. The released water evaporation is continued, and the monolayer and/or multilayer water constitutes the most strongly held materials that are supposed to remain permanently in a char particle. The authors confirmed a nearly constant total burnout time over a wide range of moisture content in coal, and even a faster burnout rate for the char from wet coal than from the nearly dried sample. This was hypothesised due to a greater porosity and/or a greater concentration of active sites of the wet coal char, rather than water–gasification reaction that was considered elsewhere [13]. Surprisingly, no research was continued further to prove these interesting but contradictory observations.

In this study, a flat flame burner reactor (FFBR) coupled with a transparent quartz reactor and advanced in-situ optical diagnosis tools was employed to examine the combustion characteristics of wet Victorian brown coal in both air-firing and oxy-fuel modes. The flat flame generated from the burning of liquid fuel provided a rapid heating rate of ~10⁵ C/s that is comparable to that in an industrial-scale power plant. Moreover, a high-speed camera with a maximum shutter speed of 5000 frames per second (fps) was used to track the behaviour of individual particles upon drying, devolatilisation, volatile cloud ignition and char particle motion [8,14,15]. Apart from air-firing, the oxy-fuel condition was also employed to examine the combined impacts, if any, of CO₂ and steam on brown coal combustion characteristics. In

order to further interpret the experimental results, a traditional one-dimensional single-film model with multiple surface reactions was applied and its results were compared with the collected experimental data. A joint effort of both experimental investigation and modelling study is expected to quantitatively clarify the role of moisture on the individual steps underpinning the combustion of brown coal in both air and O₂/CO₂ mixtures. This study has been split into two parts: part 1 for the study on volatile ignition and flame structure, and part 2 for char oxidation temperature profile.

2. Experimental facility

2.1. Non-premixed flat-flame burner reactor (FFBR)

The schematic diagram of the experimental facility is illustrated in Fig. 1. The reactor was operated at atmospheric pressure, with a non-premixed flat-flame diffusion burner (Hencken burner) that provided a heat source for coal particle heat-up and combustion. The burner is assembled from a honeycomb matrix, consisting of hundreds of fuel tubes with the inter-space between these primary tubes. The burner is equipped with a shroud ring that acts as a shield to prevent any interference to the flat flame. The coal particle streams are injected to the burner through a 1.6 mm diameter tube located at the burner centreline, entrained with CO₂ or air as the carrier gas. A piezoelectric feeder was used as the particle feeder. It was calibrated to provide a particle feeding rate of 0.1 g/min with the fixed carrier gas flow rate of 0.7 slpm (standard litre per minute). The feeder has the capability of providing wet coal with a maximum moisture content of 30 wt.%. The mixture of C₂H₄/H₂ was fed through the fuel tube as the burner fuel. The oxidant consisted of a mixture of air, CO₂ and O₂, and was fed into the interspace between the fuel tubes. The combustion chamber is also isolated within a cylindrical quartz-tube reactor with an inner diameter of 115 mm, which is also insulated by a layer of kaowool with a thickness of about 20 mm to minimise the heat loss. A portion of the insulation material was cut off at one side of the quartz reaction, creating a window for the purpose of visual flame observation and cinematography using non-intrusive optical diagnostics tools.

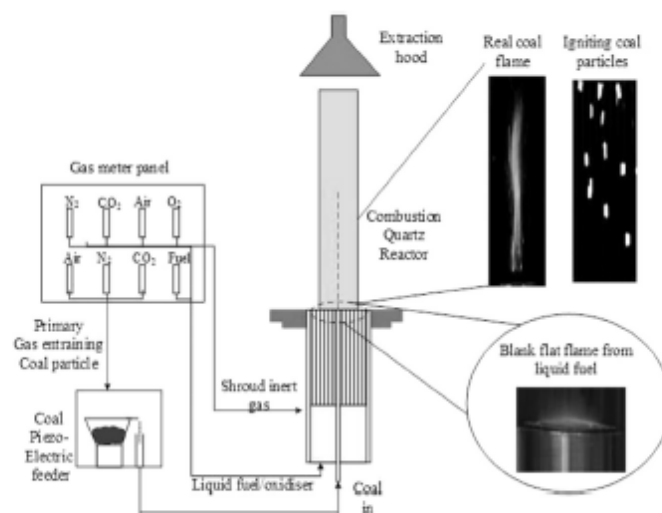


Fig. 1. Schematic diagram of entrained flow reactor flat flame burner facility.

Please cite this article as: W. Pratono, et al., Influence of inherent moisture on the ignition and combustion of wet Victorian brown coal in air-firing and oxy-fuel modes: Part 1., Fuel Processing Technology (2015), <http://dx.doi.org/10.1016/j.fuproc.2015.07.008>

The non-premixed Hencken flat-flame burner provides a wide range of flexibility on the gas temperature and the concentration of O_2 at the post-flame based on the chosen flow rates of the fuel and oxidizer gases. In this study, the fuel/oxidiser ratio was adjusted to provide a post-flame oxygen concentration of 16–31 vol%, to examine the effect of oxygen concentration on wet coal combustion, whereas the steam concentration remained constant at 17.5 vol%. It is assumed that the concentration profile of the species gas (O_2 , CO_2 , H_2O and N_2) was uniform at the cross section. The burning of liquid fuel lasted ≈ 30 min before coal was introduced into the reactor, to ensure a steady state temperature profile along the reactor height. The summary of the experimental conditions is given in Table 2. The concentration of the gaseous species in the reactor was calculated based on the stoichiometric reactions of liquid fuel with oxygen assuming a complete combustion of ethylene/ H_2 vapour. The chosen fuel/oxidiser flow rates provides an ambient temperature of 1473 K near the burner base, at the total gas flow rate of 11 slpm, regardless of the oxygen mole fraction. The gas temperature along the reactor height was measured using a type-K thermocouple and corrected for radiation loss [16]. The calculation procedure to account for the radiation loss from the thermocouple is supplied in Section A of the supporting documentation. Fig. 2 demonstrates a similar gas temperature profile along the reactor height for both O_2/N_2 and O_2/CO_2 mixtures under the blank condition (with no coal flowing). The gas temperature profiles are similar for all cases and therefore, have no effect on coal ignition and combustion under different experimental cases.

2.2. Fuel properties

The coal sample used was mined from the Loy Yang open-cut seam in the Latrobe Valley, Australia. It is milled to a size fraction of 63–104 μm , similar to that used in an industrial power plant. The proximate and ultimate analysis of the brown coal is tabulated in Table 1. The air-dried coal sample was prepared by natural drying of the as-mined wet coal in ambient air until its moisture content remained unchanged in the laboratory environment. The remaining moisture refers to the monolayer/multilayer moisture that binds atomically with the functional groups in a coal matrix. For the wet coal samples, they were prepared by mixing the de-mineralised Milli-Q water with air-dried coal, rather than drying the as-mined wet coal to a certain moisture level. The prepared wet coal samples were placed in a sealed bottle that was thoroughly mixed at a speed of 300 rpm in the rotator overnight. This is to ensure that the added water was fully adsorbed into the coal matrix. The current particle feeding system has a limited capability to supply wet coal with the maximum moisture content of 30 wt%. Therefore, the wet coal samples with two moisture contents, 22 wt% and 30 wt%, were prepared and were identified as semi-dry and wet coal hereafter, respectively. For comparison purpose, the air-dried coal with 12 wt% equilibrated moisture is denoted as dry coal throughout this study.

Table 1
Properties of brown coal sample used in this study.

Proximate analysis (wt.% dry-basis)	
Moisture content	12.0
Fixed carbon	41.4
Volatile matter	45.0
Ash	1.6
Ultimate analysis (wt.% dry-ash free)	
C	65.7
H	6.8
N	0.6
S	0.5
O (by-difference)	25.4

Table 2
Summary of the experimental condition in this study.

Gas species	Gas composition (vol.%)		
	Air	21% O_2/CO_2	31% O_2/CO_2
O_2	21.03%	21.57%	31.54%
N_2	44.04%	0.00%	0.00%
CO_2	16.44%	59.93%	49.88%
H_2O	18.49%	18.50%	18.58%

2.3. Non-intrusive in-situ optical diagnostics facility

A P7000 Nikon CCD digital camera and a Motion Pro Y3 high-speed camera from IDT lens at a shutter speed of 1000 fps were employed for coal flame image acquisition. The high speed camera was also fitted with a 25 mm micro-lens for high magnification images to capture a fast-transient event that happens during the initial heating and combustion stage. The captured images were analysed using an open-source image processing software, Image-J, to obtain information regarding coal flame length, ignition point, burning particle size and particle velocity.

The images captured with the digital camera were analysed statistically to quantify the coal flame length and the length of three combustion steps, pre-ignition, homogeneous volatile oxidation and heterogeneous char combustion regime as visualised in Fig. 3. As can be seen, the volatiles released from the coal particles burn after a certain distance which is called pre-ignition stage here. Such a stage is shown as the yellowest, blurred cloud with a very weak intensity reflecting the heat-up of a particle and the release of volatiles and/or moisture. Once ignited, the released volatiles form a continuous fireball with the strongest intensity captured by the camera. The ignition point refers to the bottom boundary between pre-ignition and volatile oxidation stages. The detailed ignition of coal particles was further observed by a high-speed camera at a shutter speed no less than 500 frames per second (fps). To maximise the number of particles captured by the high-speed camera, the sensor's gain was set to +6 dB and the exposure time was set to around 980 μs [14]. The homogeneous ignition was defined as the round or nearly round, bright spots observed in the field of view (FOV) of the high-speed camera, due to the release and residence of volatiles on the particle surface. In contrast, the heterogeneous ignition of char refers to the bright rod-like spots which have few volatiles on the surface [14]. Back to the CCD camera picture in Fig. 3, the luminous, thick flame following the ignition point and enveloping the cloud near the burner base signifies an intense release and homogeneous combustion of volatiles released from the coal pyrolysis, which in turn supplies heat feedback to ignite the char particles. The remaining

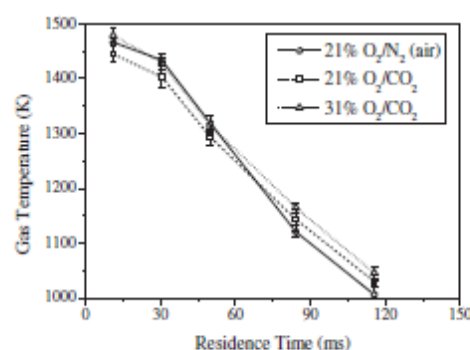


Fig. 2. Centre-line gas temperature profile in air and 21% O_2/CO_2 .

Please cite this article as: W. Pratono, et al., Influence of inherent moisture on the ignition and combustion of wet Victorian brown coal in air-firing and oxy-fuel modes: Part 1., Fuel Processing Technology (2015), <http://dx.doi.org/10.1016/j.fuproc.2015.07.008>

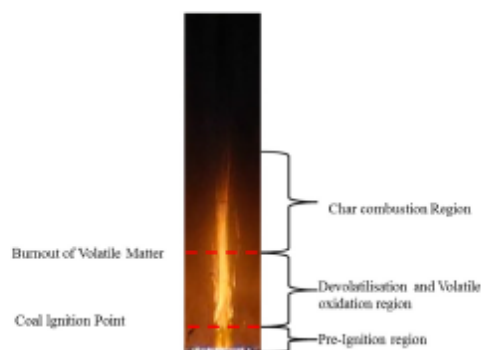


Fig. 3. Combustion region segmentation based on flame structure.

length of the flame, with the less luminous region above the volatile oxidation regime, refers to the char oxidation region. A similar analysis method has also been described elsewhere [17].

The trajectory and transformation of individual particles, including particle velocity, coal ignition point, and volatile cloud size, were tracked with the high-speed camera. The images were taken at the first 1 cm, 5 cm and 10 cm above the burner base. The particle velocity was calculated by measuring the displacement of the same individual particle between two adjacent frames, taking a 1 ms time interval between the consequent frames from the capture speed of 1000 fps. The detailed methods to calculate the particle velocity have been described previously [14]. The averaged particle velocity profile along the reactor length is given in Fig. 4. The average particle velocity in an oxy-fuel atmosphere is slightly lower as CO_2 has a higher density than N_2 . A sharp increase was observed for the particle velocity in the initial 50 mm height, which is mainly due to a rapid heat-up and expansion of the primary gas that entrains coal particles into the hot secondary gas. The particle velocity is stabilised afterwards.

The particle ignition point and volatile cloud size were measured from the high speed camera images by using Image-J. Compared with the digital camera, the high speed camera is capable of capturing individual particles, and therefore, the images created provide accurate information regarding the coal ignition point. The ignition point was measured from the burner base to the first point where the igniting bright spots were observed. The ignition time, volatile oxidation and char oxidation time were calculated by dividing measured lengths with the calculated particle velocity at their respective height. Note

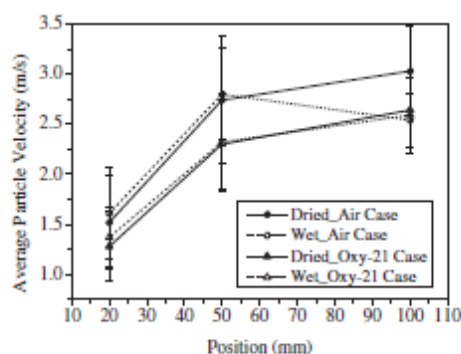


Fig. 4. Calculated average particle velocity of dried and wet coal.

that, a low particle feeding rate of ~ 0.1 g/min was used throughout this study to ensure the observation of single particles with minimal interference between one another.

3. Mathematical formulation

To interpret the experimentally observed coal particle ignition stage, numerical modelling through the use of a forward difference method and pseudo-code algorithm, as demonstrated in Fig. 5, were employed to solve the differential equations for particle heat-up, drying and devolatilisation that are three key regimes prior to particle ignition. The equations for these sub-steps are presented in the following sections.

3.1. Coal drying

The receding wet-core dry-shell model from McIntosh [4,5] was used to calculate the coal drying time by Eqs. (1) and (2). For the pulverised coal $<100 \mu\text{m}$, this model assumes a constant drying rate that is equal to the initial drying rate of a non-shrinking water droplet.

$$MC = MC_0(1 - nt) \quad (1)$$

where MC and MC_0 are the present and initial moisture contents within the coal matrix, respectively, t is the drying time required to achieve the present moisture content and n is an empirical constant expressed as:

$$n = \frac{6h(T_g - T_a)}{H_L \rho_w [MC_0] d_p} \quad (2)$$

where h = convective heat transfer coefficient, calculated based on a Nusselt number of 2 for pulverised coal combustion [18], and the properties of gas mixtures were calculated based on the Wassiljewa's equation with Maxon-Saxena formulation [19], T_g = gas temperature, T_a = coal wet bulb temperature, H_L is the latent heat of vaporisation, ρ_w is the density of wet coal and d_p particle diameter. The wet-bulb temperature of hot gas, T_a is a function of ambient gas temperature and is set at 360 K for an average hot gas temperature of 1200 K in this study.

3.2. Coal devolatilisation

The coal devolatilisation is modelled by a single kinetic rate model that assumes a first-order reaction rate [20], where the volatile release rate is proportional to the amount of volatiles released and expressed as:

$$\frac{dv}{dt} = A_{\text{devol}} \exp\left(-\frac{E_{\text{devol}}}{RT}\right) [V^* - V] \quad (3)$$

where V is the present mass of volatiles remaining and V^* is the initial volatile amount. The kinetic data for the Arrhenius form of the equation was determined from a thermo-gravimetric analyser. For Victorian brown coal studied here, the volatiles can be assumed to be dominated by light hydrocarbons of which CH_4 is the major component [21].

3.3. Coal particle heat-up by energy balance

During the particle heat up stage, the particle absorbs heat from the hot gas as well as radiation heat from the furnace wall. The particle temperature was estimated using the following energy balance equation:

$$m_p c_p \frac{dT_p}{dt} = h A_p (T_w - T_p) + \epsilon \sigma A_p (T_w^4 - T_p^4) + Q_{\text{radiation}} \quad (4)$$

where m_p is particle mass (kg), c_p is the heat capacity of a coal particle (kJ/kg K), and h is the convective heat transfer coefficient calculated

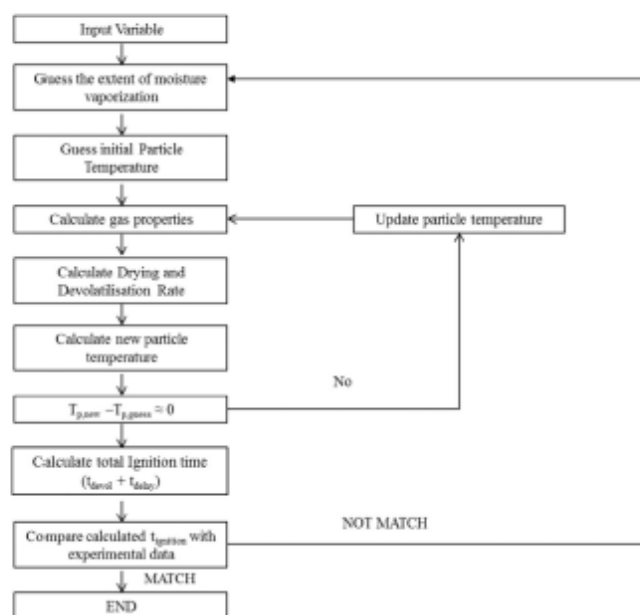


Fig. 5. Calculation procedure to determine the extent of wet coal moisture evaporation.

assuming a Nusselt number of 2. T_w is wall temperature (773 K), T_g is gas temperature measured with a thermocouple, ϵ is particle emissivity (0.8) and σ is Stefan Boltzmann constant. $Q_{reaction}$ refers to heat loss by moisture evaporation and devolatilisation.

Regarding the ignition point prior to coal volatile combustion, it corresponds to the time required for a coal particle to reach the stage where its released volatiles have a local concentration equalling its flammability. In a numerical simulation approach, such a time includes the above-mentioned particle heat-up, drying, and the release of volatiles. Once released, the volatiles are assumed to ignite instantaneously. Fig. 6 depicts the calculated mass loss profile of a dried coal in the air-firing mode, upon the variation of the particle drying extent to demonstrate how the volatile release time and local particle temperature are affected. The mass loss derivative axis, on the right hand side, depicts

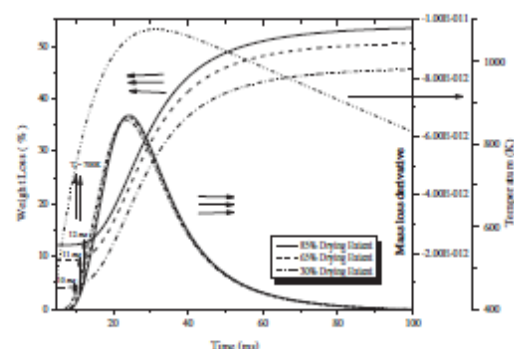


Fig. 6. Method to determine the brown coal volatile release time with the variation of the drying extent to calculate coal ignition time.

the first-order derivative of particle weight loss over time. The turning point that defines the start of the devolatilisation was derived from the sharp increase in the derivative graph. In Fig. 6 the turning points of 10.2 ms, 11 ms and 12 ms as the ignition time versus the drying extent of 30%, 65% and 85% was included, respectively.

4. Results and discussion

4.1. Experimental observation on flame structure and ignition characteristics

The representative images for the combustion of three coal samples in air are visualised in Fig. 7(a), whereas in panel (b) the axial gas temperature discrepancy measured between coal combustion and the blank case without the feeding of coal particles is shown. As demonstrated in panel (a), the flame from the combustion of dried coal has the largest intensity, whereas the boundary between different stages is rather vague. This is an indicator of an intense burning of dried Victorian brown coal due to its high reactivity, as has been confirmed previously [15,22]. The existence of moisture in the coal matrix changed the flame pattern remarkably. The semi-dried coal exhibits a clear boundary between its pre-ignition stage and volatile flame front. Such an ignition delay should be partly or entirely attributed to the evaporation of moisture within the coal particle. The flame observed also has a much weaker intensity than that observed for the dried coal. The wet coal with 30 wt.% moisture within it formed the weakest flame. The bright flame for volatile oxidation observed for the other two samples was extinguished as well. Panel (b) highlights the gas temperature profiles for the three coal samples. At the height of 50 mm which is the closest location to particle ignition location, the measured gas temperature for wet coal combustion is ~150 K lower than the gas temperature measured in the presence of dried coal combustion. This further strengthened the above flame observation that the volatile flammability was greatly reduced by the presence of the abundant moisture with the wet coal.

Please cite this article as: W. Pratono, et al., Influence of inherent moisture on the ignition and combustion of wet Victorian brown coal in air-firing and oxy-fuel modes: Part 1., Fuel Processing Technology (2015), <http://dx.doi.org/10.1016/j.fuproc.2015.07.008>

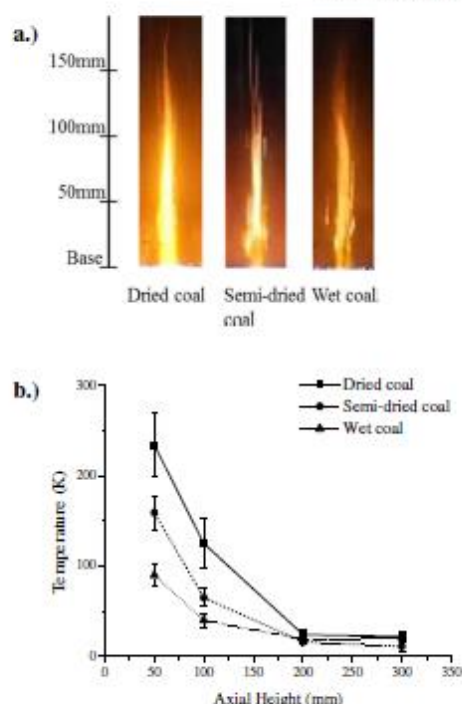


Fig. 7. Combustion of dried coal, semi-dried coal and wet coal in air (21% O_2/N_2); panel (a): flame structure; panel (b): measured axial gas temperature with coal burning in the reactor relative to blank gas temperature.

Shifting the combustion atmosphere to oxy-fuel mode resulted in an elongated coal flame with a remarkable decrease in its intensity, irrespective of the moisture content in coal. As demonstrated in Fig. 8(a), the flame formed for dried coal in 16% O_2 diluted by CO_2 exhibited the longest length, due to the large specific heat capacity of CO_2 for heat sink impact [23], and a slower diffusion rate of O_2 in a CO_2 -rich atmosphere. The combustion intensity was enhanced upon the increase of oxygen concentration in CO_2 . For the oxygen concentration of 31 vol%, the flame luminosity was found bearing a stronger intensity than in air, which should be caused by an enhanced rate for the heterogeneous oxidation of char particles. Similar results were observed for the combustion of semi-dried coal in oxy-fuel mode in panel (b), whereas its flame intensity in each case is weaker than the dried coal under the same condition. The flame length is also longer than the dried coal, which is another strong indicator of a low combustion rate including ignition for semi-dried coal. For wet coal in panel (c), its particle ignition was unstable and extinguished in the 16% O_2/CO_2 . The flame observed was also detached far away from the burner base, substantiating a significant delay by the evaporation of added moisture prior to particle ignition. The flame stability was gradually improved by increasing the oxygen fraction to 31%. Nevertheless, the flame was still unstable and lifted up from the burner, the pattern of which also differs distinctly from both dried and semi-dried coals. Fig. 9 illustrates the gas temperature discrepancy between a blank case and the combustion of a coal sample under the oxy-firing mode. Here again, the gas temperature was measured at the height of 50 mm. Similar to the trend reported in Fig. 8, the gas temperature for wet coal combustion is the lowest in each oxygen concentration, which is only 20–40 K hotter

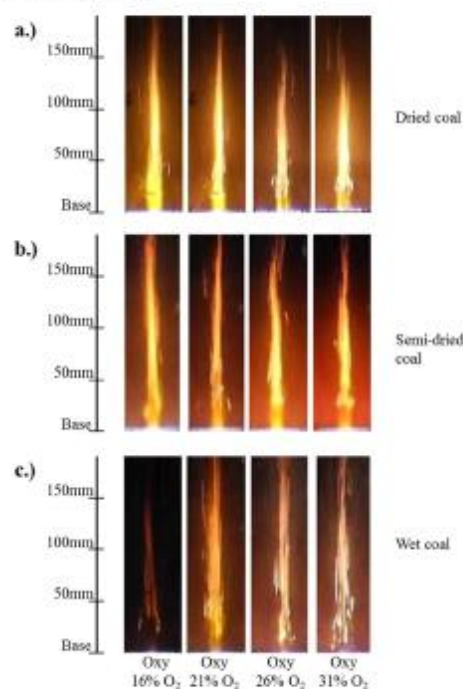


Fig. 8. Representative images of the flame structure captured with digital camera in oxy-fuel combustion case for (a) dried coal (b) semi-dried coal, and (c) wet coal.

than the blank gas. Obviously, the endothermic evaporation of coal moisture reduced both particle and gas temperatures significantly. Upon the increase of oxygen content in flue gas, the gas temperature discrepancy for dried coal was gradually narrowed down. This is due to an enhanced ignition that resulted in a quicker completion for the combustion of dried coal particles. On the contrary, the upward trend for another two coals indicates that the oxidation rate of these two wet coals at elevated oxygen concentration is still not fast enough to catch up with its dried coal counterpart.

Following the classic combustion theory which defines drying as the initial stage to be accomplished completely and separately prior to

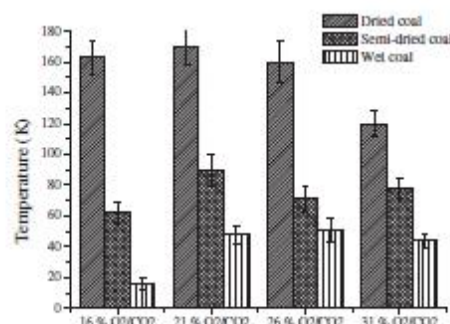


Fig. 9. Difference between measured axial gas temperature with and without coal burning for dried and wet coal samples in oxy-fuel case.

Please cite this article as: W. Pratono, et al., Influence of inherent moisture on the ignition and combustion of wet Victorian brown coal in air-firing and oxy-fuel modes: Part 1., Fuel Processing Technology (2015), <http://dx.doi.org/10.1016/j.fuproc.2015.07.008>

devolatilisation and ignition, the flame formed for wet coal should be identical with the dried coal in terms of flame intensity and shape, with the exception of a longer pre-ignition stage to accommodate time for the evaporation of inherent moisture within the particle. Moreover, the steam generated from the evaporation of coal moisture should be swept rapidly into bulk gas. Its interference to the subsequent volatile and char oxidation is thus negligible, as the maximum amount of steam derived from coal moisture accounts for only 0.03 g/min, based on the coal feeding rate of 0.1 g/min used here. This is equivalent to 0.04 slpm of extra steam contributed to flue gas which constitutes ~2–2.5 slpm of steam derived from the liquid fuel combustion. Clearly, the afore-mentioned phenomena cannot be explained by such a classic theory based on a consecutive sequence for individual steps. Fig. 10 further depicts the durations of the three steps from particle ignition to volatile combustion and char oxidation, calculated based on the statistical analysis of >100 flame images obtained from the CCD camera. For the ignition duration shown in panel (a), its change is trivial upon the shift of a coal sample from dried to wet, which accounts for 2–4 ms. The substitution of O_2/CO_2 mixtures for air narrowed down and even diminished the discrepancy in the ignition between the three coal samples, irrespective of oxygen fraction in the bulk gas. This indicates an overwhelming effect of CO_2 over the inherent moisture on coal ignition in the oxy-firing mode. Regarding the duration of volatile combustion in panel (b), although the discrepancy between three coal samples is negligible in air, an enlarged gap upon an increase in the moisture content was confirmed for all the oxy-firing cases. That is, the wet coal possessed the longest duration than its two counterparts in any oxygen fraction. The similar phenomenon was confirmed for the char oxidation stage shown in panel (c). Apparently, the steam created from the evaporation of coal moisture partially or even fully resided in the vicinity of a burning coal particle, which in turn exerted a remarkable impact on the oxidation duration of both volatiles and char particle.

4.2. Comparison of experimental observations on coal ignition with modelling prediction

Back to Fig. 7, the length of the yellowish segment in a flame refers to the initial flame front for coal volatile ignition, which is composed of moisture evaporation and volatile release. The high-speed camera observation was further conducted to accurately capture the ignition of coal particles (i.e., bright spots in the field of view of a camera) so as

to determine the distance and time for coal ignition. Subsequently, the results were compared with the modelling prediction to quantify the fraction of moisture evaporated prior to the ignition of a coal particle.

Fig. 11 demonstrates how the moisture evaporation extent affects the ignition time of a coal sample, according to the numerical approach. Irrespective of the initial moisture content, the ignition time of a coal particle increases proportionally with the increase on the evaporation extent of moisture. This is due to the fact that the drying Eqs. (1) and (2) used describe a linear relationship between the moisture evaporation rate and the required drying time. By matching the experimentally measured ignition time with the prediction curve for a coal sample, one can then quantify the moisture evaporation extent consequently. Fig. 11 illustrates the matching results for the air-firing case, from which one can reveal the evaporation of approximately 30%, 20% and 10% for the moisture out of dried, semi-dried and wet coal samples, respectively. These results substantiated an incomplete drying prior to particle ignition. In other words, the coal drying step and devolatilisation significantly overlap for the wet brown coal sample studied here. Such a conclusion is not surprising and broadly agrees with the observations in the combustion of wet brown coal in the fluidised bed reactor [12]. In addition, the descending trend for the moisture evaporation extent from dried to wet coal indicates the encapsulation of the majority of the inherent moisture in the igniting wet coal particle. This can be explained by a slow motion of the moisture evaporation front towards the core of the wet coal particle, due to less heat feedback generated from its igniting surface. Consequently, the unevaporated moisture residing inside coal particle has less opportunity to escape.

The substitution of CO_2 for N_2 to dilute oxygen is supposed to affect little on coal particle drying time, because the molar thermal conductivity of these two gases are identical. In Eq. 2, the thermal conductivity is the only property of a bulk gas affecting the moisture evaporation. A review paper on pulverised coal combustion [24] has also substantiated this statement. In this sense, the ignition delay upon shifting air to O_2/CO_2 in Fig. 7(a) is mainly caused by the large specific heat capacity of CO_2 and any other factors that are not related to the coal drying step.

Fig. 12 plots the measured ignition times for the oxy-fuel combustion of three coal samples versus the predicted values. The drying time in O_2/CO_2 was fixed the same as in air in the model. The dashed curve in a panel denotes the parity line for the match between measured and the respective prediction value. The air-firing results were also included as reference. Compared to the air-firing points falling on parity lines, the oxy-fuel results deviate remarkably from the parity lines. For

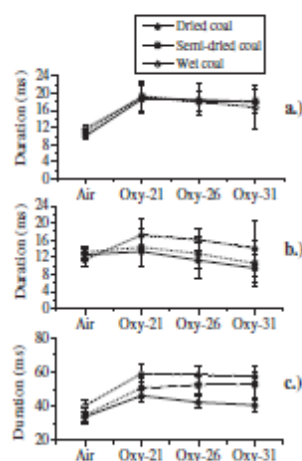


Fig. 10. Comparison of the combustion time for all coal samples in all combustion cases: (a) ignition time, (b) volatile oxidation time, and (c) char oxidation time.

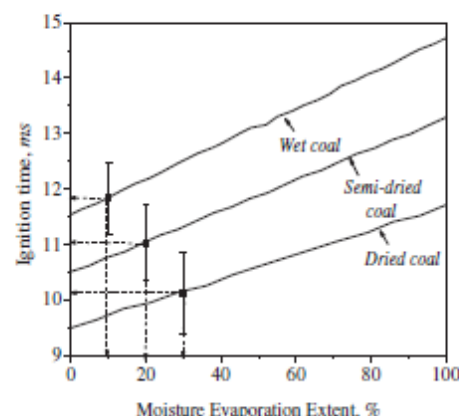


Fig. 11. Effect of the extent of moisture evaporation on the ignition time of all three brown coal samples in air.

Please cite this article as: W. Pratono, et al., Influence of inherent moisture on the ignition and combustion of wet Victorian brown coal in air-firing and oxy-fuel modes: Part 1., Fuel Processing Technology (2015), <http://dx.doi.org/10.1016/j.fuproc.2015.07.008>

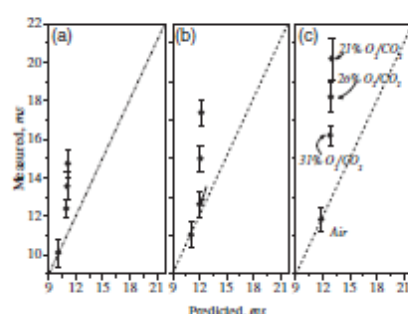


Fig. 12. Experimental and prediction of ignition time for all combustion cases: (a) dried coal, (b) semi-dried coal, and (c) wet coal.

a given O_2/CO_2 ratio, the wet coal was underestimated the most, whereas increasing the oxygen fraction in CO_2 narrowed down the discrepancy between prediction and the measurement. The ignition of dried and semi-dried coal in 31% O_2/CO_2 was predicted satisfactorily, as indicated by the insignificant gap between the experimental points and the parity line. In contrast, the gap is still rather large for the wet coal ignition in 31% O_2 . Apparently, apart from the large specific heat capacity of CO_2 that has been incorporated into the model, there are a few extra factors that negate the wet coal ignition under oxy-fuel mode. The first is the decreased flammability and ignition potential of volatiles on particle surface, due to the alteration of volatile composition and concentration by the dilution effect of CO_2 and steam. Secondly, the released steam has the potential to push the volatile flame front outwards away from the particle surface, which in turn provides less heat feedback for the continuation of particle combustion. Thirdly, the possibility of the endothermic reaction resulting from char-steam gasification reaction on a char surface reduces particle temperature. Another probable explanation is the different volatile oxidation mechanism in oxy-fuel mode, as this has already been clarified in the literature [25].

4.3. Influence of moisture on coal volatile combustion

Fig. 13 illustrates the dynamics of dried coal volatile ignition and the motion of igniting a particle in air versus the oxy-fuel mode with 21% and 31% O_2 balanced by CO_2 . In the upper panel for the air case, the dried brown coal particles were confirmed to ignite quickly once passing the flat flame layer, emitting a strong radiative heat from its surface in the FOV of the high-speed camera. The appearance of large bright spots surrounding the igniting particles is a direct sign of the release and formation of volatile flame and its preferential residence at the particle vicinity, the same as that observed for the combustion of the same coal in the drop-tube furnace [14,15]. A portion of the bright spots such as the one cycled in the left hand of the dashed line also possess a long trace, which is the indicator of a violent release and eruption of volatiles upon the provision of heat feedback from the burning of the previous volatiles released. The released volatiles were burnt gradually, changing the solid particle from a circular shape at the start to a thin rod-like shape with weak radiation intensity, as demonstrated by the last spot falling on the right end of the dashed line. The change in the particle shape was attributed to the change in the particle velocity as well as the release extent of volatiles. The residence of volatiles on the particle surface induced the formation of a volatile cloud which possesses a circular shape and moves slowly due to the buoyancy force, whereas the gradual consumption of the volatile cloud resulted in the exposure of a solid char particle in the bulk gas, which moves fast in the FOV of the high-speed camera [14]. Based on this analysis methodology, the volatile

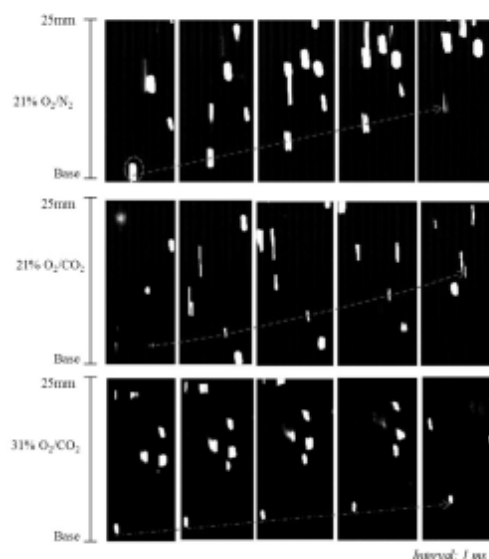


Fig. 13. Representative images of dried coal captured near the burner base.

oxidation of the traced particle in air was found to be accomplished in 5 ms.

With the substitution of air by 21% O_2/CO_2 , the igniting coal spots were much thinner and less populated in number density, as shown in the middle panel in Fig. 13. The ignition time for a luminous spot was also longer than 5 ms, as suggested by the little change on the shape of a traced particle along the dashed line. The reasons for this can be attributed to the larger specific heat capacity of CO_2 than N_2 and the slower oxygen diffusion in CO_2 . A slow ignition of the initially released volatiles induced the provision of less heat feedback to the coal particle, which in turn reduced the coal devolatilisation rate. By increasing the oxygen fraction from 21% to 31% in CO_2 , more spherical spots with a thick volatile cloud layer were produced, demonstrating the enhancement on particle ignition and volatile oxidation in the oxygen-rich environment. The bottom panel in Fig. 7 illustrated this phenomenon. Moreover, compared to the air case, the volatile cloud formed in 31% O_2/CO_2 is rather small. This is an indication that the volatile is consumed rapidly. A simultaneous oxidation of volatiles and char particles has been reported for the combustion of Victorian brown coal in the oxygen-enriched environment [23].

The progress of wet coal ignition is even more intriguing, which is illustrated in Fig. 14. For the reference air case, the igniting wet coal appears as large spots with a long trace of a volatile cloud compared to the dried coal. Such evidence strongly supports our hypothesis that moisture evaporation and volatile release overlapped remarkably in the wet coal case. It also proves the accuracy of the prediction results in Fig. 11, where the majority of the moisture (~90%) was predicted to remain in the wet coal matrix after ignition. A similar phenomenon was observed for the wet coal in 21% O_2/CO_2 shown in the middle panel of Fig. 14. Compared to the air-firing case, a slow ignition and oxidation of volatiles in 21% O_2/CO_2 induced a slow evaporation of the inherent moisture. As a result, the majority of igniting particles are present as circular spots in the FOV of the camera, relative to the abundance of rod-like spots for dried coal in Fig. 13(b). The thick volatile cloud also remained on the particle surface for a relatively long duration. Increasing oxygen fraction to 31% in CO_2 intensified the oxidation of the volatile cloud, and therefore, enhanced the moisture evaporation rate as

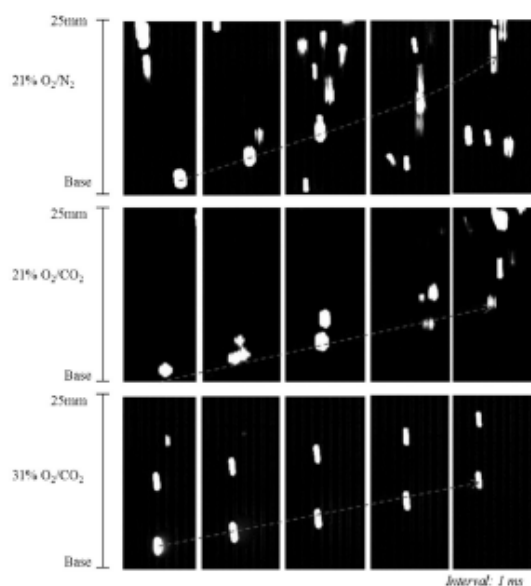


Fig. 14. Representative images of wet coal captured near the burner base.

well. Consequently, the igniting particles are mostly present as rod-like shapes with a larger width than those observed for dried coal in the bottom panel of Fig. 14.

The statistical quantification results for the shape distribution of bright spots are further summarised in Table 3. The circular shape with a circularity range of 0.8–1.0 corresponds to the solid char particles that are enveloped fully in the volatile cloud; the semi-circular shape in a range of 0.3–0.8 refers to the slight deviation caused by the volatile jet trace along the moving direction of an igniting particle, whereas the non-circular shape <0.3 corresponds to the rod-like moving char particles with fewer volatiles on the surface, undergoing heterogeneous oxidation on the surface. For the dried coal, shifting the bulk gas from air to 21% O₂/CO₂ increased the number percentage of the semi-circular spots with a long volatile jet on the surface. This reflects the ignition delay and slower volatile combustion in the CO₂-rich atmosphere. Upon the increase of oxygen fraction to 31% in CO₂, the population of semi-circular spots was decreased whereas that of the circular shape was increased to the level close to the air case, as expected. Compared to the dried coal, the semi-dried and wet coal samples had a noticeable increase in the population of semi-circular spots, particularly under the oxy-fuel mode. This is also reasonable, as the coal volatile ignition and oxidation were delayed considerably under these cases, as visualised in Figs. 13 and 14.

Fig. 15 summarised the measured size of the volatile cloud and its distribution for all three coal samples in air and oxy-fuel modes. For each given bulk gas environment, one can see the enhanced volatile cloud size of semi-dried and wet coal in place of the dried sample. In air, the mean volatile cloud size reached approximately 1400 μm for

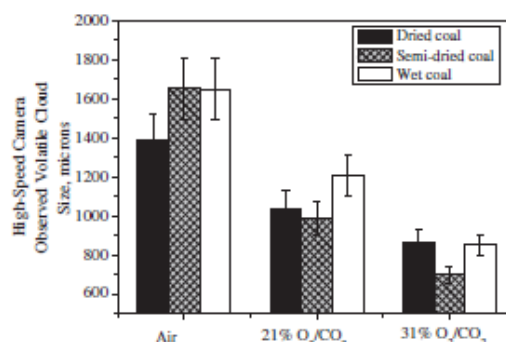


Fig. 15. Measured volatiles cloud size for all coal samples in the axial centre line of the FBFR for three different bulk gases.

the dried coal sample, which was twenty times that of the original coal size, showing the prevalence of volatiles on the particle surface [26]. This is reasonable as Victorian brown coal has abundant volatiles, which make it very reactive compared to other coals. The use of semi-dried and wet coal samples further increased the mean volatile cloud size to ~1600 μm, which echoes the co-existence of volatiles and a portion of steam derived from coal moisture on particle vicinity. The substitution of 21% O₂/CO₂ for air reduced the volatile cloud size for all the three coal samples, reflecting the slow devolatilisation rate in this bulk gas. The interesting phenomenon was observed when increasing the O₂ content to 31% in CO₂. All three samples exhibited similar cloud size. This is reasonable, as the drying time for 10% moisture only takes approximately 2 ms in a hot flue gas with a temperature of ~1273 K, as confirmed by the drying model used in the literature [4,5]. The violent oxidation of volatiles in 31% O₂ should provide a much faster heat back to the core of the coal particle for the eruption of moisture and the volatiles remaining inside.

5. Conclusion

For the first time, this paper has provided *in-situ* observations on the ignition and volatile flame propagation during the combustion of Victorian brown coal in both air-firing and oxy-fuel modes. The brown coal samples with a moisture content of 12–30 wt.% was burnt in a flat flame burner at a heating rate of ~10⁵ K, with 16–31 vol.% oxygen in the bulk gas. The major conclusions can be drawn as follows:

1. The evaporation of moisture for the drying of Victorian brown coal is incomplete prior to particle ignition. The drying extent only accounts for 31%, 20% and 10% for the air-dried coal, semi-dry coal and wet coal, respectively. This is mainly due to a quick release and ignition of the volatiles on the dried coal particle surface. The remaining moisture was released with volatiles together, forming a thick cold layer on the particle surface.
2. The co-release of moisture and volatiles affected the composition and flammability of volatile compositions on the particle surface. This played a combined role with the large specific heat capacity of CO₂ to significantly postpone the volatile ignition in oxy-fuel mode. For

Table 3
Particle shape distribution in air, 21% O₂/CO₂ and 31% O₂/CO₂.

Shape descriptions (circularity range)	Air-dried coal			Semi-dried coal			Wet coal		
	Air	Oxy-21	Oxy-31	Air	Oxy-21	Oxy-31	Air	Oxy-21	Oxy-31
Circular (0.8–1.0)	40.54	31.74	37.93	38.80	25.74	25.43	38.85	35.87	34.94
Semi-circular (0.3–0.8)	55.25	61.27	60.91	53.37	65.45	70.47	53.79	59.1	62.6
Non circular (<0.3)	4.21	6.99	1.16	7.83	8.81	4.10	7.36	5.03	2.46

Please cite this article as: W. Pratono, et al., Influence of inherent moisture on the ignition and combustion of wet Victorian brown coal in air-firing and oxy-fuel modes: Part 1., Fuel Processing Technology (2015), <http://dx.doi.org/10.1016/j.fuproc.2015.07.008>

the wet coal with 30% moisture burning in 21% O₂ balanced by CO₂, its ignition delay reached around 10 ms, which is also far larger than the model prediction due to a changed composition of a volatile and mechanisms governing its ignition in CO₂. The percentage of O₂ in bulk gas has a more overweighing influence than the negative effect of CO₂ and coal moisture. Increasing its fraction to 31% greatly narrowed the gap of coal volatile ignition time between air-firing and oxy-fuel mode.

3. The volatile cloud size of wet coal particles was significantly larger than the dried sample, due to the co-release of moisture and volatile together. Increasing the oxygen fraction to 31% in either N₂ or CO₂ eliminated the discrepancy of volatile oxidation duration between dry and wet coal samples, due to an intensified heating of coal particles in the oxygen-enriched environment.

Acknowledgement

This work is supported by Brown Coal Innovation Australia (BCIA) and Australia National Low Emission Coal Research & Development (ANLEC R&D) grant.

References

- [1] A. Tomita, Y. Ohtsuka, Gasification and combustion of brown coal, in: L.C. Zhu (Ed.), *Advances in the Science of Victorian Brown Coal*, Elsevier Ltd., Oxford 2004, pp. 252–285.
- [2] I. Ansys, *Ansys Fluent Theory Guide*, in: I. Ansys (Ed.), 2011 <http://www.ansys.com> (Cannonburg, PA).
- [3] R. Kurose, H. Tsuji, H. Malino, Effect of moisture in coal on pulverized coal combustion characteristics, *Fuel* 80 (2001) 1457–1465.
- [4] M.J. McIntosh, Mathematical model of drying in a brown coal mill system. 1. Formulation of model, *Fuel* 55 (1976) 47–52.
- [5] M.J. McIntosh, Mathematical model of drying in a brown coal mill system. 2. Testing of model, *Fuel* 55 (1976) 53–58.
- [6] E.S. Hetch, C.R. Shaddix, A. Molina, B.S. Haynes, Effect of CO₂ gasification reactions on oxy-combustion of pulverized coal char, *Proc. Combust. Inst.* 33 (2011) 1699–1706.
- [7] S. Hu, D. Zeng, A.N. Sayre, H. Sarv, Effect of Moisture on Char Burnout During Warm-recycle Oxy-fuel Combustion, Babcock & Wilcox Power Generation Group, 2011.
- [8] E. Binner, I. Zhang, C.Z. Li, S. Bhattacharya, In-situ observation of the combustion of air-dried and wet Victorian brown coal, *Proc. Combust. Inst.* 33 (2011) 1739–1746.
- [9] K. Yip, H.W. Wu, D.K. Zhang, Effect of inherent moisture in Collie coal during pyrolysis due to in-situ steam gasification, *Energy Fuels* 21 (2007) 2883–2891.
- [10] J. Hayashi, K. Nonaka, T. Yamashita, T. Chiba, Effect of sorbed water on conversion of coal by rapid pyrolysis, *Energy Fuels* 13 (1999) 611–616.
- [11] S.C. Yao, L. Liu, Behaviour of the suspended coal–water slurry droplet in combustion environment, *Combust. Flame* 51 (1983) 335–345.
- [12] K. Jung, B.R. Stanmore, Fluidised bed combustion of wet brown coal, *Fuel* 59 (1980) 74–80.
- [13] K. Matsunaka, D. Kajiura, K. Kusumoto, A. Sharma, Y. Suzuki, Factor affecting steam gasification rate of low rank coal in a pressurized fluidized bed, *Fuel Process. Technol.* 90 (2009) 895–900.
- [14] I. Zhang, E. Binner, Y. Qiao, C.Z. Li, High-speed camera observation of coal combustion in air and O₂/CO₂ mixtures and measurement of burning coal particle velocity, *Energy Fuels* 24 (2010) 29–31.
- [15] I. Zhang, E. Binner, Y. Qiao, C.Z. Li, In situ diagnostics of Victorian brown coal combustion in O₂/N₂ and O₂/CO₂ mixtures in drop-tube furnace, *Fuel* 89 (2010) 2703–2712.
- [16] C.R. Shaddix, Correcting thermocouple measurements for radiation loss: a critical review, *National Heat Transfer Conference NHTC99* 33rd, American Society of chemical Engineer, Albuquerque, NM 1999, pp. HTD99–HTD282.
- [17] J.D. Kim, G.B. Kim, Y.J. Chang, J.H. Song, C.H. Jeon, Examination of flame length for burning pulverized coal in laminar flow reactor, *J. Mech. Sci. Technol.* 24 (2010) 2567–2575.
- [18] J.J. Murphy, C.R. Shaddix, Combustion kinetics of coal chars in oxygen-enriched environments, *Combust. Flame* 144 (2006) 710–729.
- [19] S.C. Saxena, Transport properties of gases and gaseous mixtures at high temperatures, *High Temp. Sci.* 3 (1971) 168–188.
- [20] M.M. Baum, P.J. Street, Predicting the combustion behaviour of coal particles, *Combust. Sci. Technol.* 3 (1971) 231–243.
- [21] J. Zhang, W. Pratiño, I. Zhang, Z.X. Zhang, Computational fluid dynamics modelling on the air-firing and oxy-fuel combustion of dried Victorian brown coal, *Energy Fuels* 27 (2013) 4258–4269.
- [22] A.J. Stevenson, R.G. Thomas, D.G. Evan, Modelling the ignition of brown-coal particles, *Fuel* 52 (1973) 281–287.
- [23] C. Shaddix, A. Molina, Particle imaging of ignition and devolatilisation of pulverized coal during oxy-fuel combustion, *Proc. Combust. Inst.* 32 (2009) 2091–2098.
- [24] I. Chen, S.Z. Yong, A.F. Ghoniem, Oxy-fuel combustion of pulverized coal: characterization, fundamentals, stabilization and CFD modelling, *Prog. Energy Combust. Sci.* 38 (2012) 156–214.
- [25] P. Glarborg, L.L.B. Bentzen, Chemical effects of a high CO₂ concentration in oxy-fuel combustion of methane, *Energy Fuels* 22 (2008) 291–296.
- [26] R. Khatami, C. Stivers, Y.A. Levendis, Ignition characteristics of single coal particles from three different ranks in O₂/N₂ and O₂/CO₂ atmospheres, *Combust. Flame* 159 (12) (2012) 3554–3568.



Contents lists available at ScienceDirect

Fuel Processing Technology

journal homepage: www.elsevier.com/locate/fuproc

Research article

Clarifying the influence of moisture on the ignition and combustion of wet Victorian brown coal in air-firing and oxy-fuel modes: Part 2: Contribution of gasification reaction to char oxidation rate

Wirhan Pratio^a, Jian Zhang^a, Jianfang Cui^b, Yatao Wang^b, Lian Zhang^{a,*}^a Department of Chemical Engineering, Monash University, Clayton, Victoria 3800, Australia^b Coal Chemical R&D Center of Kailuan Group, South No. 3 Road, Seaport Economic Development Zone, Tangshan, Hebei Province 063611, China

ARTICLE INFO

Article history:

Received 20 May 2015

Received in revised form 6 July 2015

Accepted 8 July 2015

Available online xxxxx

Keywords:

Oxy-fuel combustion

Wet Victorian brown coal

Inherent moisture

Char-steam gasification reaction

ABSTRACT

This paper is the second part of the study to clarify the influence of moisture in Victorian brown coal oxy-fuel combustion, with a focus on char oxidation and gasification reaction through experimental and modelling efforts. An in-situ high-speed two-colour pyrometer with the wavelength band of 0.85–1.05 μm was employed to measure particle temperature in the flat flame burner reactor. The combustion stage of carbon particle was simulated for the transient phenomena with particle heating and radiative heat transfer. The multiple surface reaction single-film approach, including char- O_2 , char- CO_2 and char-steam reactions, was employed and the contribution of individual reactions to carbon consumption rate was determined via matching with the measured particle temperature. Irrespective of the initial moisture content, the extent of char-steam gasification reaction was found to account for ~15% in the air-firing case. This reaction was mainly triggered by the external steam in the reactor, rather than the inherent moisture that resided preferentially as volatile cloud on char particle surface. The combined effect of both char- CO_2 and char-steam gasification was significant in oxy-fuel combustion mode, especially for the wet coal. In the oxy-21 case, these two reactions have a total extent of around 8% and 18% on the burning char surface of dried and wet coal, respectively. The char- CO_2 gasification is insignificant because the char particle temperature was low. Increasing the oxygen percentage to 31% in CO_2 enhanced the total extent of these two gasification reactions to 28%, based on the mass of total carbon. Such an extent is comparable with the literature. However, the steam gasification rate for brown coal char was far higher, ~26% relative to ~10% for high-rank bituminous coal reported in the literature. This substantiates the strong steam gasification reactivity of Victorian brown coal char. The contribution of inherent moisture to char-steam gasification reaction is crucial in the combustion of wet coal in the oxy-21 case, accounting for ~10%. This is due to the long residence of the unevaporated steam as a thick cloud on the char surface. Increasing the oxygen concentration in CO_2 enhanced the char- O_2 reaction, the release rate of volatiles and inherent moisture. Therefore, the char-steam reaction caused by the inherent moisture within coal matrix was minimised and eventually diminished in the oxy-31 case.

© 2015 Elsevier B.V. All rights reserved.

1. Introduction

Oxy-fuel combustion is a promising low-emission technology that can be implemented in the short term to mitigate the carbon dioxide emitted from the stationary power plants. To date, most of the investigations focused on the combustion of high-rank bituminous coals [1–6]. The test of Victorian brown coal, which is abundant in moisture [7], in oxy-fuel mode generates abundant steam in the furnace, due to the recirculation of flue gas. Wall et al. has pointed the necessity of the investigation of steam dilution in oxy-firing furnace [8]. In our previous lab-scale drop-tube furnace (DTF) study on wet coal combustion, the

reduction on the temperature of burning wet coal particle has been witnessed, which was supposedly caused by the contribution of steam gasification reaction towards the char matrix as opposed to the steam gasification from the ambient steam [9]. In contrast, another study on brown coal (~10%–60% moisture) in fluidised bed showed no change on the char oxidation regime with increasing the moisture content in brown coal, as the moisture has been suggested to fully evaporate prior to the beginning of the release of volatiles [10]. A clear and generalised view on the oxy-firing of Victorian brown coal has not yet been reached.

Numerous approaches on the CFD modelling have been conducted for coal oxy-fuel combustion [11,12]. Our previous modelling works have successfully utilised multiple reaction model, including char- O_2 , char- CO_2 and char-steam in the CFD to predict the brown coal burning

<http://dx.doi.org/10.1016/j.fuproc.2015.07.009>
0378-3820/© 2015 Elsevier B.V. All rights reserved.

Please cite this article as: W. Pratio, et al., Clarifying the influence of moisture on the ignition and combustion of wet Victorian brown coal in air-firing and oxy-fuel modes: ..., Fuel Processing Technology (2015), <http://dx.doi.org/10.1016/j.fuproc.2015.07.009>

temperature profile and carbon burnout in a drop-tube furnace [13]. One-dimensional modelling approach using SKPPY (Surface Kinetics in Porous Particles) has also successfully clarified the effect of CO₂ and steam gasification reaction on the oxidation of bituminous coal char [14,15]. These modelling approaches utilised traditional combustion model where coal is assumed to be completely dried prior to ignition and there is no overlapping of individual steps including moisture evaporation and volatile release/ignition. Clearly, this is not the case for the oxy-firing of wet Victorian brown coal that has been observed in flat flame burner reactor [16] and in drop-tube furnace [9].

This paper is the second part of the study on wet Victorian brown coal combustion in flat flame burner reactor that employs a similar heating rate with the industrial boiler [16]. Complementing to the first part focusing on the ignition and volatile oxidation, this paper aims to assess whether the inherent moisture affects char oxidation rate and particle temperature through char–steam gasification reaction. As has been clarified in the first part, the inherent moisture is only partially evaporated prior to volatile ignition; whereas the remaining moisture and volatiles are co-released as a thick could layer on the char surface, which is supposed to increase the local steam partial pressure and hence trigger the char–steam gasification reaction. This is different from the previous studies in the literature where only the external steam in flue gas has been considered.

2. Experimental set-up

2.1. High-speed infrared pyrometer for coal particle temperature measurement

The coal samples and the flat flame burner reactor (FFBR) for coal combustion have been detailed in part 1 [16]. For char particle temperature measurement, a Kleiber-GmbH high-speed infrared pyrometer KS-740 LO was installed next to the observation window along the quartz reactor on the FFBR. The pyrometer captured signal at the rate of 5 MHz with the linear voltage output of 0–10 V. It has the capability of measuring the surface temperature in the range of 1073–2573 K. The pyrometer is operated at the wavelength between 0.85 μm and 1.05 μm to avoid the interference of the CO₂ and water vapour [17], which are abundant in oxy-fuel atmosphere. The emissivity of the pyrometer was adjusted to 0.8, based on the suggestion from Baum [18]. The data was captured using an oscilloscope and data acquisition instrument. The measurements were taken at the reactor height of 50 mm and 75 mm above the burner base. These two distances chosen refer to char oxidation stage with the first distance 50 mm for the simultaneous volatile and char oxidation and the second distance 75 mm for char oxidation alone.

3. Mathematical model

The modelling of single coal particle combustion here was modified based on the previous model described in the literature [13,18]. The code employed only focused on one-dimensional transient calculations. The gas mixture properties, including thermal conductivity, heat capacity, viscosity and density was calculated using the Wilke's Mixture rule and Maxon–Saxena formulation, corresponding to the statistical collision theory [19].

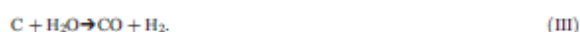
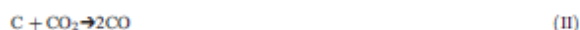
3.1. Modelling approach

Coal particles undergo rapid heating once being introduced to the furnace. The heat transferred to particle is driven by the convection from hot gas and radiation from the surrounding volatile flame as well as radiation from the furnace wall, which has the potential to increase particle temperature in the magnitude of ~10⁵ K/s. The transient model of single spherical coal particle with a diameter d_p immersed in the hot gas of temperature T_g , was used to simulate its combustion

behaviour. The following sub-models were applied in sequence, drying model, devolatilisation model and finally char oxidation model. The former two have been detailed in part 1 [16], whereas the last one is detailed below.

3.1.1. Char oxidation model

The three heterogeneous char surface reactions, as listed in Reactions (I)–(III) were assumed to occur with first-order global Arrhenius rates.



The rate of char burning is described using the multiple surface reactions' kinetic-diffusion single-film approach, assuming that the above-listed multiple reactions occur in a frozen boundary layer at the particle surface with no gas-phase reactions. This model has been proven to work satisfactorily for the combustion of pulverised coal less than 100 μm in diameter [20]. For the combustion of particles larger than 100 μm, Mitchell suggested that the conversion of CO to CO₂ in boundary layer is non-negligible [21]. It has also been postulated by Law that the characteristics diffusion time is normally negligible for the droplets less than 100 μm in diameter [22]. In other words, the droplets less than 100 μm in diameter are too small to support the existence of a gaseous flame on its surface. Therefore, it is safe to assume that the frozen boundary layer assumption can be used in this numerical study. The char combustion rate can be written as:

$$q = \frac{P_{O_2}}{\frac{1}{k_{c,o}} + \frac{1}{k_{d,o}}} + \frac{P_{CO_2}}{\frac{1}{k_{c,c}} + \frac{1}{k_{d,c}}} + \frac{P_{H_2O}}{\frac{1}{k_{c,s}} + \frac{1}{k_{d,s}}} \quad (1)$$

$$k_c = A \exp\left(-\frac{E}{RT}\right) \quad (2)$$

$$k_d = C_2 \frac{(T_g + T_s)^{0.75}}{d_p} \quad (3)$$

$$\frac{\partial d}{\partial t} = -\frac{2q}{\rho} \quad (4)$$

With k_c and k_d are chemical reaction rate coefficient and diffusion reaction rate coefficient, respectively. The chemical reaction rate coefficient is expressed in an Arrhenius form with A being the pre-exponential factor and E as the activation energy for Reactions (I)–(III). The intrinsic kinetic parameters for Reactions (I)–(III) are obtained from thermo-gravimetric analyser (TGA) measurement. For Reactions (I) and (II), the TGA experiments were conducted at different heating rates (10–50 K/min) for devolatilised char in both air and pure CO₂ (grade 5) atmosphere, which have proven accurate in our previous work [13,23,24].

For the char–steam gasification Reaction (III), it is considered to include two reactions for wet coal combustion, one being induced by the external steam in bulk gas, and another one occurring within char matrix that is triggered by the internal moisture remaining 'permanently' after volatile ignition and those produced from the pyrolysis of coal. Due to the abundance of hydrogen and oxygen, Victorian brown coal pyrolysis results in the yield of 5–15 wt.% steam in the products [25]. Such a steam is non-distinguishable from the remaining moisture after the drying stage. The kinetic parameters for steam gasification

were obtained from a steam-injected TGA at a heating rate of 40 K/min, with steam concentrations of 5%, 10% and 20% balanced by nitrogen. The resulting datasets were analysed using a Coats–Redfern method, shown in Eq. (5), by assuming a first order for the carbon–steam gasification reaction [26].

$$\ln \frac{g(x)}{1-x} = \ln \frac{AR}{\beta E} - \frac{E}{RT} \quad (5)$$

With x is char conversion fraction, T is temperature (K), R is universal gas constant, β is heating rate, with A and E as the kinetic parameter for steam gasification. The variable $g(x)$ is the algebraic expressions of function of the common reaction mechanisms in solid-phase reactions. The assumption of the first order reaction yields the expression of $g(x) = -\ln(1-x)$. The kinetic parameters were calculated by plotting the graph of $\ln \frac{g(x)}{1-x}$ versus $1/T$, as shown in Fig. 1. The rate constant of $3.6 \times 10^6 \text{ s}^{-1}$ and activation energy of 206 kJ/mol were chosen for the Victorian brown coal studied here. The steam gasification kinetic rate used in this study is also comparable with the kinetics data for lignite steam gasification used in the literature, which are also far more reactive than bituminous coal [27–29], as demonstrated in Fig. 2. In general, the steam gasification reaction for brown coal is significant with the reaction temperature exceeding 1000 K.

3.1.2. Particle heat-up

The coal particle temperature profile in the furnace was calculated by using an unsteady-state energy balance Eq. (6) shown below, considering both radiative and convective heat transfer between particle and surrounding gas.

$$m_p c_p \frac{dT_p}{dt} = h A_p (T_w - T_p) + \epsilon \sigma A_p (T_w^4 - T_p^4) + H_{gen} \quad (6)$$

where m_p is particle mass (kg), c_p is the heat capacity of coal particle (kJ/kg·K), h is the convective heat transfer coefficient calculated assuming Nusselt number of 2, T_w is the wall temperature (773 K), T_g is the gas temperature measured with thermocouple, ϵ is the particle emissivity (0.8) and σ is the Stefan Boltzmann constant.

The term H_{gen} is the total heat generated/released from the Reactions (I)–(IV). The heat generated from char oxidation reaction was calculated from the amount of CO/CO₂ produced. The ratio of CO₂/CO production at particle surface was determined based on the coefficient suggested by Arthur [30].

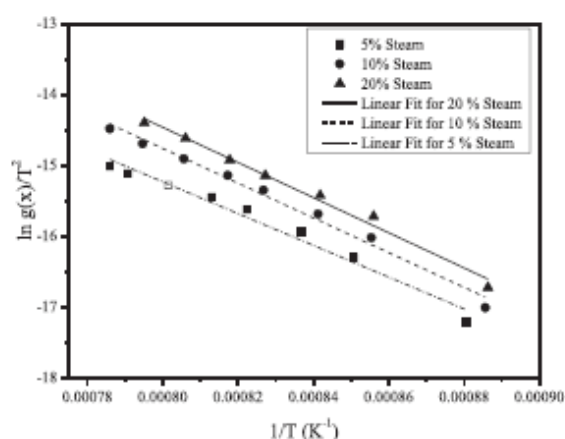


Fig. 1. Linear plot of Coats–Redfern method for Loy Yang coal to determine the kinetic parameters for its char–steam gasification rate.

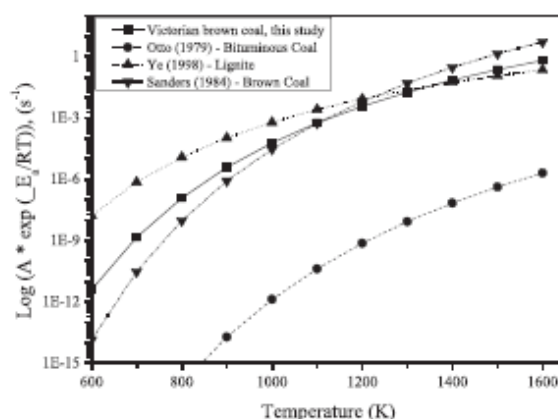


Fig. 2. Comparison of measured gasification rate with other brown coals available in the literature [24–26].

3.2. Numerical calculation procedure

The series of differential equations to describe the transient change in particle temperature were programmed and solved numerically using MATLAB. The particle temperature and char oxidation rate were calculated using Euler's method, as shown in Eq. (7) below. The time step chosen was determined based on the trial and error method to ensure that the solution stabilizes. A pseudo-code algorithm shown in Fig. 3 has been developed to solve particle temperature history.

$$y(t + \Delta t) = y(t) + dt \times \frac{dy}{dt} \quad (7)$$

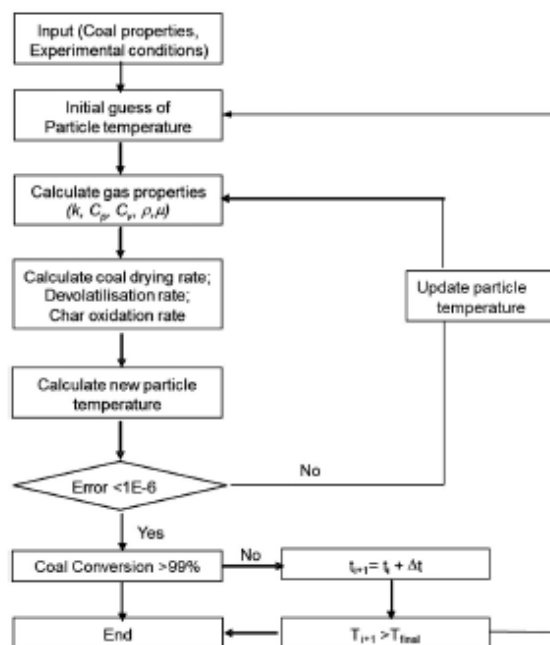


Fig. 3. Schematic of the numerical procedure applied to determine the contribution of gasification reaction.

4. Results and discussion

4.1. Influence of moisture and char–H₂O gasification on particle temperature in air-firing case

Fig. 4 depicts the temperature profile for the burning coal particles in the air-firing case. Irrespective of the original moisture content, most of the burning char particle temperature falls in the range of 1373–1520 K, which is approximately 100–200 K above the surrounding gas temperature at the respective location. This measurement is consistent with our previous study on the combustion of the same coal in drop-tube furnace [9,13]. The temperature gap between burning brown coal particle and surrounding gas, as observed here is also slightly lower than that observed for bituminous coal, which was found to be 200–400 K [3]. For the dried coal sample, its temperature distribution at 50 mm has a peak at around 1120 K, with a considerable fraction larger than 1433 K. With the reactor distance extending to 75 mm, the peak temperature was lowered to ~1373 K. The fraction for the particle hotter than 1433 K was also decreased. The wet coal particle has a lower peak temperature than the dried coal at a same reactor distance. Its peak temperature is centred at 1373 K for both two distances; and less of hot particles above 1433 K have been observed. This is another direct sign of the ‘permanent’ residence of inherent moisture on char matrix, which negated both volatile oxidation and char consumption over a long duration.

Considering that the remaining moisture was released with volatiles together to form a thick cloud layer on char surface, it is hypothesised that such a thick cloud layer may increase the partial pressure of steam in char vicinity so as to trigger and/or enhance the char–steam gasification reaction consequently. The brown coal has been proven highly reactive for such a reaction from 1000 K onwards, as shown in Fig. 2. Moreover, considering that a direct measurement on the partial pressure of steam derived from remaining moisture and pyrolysis of coal is implausible, we did not differentiate the two different steams during modelling. Instead, we simply varied the partial pressure of steam in the model to reveal the sensitivity of the change on char particle temperature. The prediction results are depicted as lines in Fig. 5 for the combustion of both dried and wet coal in air. The distance of 75 mm was chosen here to avoid the interference of volatile combustion which is not fully finished at 50 mm. For both samples, the char particle temperature drops quickly upon increasing the extent of steam gasification reaction on the char surface. The dried coal particle temperature reaches 1523 K for the absence of char–steam gasification reaction. However, it drops to 1273 K upon a contribution of 67% from such an endothermic reaction to the total carbon burnout. For the combustion

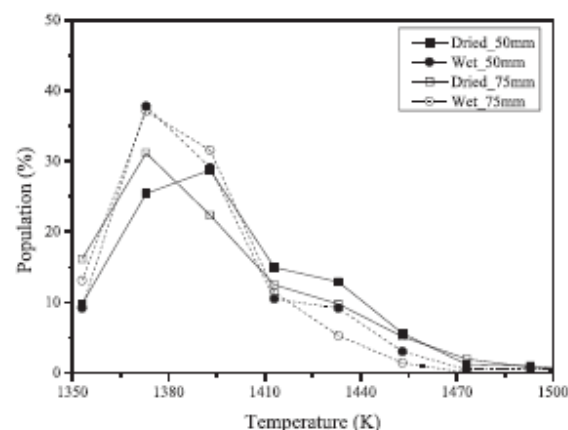


Fig. 4. Distribution of measured char particle temperature of dried and wet coal in air.

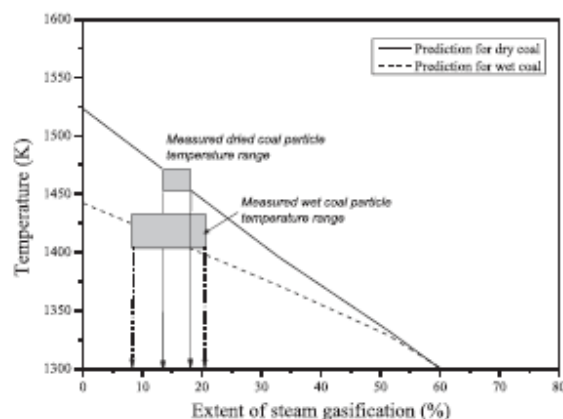


Fig. 5. Method to determine the contribution of steam gasification reaction in air-firing case.

of wet coal, its particle temperature without char–steam gasification reaches only 1448 K, which is around 80 K lower than the dried coal, due to evaporation of coal moisture that in turn reduced the amount of heat fed back to char particle. In Fig. 5 the pyrometer data were also added on the respective prediction curve, as rectangular boxes with its length representing the variation of the particle temperatures measured. Clearly, one can conclude that the extent of steam gasification reaction reaches 14–17% (median 15.5%) for dried coal and 8–20% (median 14%) for wet coal, respectively. Considering that the median extent for such a reaction is very close for both two coals, it is safe to conclude that the inherent moisture in wet coal contributed little to char–steam gasification in the air-firing case, although it co-exists with volatiles to form a thick cloud on char surface. In other words, the partial pressure of steam in volatile cloud should be very low, or the residence time of volatile could be very short, therefore, there was little opportunity for the char–steam reaction to take place on the char surface. In addition, it is noteworthy that, the char–CO₂ gasification reaction was also included during the modelling for the air-firing case. It was however found insignificant with the contribution of less than ~1%. This is due to the low partial pressure of CO₂ (~15 vol%) and a low gas temperature in the reactor.

4.2. Combined effect of char–H₂O and char–CO₂ gasification reaction in oxy-fuel mode

Fig. 6(a) and (b) shows the measured burning char temperature profile at 50 mm and 75 mm for oxy-21 and oxy-31, respectively. For dried coal in oxy-21 case in panel (a), a noticeable fraction of hot particles with temperature above 1413 K has been confirmed at the reactor height of 75 mm, which is opposite against the trend that is observed in the air case where more hot particles are present at 50 mm. This is due to the delayed ignition in oxy-21 case which in turn postponed char combustion stage. The similar phenomenon was confirmed for the wet coal particle temperature profile in oxy-21. In oxy-31 case shown in panel (b), the dried coal has a peak temperature of 1373 K and a rather narrow distribution compared to wet coal at the reaction height of 50 mm. This is mainly due to a faster combustion of the dried coal which even occurred before 50 mm for a concurrent ignition and oxidation of both its volatiles and char in the elevated oxygen concentration. With the reactor height increasing to 75 mm, the gap between two coal samples is narrowed, indicating that the combustion for wet coal is even close to the end at this distance.

Modelling work was conducted to compare with the pyrometer data to quantify the impact of the endothermic gasification reactions. Due to

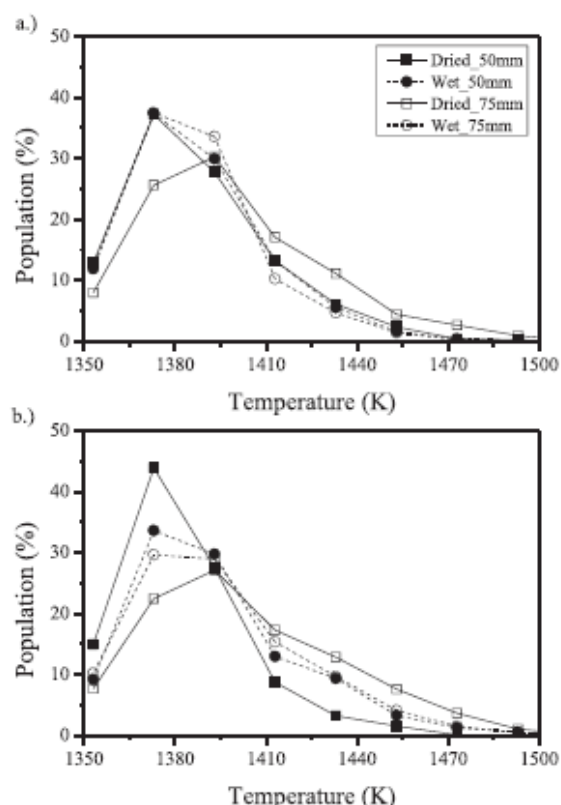


Fig. 6. Measured pyrometer data for dried and wet brown coal at 50 mm and 75 mm height for (a) oxy-21 case and (b) oxy-31 case.

the co-existence of CO_2 and steam, both char- CO_2 and char-steam gasification reactions could occur concurrently on the char surface, which in turn reduces the char particle temperature significantly. Apparently, these two reactions could also affect each other. To assess the significance of each gasification reaction, the modelling was first conducted by only considering the char- CO_2 gasification reaction. In other words, the char-steam reaction was switched off in the model.

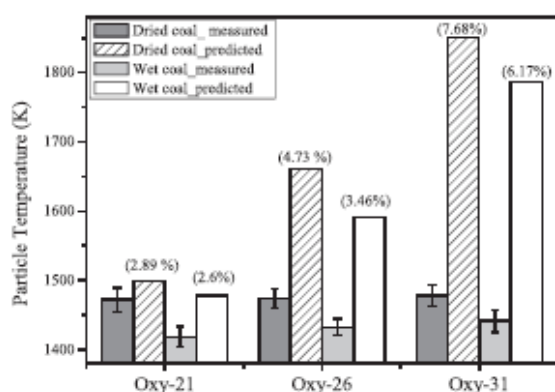


Fig. 7. Predicted char particle temperature for dried coal and wet coal at 75 mm at oxy-fuel combustion case with the consideration of char- CO_2 gasification reaction ONLY. The extent of char- CO_2 reaction is shown above the prediction bars in the figure.

Fig. 7 demonstrates the predicted particle temperatures for both dried and wet coal samples in the three oxy-fuel cases, at the reactor height of 75 mm. The experimentally measured data were included for comparison. In addition, the numbers in parenthesis on the prediction bars refer to the extent of char- CO_2 gasification reaction that was determined by the molar ratio of this reaction to the overall reaction. Irrespective of the moisture content in coal, the contribution of char- CO_2 reaction was relatively low, reaching 2.6–2.89% and 6.17–7.68% for oxy-21 and oxy-31, respectively. This is much lower than ~20% observed for the bituminous coal at the oxygen concentration of 27% [28]. Again, this can be due to the low flue gas temperature used throughout this study. Moreover, one can see a large disagreement between the measured particle temperature and its prediction, particularly for the oxy-26 and oxy-31 cases. In both cases, the temperature predicted is far higher than the measured value, irrespective of moisture content in coal. Clearly, the char-steam reaction is more influential than the char- CO_2 reaction for the oxy-fuel combustion of Victorian brown coal, either dry or wet. This can be the case, as char-steam gasification reaction for Victorian brown coal reaches $3.66 \times 10^{-6} \text{ s}^{-1}$ at 1000 K, which is 1000 times higher than the char- CO_2 reaction at the same temperature.

Fig. 8 demonstrates the influence of char- CO_2 and char-steam reactions for particle temperature in the oxy-21 case. In Fig. 8, the predicted particle temperature was plotted as a function of the total contribution of these two gasification reactions at the reaction height of 75 mm, and the pyrometer data were added on the respective curve to match the predicted value. From the match between the pyrometer data and prediction curve, the extent of each gasification reaction was further calculated and plotted as pie chart next to the respective pyrometer point. For the combustion of dried coal in oxy-21, a total contribution of gasification reactions accounts for only 8%, with 5.53% for char-steam reaction and 2.35% for char- CO_2 reaction. The extent of char-steam reaction is obviously low compared to that in the air case shown in Fig. 5, where the extent of char-steam reaction reaches 14–17% for the same coal. This should be attributed to the large specific heat capacity of CO_2 which cooled down the particles dramatically. For the wet coal combustion in 21% O_2 balanced by CO_2 , the total contribution of ~18% from the two gasification reactions was observed, which was approximately 10% higher than that for the dried coal in the same bulk gas. In addition, the total gasification reaction contribution for wet coal in oxy-21 case is close to the air-firing case as shown in Fig. 5. Clearly, although the ignition delay and lower char particle temperature are expected for the wet coal, the extra moisture within it increased the partial pressure of steam in the char particle vicinity. It thus enhanced the char-steam gasification reaction extent to a level that is comparable with the external

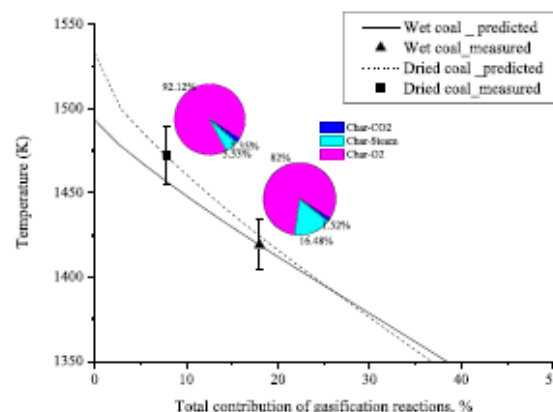


Fig. 8. Contribution of char- CO_2 and char-steam gasification reactions for dried coal and wet coals in oxy-21 case.

steam in the bulk gas. The influence of pyrolytic water on the observed discrepancy between dry and wet coal should be negligible here, based on the assumption that its content is independent on the moisture content in coal.

The contribution from two gasification reactions is more influential upon the rise of oxygen concentration. As illustrated in Fig. 9 for the oxy-26 case, the extent of char–steam gasification reaction was increased to 17.4% and 22.2% for the dried and wet coal, respectively. This is attributed to the increase in the reaction rate for the exothermic char–O₂ reaction which in turn improved the char particle temperature. Moreover, compared to a discrepancy of about 11% for the extent of char–steam reaction between the dried and wet coal in oxy-21 case, the gap was narrowed to about 4.8% for the oxy-26 case. Apparently, compared to the internal steam derived from inherent moisture, the external steam in bulk gas has a comparable and even larger role in triggering the char–steam gasification in the oxy-26 case. This should also be due to the enhanced char–O₂ reaction that led to a rapid release of the internal moisture out of char matrix. The CO₂ gasification is still insignificant in the oxy-26 case. This is because the char particle temperature is still fairly low, which, unless reaching 1600 K, has no potential to trigger the char–CO₂ gasification reaction for the Victorian brown coal studied here [13].

The enhanced char–steam gasification reaction was further confirmed in the oxy-31 case, as substantiated in Fig. 10. The extent of char–steam gasification reaction reaches 26.6% and 26.55% for the dried and wet coal sample, respectively. The gap between two coal samples is negligible, strongly supporting an insignificant role of the internal steam (derived from the inherent moisture and from pyrolysis) on the combustion of wet coal in oxy-31 mode. The char–steam reaction was merely induced by the external steam in the reactor. To reiterate, this is due to a rapid release and escape of the inherent moisture from char surface. The high-speed camera imaging results in part 1 [16] support such a hypothesis.

Table 1 depicts the summary on the contribution of char–CO₂ and char–steam reactions for both dried and wet coals in the oxy-fuel cases with the oxygen concentration increasing from 21% to 31% in CO₂ including some of the literature study related to bituminous coal for comparison. To reiterate, the contribution of char–CO₂ reaction here is approximately less than 3% in all cases, and no significant change was observed with increasing oxygen concentration. Such a value is low compared to the literature results. The char–CO₂ gasification accounted for ~15% for sub-bituminous and bituminous coal burnt at around 1773 K in lab-scaled combustor [14,31]. The numerical study of wet recycle of bituminous coal in oxy-fuel combustion also confirmed the

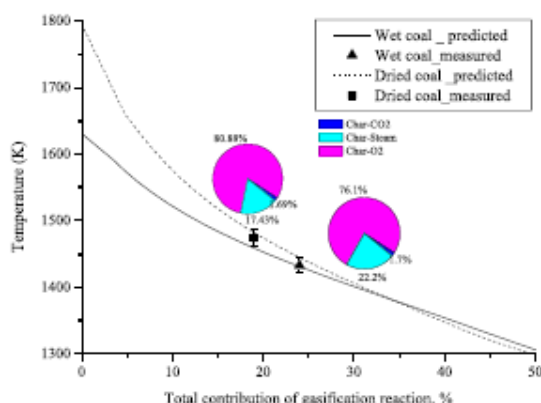


Fig. 9. Contribution of char–CO₂ and char–steam gasification reaction for dried coal and wet coal in oxy-26 case.

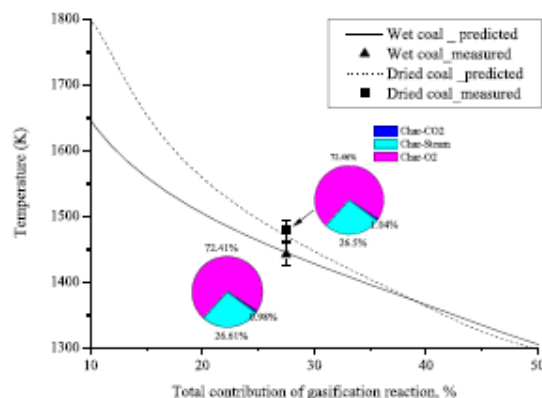


Fig. 10. Contribution of char–CO₂ and char–steam gasification reaction for dried coal and wet coal in oxy-31 case.

contribution of char–CO₂ and char–steam gasification as ~21% and 7.5% in the case of 24% O₂ balanced by CO₂ [15]. Instead, the char–steam gasification reaction was found more influential for Victorian brown coal tested in this study. For either dried or wet brown coal, its contribution increases upon increasing oxygen concentration in the bulk gas, reaching about 26% for both coal samples in the oxy-31 case. Such a value is obviously higher than that reported in the numerical study reported earlier for bituminous coal [15]. This is due to the abundance of alkali and alkaline earth metals in brown coal that can catalytically trigger the char–steam gasification from 1207 K onwards [32]. In terms of the extent of char–steam gasification reaction, the discrepancy between dried and wet coal samples is noteworthy. It is as broad as approximately 10% in the oxy-21 case, and is gradually narrowed down to only 5% in oxy-26 case and insignificant at the oxy-31 case. Such a discrepancy is mainly induced by the extra moisture in the wet coal, which formed a thick cloud on the char surface in the oxy-21 case. The lowest oxidation of volatiles and char in the oxy-21 case caused a long duration of the evaporated steam in the char particle vicinity. Consequently, the char–steam reaction was triggered. Increasing the oxygen concentration in bulk gas enhanced the release and combustion of volatiles, which in turn fastened the eruption of inherent moisture with few residing on the char surface to trigger any extra gasification reaction. The similar phenomenon was confirmed for the air-firing of wet coal [9].

5. Conclusions

A Hencken flat-flame burner was used to study the combustion of wet Victorian brown coal in air-firing and oxy-fuel modes with 21–31 vol.% oxygen in the bulk gas. A two-colour pyrometer was used to measure burning char particle temperature, and the results were compared with 1-D modelling considering all the surface reactions in char particle vicinity. The major conclusions can be drawn as follows:

1. Irrespective of the initial moisture content, the extent of char–steam gasification reaction was found to be ~15% in the air-firing case. Such a reaction was solely triggered by the external steam in the reactor, rather than the inherent moisture and pyrolytic water that has been fully released prior to char oxidation stage, which has little interference on char consumption rate.
2. The combined effect of both char–CO₂ and char–steam gasification was significant in oxy-fuel combustion mode, especially for the wet coal. In the oxy-21 case, these two reactions have a total extent of around 8% and 18% on the burning particle surface of dried coal and wet coal, respectively. The char–CO₂ gasification is insignificant,

Table 1

Summary of the CO₂ and H₂O gasification reaction evaluated in this study compared with literature data [14,15,28].

Case study	Coal type	Facility	Temperature (K)	Gas atmosphere	Particle size (μm)	Contribution of gasification (%)	
						CO ₂	H ₂ O
This study	Dried brown coal	Flat flame burner	1373	21% O ₂ /CO ₂ –18% H ₂ O	63–104	2.5	5.2
				31% O ₂ /CO ₂ –18% H ₂ O		1	26
	Wet brown coal			21% O ₂ /CO ₂ –18% H ₂ O		1.9	16.1
				31% O ₂ /CO ₂ –18% H ₂ O		0.9	26.2
Hetch et al. (2012)	Bituminous coal	SKIPPY 1-D programme	1690	Dry recycle (14% H ₂ O)–24% O ₂ /CO ₂	100	23.5	3.9
				Wet recycle (25% H ₂ O)–24% O ₂ /CO ₂		21	7.4
Kim et al. (2014)	Sub-bituminous coal	Flat flame burner	1700	21% O ₂ /CO ₂	75–106	15.3	–
				30% O ₂ /CO ₂		15.5	–

because the char particle temperature was low in this study. Increasing the oxygen percentage to 31% in CO₂ enhanced the extent of these two gasification reactions to reach 28% based on the mass of total carbon. Such an extent is comparable with the literature. However, the steam gasification rate was far higher (~26% compared to ~10% in literature) substantiating the strong steam gasification reactivity of Victorian brown coal char.

- The contribution of inherent moisture to char–steam gasification reaction is crucial in the combustion of wet coal in the oxy–21 case, accounting for ~10%. This is due to the long residence of the unevaporated steam as a thick cloud on the char surface. Increasing the oxygen concentration in CO₂ enhanced the char–O₂ reaction, the release of volatiles and inherent moisture, and hence, the char–steam reaction caused by the inherent moisture was minimised and eventually diminished in the oxy–31 case.

Acknowledgement

This work is supported by the Brown Coal Innovation Australia (BCIA) and Australia National Low Emission Coal Research & Development (ANLEC R&D) grant. The authors would like to extend their gratitude to Professor Brian Haynes from the University of Sydney for his suggestions in our single-film modelling approach. We also would like to thank Professor Dunxi Yu and the State Key Laboratory of Coal Combustion in Huazhong University of Science and Technology for the support on the experimentation of brown coal steam gasification.

References

- R. Khatami, C. Stivers, Y.A. Levendis, Ignition characteristics of single coal particles from three different ranks in O₂/N₂ and O₂/CO₂ atmospheres, *Combust. Flame* 159 (12) (2012) 3554–3568.
- A. Molina, C. Shaddix, Ignition and devolatilisation of pulverized bituminous coal particles during oxygen/carbon dioxide coal combustion, *Proc. Combust. Inst.* 31 (2) (2007).
- J.J. Murphy, C.R. Shaddix, Combustion kinetics of coal chars in oxygen-enriched environments, *Combust. Flame* 144 (2006) 710–729.
- M. Schiemann, V. Scherer, S. Wirtz, Optical coal particle temperature measurements under oxy-fuel conditions: measurement methodology and initial results, *Chem. Eng. Technol.* 32 (12) (2009) 2000–2004.
- C. Shaddix, A. Molina, Particle imaging of ignition and devolatilisation of pulverized coal during oxy-fuel combustion, *Proc. Combust. Inst.* 32 (2009) 2091–2098.
- S. Hu, D. Zeng, A.N. Sayre, H. Sarv, Effect of Moisture on Char Burnout During Wamrecycle Oxy-fuel Combustion, Babcock & Wilcox power generation group, 2011.
- D.J. Allardice, A.J. Chaffee, R.W. Jackson, M. Marshall, Water in brown coal and its removal, in: C.Z. Li (Ed.), *Advances in the Science of Victorian Brown Coal*, Elsevier 2004, pp. 85–133.
- T. Wall, et al., An overview on oxy-fuel coal combustion—state of the art research and technology development, *Chem. Eng. Res. Des.* 87 (2009) 1003–1016.
- E. Binner, I. Zhang, C.Z. Li, S. Bhattacharya, In-situ observation of the combustion of air-dried and wet Victorian brown coal, *Proc. Combust. Inst.* 33 (2011) 1739–1746.
- K. Jung, B.R. Stanmore, Fluidised bed combustion of wet brown coal, *Fuel* 59 (1980) 74–84.
- A.H. Al-Abbas, J. Naser, D. Dodds, CFD modelling of air-fired and oxy-combustion of lignite in a 100 kW furnace, *Fuel* 90 (5) (2011).
- A.H. Al-Abbas, J. Naser, D. Dodds, CFD modelling of air-fired and oxy-fuel combustion in a large-scale furnace at Loy Yang A brown coal power station, *Fuel* 102 (2012).
- J. Zhang, W. Pratiño, I. Zhang, Z.X. Zhang, Computational Fluid Dynamics modelling on the air-firing and oxy-fuel combustion of dried Victorian brown coal, *Energy Fuel* 27 (8) (2013) 4258–4269.
- E.S. Hetch, C.R. Shaddix, A. Molina, B.S. Haynes, Effect of CO₂ gasification reactions on oxy-combustion of pulverized coal char, *Proc. Combust. Inst.* 33 (2011) 1699–1706.
- E.S. Hetch, C.R. Shaddix, M. Geier, A. Molina, B.S. Haynes, Effect of CO₂ and steam gasification reactions on the oxy-combustion of pulverized coal char, *Combust. Flame* 159 (2012) 3437–3447.
- W. Pratiño, J. Zhang, X.D. Chen, I. Zhang, Clarifying the Influence of Moisture on the Ignition and Combustion of Wet Victorian Brown Coal in Air-Firing and Oxy-Fuel Modes: Part 1: Volatile Ignition and Flame Propagation, Submitted to *Energy & Fuels* 2014.
- K.P. Mollman, F. Pinno, M. Vollmer, Two-Color or Ratio Thermal Imaging – Potentials and Limits, *FLIR Technical Series*, FLIR, 2010.
- M.M. Baum, P.J. Street, Predicting the combustion behaviour of coal particles, *Combust. Sci. Technol.* 3 (1971) 231–243.
- J.P. Smith, D.L. Smoot, One-dimensional model for pulverized-coal combustion and gasification, *Combust. Sci. Technol.* 23 (1–2) (1980) 17–31.
- R.E. Mitchell, Experimentally determined overall burning rates of coal chars, *Combust. Sci. Technol.* 53 (1987) 165–186.
- R.E. Mitchell, R.J. Kee, P. Glarborg, M.E. Coltrin, The effect of CO conversion on the boundary layers surrounding pulverized coal–char particles, *Proc. Combust. Inst.* 23 (1991) 1169–1176.
- C.K. Law, *Combustion Physics*, Cambridge University Press, Cambridge, 2006.
- J. Zhang, Q.Y. Wang, Y.J. Wei, I. Zhang, Numerical modelling and experimental investigation on the use of brown coal and its beneficiated semicoke for coal blending combustion in a 600 MW_e utility furnace, *Energy Fuel* 29 (2) (2015) 1196–1209.
- J. Zhang, B.Q. Dai, Y. Meng, X. Wu, J. Zhang, Y. Ninomiya, Z. Zhang, I. Zhang, Pilot-scale experimental and CFD modelling investigations of oxy-fuel combustion of Victorian brown coal, *Fuel* 144 (2015) 111–120.
- J.-I. Hayashi, K. Miura, in: C.Z. Li (Ed.), *Advances in the Science of Victorian Brown Coal*, Elsevier 2004, pp. 134–222.
- A.W. Coats, J.P. Redfern, Kinetic parameters from thermogravimetric data, *Nature* 201 (1964) 68–69.
- K. Otto, L. R. M. Shelef, Catalysis of carbon–steam gasification by ash components from two lignites, *Fuel* 58 (2) (1979) 85–91.
- G.A. Sandars, C.K.S. Jones, Study of the gasification of various Victorian brown coals by the non-isothermal thermo-gravimetric measurement, *Proc. Aust. Coal Science Conf.*, Churchill, Victoria, 1984.
- D.P. Ye, J.B. Agnew, D.K. Zhang, Gasification of a South Australian low rank coal with carbon dioxide and steam: kinetics and reactivity studies, *Fuel* 77 (1998) 1209–1219.
- J.R. Arthur, Reactions between carbon and oxygen, *Trans. Faraday Soc.* 47 (1951) 164–178.
- D. Kim, S. Choi, C.R. Shaddix, M. Geier, Effect of CO₂ gasification reaction on char particle combustion in oxy-fuel conditions, *Fuel* 120 (2014) 130–140.
- S. Kajitani, H.J. Tay, S. Zhang, C.Z. Li, Kinetics of steam gasification of brown coal and volatile–char interactions, *Chemeca*, ICMS Pty Ltd, Adelaide, SA, 2010.

This page is intentionally left blank

APPENDIX C

Published Second-Author Paper Not
Included in the Main Body of Thesis

This page is intentionally left blank

Computational Fluid Dynamics Modeling on the Air-Firing and Oxy-fuel Combustion of Dried Victorian Brown Coal

Jian Zhang,[†] Wirhan Pratiomo,[†] Lian Zhang,^{†,*} and Zhongxiao Zhang[‡]

[†]Department of Chemical Engineering, Monash University, GPO Box 36, Clayton, Victoria 3800, Australia

[‡]Institute of Thermal Energy Engineering, Shanghai Jiaotong University, Shanghai 200240, China

ABSTRACT: The numerical modeling of the combustion of air-dried Victorian brown coal in O₂/N₂ and O₂/CO₂ mixtures with 21–30% O₂ has been conducted via the use of computational fluid dynamics (CFD), ANSYS FLUENT 13.0, with the refined weighted-sum-of-gray-gases model (WSGGM), the single-film model with multiple surface reactions (i.e., char-O₂, char-CO₂, and char-H₂O) for char particle, and the refined two-step mechanism for the oxy-firing of methane to mimic the volatile oxidation. The purpose of this study is to verify the experimental observations in a lab-scale drop-tube furnace (DTF) and to promote the understanding on the details underpinning the combustion characteristics of Victorian brown coal, the youngest coal in the world and the single largest source for power generation in Victoria, Australia. As confirmed, the modeling results show good agreement with the experimental measurements on the particle temperature, coal ignition delay photographed by a high-speed camera, carbon burnout rate, and particle velocity. The air-dried Victorian brown coal bears an extremely high reactivity for devolatilization and char-O₂ and char-CO₂ reactions. The inherent moisture in coal was released with volatile matter simultaneously rather than as that predicted by the CFD wet combustion module for pulverized coal with surface moisture. Increasing the secondary gas temperature greatly narrowed coal ignition delay caused by the substitution of 21% O₂ balanced in CO₂ for air. At the furnace temperatures of 1073 and 1273 K, the contribution of char-CO₂ to coal burnout reached approximately 10 and 25% in the oxy-fuel mode, respectively, which, in turn, reduced the coal particle temperature by a maximum of 300 K. To achieve an identical flue gas temperature with the air-firing case, the use of 30% O₂ in CO₂ is essential. However, the radiation heat flux match can be achieved by the substitution of 27% O₂ in CO₂ for air.

INTRODUCTION

The large quantities of greenhouse gas emitted upon industrialization have been causing significant global climate warming. A variety of carbon capture, utilization, and storage (CCUS) technologies have been under development for the CO₂ mitigation in both short and long terms.^{1,2} Of those, oxy-fuel combustion is one of the most promising options that can be retrofitted to existing air-fired power plants or in a purpose-designed oxy-fired system. With the burning of coal in a mixed gas of pure oxygen and recirculated flue gas (RFG), oxy-fuel combustion delivers high-purity CO₂ in flue gas that can be sequestered directly.^{3–5}

Extensive studies on both lab and pilot scales have pointed out the pronounced influences of gas shift from air to O₂/CO₂ on coal combustion characteristics and pollutant emissions. The distinct specific heat capacity and density of CO₂ relative to N₂ alter the flue gas mass flow pattern, velocity profile, and heat-transfer distribution in an oxy-fuel furnace.^{6,7} The increased concentrations of CO₂ and water vapor substantially increase the emissivity of flue gas and, hence, the radiative heat transfers in the furnace.⁸ In terms of coal ignition and char burnout, a noticeable ignition delay has been confirmed in O₂/CO₂ in comparison to O₂/N₂ with the same O₂ concentration.⁹ The high concentrations of CO₂ and water vapor have the potential to lower the gaseous diffusion in char particle vicinity and even trigger char-CO₂ and char-H₂O gasification reactions,^{10,11} which, in turn, affect the char burnout rate, its pollutant emissions, and ash slagging/fouling in a complex manner.^{12–14} To date, extensive studies have been conducted for the oxy-fuel combustion of bituminous coal, sub-bituminous coal, and European lignite,

reaching a conclusion that a typical oxygen concentration of 28–35% in CO₂ is essential to match the flame temperature and heat flux in the air-fired system. It is also argued that the matching oxygen level in an oxy-fuel flame should vary with the operating conditions, including coal properties and wet/dry flue gas recirculation.²

Apart from experimental investigation, computational fluid dynamics (CFD) modeling has been widely employed to clarify the mechanisms underpinning the oxy-fuel combustion phenomena and to optimize the design and configuration of a coal-fired burner and furnace.^{2,15–18} To improve the CFD prediction accuracy on oxy-fuel combustion, efforts have been made extensively in the past 5 years, which mainly focused on the following three aspects.

Radiation Models in CFD. The radiative heat transfer in an oxy-firing furnace is supposed to differ from the air-firing boiler remarkably, because of the abundance of CO₂, H₂O, and different H₂O/CO₂ ratios in flue gas. The weighted sum of gray gases model (WSGGM), originally proposed by Hottel and Sarofim,¹⁹ was used to calculate the total emissivity as a weighted sum of *j*th gray gases and one clear gas. The air-firing modeling results by Smith et al.²⁰ were widely used, which were also employed in ANSYS FLUENT. However, the spatial variations in the mean H₂O/CO₂ ratios within the flame are supposed to vary widely and even beyond the range of the WSGGM

Special Issue: Accelerating Fossil Energy Technology Development through Integrated Computation and Experiment

Received: January 6, 2013

Revised: July 1, 2013

Published: July 3, 2013

parameters. Because of this consideration, a refined WSGGM has been developed,^{21,22} which is applicable to both air- and oxy-firing as well as to both gray and non-gray gases. The model extends its applicability to cover a broader range of parameters, $0.001 \leq L \leq 60$ m, $0.001 \leq PL \leq 60$ atm m, and $500 \leq T_g \leq 3000$ K, and includes broader conditions to accommodate the variation of the molar ratio of H_2O/CO_2 in an oxy-fuel flame. The new modeling results have witnessed a significant difference from the model by Smith et al. in particular at large beam length under oxy-enriched mode. Similarly, Krishnamoorthy developed another new WSGGM from the emissivity curves based on the correlations in *Perry's Chemical Engineering Handbook* to cover the H_2O/CO_2 ratio ranges of 0.25–0.67, 0.67–1.5, 1.5–2.33, and 2.33–4.^{23,24} The model was also proven more accurate in terms of matching the experimental data. Furthermore, Johansson modified another WSGGM applicable for the ratio of H_2O/CO_2 from 0.125 to 2.0.²⁵

Char Oxidation Model in CFD. The single-film char oxidation model is mainly applied to predict the char particle temperature and burnout rate in the air-firing flame. As for oxy-fuel combustion, the existence of elevated CO_2 and/or H_2O levels in the furnace has the potential to trigger the endothermic gasification reactions on the char surface, which, in turn, lower the particle temperature while improving the coal burnout rate. Using the surface kinetics in porous particle (SKIPPY) code to compare to the burning coal particle temperature measured by the pyrometer, Hecht et al.²⁶ have clarified the remarkable contribution of gasification on char consumption at the O_2 concentration of 12% in CO_2 , whereas its significance was reduced for 36% O_2 diluted by CO_2 . Clearly, to improve the predictive accuracy of the particle temperature profile, the multiple reactions on the char surface have to be incorporated in the CFD model, as conducted in the literature.^{2,27}

Homogeneous Volatile (Gas) Oxidation Model in CFD. During the pulverized coal combustion process, a large quantity of hydrocarbons derived from coal volatiles burn homogeneously in the gas phase. For the oxy-firing case, the hydrocarbon gas oxidation could be inhibited by abundant CO_2 , which, in turn, leads to a dramatic increase in the concentration of carbon monoxide (CO) at flame temperatures. The experimental and CHEMKIN modeling investigations²⁸ have been conducted at atmospheric pressure and 1200–1800 K to clarify the effect of the direct chemical reactions of CO_2 on methane oxidation. Upon the substitution of CO_2 for N_2 , the CO concentration profile has been reported to increase to 1000–3500 ppm relative to the stabilized level of 0–1000 ppm in N_2 at the temperature above 1400 K. In comparison to the above-mentioned assessment on the fundamental chemical reactions, the updated global mechanisms of methane oxidation have been suggested to be more useful for CFD modeling, such as the refined two-step mechanism by Westbrook and Dryer (WD)²⁹ and the refined four-step mechanism by Jones and Lindstedt (JL),^{30,29} which have been proposed and fully validated.

This paper aims to apply the modified CFD codes to the oxy-fuel combustion of a low-rank brown coal (i.e., lignite) in a lab-scale drop-tube furnace (DTF). In comparison to the conventional one-dimensional modeling for the lab-scale DTF, where particle Reynolds number is generally assumed small enough to ignore the particle slip velocity, the three-dimensional CFD modeling is beneficial for providing the information regarding the trajectory and temperature for individual coal particle sizes. It is also easy to be coupled with a variety of submodels to describe the impacts of rather complex factors on coal ignition and the

combustion process, e.g., the greenhouse gas radiation heat transfer, as mentioned above.

The brown coal examined is named Victorian brown coal, which is the single largest source for power generation in the state of Victoria, Australia. With the inherent moisture content up to 70 wt %, Victorian brown coal has a notoriously larger carbon emission rate than the high-rank black coal and natural gas. As a continuation of our previous feasibility studies on experimental investigation,^{31–34} this study aims to establish a mature CFD code for the unique DTF constructed in our laboratory, to verify the experimental observations achieved for the combustion of Victorian brown coal in both air- and oxy-fuel modes and to further explore the unknown transport phenomena governing the combustion of this low-rank coal. Our focus here is the dried Victorian brown coal, which has yet to be understood completely compared to the as-received wet coal that has been burnt in the industry. A prior drying to remove the inherent moisture is primarily important and most practical to improve the combustion efficiency for Victorian brown coal. Its integration with either an existing air-fired system or a purpose-designed oxy-fuel boiler has been deemed a step-change process to mitigate the carbon footprint of Victorian brown coal in the foreseeable future. Moreover, apart from the use of the modified CFD codes, the novel methods for the CFD data interpretation have been proposed here to quantitatively examine the variation of the coal ignition point and flame temperature with the coal particle size and flue gas temperature, as well as the ignition delay upon gas shift. The results here are expected to shed new light on the combustion characteristics of dried Victorian brown coal in both air- and oxy-fuel modes and its difference to high-rank bituminous coal.

■ EXPERIMENTAL SECTION

Victorian Brown Coal Combustion. The coal sample tested is a Victorian brown coal, namely, Loy Yang, with a size range of 106–153 μm (mean size of 130 μm) and air dried prior to use. As tabulated in Table 1,

Table 1. Properties of Victorian Brown Coal

Victorian brown coal		
Proximate Analysis		
moisture (% ar)		10.1
ash (% db)		3.0
volatile (% db)		50.1
fixed carbon (% db)		46.9
Ultimate Analysis		
C (% db)		65.9
H (% db)		4.7
N (% db)		0.6
S (% db)		0.5
specific energy (gross dry, MJ/kg)		25.3
reaction kinetics	raw coal	ammonia-acetate-washed coal
(1) Devolatilization Rate		
pre-exponential coefficient (s^{-1})	5.18×10^{16}	1.92×10^{11}
activation energy (kJ/mol)	217.27	152.22
(2) Char Oxidation Rate		
pre-exponential coefficient ($\text{kg m}^{-2} \text{s}^{-1} \text{Pa}^{-1}$)	0.0024	0.0014
activation energy (kJ/mol)	69.06	68.54
(3) Char Gasification Rate with CO_2		
pre-exponential coefficient ($\text{kg m}^{-2} \text{s}^{-1} \text{Pa}^{-1}$)	0.0053	1.2659
activation energy (kJ/mol)	125.5	195.0

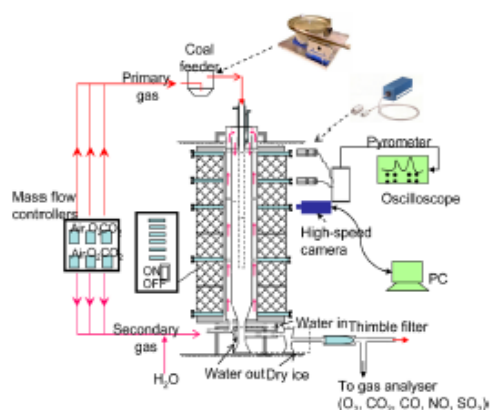


Figure 1. Schematic diagram of the DTF. Reprinted with permission from ref 32. Copyright 2010 from the American Chemical Society.

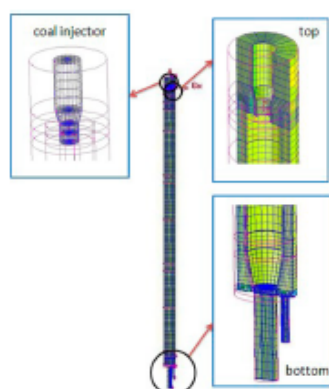


Figure 2. Modeling geometry and local expansion diagrams for the DTF.

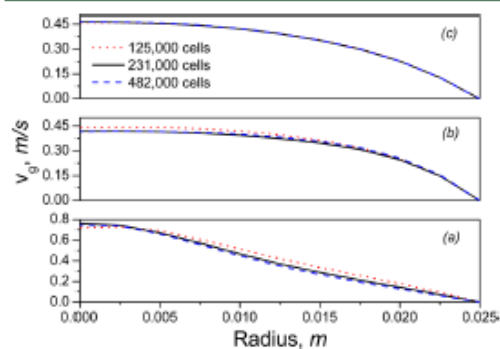


Figure 3. Grid independence test for 125,000, 231,000, and 482,000 cells drawn in the DTF geometry, which shows predicted axial gas velocity profiles at radial positions with different heights in the 1073 K furnace without coal feeding. Panels a, b, and c are 0.1, 0.2, and 0.4 m distance from the coal injector tip, respectively.

the air-dried brown coal has the moisture content of 10 wt %, which reaches its equilibrium state after being exposed to the air for several

weeks. On the dried mass basis, the volatile matter content is comparable to fixed carbon. The devolatilization, char O_2 oxidation, and char CO_2 gasification reactions occur fast for the coal tested here. The kinetics of coal devolatilization and char surface reactions were measured by a non-isothermal heating program, with the heating rate varying from 10 to 50 K/min in a thermogravimetric analyzer (TGA, Shimadzu, 60H).

A lab-scale DTF with a detailed schematic in Figure 1 was used for coal combustion experiments. As detailed elsewhere,³² the furnace is 2.0 m long and consists of six heating sections with the same length that are controlled individually. A tubular quartz reactor consisting of two layers with inner diameters of 50 and 80 mm was designed for experiments. It is fitted at the top with a piezoelectric coal feeder and a water-cooled injector to continuously introduce coal particles into the inner chamber. The combustion gas, namely, secondary gas, is introduced from the bottom of the outer chamber of the reactor, is heated to the furnace temperature during passing of the outer tube, and then mixed with coal and primary gas at the top of the chamber. In comparison to the conventional DTF, in which the second gas remains cold prior to mixing with coal power, the DTF used here is supposed to prevent the influence of gas preheating on coal ignition. Otherwise, the substitution of CO_2 for N_2 may pose a different preheating rate for the bulk gas, which, in turn, affects coal particle heating and its ignition.

For each run, coal was entrained by primary air and fed at a rate of approximately 0.5 g/min. The temperature of the furnace wall was kept at 1073 or 1273 K. The fluxes of primary and secondary gas were set as 1.0 and 9.0 L/min (cold), respectively. The average oxygen content in bulk gas varies from 21 to 30% in volume, balanced by either N_2 or CO_2 . Apart from the sampling of unburnt carbon, imaging of flame ignition and propagation was also taken during experiments. The flame observation holes with a diameter of 20 mm are located at five levels

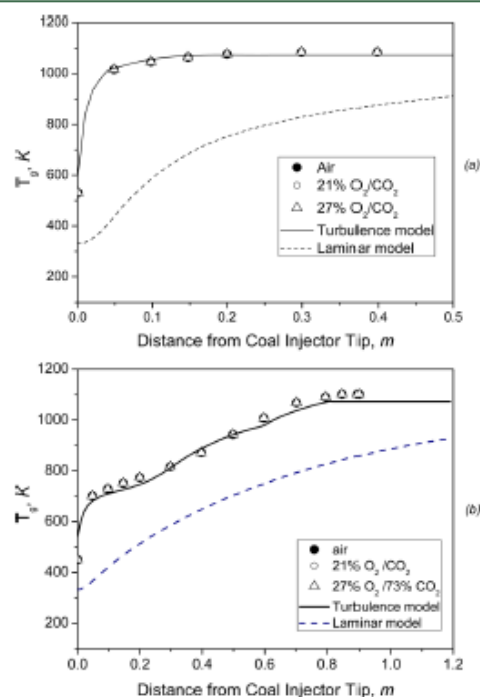


Figure 4. Experimentally measured (dots) and predicted centerline gas temperature (T_g) profiles at the DTF furnace temperature of 1073 K without coal feeding. Panels a and b are for the DTF with and without the first two heating zones, respectively.

on the furnace wall, as shown in Figure 1. The burning coal particle temperatures were also measured, using a two-color pyrometer.³⁴

CFD Modeling Approach. The commercial CFD software, ANSYS FLUENT 13.0, has been employed to predict coal combustion in the DTF. The submodels chosen and the other methods incorporated into FLUENT are summarized as follows.

DTF Geometry and Grid. The modeling geometry was created by the GAMBIT 2.4.6 preprocessor based on the size of the DTF furnace, as illustrated in Figure 2. A grid independence test was first conducted to

elucidate the minimum cell number in a grid to ensure the accuracy of modeling results and least calculation time. As demonstrated in Figure 3 for the predicted gas-phase axial velocities as a function of radial positions/heights, the grid of 231 000 cells yielded almost the same results as the grid with 482 000 cells. It was thus selected and used throughout this study.

Flow Model. For the gas flow pattern in the lab-scale DTF, Figure 4 suggests that, for the two blank cases without the feeding of the coal particle, the predicted gas temperatures based on a laminar gas model are much lower than the measured values. Instead, the use of a turbulent model with a realizable $k-\epsilon$ model exhibits a good agreement with the experimental observations. The turbulence of the mixed gas in the DTF is most likely attributed to the mixing of two gas streams at the coal injector tip where the cold primary gas is suspected to expand rapidly upon meeting the hot secondary gas. The introduction of coal into the DTF may further intensify the turbulence of gas mixing and flow in the combustion chamber.

Particle Trajectory Model. Coal particle trajectory was simulated by the discrete phase model (DPM) in FLUENT. The impact of the drag force and gravity force acting on the particle phase was taken into account during calculation. A total of 800 coal particle trajectories were tracked at each step of the DPM coupling. During combustion, the coal particle size was assumed to remain constant, while its particle density varies. The particle size was assumed to obey the Rosin–Rammler distribution with a spread parameter of 3.5 and 10 groups.

Radiation Model. The discrete ordinates (DO) model was applied here for radiation modeling, in which gas was assumed being a gray body. The refined WSGGM^{21,22} was implemented in the CFD model via the user-defined function in ANSYS FLUENT. The total emissivity and the effective absorption coefficient of flue gas are described as

$$e = \sum_{i=1}^I a_{e,i}(T_g)(1 - e^{-k_i P_L}) \quad (1)$$

$$a_{e,i}(T) = \sum_{j=1}^J b_{e,i,j} \left(\frac{T_g}{1200.0} \right)^{j-1} \quad (2)$$

$$\bar{k}_a = -\frac{1}{L} \ln(1 - e) \quad (3)$$

where $b_{e,i,j}$ and k_i were given in the 10 suites of the refined WSGGM database in ref 21, including the cases of variable H_2O/CO_2 ratios of 0.125, 0.25, 0.5, 0.75, 1, 2, and 4 for oxy-firing mode and the H_2O mole fractions of 0, 0.1, and 0.3 in the air-firing mode. The data of these 10 suites were included in our written user-defined function code that is incorporated into the CFD. However, it is noteworthy that most of the calculation cases fell in the cases of $P_{H_2O} + P_{CO_2} = 0.0$ for air-firing and $P_{H_2O}/P_{CO_2} = 0.125$ for oxy-firing in the modeling work here. This is because the coal feeding rate in the DTF was only 0.5 g/min in 10.0 L/min

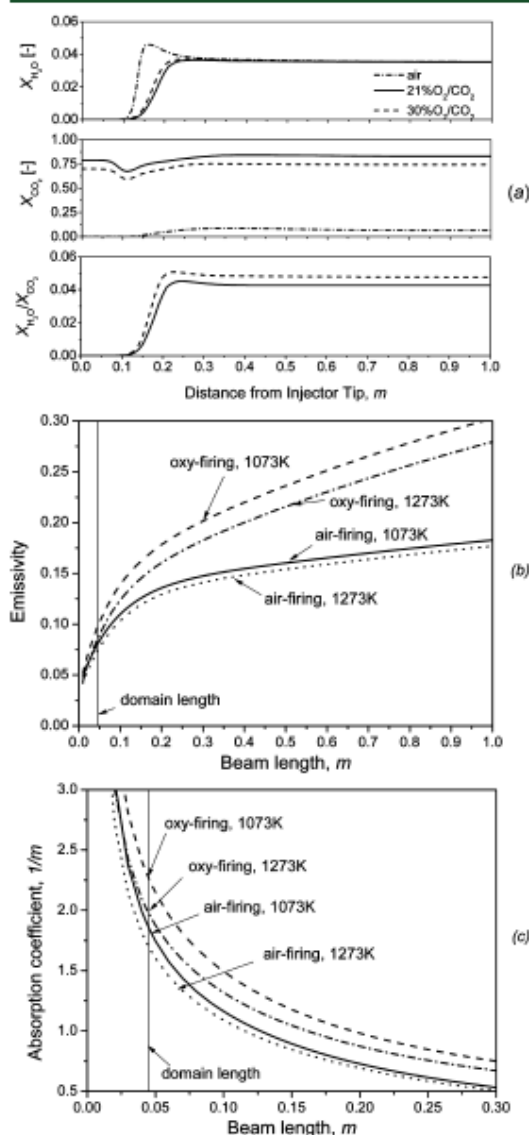


Figure 5. Concentrations of H_2O and CO_2 in DTF and the comparison of gas radiation characteristics of air- and oxy-firing modes in DTF, predicted through the refined WSGGM^{21,22} Panel (a) was the predicted gas composition profiles along the DTF centerline at 1273 K of furnace (b) for the total gas emissivity versus beam length and (c) for the effective absorption coefficient versus beam length.

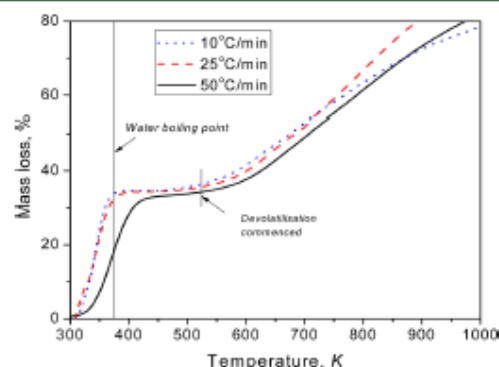


Figure 6. Mass loss curves for the wet Victorian brown coal containing 35 wt % moisture as a function of the particle heating rate in TGA.

gas, and the water vapor yielded in flue gas was very tiny, as substantiated in Figure 5a, where the maximum mole fraction of steam (X_{H_2O}) reached 0.045 in the air case and the maximum X_{H_2O}/X_{CO_2} was 0.05 in oxy-fuel cases.

The emissivity and the absorption coefficient of flue gas depend upon the characteristic length of the computational domain, a mean beam length, which is calculated as $L = 3.6V/A$, where V is the volume of the domain and A is the corresponding surface area.¹⁹ The domain-based length is normally recommended, because the other method (cell-based length) could bring up more grid-dependent error as the grid is refined.³⁵ With regard to the lab-scale DTF, its domain length was determined by its inner diameter of 0.05 m and height of 2 m. Panels b and c of Figure 5 depict the gas emissivity and absorption coefficient versus domain length and gas temperature for the above-mentioned two specific suites of the WSGGM database. Clearly, at the DTF domain length, the emissivity and absorption coefficient of the oxy-fuel case are higher than the corresponding air-firing mode at the same temperature, which, in turn, enhances the radiative heat transfer in the furnace. Note that, in the CFD model here, the emissivity of the quartz glass wall and burning coal particle surface were set as 0.9 and 0.85, respectively.

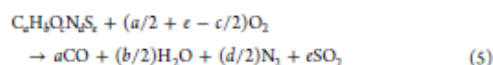
Drying Modeling of Inherent Moisture in Brown Coal. The moisture in coal is defined according to the manner in which they are measured. Broadly, the moisture in a coal can be either inherent moisture embedded chemically within a coal matrix or free moisture remaining on the coal surface. The former portion is held within the pore and capillaries of coal, requiring more energy to break the chemical bonds for the release. In contrast, the surface moisture is the portion to be released spontaneously once the coal particle temperature reaches the water evaporation/boiling point. The coal particle temperature remains at a plateau of 373 K during the evaporation of the surface moisture. This is also the methodology for the wet combustion model in FLUENT.³⁶

With regard to the Victorian brown coal tested here, the drying and devolatilization processes of its wet sample containing 35 wt % moisture in inert argon, as demonstrated in Figure 6, exhibit a shift of the moisture evaporation beyond 373 K upon increasing the coal particle heating rate from 10 to 50 K/min. Considering that the particle heating rate is on the order of 10^4 K/s in a lab-scale DTF, it is inferable that the moisture of coal should be evaporated at the temperatures above 373 K in our study case, which could even occur in parallel to devolatilization. This viewpoint agrees with a previous investigation on the temperature of the suspended American coal–water slurry droplets (60 wt % lignite coal and 490–730 μ m droplet size) in a combustion environment,³⁷ in which the 373 K plateau referring to surface moisture evaporation was not observed. This was explained by a simultaneous moving of both the water evaporation front and thermal front toward the center of the droplet, as well as a violent devolatilization of brown coal even at very low temperatures. In this model, the equilibrated 10 wt % moisture in the dried Victorian brown coal was assumed as the inherent moisture that is released at the same rate as volatile matter.

Devolatilization Modeling of the Coal Particle. The devolatilization process is determined by a first-order model.³⁸ The rate of volatile matter loss from coal is expressed as

$$\frac{dV}{dt} = A \exp(-E_v/RT_p)(V_\infty - V) \quad (4)$$

The volatile matter (VM) was assumed as a single hypothetical hydrocarbon component $C_aH_bO_cN_dS_e$, whose subscripts were determined by subtracting the contents of C, H, N, S, and O of the pyrolytic char from the raw coal. The pyrolytic char refers to the char sample created by pyrolyzing the raw coal in pure N_2 at the furnace temperature of 1273 K and a short residence time of around 0.6 s in the DTF. The combustion rate of volatiles was simplified as the oxidation rate of methane. Considering the influence of a higher CO_2 level, the original or refined two-step mechanism by Westbrook and Dryer (WD) was employed in air- and oxy-fuel modes, respectively.^{29,30} The reactions for volatile oxidation follow eqs 5 and 6, and the kinetic data are tabulated in Table 2.



Single-Film Model with Multiple Surface Reactions. The three heterogeneous reactions, as listed below, were assumed to occur at the particle external surface with first-order global Arrhenius kinetics.² The overall carbon consumption rate equals the sum of the rates from each individual surface reaction.³⁹

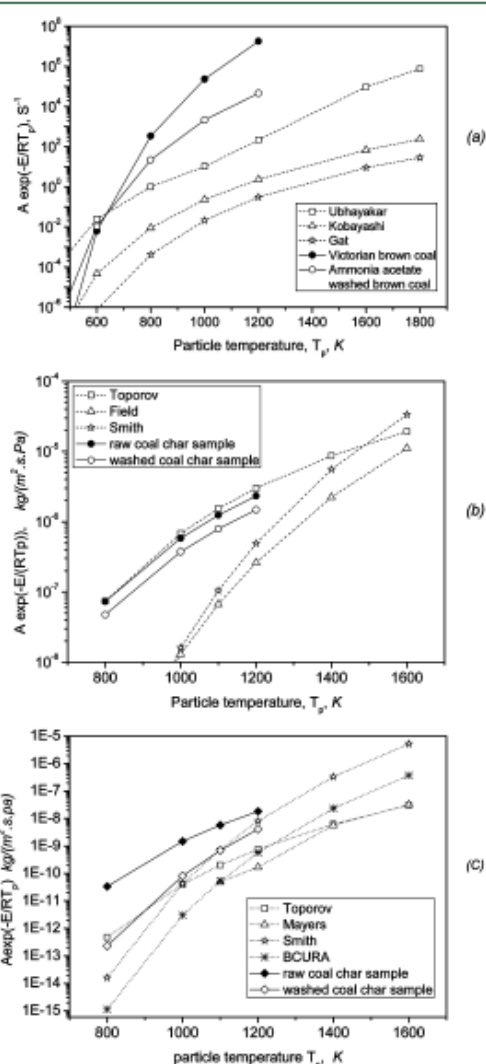
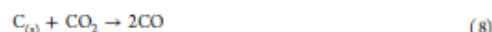


Figure 7. Comparison of measured kinetics of Victorian brown coal and those reported in refs 40–47. Panels a, b, and c are for devolatilization, char oxidation, and char gasification reactions with CO_2 , respectively. Copyright from Elsevier for the reprinted use of the results in refs 40–47.

Table 2. Global Mechanisms of Gas-Phase Reactions^a

number	reaction	rate equation (kmol m ⁻³ s ⁻¹)	A	b	E (J/kmol)
(1) Original WD: Westbrook and Dryer Two-Step Mechanism for Methane Combustion in Air ^{29,30}					
1	CH ₄ + 1.5O ₂ → CO + 2H ₂ O	d[CH ₄]/dt = A ⁹ exp(-E/RT)[CH ₄] ^{0.5} [O ₂] ^{0.8}	5.012 × 10 ¹¹	0	200.0
2	CO + 0.5O ₂ → CO ₂	d[CO]/dt = A ⁹ exp(-E/RT)[CO][O ₂] ^{0.25} [H ₂ O] ^{0.5}	2.239 × 10 ¹²	0	170.0
(2) Refined WD: Refined Westbrook and Dryer Two-Step Mechanism for Oxy-fuel Combustion of Methane ^{29,30}					
1	CH ₄ + 1.5O ₂ → CO + 2H ₂ O	d[CH ₄]/dt = A ⁹ exp(-E/RT)[CH ₄] ^{0.5} [O ₂] ^{0.8}	5.03 × 10 ¹¹	0	200.0
2	CO + 0.5O ₂ → CO ₂	d[CO]/dt = A ⁹ exp(-E/RT)[CO][O ₂] ^{0.25} [H ₂ O] ^{0.5}	2.239 × 10 ¹²	0	41.8
3	CO ₂ → CO + 0.5O ₂	d[CO]/dt = A ⁹ exp(-E/RT)[CO ₂][O ₂] ^{-0.25} [H ₂ O] ^{0.5}	1.10 × 10 ¹³	-0.97	328.0
(3) Hydrogen Oxidation ³⁶					
1	H ₂ + 0.5O ₂ → H ₂ O	d[H ₂]/dt = A ⁸ exp(-E/RT)[H ₂][O ₂]	9.87 × 10 ⁸	0	31.0

^aThe methane oxidation kinetics was used for volatile oxidation in air- and oxy-fuel modes.

Table 3. Global Mechanisms of Char Surface Reactions

number	reaction	A (kg m ⁻² s ⁻¹ Pa ⁻¹)	E (J/kmol)	reference	C _{diff} in air	C _{diff} in CO ₂
1	C + 0.5O ₂ → CO		in Table 1		5.0 × 10 ⁻¹²	4.0 × 10 ⁻¹²
2	C + CO ₂ → 2CO		in Table 1		2.0 × 10 ⁻¹²	1.8 × 10 ⁻¹²
3	C + H ₂ O → CO + H ₂	0.00635	162.0	45	3.4 × 10 ⁻¹²	2.2 × 10 ⁻¹²

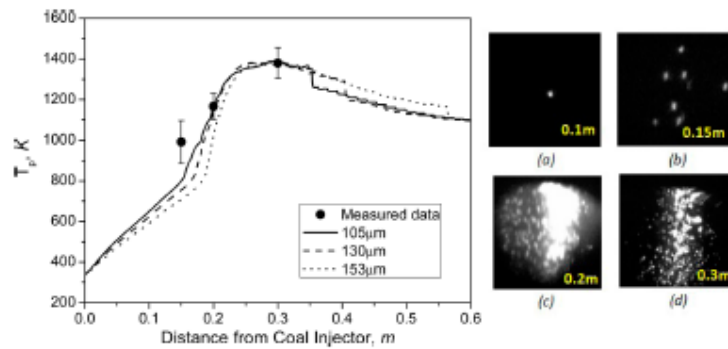


Figure 8. Measured and predicted char particle temperature profiles for different particle sizes in air and the furnace temperature of 1073 K. Photos a, b, c, and d are for the flame observed at reactor distances of 0.1, 0.15, 0.2, and 0.3 m, respectively.³⁴ The photographs were reprinted with permission from the copyright of Elsevier.

$$q = \sum_{j=1}^3 q_j = \frac{P_{g,O_2}}{K_{s,1} + \frac{1}{K_{d,1}}} + \frac{P_{g,CO_2}}{K_{s,2} + \frac{1}{K_{d,2}}} + \frac{P_{g,H_2O}}{K_{s,3} + \frac{1}{K_{d,3}}} \quad (10)$$

where kinetic and mass diffusion coefficients for each reaction above were decided by

$$K_{s,j} = A \exp\left(\frac{-E_j}{RT_p}\right) \quad (11)$$

$$K_{d,1} = \frac{2D_{m,O_2}M_C}{r_p RT_m} \quad (12)$$

$$K_{d,2} = \frac{D_{m,CO_2}M_C}{r_p RT_m} \quad (13)$$

$$K_{d,3} = \frac{D_{m,H_2O}M_C}{r_p RT_m} \quad (14)$$

$$K_{d,j} = C_{diff} \frac{[(T_p + T_g)/2]^{0.75}}{d_p} \quad (15)$$

Note that the gas-phase diffusion coefficients (D_{O_2} , D_{CO_2} , and D_{H_2O}) are different in diluent CO₂ and N₂. Once the diffusion coefficients are determined, C_{diff} is calculated by eq 15, as tabulated in Table 3.

The particle temperature was calculated by considering heat transfer from convection, radiation, and surface heat gain/loss because of char heterogeneous reactions, using the following equation:

$$m_p c_p \frac{dT_p}{dt} = \frac{2\lambda}{d_p} A_p (T_\infty - T_p) + A_p \epsilon_p \sigma (T_g^4 - T_p^4) + f_h A_p (q_1 H_1 - q_2 H_2 - q_3 H_3) \quad (16)$$

Gaseous Homogeneous Reactions. The primary products (CO and H₂) yielded from char surface reactions burn further in the bulk gas, depicted as reactions 6 and 17.



The turbulent combustion of fuel gases was predicted using the finite-rate/eddy-dissipation model, taking into account the Arrhenius laminar reaction and turbulent fluctuation. The reaction kinetic data are also listed in Table 2.

RESULTS AND DISCUSSION

Devolatilization and Char O₂ and Char CO₂ Reactivities of Victorian Brown Coal. Once being dried, the Victorian brown coal bears a very high reaction rate for both devolatilization and char oxidation. Figure 7 summarizes the kinetic parameters for this coal, its ammonia-acetate-washed residue, and the bituminous coals reported in refs 40–47.

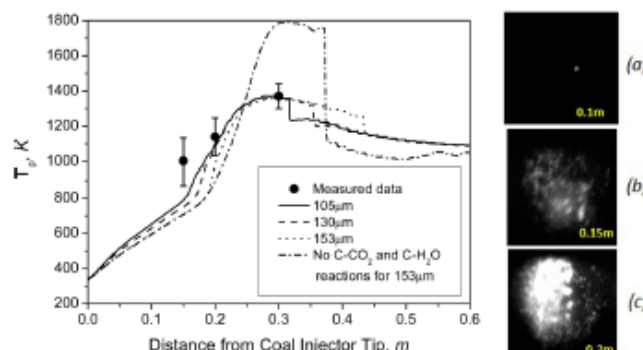


Figure 9. Measured and predicted particle–temperature profiles for different particle sizes in 1073 K and 27% O_2 in diluted CO_2 . Photos a, b, and c are for the flame observed at reactor distances of 0.1, 0.15, and 0.2 m, respectively. The photographs were reprinted with permission from the copyright of Elsevier.

Ammonia acetate was used to remove the alkali and alkaline earth metals that are supposed to be the catalysts for brown coal oxidation. In Figure 7a showing the devolatilization rate, one can see that both Victorian brown coal and its washed residue were pyrolyzed quickly from 800 K onward. Their devolatilization rates are 10^2 – 10^6 faster than the bituminous coals. This is due to the youngest age and shortest coalification time for this brown coal. Its volatile matter is mainly composed of light/gaseous hydrocarbons accounting for more than half on the mass basis of the total volatiles. With regard to the brown coal char O_2 oxidation rate in Figure 7b, it is close to that reported by Toporov et al. in ref 44, being fast compared to the bituminous coal char. The ammonia acetate washing affected little on the char O_2 oxidation rate. For the char CO_2 gasification rate, it is obviously higher than the reported high-rank coal at the temperatures below 1200 K. The removal of the ash-forming metals by ammonia acetate washing dropped the magnitude of this reaction to the same level as the reported bituminous coals, which substantiates the catalytic role of ash-forming metals on the high char CO_2 reactivity of this coal.

CFD Model Verification by Particle Temperature. The CFD modeling program, such as ANSYS FLUENT, tracks the trajectories of plenty particles and simultaneously records the temperature and reactivity of the individual particles over time. The particles were grouped into grid meshes, and in each group, the particles were differentiated in size. Considering that the majority of the particles are moving in the axial way in the DTF and there is little interaction of particles along the radial direction, the information for the particles with the same size was extracted from different meshes and interpreted statistically for its particle temperature profile and ignition characteristics hereafter.

Figures 8 and 9 demonstrate the CFD-predicted particle temperature profile for three different coal sizes (i.e., maximum, minimum, and mean diameter) as a function of the reactor distance in air versus 27% O_2 in CO_2 , respectively. In each figure, the pyrometer-measured data and high-speed camera photographs for three distances are also displayed. Irrespective of the particle size, the Victorian brown coal exhibits a single peak in its temperature profile, which is broadly consistent with the lignites reported in the literature.⁴⁸ In comparison to bituminous coals possessing a bimodal distribution for a rather separate oxidation of volatile and char, the single peak for brown coal (i.e., lignite) is

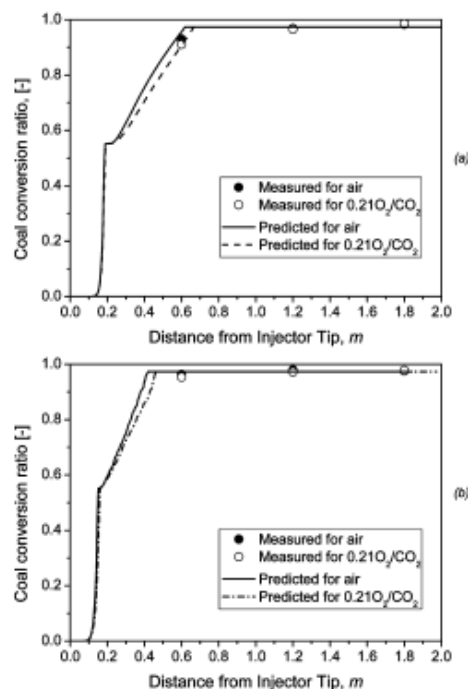


Figure 10. Brown coal burnout rates as a function of the reactor distance for air versus 21% O_2/CO_2 in DTF for the furnace temperatures of (a) 1073 K and (b) 1273 K. The experimental data were reprinted with permission from the copyright of Elsevier. The experimental results were reprinted with permission from ref 34. Copyright 2010 from Elsevier.

a direct sign of its hetero- and homogeneous ignitions and/or a large overlapping of the oxidation of both volatiles (in the gas phase) and char particles (in the solid phase). This is also consistent with our previous observation for the ignition of the same coal in a wire-mesh reactor.³³

In Figure 8, one can see that the pyrometer data in air-firing experiments were matched reasonably well by the CFD modeling

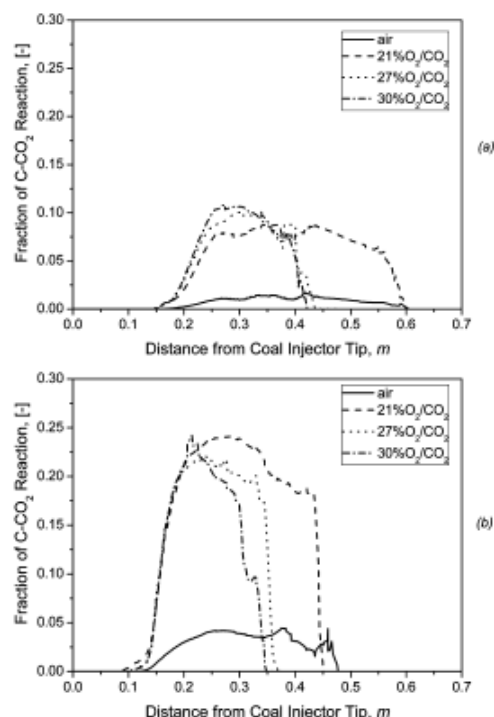


Figure 11. Fraction of the char CO_2 gasification reaction contribution to the coal burnout rate. Panels a and b are for the furnace temperatures of 1073 and 1273 K, respectively.

results, regarding different particle sizes. In Figure 9 for the 27% O_2 balanced by CO_2 , it is proven essential to include the char CO_2 and char H_2O gasification reactions in the model; otherwise, the prediction (top dash-dot curve) would stay far away from the pyrometer measurement (solid dots with error bars). This is very intriguing and further confirms the high C- CO_2 gasification reactivity for the brown coal tested here, which even occurs at a low furnace wall temperature of 1073 K.

CFD Model Verification by the Coal Burnout Rate and Particle Velocity. The high reactivity of the dried Victorian brown coal tested was also demonstrated by its burnout rate versus DTF reactor distance in Figure 10. In the furnace temperature of 1073 K (Figure 10a), the coal conversion even reached 90% at the reactor distance of 0.6 m, in either air or 21% O_2 balanced by CO_2 . Such a fast burnout rate in DTF was also predicted accurately by the CFD modeling, via the use of the kinetic parameters in Table 1 and the submodels described above. The model also predicts a completion of the release of volatiles at the reactor distance of 0.2 m, which corresponds to a particle residence time as short as 0.2 s. Moreover, from both experimental measurement and CFD modeling, one can see that the difference between the two bulk gases, air and 21% O_2 in CO_2 , is negligible in terms of the coal burnout rate for Victorian brown coal. Because the substitution of 21% O_2 in CO_2 for air caused the significant ignition delay (as shown later) and lower particle temperature, a nearly identical coal burnout rate between the two cases observed here echoes Figure 9 to prove the strong char CO_2 gasification reactions for the brown coal tested here.

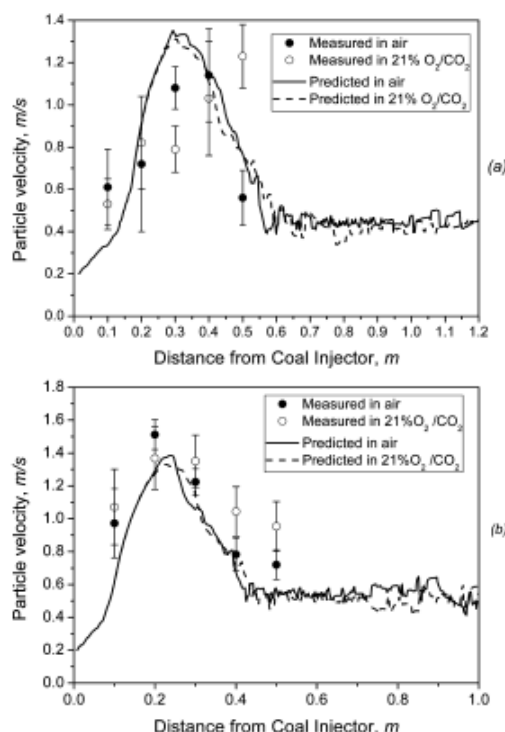


Figure 12. CFD-predicted particle velocity profile of the mean particle size and comparison to experimental observation by *in situ* diagnosis for the furnace temperatures of (a) 1073 K and (b) 1273 K. Experimental results were reprinted with permission from ref 32. Copyright 2010 from the American Chemistry Society.

When the pyrometer-measured burning coal particle temperature was matched with modeling results, a contribution of approximately 10% from the char CO_2 reaction has been reported in the literature.³⁶ Following the same idea, Figure 11 plotted the char CO_2 contribution as a function of the bulk gas composition and furnace temperature. The fraction of the char CO_2 reaction was defined here by the equation of $q_2/(q_1 + q_2 + q_3)$. Even at the furnace wall temperature of 1073 K, around 10% contribution can be attributed to the char CO_2 reaction that preferentially occurs at the particle peak temperature where the volatile flame is formed. Increasing the oxygen fraction in CO_2 gradually dropped the contribution of the char CO_2 reaction at the particle peak temperature, from around 10% in 21% O_2 to 8% in 26% O_2 and then 7.0% in 30% O_2 . This is an indicator of the enhanced char O_2 reaction at the elevated oxygen content in the bulk gas, as expected. The consequence of this enhanced char O_2 reaction is also obvious, which resulted in a longer duration for the char CO_2 gasification reaction to occur on the char particle surface. Increasing the furnace temperature to 1273 K clearly improved the char CO_2 contribution to coal burnout, reaching around 25% at the peak temperature for the 21% O_2 in CO_2 case. Moreover, the duration for the char CO_2 reaction was enlarged at the elevated oxygen fraction in CO_2 , the same as the low furnace temperature discussed above.

The accuracy of the CFD modeling was further verified by the particle velocity profile in Figure 12. Although the particle trajectory in the DTF was supposed to be complex because of the

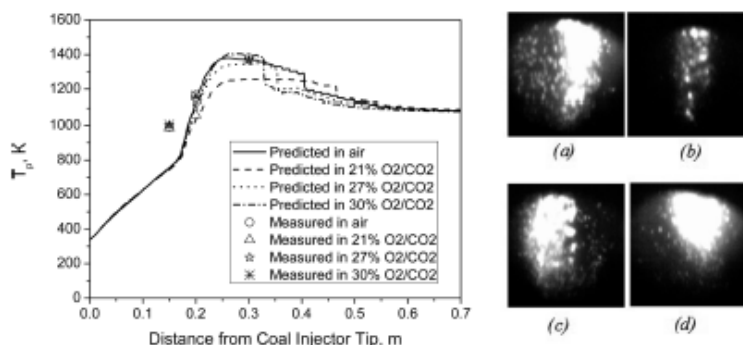


Figure 13. Measured and predicted particle temperature and flame propagation as a function of the reactor distance and bulk gas composition. The calculation on the particle temperature was made for the mean particle size of $130\ \mu\text{m}$ at the furnace wall temperature of $1073\ \text{K}$. Photos a, b, c, and d are for the flame observed at the reactor distance of $0.2\ \text{m}$ for air, $21\%\ \text{O}_2/\text{CO}_2$, $27\%\ \text{O}_2/\text{CO}_2$, and $30\%\ \text{O}_2/\text{CO}_2$, respectively.³⁴ The photographs were reprinted with permission from the copyright of Elsevier.

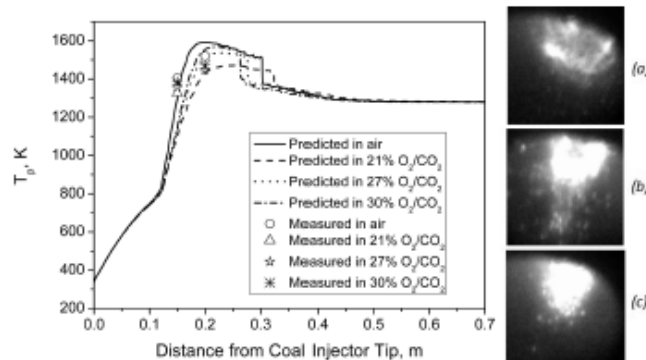


Figure 14. Measured and predicted particle temperature and flame propagation as a function of the reactor distance and bulk gas composition. The calculation on the particle temperature was made for the mean particle size of $130\ \mu\text{m}$ at the furnace wall temperature of $1273\ \text{K}$. Photos a, b, and c are for the flame observed at the reactor distance of $0.15\ \text{m}$ for $21\%\ \text{O}_2/\text{CO}_2$, $27\%\ \text{O}_2/\text{CO}_2$, and $30\%\ \text{O}_2/\text{CO}_2$, respectively.

feeding of the coal particles with a broad size range and broad variation of the position to enter the furnace, the predicted particle velocity for the mean size of $130\ \mu\text{m}$ was found falling in the error range of the measured data. In both furnace temperatures, the particle velocities measured by a high-speed camera follow the same trend as that predicted by the CFD model. In each case, the particle velocity was maximized at a reactor distance of 0.3 or $0.2\ \text{m}$, which corresponds to the complete burnout of coal volatiles. The rapid release of coal volatiles as a jet out of the coal matrix clearly formed an extra momentum, pushing the forward motion of char particles.

Coal Particle Ignition versus O_2 Fraction and Secondary Gas Temperature. Upon the verification of the CFD module developed here, a variety of extra prediction was conducted on the coal particle temperature, flue gas temperature, and radiation heat flux to compare the different combustion cases. The coal ignition point was also extracted from the particle temperature and compared between different cases to address its variation with the secondary gas temperature and the oxygen fraction in CO_2 .

Figures 13 and 14 illustrate coal particle temperature profiles, both predicted and measured, for the four furnace temperatures of 1073 and $1273\ \text{K}$, respectively. For either furnace temperature,

the use of $21\%\ \text{O}_2/\text{CO}_2$ in place of air caused a significant delay on coal ignition, the longest duration of the endothermic char CO_2 gasification reactions (see Figure 11), and hence, the lowest particle temperature at each distance. Increasing the oxygen percentage to 30% in CO_2 enhanced the exothermic char O_2 reaction rate, which thus offset the negative contribution from the char CO_2 gasification reaction and narrowed the discrepancy of both flame intensity and particle temperature to the air case.

Considering that it is very likely that both homo- and heterogeneous ignitions occur simultaneously for the air-dried Victorian brown coal, the ignition time of coal was further extracted from particle temperature profiles in Figure 15. For each panel in Figure 15, the intersection between the tangent curves of the two sections (slow rise versus quick rise) of a char temperature profile was deduced as the coal ignition time. Clearly, at the furnace/gas temperature of $1273\ \text{K}$ in Figure 15a, the brown coal ignition occurred at approximately $0.121\ \text{s}$ in air, relative to $\sim 0.125\ \text{s}$ in $21\%\ \text{O}_2/\text{CO}_2$, $27\%\ \text{O}_2/\text{CO}_2$, and $30\%\ \text{O}_2/\text{CO}_2$ with insignificant difference among the three oxy-firing cases. Panels b and c of Figure 15 illustrate the analysis on coal ignition temperatures at two lower temperatures for the secondary gas, 1073 and $900\ \text{K}$. The former temperature was achieved by simply setting the size zones of the furnace at $1073\ \text{K}$,

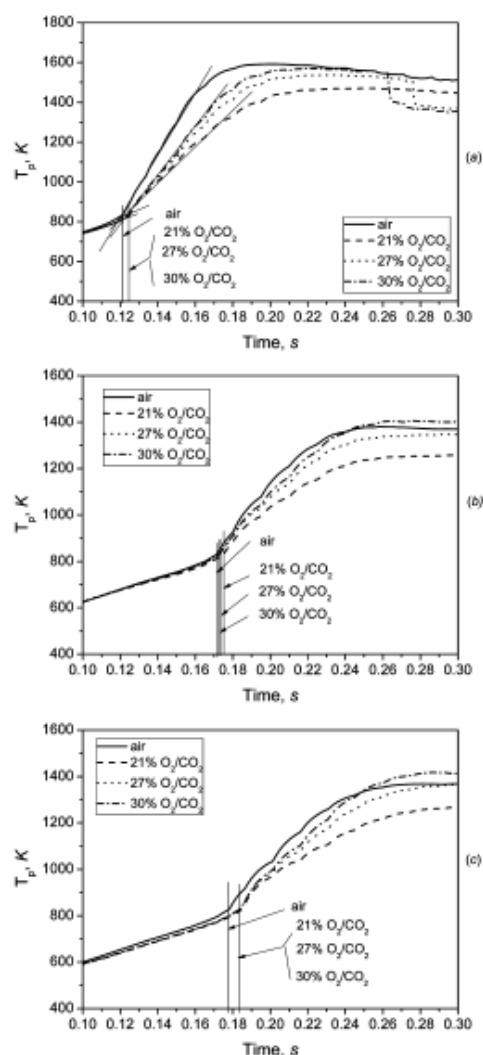


Figure 15. Method to determine the brown coal particle ignition temperature and its variation with bulk gas composition at the secondary gas temperature of (a) 1273 K, (b) 1073 K, and (c) 900 K.

whereas the latter two were achieved by turning off the top two and four zones of the furnace, respectively. By reducing the secondary gas temperature, one can see that the discrepancy of the coal ignition time between air and 21% O_2 in CO_2 and other oxy-fuel cases is clearly widened. This was further quantified in Figure 16, where the ignition times of Victorian brown coal for four cases and the ignition delay between 21% O_2/CO_2 and air were plotted as a function of the secondary gas temperature. Irrespective of bulk gas composition, increasing the secondary gas temperature shortened the coal ignition time quickly as well as narrowed the ignition delay between air and 21% O_2 balanced in CO_2 . At the gas temperature of 700 K, a coal ignition time of 0.235 s was required in air, which changed little at 900 K but was reduced to 0.184 s and then 0.171 and 0.121 s for 1073 and 1273 K,

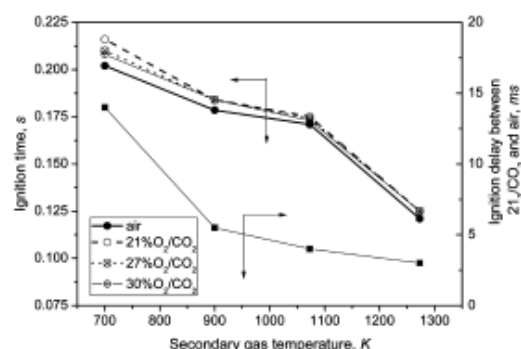


Figure 16. Air-dried Victorian brown coal ignition time and delay as a function of the secondary gas temperature.

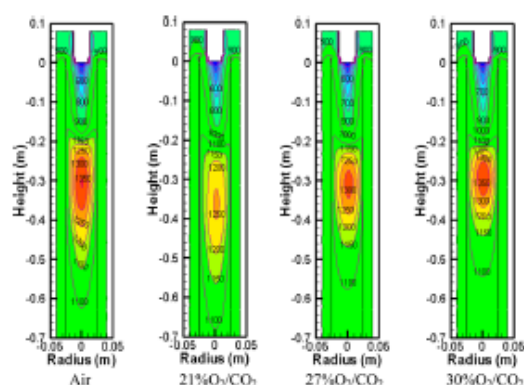


Figure 17. Predicted gas temperature distribution at the DTF furnace temperature of 1073 K.

respectively. In addition, at the low gas temperature of 700 K, the ignition delay between 21% O_2/CO_2 and air reached ~ 14 ms, which was narrowed remarkably to about 5, 4, and 3.5 ms at 900, 1073, and 1273 K, respectively. Clearly, the temperature of the secondary gas plays a critical role in particle ignition. It has the potential to offset the negative impact of the large specific heat capacity of CO_2 . Here, it can be concluded that the coal ignition delay upon gas shift from air to 21% O_2/CO_2 can be eliminated by increasing the second gas temperature to approximately 1273 K. Apparently, such a high temperature can be achieved by employing a regenerator via the use of internal flue gas recirculation to efficiently preheat the combustion gas, the same as the concept of high-temperature air combustion.⁴⁹ The application of such a technology to the oxy-fuel combustion of Victorian brown coal may be plausible, because the low ash content in Victorian brown coal can assist in minimizing the ash fouling in the regenerator.

Flue Gas Temperature Profile and Radiative Heat Flux in DTF. The match of the flue gas temperature profile and radiative heat flux in a furnace is crucial for the retrofitting of oxy-fuel technology to an existing air-fired boiler, in which the heat flux must be match. As shown in Figure 17 for the flue gas temperature extracted from the CFD model, for the same O_2 concentration of 21%, the substitution of N_2 by CO_2 led to the disappearance of the highest temperature of 1350 K corresponding to coal flame in air. Instead, the flue gas remained hotter close

to the bottom of the furnace. This is attributed to delay on coal ignition and oxidation. Increasing the O_2 fraction in CO_2 caused an upward shift of the flue gas temperature and the increase in the flue gas temperature at the coal flame zone, as expected. For the use of 30% O_2/CO_2 in place of air, the highest flame temperature of 1350 K was achieved at nearly the same distance as in air, whereas in the bottom post-flame zone, the flue gas temperature was dropped quickly, because of an intensified and quicker burnout of coal in the furnace. Figure 18 further substantiates a

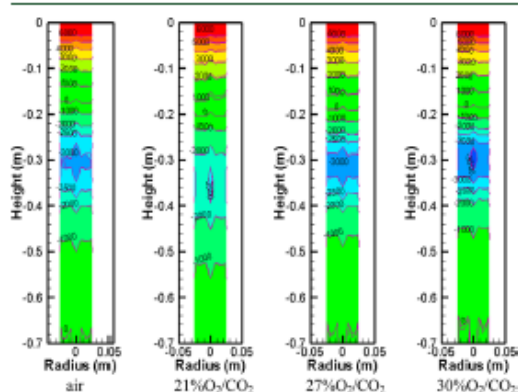


Figure 18. Predicted radiation heat flux distribution at the furnace temperature of 1073 K (J/m^2).

much stronger radiation heat flux for 30% O_2 in CO_2 than in air. Instead, the use of 27% O_2 in CO_2 shows a good match with the air in radiation heat flux in the furnace, although its flue gas temperature is lower than the air case.

CONCLUSION

The numerical modeling of the combustion of air-dried Victorian brown coal in O_2/N_2 and O_2/CO_2 mixtures with 21–30% O_2 has been conducted via the use of CFD, ANSYS FLUENT 13.0. The purpose of this study is to verify the experimental observations as well as to promote our understanding on the details underpinning the combustion characteristics of Victorian brown coal. The major conclusions achieved are drawn as follows: (1) From the methodology perspective, theoretical descriptions of gas radiation and char heterogeneous reactions are key factors determining the simulation accuracy of oxy-fuel combustion. The refined WSGGM, the single-film model with multiple surface reactions, and the refined two-step mechanism for methane oxy-firing that was used to depict volatile oxidation were proven applicable to the oxy-fuel combustion of Victorian brown coal. The turbulence model was found more suitable than the laminar model in terms of estimating the gas temperature profile in the DTF. This is caused by the mixing of cold and hot gas streams nearby the coal injector tip. Moreover, the drying of residual moisture of the air-dried brown coal sample assumed the releasing process of inherent moisture, which was deemed to release with volatile matter simultaneously rather than the wet combustion mode of pulverized coal with surface moisture. (2) The air-dried Victorian brown coal bears a high reactivity for devolatilization and char O_2 and char CO_2 gasification reactions. From both CFD modeling and experimental measurement, the oxidation of air-dried Victorian brown coal is completed in less

than 0.6 m from the DTF coal injector tip, irrespective of bulk gas composition and the oxygen fraction in CO_2 . In comparison to the furnace temperature of 1073–1173 K, the particle peak temperature reached 1300–1600 K after ignition, contributed by approximately 10 and 25% from the char CO_2 gasification reaction at the furnace temperatures of 1073 and 1273 K, respectively. (3) Apart from increasing the oxygen fraction in CO_2 , the increase in the secondary gas temperature is also pivotal in narrowing coal ignition delay between air- and oxy-firing the delay interval to a certain extent. (4) In terms of matching air-firing for radiation heat flux, the presence of 27% O_2 in CO_2 is essential, as an expense of a lower flue gas temperature in the coal volatile flame zone.

AUTHOR INFORMATION

Corresponding Author

Notes

The authors declare no competing financial interest.

ACKNOWLEDGMENTS

This study is supported by the Australian National Low Emission Coal (ANLEC) Research and Development Fund and Brown Coal Innovation Australia (BCIA). We are also grateful to two Monash graduates, Mohammed Al-Bahri and John M. Headberry, for their assistance on the DTF experiment. Dr Lian Zhang is the awardee of 2009–13 Australian Research Council (ARC) Future Fellow under the grant FT0991010, and Prof Zhongxiao Zhang is also grateful for the travel support from Australia–China JCG Round 1 (2012–13) Partnership fund, which allowed him to discuss with the other authors face-to-face in Monash University.

NOMENCLATURE

- A = pre-exponential factor
- A_p = particle external surface (m^2)
- $a_{k,i}$ = coefficient in WSGGM
- $b_{k,i,j}$ = coefficient in WSGGM
- c_p = specific heat ($J\ kg^{-1}\ K^{-1}$)
- C_{diff} = diffusion-limited constant in ANSYS FLUENT ($s\ K^{0.75}$)
- D = diffusion coefficient (m^2/s)
- d_p = particle diameter (m)
- E = activation energy of the reaction ($J/kmol$)
- f_h = heterogeneous reaction heat coefficient absorbed by the particle
- H = heat of the heterogeneous reaction (J/kg of carbon)
- \bar{k}_a = gas absorption coefficient (m^{-1})
- K_d = diffusion-limited reaction rate coefficient ($kg\ m^{-2}\ s^{-1}\ Pa^{-1}$)
- k_i = coefficient in WSGGM
- K_s = surface reaction rate coefficient ($kg\ m^{-2}\ s^{-1}\ Pa^{-1}$)
- \bar{L} = domain length (m)
- M = molecular weight ($kg/kmol$)
- m_p = particle mass (kg)
- r_p = radius of the particle (m)
- P = total or partial pressure (Pa)
- q = reaction rate of carbon per unit surface area ($kg\ m^{-2}\ s^{-1}$)
- R = universal gas constant ($J\ kmol^{-1}\ K^{-1}$)
- T = temperature (K)
- V_{∞} = maximum volume of volatile matter
- ρ = gas density (kg/m^3)

λ = thermal conductivity ($\text{W m}^{-1} \text{K}^{-1}$)

ε = gas emissivity

ε_p = emissivity of the particle surface

θ_R = radiation temperature (K)

σ = Stefan-Boltzmann constant ($\text{W m}^{-2} \text{K}^{-4}$)

Subscripts

d = diffusion

v = volatile matter

g = ambient

m = average in the particle boundary layer

p = particle

1 = reaction of $\text{C} + 0.5\text{O}_2 \rightarrow \text{CO}$

2 = reaction of $\text{C} + \text{CO}_2 \rightarrow 2\text{CO}$

3 = reaction of $\text{C} + \text{H}_2\text{O} \rightarrow \text{CO} + \text{H}_2$

REFERENCES

- Wall, T.; Liu, Y.; Spero, C.; Elliott, L.; Khare, S.; Rathnam, R.; Zeenathal, F.; Moghtaderi, B.; Buhre, B.; Sheng, C.; Gupta, R.; Yamada, T.; Malino, K.; Yu, J. *Chem. Eng. Res. Des.* **2009**, *87*, 1003–1016.
- Chen, L.; Yong, C.; Ghoniem, A. F. *Prog. Energy Combust. Sci.* **2012**, *38*, 156–214.
- Smart, J.; Lu, G.; Yan, Y.; Riley, G. *Combust. Flame* **2010**, *157*, 1132–1139.
- Buhre, B. J. P.; Elliott, L. K.; Sheng, C. D.; Gupta, R. P.; Wall, T. F. *Prog. Energy Combust. Sci.* **2005**, *31* (4), 283–307.
- Molina, A.; Shaddix, C. R. *Proc. Combust. Inst.* **2007**, *31*, 1905–1912.
- Kakaras, E.; Koumanakos, A.; Doukelis, A.; Giannakopoulos, D.; Vorrilas, I. *Fuel* **2007**, *86*, 2144–2150.
- Khare, S. P.; Wall, T. F.; Farida, A. Z.; Liu, Y.; Moghtaderi, B.; Gupta, R. P. *Fuel* **2008**, *87*, 1042–1049.
- Tan, Y.; Croiset, E.; Douglas, M. A.; Thambimuthu, K. V. *Fuel* **2006**, *85*, 507–512.
- Suda, T.; Masuko, K.; Sato, J.; Yamamoto, A.; Okazaki, K. *Fuel* **2007**, *86*, 2008–2015.
- Liu, Y.; Geier, M.; Molina, A.; Shaddix, C. R. *Int. J. Greenhouse Gas Control* **2011**, *55*, 36–46.
- Riaza, L.; Alvarez, L.; Gil, M. V.; Pevida, C.; Pis, J. J.; Rubiera, F. *Energy* **2011**, *36*, 5314–5319.
- Liu, H.; Zailani, R.; Gibbs, B. *Fuel* **2005**, *84*, 833–840.
- Anderson, K.; Johansson, R.; Hjartstam, S.; Johnson, F.; Leckner, B. *Fuel* **2008**, *33*, 67–76.
- Zhang, L.; Jiao, F.; Binner, E.; Bhattacharya, S.; Ninomiya, Y.; Li, C. Z. *Fuel* **2011**, *90*, 1361–1369.
- Haryanto, A.; Hong, K.-S. *Comput. Chem. Eng.* **2011**, *35*, 25–40.
- Al-Abbas, A. H.; Naser, J.; Dodds, D. *Fuel* **2011**, *90*, 1778–1795.
- Al-Abbas, A. H.; Naser, J.; Dodds, D. *Fuel* **2012**, *102*, 646–665.
- Edge, P.; Gubba, S. R.; Ma, L.; Porter, R.; Pourkashanian, M.; Williams, A. *Proc. Combust. Inst.* **2011**, *33*, 2709–2716.
- Hottel, H. C.; Sarofim, A. F. *Radiative Transfer*, 1st ed.; McGraw-Hill: New York, 1967.
- Smith, T. F.; Shen, Z. F.; Friedman, J. N. *J. Heat Transfer* **1982**, *104*, 602–608.
- Yin, C. G.; Johansen, L. C. R.; Rosendahl, L. A.; Kar, S. K. *Energy Fuels* **2010**, *24*, 6275–6282.
- Yin, C. G. *Energy Fuels* **2012**, *26*, 3349–3356.
- Krishnamoorthy, G.; Jimenez, M. *Int. J. Energy Res.* **2012**, *36*, 789–797.
- Krishnamoorthy, G. *Int. Commun. Heat Mass Transfer* **2010**, *37*, 1182–1186.
- Johansson, R.; Leckner, B.; Andersson, K.; Johansson, F. *Combust. Flame* **2011**, *158*, 893–901.
- Hecht, E. S.; Shaddix, C. R.; Molina, A.; Haynes, B. S. *Proc. Combust. Inst.* **2011**, *33*, 1699–1706.
- Geier, M.; Shaddix, C. R.; Davis, K. A.; Shim, H. S. *Appl. Energy* **2012**, *93*, 675–679.
- Glarborg, P.; Bentzen, L. I. B. *Energy Fuels* **2008**, *22*, 291–296.
- Andersen, J.; Rasmussen, C. L.; Giselsson, T.; Glarborg, P. *Energy Fuels* **2009**, *23*, 1379–1389.
- Yin, C.; Rosendahl, L. A.; Kar, S. K. *Fuel* **2011**, *90*, 2519–2529.
- Binner, E.; Zhang, L.; Li, C. Z.; Bhattacharya, S. *Proc. Combust. Inst.* **2011**, *33*, 1739–1746.
- Zhang, L.; Binner, E.; Qiao, Y.; Li, C. Z. *Energy Fuels* **2010**, *24*, 29–37.
- Qiao, Y.; Zhang, L.; Binner, E.; Xu, M.; Li, C. Z. *Fuel* **2010**, *89*, 3381–3387.
- Zhang, L.; Binner, E.; Qiao, Y.; Li, C. Z. *Fuel* **2010**, *89*, 2703–2712.
- Johansson, R.; Leckner, B.; Andersson, K.; Johansson, F. *Combust. Flame* **2011**, *158*, 893–901.
- ANSYS, Inc. *FLUENT User's Guide, Version 13.0*; ANSYS, Inc.: Canonsburg, PA, 2013.
- Yao, S. C.; Liu, L. *Combust. Flame* **1983**, *51*, 335–345.
- Badzioch, S.; Hawksley, P. G. W. *Ind. Eng. Chem. Process Des. Dev.* **1970**, *9*, 521–530.
- Zhang, J.; Zhang, M. C.; Yu, J. *Energy Fuels* **2010**, *24* (2), 871–879.
- Field, M. A.; Gill, D. W.; Morgan, B. B.; Hawksley, P. G. W. *Combustion of Pulverized Coal*; British Coal Utilisation Research Association (BCURA): Leatherhead, U.K., 1967; p 186.
- Ubhayakar, S. K.; Stickler, D. B.; Von Rosenberg, C. W.; Gannan, R. S. *Symp. (Int.) Combust., [Proc.]* **1976**, 427–436.
- Kobayashi, H.; Howard, J. B.; Sarofim, A. F. *Symp. (Int.) Combust., [Proc.]* **1976**, 411–425.
- Gururajan, V. S.; Wall, T. F.; Truelove, J. S. *Combust. Flame* **1988**, *72*, 1–12.
- Toporov, D.; Bocian, P.; Heil, P.; Kellermann, A.; Stadler, H.; Tschunko, S.; Förster, M.; Kneer, R. *Combust. Flame* **2008**, *155*, 605–618.
- Smith, I. W. *Combust. Flame* **1971**, *17*, 303–314.
- Mayers, A. M. *J. Am. Chem. Soc.* **1934**, *56*, 1879–1881.
- British Coal Utilisation Research Association (BCURA). *Laboratory Studies of Combustion, BCURA Annual Report*; BCURA: Cheltenham, U.K., 1966.
- Bejarano, P. A.; Levendis, Y. A. *Combust. Flame* **2008**, *153*, 270–287.
- Suda, T.; Takafuji, M.; Hirata, T.; Yoshino, M.; Sato, J. *Proc. Combust. Inst.* **2002**, *29*, 503–509.

APPENDIX D

Simulation Code used in this thesis

This page is intentionally left blank

D.1. MATLAB code for calculating the amount inherent moisture (Chapter 5)

Main code:

```
function [timedry, disdry, tdevol, disdevol, tempdevol, tignition, Tm, index] =  
Comb_inherent(inher, mcoinput, comb, Drying)  
  
diam = 0.000084;  
  
%Problem Constant  
hd = 2.26E6; %Heat of water evaporation (J/kgK)  
hpyro = 8.37*10^5; %J/kgK of coal  
e = 0.8; %Particle Emissivity  
sig = 5.67E-8; %Stefan-Boltzmann Constant  
tw = 773; %Wall temperature (K)  
r = 8.314; %Universal gas constant (J/kgK)  
cpcoal = 1150; %Lignite Heat Capacity from Fluent (J/kgK)  
pdried = 1150; %Dried Coal Density (kg/m3)  
ta = 365; %Wet bulb temperature(K)  
na = 0.3468; %Total Time in air (s)  
no = 0.4132; %Total Time in CO2 (s)  
fv = 0.4495; %Volatile Fraction in air-dried  
fvdb = fv/0.88; %Vol Fraction in dry basis  
dt = 0.00005; %Integration time step  
  
if comb == 1  
fo = 0.2103; fn = 0.4404; fc = 0.1644; fs = 0.1849; n = (0:dt:na);  
elseif comb == 2  
fo = 0.1664; fn = 0; fc = 0.649; fs = 0.1846; n = (0:dt:no);  
elseif comb == 3  
fo = 0.2157; fn = 0; fc = 0.5992; fs = 0.185; n = (0:dt:no);  
elseif comb == 4  
fo = 0.2654; fn = 0; fc = 0.5492; fs = 0.1855; n = (0:dt:no);  
elseif comb == 5  
fo = 0.3154; fn = 0; fc = 0.4989; fs = 0.1859; n = (0:dt:no);  
end  
  
%Solution Initialization  
tf = zeros(length(n),1); tp = zeros(length(n),1); Tm = zeros(length(n),1);  
tgas = zeros(length(n),1);  
mv = zeros(length(n),1);  
devolrate = zeros(length(n),1);  
area = zeros(length(n),1);  
b = zeros(length(n),1);  
distance = zeros(length(n),1);  
nn = zeros(length(n),1); dryrate = zeros(length(n),1); totconv =  
zeros(length(n),1);  
reaction = zeros(length(n),1);  
rate = zeros(length(n),1);  
  
%Input Parameter  
d(1:length(n),1) = diam;  
mco(1:length(n),1) = mcoinput;  
pwc = pdried*(1-mcoinput)+mcoinput*1000;  
mdried = (pdried*3.14/6*diam^3);  
mi = (pdried*3.14/6*diam^3)+(mcoinput*mdried/(1-mcoinput));  
ft = fvdb*mdried;
```

```

unburnt = 0.03*mdried;
mt(1:length(n),1) = mi;
tp(1) = 298;
tf(2) = tf(1) +dt;
i = 2;
iagain = 1;
m = 2;
err(1:length(n),1) = 0;

%Coal Properties dried basis
FC = 0.470455;          %Fixed carbon
VM = 0.510795;          %Volatile matter
A = 0.018750;           %Ash
C = 0.657;              %Carbon
H = 0.068;              %Hydrogen
N = 0.06;               %Nitrogen
S = 0.05;               %Sulphur
O = 0.258;              %Oxygen

%Method 2
Cvol = C - FC;
hvol = ((3.55*Cvol^2-232*Cvol - 2230*H +51.2*Cvol*H+131*N +
20600))*1000-hd;

clc
fprintf('Time Step: %6d%10s:%10.4f Total
Conversion:%10.4f\n',1,'Error',0,0);
while iagain == 1
    if tf(i) == 0
        distance(i) = 0;
    elseif tf(i) > 0 && tf(i) <= 0.048
        if comb == 1
            distance(i) = (-
0.0003*(tf(i)*1000)^3+0.0411*(tf(i)*1000)^2+0.7678*(tf(i)*1000)-
2.7809)/10;
        elseif comb >=2&&comb<=5
            distance(i) = (-0.0003*(tf(i)*1000)^3+0.0468*(tf(i)*1000)^2-
0.2070*(tf(i)*1000)+1.0267)/10;
        end
    elseif tf(i)>0.048
        if comb == 1
            distance(i) = (0.0041*(tf(i)*1000)^2+2.3791*(tf(i)*1000)-29.012)/10;
        elseif comb >=2&&comb<=5
            distance(i) = (0.0045*(tf(i)*1000)^2+1.8867*(tf(i)*1000)-
37.528)/10;
        end
    end
    if distance(i) < 0
        distance(i) = distance(i-1)+0.0001;
    end
    if comb == 1
        %
        tgas(1) = 414.96 + 820.13576;
        %
        tgas(i) = 414.96 + 820.13576*exp(-distance(i)/30.77);
        tgas(i) = -4259.2*tf(i) + 1232.3;
    elseif comb >=2&&comb<=5
        %
        tgas(1) = 276.465 + 930.52797;
        %
        tgas(i) = 276.465 + 930.52797*exp(-distance(i)/43.834);
    end
end

```

```

        tgas(i) = -4756.4*tf(i) + 1265.4;
    end%-- from if comb == 1 loop --%

    if tgas(i) <=tw
        tgas(i) = tw;
    end

    if tf(i)<=0.0025
        parvel = 0;
    elseif tf(i)>0.0025
        if comb == 1
            parvel = 0.7224*log(tf(i)*1000)-0.1205;
        elseif comb >=2&& comb <=5
            parvel = 0.897*log(tf(i)*1000)-1.3227;
        end
    end

    %Kinetic Parameter
    %A is in s-1 and E is J/mole
    %Devolatilisation
    %
    if comb == 1
        av = 104475.6;ev=66526.13;
    %
    elseif comb >=2&& comb <=5
    %
        av = 207744.8;ev=67785.7;
    %
    end

    %Guess the particle temperature at t + dt
    tpi = tp(i-1)+10;
    err(i) = 1;
    b(m) = 0;

    %Iterative procedure
    for m = 1:10
        %Dimensionless Coefficient
        Tm(1) = (tpi+tgas(1))/2;
        Tm(i) = (tpi+tgas(i))/2;
        [miut,pt,cpt,lt] = Gprop(Tm,i,fo,fs,fc,fn);

    %Dimensionless Correlation
        gasvel = (11.7/60*10^-3)*(tgas(i)/298)/(pi*0.115^2);
        urel = abs(parvel-gasvel);
        Re = pt*urel*d(i)/miut;
        Pr = cpt*miut/lt;
        Nu = 2 + ((0.555*Re^0.5*Pr^(1/3))/(1+(1.232*(1/Re)*(Pr)^(-4/3))))^0.5);
        h = Nu*lt/d(i);

    %Constant Calculation
        area(1) = pi*d(1)^2;
        area(i) = pi*d(i)^2;

        %Rate of Drying
        if Drying == 1
            nn(i) = (6*h*(tgas(i)-ta))/(hd*pwc*(mco(1)/(1+mco(1)))*d(i));
            dryrate(i) = mco(1)*nn(i)*mi/area(i);
        elseif Drying == 2
            dryrate(i) = h*(tgas(i)-ta)/hd;
        end
    end

```

```

        %Rate of Devolatilisation
        kv(i) = av*exp(-ev/(r*tpi));
        devolrate(i) = kv(i)*(ft-mv(i))/area(i);
        reaction(i) = -devolrate(i-1)*area(i-1)*hpyro;
        rate(i) = devolrate(i-1)*area(i-1)*dt;

        % Transient Code algorithm
        if mco(i-1) > inher
            if tp(i-1) < ta
                tp(i) = tp(i-1) + area(i-1)/(mt(i-
1)*cpcoal)*dt*(e*sig*(tw^4-tp(i-1)^4)+h*(tgas(i-1)-tp(i-1)));
            elseif tp(i-1) >= ta
                mt(i) = mt(i-1)-(dryrate(i-1)*dt*area(i-1));
                tp(i) = tp(i-1) + area(i-1)/(mt(i-
1)*cpcoal)*dt*(e*sig*(tw^4-tp(i-1)^4)+h*(tgas(i-1)-tp(i-1))-dryrate(i-
1)*hd);
                mco(i) = (mco(i-1)*mt(1)-dt*dryrate(i-1)*area(i-
1))/mt(1);
            if tp(i)<ta
                tp(i) = ta;
            end
        end
        if mco(i) < inher
            mco(i) = inher;
        end
        timedry = tf(i);
        disdry = distance(i);
        elseif mco(i-1)<=inher
        mco(i) = inher;
            mt(i) = mt(i-1)-rate(i-1);
            mv(i) = mv(i-1)+devolrate(i-1)*area(i-1)*dt;
            tp(i) = tp(i-1) + area(i-1)/(mt(i-1)*cpcoal)*dt*(e*sig*(tw^4-tp(i-
1)^4)+h*(tgas(i-1)-tp(i-1))+reaction(i-1));
            if mt(i) <= unburnt,break,end
            end%-- exit from if mco < inher loopx
            err = abs((tp(i)-tpi)/tpi);
            tpi = tp(i);
            totconv(i) = (mi-mt(i))/mi;
        end%-- Exit from for m= 1:50 loop
            fprintf('Time Step: %6d%10s:%10.4f Total
Conversion:%10.4f\n',i,'Error',err,totconv(i));
            i = i+1;
            if distance(i-1) <= 100
                iagain = 1;
                tf(i) = tf(i-1)+dt;
                if mt(i-1) <= unburnt
                    iagain = 0;
                    i = i-1;
                end
                if tf(i) >=0.03
                    iagain = 0;
                    i = i-1;
                end
            else
                i = i-1;
                iagain = 0;
            end% -- Exit from if i > length(n)

```

```

end%-- From while iagain == 1

%Final Solution
tff = tf(1:i,1);tpf = tp(1:i,1);mvf=mv(1:i,1);
devolratef = devolrate(1:i,1);distancef = distance(1:i,1);
maxrate2 = gradient(devolratef,tff);
maxrate = gradient(maxrate2,tff);
index = find(maxrate==max(maxrate));
% maxrate = find(tpf>673);
% index = min(maxrate);
tdevol = tff(index);
tempdevol = tpf(index);
disdevol = distancef(index);

A = 5.012E11;
Ea = 200000;
% A = 2.239E12;
% Ea = 170000;
[miutff,ptff,cptff,ltff,do2mff,dn2mff,dco2mff,dh2omff,cvtff] =
Gprop(Tm,index,fo,fs,fc,fn);%J/molK
tignition = cvtff*(Tm(index)^2*r/Ea)/(hvol/18*0.33*A*exp(-
Ea/(r*Tm(index))));

fprintf('\nEnd of Calculation\n');

```

Code for calculating gas property:

```

function[miut,pt,cpt,lt,do2m,dn2m,dco2m,dh2om,cvt] =
Gprop(Tm,i,fo,fs,fc,fn)

%Gas properties Calculation at mean temperature
%Thermal Conductivity (W/mK), Heat capacity (J/kgK), Density (kg/m3),
%Viscosity (kg/m.s)
%C denote CO2, n denote N2, O denote O2 and s denote steam

mo2 = 32;
mco2 = 44;
mn2 = 28;
mh2o = 18;
r = 8.314;
p = 101325;
tw = fo*mo2+fc*mco2+mn2*fn+mh2o*fs;
wo = fo*mo2/tw;
wc = fc*mco2/tw;
wn = fn*mn2/tw;
ws = fs*mh2o/tw;
mmix = wo*mo2+wc*mco2+wn*mn2+mh2o*ws;

%Transport Properties Data
cpc = (23.5061 + 0.03807*Tm(i) + 7.40233E-05 *Tm(i)^2 - 2.22713E-
07*Tm(i)^3+2.34E-10*Tm(i)^4-1.1E-13*Tm(i)^5+2.17E-17*Tm(i)^6);
cps = (33.1744 - 0.00325*Tm(i) + 1.74365E-05 *Tm(i)^2 - 5.97958E-
09*Tm(i)^3);
cpn = (28.7168 + 0.00735*Tm(i) - 4.54759E-05 *Tm(i)^2 + 1.16406E-
07*Tm(i)^3-1.2E-10*Tm(i)^4+5.9E-14*Tm(i)^5-1.1E-17*Tm(i)^6);

```

```

cpo = (29.7902 - 0.00949*Tm(i) + 2.85799E-05 *Tm(i)^2 + 9.87286E-
09*Tm(i)^3-5.7E-11*Tm(i)^4+4.3E-14*Tm(i)^5-1E-17*Tm(i)^6);
miuc = (11.8109 + 0.49838 *Tm(i) -0.00011 * Tm(i)^2)*10^-6;
miun = (4.465558 + 0.638138*Tm(i) - 0.00027 *Tm(i)^2 + 5.41E-8
*Tm(i)^3)*10^-6;
miuo = (-4.94329 + 0.806733 *Tm(i) - 0.0004 *Tm(i)^2 + 1.01E-7
*Tm(i)^3)*10^-6;
mius = (22.82112E-3 + 0.173868*Tm(i) + 0.000325 *Tm(i)^2 - 1.4E-7
*Tm(i)^3)*10^-6;
cvc = (cpc)/1.18;
cvs = (cps)/1.25;
cvn = (cpn)/1.34;
cvo = (cpo)/1.313;
lc = -6.708E-3 + 7.535E-5 *Tm(i) +9.493E-9 * Tm(i)^2 - 1.127E-11
*Tm(i)^3;
ln = -2.268E-4 + 1.027E-4 *Tm(i) - 6.015E-8 *Tm(i)^2 + 2.233E-11
*Tm(i)^3;
lo = 1.547E-4 + 9.415E-5 *Tm(i) -2.753E-8 *Tm(i)^2 + 5.207E-12 *Tm(i)^3;
ls = 5.62E-3 + 1.57E-5 *Tm(i) +1.01E-7 *Tm(i)^2 - 2.428E-11 *Tm(i)^3;

```

```

%Interaction Parameter for viscosity
psio2co2 = (1/8)^0.5*(1+(mo2/mco2))^0.5*(1+(miuo/miuc)^0.5*(mco2/mo2)^0.25)^2;
psio2n2 = (1/8)^0.5*(1+(mo2/mn2))^0.5*(1+(miuo/miun)^0.5*(mn2/mo2)^0.25)^2;
psio2h2o = (1/8)^0.5*(1+(mo2/mh2o))^0.5*(1+(miuo/mius)^0.5*(mh2o/mo2)^0.25)^2;
psico2o2 = (1/8)^0.5*(1+(mco2/mo2))^0.5*(1+(miuc/miuc)^0.5*(mo2/mco2)^0.25)^2;
psico2n2 = (1/8)^0.5*(1+(mco2/mn2))^0.5*(1+(miuc/miun)^0.5*(mn2/mco2)^0.25)^2;
psico2h2o = (1/8)^0.5*(1+(mco2/mh2o))^0.5*(1+(miuc/mius)^0.5*(mh2o/mco2)^0.25)^2;
psin2o2 = (1/8)^0.5*(1+(mn2/mo2))^0.5*(1+(miun/miuc)^0.5*(mo2/mn2)^0.25)^2;
psin2co2 = (1/8)^0.5*(1+(mn2/mco2))^0.5*(1+(miun/miuc)^0.5*(mco2/mn2)^0.25)^2;
psin2h2o = (1/8)^0.5*(1+(mn2/mh2o))^0.5*(1+(miun/mius)^0.5*(mh2o/mn2)^0.25)^2;
psih2oo2 = (1/8)^0.5*(1+(mh2o/mo2))^0.5*(1+(miun/miuc)^0.5*(mo2/mh2o)^0.25)^2;
psih2oco2 = (1/8)^0.5*(1+(mh2o/mco2))^0.5*(1+(miun/miuc)^0.5*(mco2/mh2o)^0.25)^2;
psih2on2 = (1/8)^0.5*(1+(mh2o/mn2))^0.5*(1+(miun/miun)^0.5*(mn2/mh2o)^0.25)^2;

```

```

%Interaction Parameter for thermal conductivity

```

```

psio2co2k = (1/8)^0.5*(1+(mo2/mco2))^0.5*(1+(lo/lc)^0.5*(mo2/mco2)^0.25)^2;
psio2n2k = (1/8)^0.5*(1+(mo2/mn2))^0.5*(1+(lo/ln)^0.5*(mo2/mn2)^0.25)^2;
psio2h2ok = (1/8)^0.5*(1+(mo2/mh2o))^0.5*(1+(lo/ls)^0.5*(mo2/mh2o)^0.25)^2;
psico2o2k = (1/8)^0.5*(1+(mco2/mo2))^0.5*(1+(lc/lo)^0.5*(mco2/mo2)^0.25)^2;
psico2n2k = (1/8)^0.5*(1+(mco2/mn2))^0.5*(1+(lc/ln)^0.5*(mco2/mn2)^0.25)^2;

```

```

psico2h2ok = (1/8)^0.5*(1+(mco2/mh2o))^0.5*(1+(lc/ls)^0.5*(mco2/mh2o)^0.25)^2;
psin2o2k = (1/8)^0.5*(1+(mn2/mo2))^0.5*(1+(ln/lo)^0.5*(mn2/mo2)^0.25)^2;
psin2co2k = (1/8)^0.5*(1+(mn2/mco2))^0.5*(1+(ln/lc)^0.5*(mn2/mco2)^0.25)^2;
psin2h2ok = (1/8)^0.5*(1+(mn2/mh2o))^0.5*(1+(ln/ls)^0.5*(mn2/mh2o)^0.25)^2;
psih2oo2k = (1/8)^0.5*(1+(mh2o/mo2))^0.5*(1+(ls/lo)^0.5*(mh2o/mo2)^0.25)^2;
psih2oco2k = (1/8)^0.5*(1+(mh2o/mco2))^0.5*(1+(ls/lc)^0.5*(mh2o/mco2)^0.25)^2;
psih2on2k = (1/8)^0.5*(1+(mh2o/mn2))^0.5*(1+(ls/ln)^0.5*(mh2o/mn2)^0.25)^2;

%Total in Gas Mixtures
% cpt = ((fo*cpo)/32+(fn*cpn)/28+(fc*cpc)/44+(fs*cps)/18)*1000;
cpt = ((fo*cpo)+(fn*cpn)+(fc*cpc)+(fs*cps));
cvt = (fo*cvo+fn*cvn+fc*cvc+fs*cvs);
pt = p*mmix/r/Tm(i)*10^-3;

%Wassiljewa Equation with Mason-Saxena Formulation
lof =
lo*(1+(0.85*(psio2co2k*(fc/fo)+psio2n2k*(fn/fo)+psio2h2ok*(fs/fo))))^-1;
lcf =
lc*(1+(0.85*(psico2o2k*(fo/fc)+psico2n2k*(fn/fc)+psico2h2ok*(fs/fc))))^-1;
lnf =
ln*(1+(0.85*(psin2o2k*(fo/fn)+psin2co2k*(fc/fn)+psin2h2ok*(fs/fn))))^-1;
lsf =
ls*(1+(0.85*(psih2oo2k*(fo/fs)+psih2on2k*(fn/fs)+psih2oco2k*(fc/fs))))^-1;

%Wilke mixture rule with Chapman-Enskog approximation
miuof = miuo*(1+(psio2co2*(fc/fo)+psio2n2*(fn/fo)+psio2h2o*(fs/fo))))^-1;
miucf = miuc*(1+(psico2o2*(fo/fc)+psico2n2*(fn/fc)+psico2h2o*(fs/fc))))^-1;
miunf = miun*(1+(psin2o2*(fo/fn)+psin2co2*(fc/fn)+psin2h2o*(fs/fn))))^-1;
miusf = mius*(1+(psih2oo2*(fo/fs)+psih2on2*(fn/fs)+psih2oco2*(fc/fs))))^-1;

if fn > 0
    miut = miuof+miucf+miunf+miusf;
    lt = lof+lcf+lnf+lsf;
elseif fn == 0
    lt = lof+lcf+lsf;
    miut = miuof+miucf+miusf;
end
%Diffusional coefficient

dco2o2 = 1.59E-5;
dh2oo2 = 2.44E-5;
dn2o2 = 2.02E-5;
do2n2 = 2.07E-5;
dco2n2 = 1.54E-5;
dh2on2 = 2.53E-5;
do2co2 = 0.8*do2n2;
dh2oco2 = 0.8*dh2on2;
dn2co2 = 0.8*dn2o2;

```



```

do2h2o = 1.2*do2n2;
dco2h2o = 1.2*dco2n2;
dn2h2o = 1.2*dn2o2;

do2m = (1-fo)/((fc/do2co2)+(fn/do2n2)+(fs/do2h2o));
dn2m = (1-fn)/((fc/dn2co2)+(fo/dn2o2)+(fs/dn2h2o));
dco2m = (1-fc)/((fo/dco2o2)+(fn/dco2n2)+(fs/dco2h2o));
dh2om = (1-fs)/((fc/dh2oco2)+(fn/dh2on2)+(fo/dh2oo2));
end

```

The above function can be invoked by:

```

clc
clear
fout = fopen('Dried_Air.txt','w+');
inher = 0;
i = 1;
mcoinput = 0.14;

%Input Drying Model
fprintf('Coal Moisture Content');
fprintf('\n1.Air\n2.Oxy16\n3.Oxy21\n4.Oxy26\n5.Oxy31');
comb = 1;
fprintf('\n1.McIntosh model\n2.General Model\n');
Drying = 1;
fprintf(fout,'Inherent Moisture\tDrying Time (ms)\tDrying
Distance\tIgnition Time (ms)\tIgnition Distance\tDevolatilisation Temp\t
Ignition Delay(ms)\n');
while inher < mcoinput
    [timedry,disdry,tdevol,disdevol,tempdevol,tignition,Tmf,index] =
Comb_inherent(inher,mcoinput,comb,Drying);
    a(i) = inher;
    bb(i) = timedry*1000;
    c(i) = disdry;
    dd(i) = tdevol*1000;
    e(i) = disdevol;
    f(i) = tempdevol;
    g(i) = tignition*1000;

    fprintf(fout,'%10.4f\t%10.4f\t%10.4f\t%10.4f\t%10.4f\t%10.4f\t%10.4f\n',
a(i),bb(i),c(i),dd(i),e(i),f(i),g(i));
    inher = inher + 0.01;
    i = i+1;
end

fclose('all');

```

D.2. MATLAB code to calculate the contribution of steam gasification (Chapter 6)

Code for calculating the rate of steam gasification (Figure 6.2):

```

clc
clf
clear

A1 = [3.58E6;4.26E4;2.61E5/60;3E9];
Ea1 = [206174/8.314;3.16E5/8.314;1.31E5/8.314;2.68E5/8.314];
T = linspace(400,1600,13);
shape(1,:) = 'b-';
shape(2,:) = 'r-';
shape(3,:) = 'g-';
shape(4,:) = 'm-';

for i = 1:length(A1)
    Rate = A1(i)*exp(-Ea1(i)./T);
    semilogy(T,Rate,shape(i,:));
    hold all
    g(:,1) = T;
    g(:,i+1) = Rate;
end

xlabel('Temperature(K)');
ylabel('log (A*exp(-Ea/RT)) (s-1)');
legend('Our coal','Otto et al(1988)','Ye et al (1998)','Demineralized  
Loy Yang Coal');
legend('Location','East');
legend BOXOFF

```

Main Code for calculating the extent of steam gasification in air case:

```

function [tff,tpf,qsf,qtf,qcf] =
Aircasemodel(mcoinput,comb,inher,alphas,alphac)

%One-Dimensional Code for Coal Combustion and Gasification Study

diam = 0.000084;

%Problem Constant
hd = 2.26E6; %Heat of water evaporation (J/kgK)
hco = 9.208*10^6; %Heat of CO formation (J/kgK)
hcd = 3.28*10^7; %Heat of CO2 formation (J/kgK)
hcdg = 1.438*10^7; %Heat of CO2 gasification (J/kgK)
hsg = 1.094*10^7; %Heat of steam gasification (J/kgK)
hh = 1.43*10^8; %Heat of H2 combustion (J/kgK)
hpyro = 8.37*10^5; %J/kgK of coal
hms = 1.145*10^7; %Methane Steam Reforming Endothermic Reaction
(J/kgK)
e = 0.8; %Particle Emissivity
sig = 5.67E-8; %Stefan-Boltzmann Constant

```

```

tw = 773; %Wall temperature (K)
r = 8.314; %Universal gas constant (J/kgK)
cpcoal = 1150; %Lignite Heat Capacity from Fluent (J/kgK)
pdried = 1150; %Dried Coal Density (kg/m3)
ta = 365; %Wet bulb temperature(K)
na = 0.3468; %Total Time in air (s)
no = 0.4132; %Total Time in CO2 (s)
fv = 0.4495; %Volatile Fraction in air-dried
fvdb = fv/0.88; %Vol Fractionin dry basis
P = 101325; %Total Pressure (Pa)
dt = 0.00005; %Integration time step
hchar = 3.28E7; %Heating value of Carbon Char (J/kg)

%Coal Properties dried basis
FC = 0.470455; %Fixed carbon
VM = 0.510795; %Volatile matter
A = 0.018750; %Ash
C = 0.657; %Carbon
H = 0.068; %Hydrogen
N = 0.06; %Nitrogen
S = 0.05; %Sulphur
O = 0.258; %Oxygen

%Method 1
%Conversion ratio btu/lb to kJ/kg
ratio = 2.326;
coalhhvdb = (146.58*C*100+568.78*H*100+29.4*S*100-6.58*A*100-
51.53*(O+N)*100)*ratio*1000;
coalhhvar = coalhhvdb*(1-mcoinput);
coalhhvdb = coalhhvdb-(1+H/2*18)*hd;
coalhhvar = coalhhvar-(1+H/2*18)*hd;
hvol2 = (coalhhvar-(hchar*FC*(1-mcoinput)))/(VM*(1-mcoinput));
hvol3 = (coalhhvdb-(hchar*FC))/VM;

%Method 2
Cvol = C - FC;
hvol = ((3.55*Cvol^2-232*Cvol - 2230*H +51.2*Cvol*H+131*N +
20600))*1000-hd;

if comb == 1
    fo = 0.2103;fn=0.4404;fc = 0.1644;fs = 0.1849;n = (0:dt:na);limit =
na;
elseif comb == 2
    fo = 0.1664;fn = 0;fc = 0.649;fs = 0.1846;n = (0:dt:no);limit = no;
elseif comb == 3
    fo = 0.2157;fn = 0;fc = 0.5992;fs = 0.185;n = (0:dt:no);limit = no;
elseif comb == 4
    fo = 0.2654;fn = 0;fc = 0.5492;fs = 0.1855;n = (0:dt:no);limit = no;
elseif comb == 5
    fo = 0.3154;fn = 0;fc = 0.4989;fs = 0.1859;n = (0:dt:no);limit = no;
end

%Solution Initialization
tf = zeros(length(n),1);tp = zeros(length(n),1);Tm = zeros(length(n),1);
tgas = zeros(length(n),1);
mv = zeros(length(n),1);
rat = zeros(length(n),1);
qo = zeros(length(n),1);qc = zeros(length(n),1);qs = zeros(length(n),1);

```

```

qssurf = zeros(length(n),1);
qt = zeros(length(n),1);
devolrate = zeros(length(n),1);
area = zeros(length(n),1);
b = zeros(length(n),1);
psi = zeros(length(n),1);
vco = zeros(length(n),1);vco2 = zeros(length(n),1);
hcomb = zeros(length(n),1);mech = zeros(length(n),1);
distance = zeros(length(n),1);
nn = zeros(length(n),1);dryrate = zeros(length(n),1);totconv =
zeros(length(n),1);
massrem = zeros(length(n),1);tc = zeros(length(n),1);reaction =
zeros(length(n),1);
rate = zeros(length(n),1);

%Input Parameter
d((1:length(n)),1) = diam;
mco(1:length(n),1) = mcoinput;
pwc = pdried*(1-mcoinput)+mcoinput*1000;
mdried = (pdried*3.14/6*diam^3);
mi = (pdried*3.14/6*diam^3)+(mcoinput*mdried/(1-mcoinput));
ft = fvd*b*mdried;
unburnt = A*mdried;
carbon = mdried-ft-unburnt;
mt(1:length(n),1) = mi;
tp(1) = 298;
tf(2) = tf(1) +dt;
i = 2;
iagain = 1;
m = 2;
err(1:length(n),1) = 0;
pchar = 615;%kg/m3

% %Input Drying Model
% fprintf('\n1.McIntosh model\n2.General Model\n');
% Drying = input('Drying model :');
Drying = 1;

clc
fprintf('Time Step: %6d%10s:%10.4f Total
Conversion:%10.4f\n',1,'Error',0,0);
while iagain == 1
    if tf(i) == 0
        distance(i) = 0;
    elseif tf(i) > 0 && tf(i) <= 0.048
        if comb == 1
            distance(i) = (-
0.0003*(tf(i)*1000)^3+0.0411*(tf(i)*1000)^2+0.7678*(tf(i)*1000)-
2.7809)/10;
        elseif comb >=2&&comb<=5
            distance(i) = (-0.0003*(tf(i)*1000)^3+0.0468*(tf(i)*1000)^2-
0.2070*(tf(i)*1000)+1.0267)/10;
        end
    elseif tf(i)>0.048
        if comb == 1
            distance(i) = (0.0041*(tf(i)*1000)^2+2.3791*(tf(i)*1000)-29.012)/10;
        elseif comb >=2&&comb<=5

```

```

        distance(i) = (0.0045*(tf(i)*1000)^2+1.8867*(tf(i)*1000) -
37.528)/10;
end
    end
    if distance(i) < 0
        distance(i) = distance(i-1)+0.0001;
    end
    if comb == 1
%       tgas(1) = 414.96 + 820.13576;
%       tgas(i) = 414.96 + 820.13576*exp(-distance(i)/30.77);
        tgas(i) = -4259.2*tf(i) + 1232.3;
    elseif comb >=2&&comb<=5
%       tgas(1) = 276.465 + 930.52797;
%       tgas(i) = 276.465 + 930.52797*exp(-distance(i)/43.834);
        tgas(i) = -4756.4*tf(i) + 1265.4;
    end%-- from if comb == 1 loop --%

    if tgas(i) <=tw
        tgas(i) = tw;
    end

    if tf(i)<=0.0025
        parvel = 0;
    elseif tf(i)>0.0025
        if comb == 1
            parvel = 0.7224*log(tf(i)*1000)-0.1205;
        elseif comb >=2&& comb <=5
            parvel = 0.897*log(tf(i)*1000)-1.3227;
        end
    end
end

%Kinetic Parameter
%A is in s-1 and E is J/mole
%Devolatilisation

%   if comb == 1
%       av = 104475.6;ev=66526.13;
%   elseif comb >=2&& comb <=5
%       av = 207744.8;ev=67785.7;
%   end
%Char oxidation kinetic
ao = 0.0024;eo = 69060;
%CO2 gasification kinetic
ac = 0.0053;ec = 125500;
%Steam Gasification Kinetic
as = 3.6E6*pchar*d(1);es = 206000;
%Arthur Coefficient for CO/CO2 Ratio
at = 2511.9;bt = 52080;

%Guess the particle temperature at t + dt
tpi = tp(i-1)+10;
err(i) = 1;
b(m) = 0;

%Iterative procedure
for m = 1:10
    %Dimensionless Coefficient

```

```

Tm(1) = (tpi+tgas(1))/2;
Tm(i) = (tpi+tgas(i))/2;
[miut,pt,cpt,lt,do2m,dn2m,dco2m,dh2om,cvt] =
Gprop(Tm,i,fo,fs,fc,fn);
kdo = 24*do2m*(1/(293)^1.75*1/r);kdc =
24*dco2m*(1/(293)^1.75*1/r);
kds = 24*dh2om*(1/(293)^1.75*1/r);
%
psat = P*exp(hd/1000*18/r*((1/373)-(1/tpi)));

%Dimensionless Correlation
gasvel = (11.7/60*10^-3)*(tgas(i)/298)/(pi*0.115^2);
urel = abs(parvel-gasvel);
Re = pt*urel*d(i)/miut;
Pr = cpt*miut/lt;
Scs = miut/(pt*dh2om);
Shs = 2 + 0.6*Re^0.5*Scs^(1/3);
kcs = Shs*dh2om/d(i);
Nu = 2 + ((0.555*Re^0.5*Pr^(1/3))/(1+(1.232*(1/Re)*(Pr)^(-4/3))))^0.5);
h = Nu*lt/d(i);

%Constant Calculation
area(1) = pi*d(1)^2;
area(i) = pi*d(i)^2;

%Rate of Drying
if Drying == 1
nn(i) = (6*h*(tgas(i)-ta))/(hd*pwc*(mco(1)/(1+mco(1)))*d(i));
dryrate(i) = mco(1)*nn(i)*mi/area(i);
elseif Drying == 2
dryrate(i) = h*(tgas(i)-ta)/hd;
end

%Rate of Devolatilisation
kv(i) = av*exp(-ev/(r*tpi));
devolrate(i) = kv(i)*(ft-mv(i))/area(i);

%Ratio of CO/CO2 produced at particle surface
rat(i) = at*exp(-bt/(r*tpi));
psi(i) = 1/(1+rat(i));
vco(i) = 1-psi(i);vco2(i) = psi(i);
mech(i) = 2*(1-psi(i))+psi(i);

%Kinetic and Diffusion Coefficient
ko(i) = ao*exp(-eo/(r*tpi));
kc(i) = ac*exp(-ec/(r*tpi));
ks(i) = as*exp(-es/(r*tpi));
%ks(i) = 1.9E-3*pchar*diam/6/(P*fs);
kdot(i) = mech(i)*kdo*Tm(i)^0.75/d(i)*1E-3;
kdct(i) = kdc*Tm(i)^0.75/d(i)*1E-3;
kdst(i) = kds*Tm(i)^0.75/d(i)*1E-3;
hcomb(i) = hcd*((2/mech(i))-1)+hco*(2-(2/mech(i)));
qo(i) = 1/((1/kdot(i))+(1/ko(i)))*fo*P;
qc(i) = alphac*1/((1/kdct(i))+(1/kc(i)))*fc*P;
qs(i) = alphas*1/((1/kdst(i))+(1/ks(i)))*fs*P;
qt(i) = qo(i)+qc(i)+qs(i);
reaction(i) = -devolrate(i-1)*area(i-1)*hpyro +qo(i-1)*hcomb(i-
1)-qc(i-1)*hcdg-qs(i-1)*hsg;

```

```

rate(i) = devolrate(i-1)*area(i-1)*dt+qt(i-1)*area(i-1)*dt;

    % Transient Code algorithm
    if mco(i-1) > inher
        if tp(i-1) < ta
            tp(i) = tp(i-1) + area(i-1)/(mt(i-
1)*cpcoal)*dt*(e*sig*(tw^4-tp(i-1)^4)+h*(tgas(i-1)-tp(i-1)));
            elseif tp(i-1) >= ta
                mt(i) = mt(i-1)-(dryrate(i-1)*dt*area(i-1));
                tp(i) = tp(i-1) + area(i-1)/(mt(i-
1)*cpcoal)*dt*(e*sig*(tw^4-tp(i-1)^4)+h*(tgas(i-1)-tp(i-1))-dryrate(i-
1)*hd);
mco(i) = (mco(i-1)*mt(1)-dt*dryrate(i-1)*area(i-1))/mt(1);
if tp(i)<ta
            tp(i) = ta;
        end
    end
    if mco(i) < inher
        mco(i) = inher;
    end
    timedry = tf(i);
    disdry = distance(i);
    elseif mco(i-1)<=inher
mco(i) = inher;
        mv(i) = mv(i-1)+devolrate(i-1)*area(i-1)*dt;
if mv(i-1) >= ft
            mt(i) = mt(i-1)-rate(i-1)+devolrate(i-1)*area(i-1)*dt;
            else
                mt(i) = mt(i-1)-rate(i-1);
            end
            tp(i) = tp(i-1) + area(i-1)/(mt(i-
1)*cpcoal)*dt*(e*sig*(tw^4-tp(i-1)^4)+h*(tgas(i-1)-tp(i-1))+reaction(i-
1));
d(i) = d(i-1)-2*qo(i-1)*dt/pdried;
if mt(i) <= unburnt,break,end
    end%-- exit from if mco < inher loopx
    err = abs((tp(i)-tpi)/tpi);
    tpi = tp(i);
tgas(i) = tgas(i);
    totconv(i) = (mi-mt(i))/mi;
end%-- Exit from for m= 1:50 loop
    if i == 2400
        ltf = lt;
        cpf = cpt;
    end
    fprintf('Time Step: %6d%10s:%10.4f Total
Conversion:%10.4f\n',i,'Error',err,totconv(i));
    i = i+1;
    if distance(i-1) <= 100
        iagain = 1;
        tf(i) = tf(i-1)+dt;
        if mt(i-1) <= unburnt
            iagain = 0;
            i = i-1;
        end
        if tf(i) >=0.055
            iagain = 0;
            i = i-1;

```

```

        end
    else
        i = i-1;
        iagain = 0;
        end% -- Exit from if i > length(n)
        z = i;
    end%-- From while iagain == 1

%Final Solution
tff = tf(1:i,1);tpf = tp(1:i,1);
mtf = mt(1:i,1);mvf = mv(1:i,1);mcof = mco(1:i,1);
qof = qo(1:i,1);qcf = qc(1:i,1);qsf = qs(1:i,1);qtf = qt(1:i,1);
df = d(1:i,1);areaf = area(1:i,1);tgasf = tgas(1:i,1);
devolratef = devolrate(1:i,1);distancef = distance(1:i,1);
totconvf = totconv(1:i,1);

maxrate2 = gradient(devolratef,tff);
maxrate = gradient(maxrate2,tff);
index = find(maxrate==max(maxrate));
tdevol = tff(index);
tempdevol = tpf(index);
disdevol = distancef(index);
A = 5.012E11;%Fluent = 2.119E11;
Ea = 200000;%Fluent = 202700;
[miutff,ptff,cptff,ltff,do2mff,dn2mff,dco2mff,dh2omff,cvtff] =
Gprop(Tm,index,fo,fs,fc,fn);%J/molK
tignition = cvtff*(Tm(index)^2*r/Ea)/(hvol/18*0.33*A*exp(-
Ea/(r*Tm(index))));

fprintf('\nEnd of Calculation\n');

```

Main code to calculate the extent of steam gasification in oxy-fuel mode:

```

function[tpf,tff] = Comb_function(mcoinput,comb,alphac,alphas,Drying)

%One-Dimensional Code for Coal Combustion and Gasification Study

diam = 0.000084;
alphao = 1-alphac-alphas;
if mcoinput == 0.14
    inher = 0.098;
elseif mcoinput == 0.22
    inher = 0.176;
elseif mcoinput == 0.3
    inher = 0.27;
end

%Problem Constant
hd = 2.26E6; %Heat of water evaporation (J/kgK)
hco = 9.208*10^6; %Heat of CO formation (J/kgK)
hcd = 3.28*10^7; %Heat of CO2 formation (J/kgK)
hcdg = 1.438*10^7; %Heat of CO2 gasification (J/kgK)
hsg = 1.094*10^7; %Heat of steam gasification (J/kgK)
hpyro = 8.37*10^5; %J/kgK of coal
e = 0.8; %Particle Emissivity
sig = 5.67E-8; %Stefan-Boltzmann Constant
tw = 773; %Wall temperature (K)

```



```

r = 8.314; %Universal gas constant (J/kgK)
cpcoal = 1150; %Lignite Heat Capacity from Fluent (J/kgK)
pdried = 1150; %Dried Coal Density (kg/m3)
ta = 365; %Wet bulb temperature(K)
na = 0.3468; %Total Time in air (s)
no = 0.4132; %Total Time in CO2 (s)
fv = 0.4495; %Volatile Fraction in air-dried
fvdb = fv/0.88; %Vol Fractionin dry basis
P = 101325; %Total Pressure (Pa)
dt = 0.00005; %Integration time step
hchar = 3.28E7; %Heating value of Carbon Char (J/kg)

%Coal Properties dried basis
FC = 0.470455; %Fixed carbon
VM = 0.510795; %Volatile matter
A = 0.018750; %Ash
C = 0.657; %Carbon
H = 0.068; %Hydrogen
N = 0.06; %Nitrogen
S = 0.05; %Sulphur
O = 0.258; %Oxygen

%Method 1
%Conversion ratio btu/lb to kJ/kg
ratio = 2.326;
coalhhvdb = (146.58*C*100+568.78*H*100+29.4*S*100-6.58*A*100-
51.53*(O+N)*100)*ratio*1000;
coalhhvar = coalhhvdb*(1-mcoinput);
coalhhvdb = coalhhvdb-(1+H/2*18)*hd;
coalhhvar = coalhhvar-(1+H/2*18)*hd;
hvol2 = (coalhhvar-(hchar*FC*(1-mcoinput)))/(VM*(1-mcoinput));
hvol3 = (coalhhvdb-(hchar*FC))/VM;

%Method 2
Cvol = C - FC;
hvol = ((3.55*Cvol^2-232*Cvol - 2230*H +51.2*Cvol*H+131*N +
20600))*1000-hd;

if comb == 1
    fo = 0.2103;fn=0.4404;fc = 0.1644;fs = 0.1849;n = (0:dt:na);limit =
na;
elseif comb == 2
    fo = 0.1664;fn = 0;fc = 0.649;fs = 0.1846;n = (0:dt:no);limit = no;
elseif comb == 3
    fo = 0.2157;fn = 0;fc = 0.5992;fs = 0.185;n = (0:dt:no);limit = no;
elseif comb == 4
    fo = 0.2654;fn = 0;fc = 0.5492;fs = 0.1855;n = (0:dt:no);limit = no;
elseif comb == 5
    fo = 0.3154;fn = 0;fc = 0.4989;fs = 0.1859;n = (0:dt:no);limit = no;
end

%Solution Initialization
tf = zeros(length(n),1);tp = zeros(length(n),1);Tm = zeros(length(n),1);
tgas = zeros(length(n),1);
mv = zeros(length(n),1);
rat = zeros(length(n),1);
qo = zeros(length(n),1);qc = zeros(length(n),1);qs = zeros(length(n),1);
qt = zeros(length(n),1);

```

```

devolrate = zeros(length(n),1);
area = zeros(length(n),1);
b = zeros(length(n),1);
psi = zeros(length(n),1);
vco = zeros(length(n),1);vco2 = zeros(length(n),1);
hcomb = zeros(length(n),1);mech = zeros(length(n),1);
distance = zeros(length(n),1);
nn = zeros(length(n),1);dryrate = zeros(length(n),1);totconv =
zeros(length(n),1);
massrem = zeros(length(n),1);tc = zeros(length(n),1);reaction =
zeros(length(n),1);
rate = zeros(length(n),1);

%Input Parameter
d((1:length(n)),1) = diam;
mco(1:length(n),1) = mcoinput;
pwc = pdried*(1-mcoinput)+mcoinput*1000;
mdried = (pdried*3.14/6*diam^3);
mi = (pdried*3.14/6*diam^3)+(mcoinput*mdried/(1-mcoinput));
ft = fvd*mdried;
unburnt = A*mdried;
carbon = mdried-ft-unburnt;
mt(1:length(n),1) = mi;
tp(1) = 298;
tf(2) = tf(1) +dt;
i = 2;
iagain = 1;
m = 2;
err(1:length(n),1) = 0;
pchar = 615;%kg/m3

fprintf('Time Step: %6d%10s:%10.4f Total
Conversion:%10.4f\n',1,'Error',0,0);
while iagain == 1
    if tf(i) == 0
        distance(i) = 0;
    elseif tf(i) > 0 && tf(i) <= 0.048
        if comb == 1
            distance(i) = (-
0.0003*(tf(i)*1000)^3+0.0411*(tf(i)*1000)^2+0.7678*(tf(i)*1000)-
2.7809)/10;
        elseif comb >=2&&comb<=5
            distance(i) = (-0.0003*(tf(i)*1000)^3+0.0468*(tf(i)*1000)^2-
0.2070*(tf(i)*1000)+1.0267)/10;
        end
    elseif tf(i)>0.048
        if comb == 1
            distance(i) = (0.0041*(tf(i)*1000)^2+2.3791*(tf(i)*1000)-29.012)/10;
        elseif comb >=2&&comb<=5
            distance(i) = (0.0045*(tf(i)*1000)^2+1.8867*(tf(i)*1000)-
37.528)/10;
        end
    end
    if distance(i) < 0
        distance(i) = distance(i-1)+0.0001;
    end
    if comb == 1
        %
        tgas(1) = 414.96 + 820.13576;
    end
end

```

```

%      tgas(i) = 414.96 + 820.13576*exp(-distance(i)/30.77);
      tgas(i) = -4259.2*tf(i) + 1232.3;
elseif comb >=2&&comb<=5
%      tgas(1) = 276.465 + 930.52797;
%      tgas(i) = 276.465 + 930.52797*exp(-distance(i)/43.834);
      tgas(i) = -4756.4*tf(i) + 1265.4;
end%-- from if comb == 1 loop --%

if tgas(i) <=tw
      tgas(i) = tw;
end

if tf(i)<=0.0025
      parvel = 0;
elseif tf(i)>0.0025
      if comb == 1
            parvel = 0.7224*log(tf(i)*1000)-0.1205;
      elseif comb >=2&& comb <=5
            parvel = 0.897*log(tf(i)*1000)-1.3227;
      end
end

%Kinetic Parameter
%A is in s-1 and E is J/mole
%Devolatilisation

%      if comb == 1
%            av = 104475.6;ev=66526.13;
%      elseif comb >=2&& comb <=5
%            av = 207744.8;ev=67785.7;
%      end

%Char oxidation kinetic
ao = 0.0024;eo = 69060;
%CO2 gasification kinetic
ac = 0.0053;ec = 125500;
%Steam Gasification Kinetic
as = 3.6E6*pchar*d(1);es = 206000;
%Arthur Coefficient for CO/CO2 Ratio
at = 2511.9;bt = 52080;

%Guess the particle temperature at t + dt
tpi = tp(i-1)+10;
err(i) = 1;
b(m) = 0;

%Iterative procedure
for m = 1:10
      %Dimensionless Coefficient
      Tm(1) = (tpi+tgas(1))/2;
      Tm(i) = (tpi+tgas(i))/2;
      [miut,pt,cpt,lt,do2m,dn2m,dco2m,dh2om,cvt] =
Gprop(Tm,i,fo,fs,fc,fn);
      kdo = 24*do2m*(1/(293)^1.75*1/r);kdc =
24*dco2m*(1/(293)^1.75*1/r);
      kds = 24*dh2om*(1/(293)^1.75*1/r);
%      psat = P*exp(hd/1000*18/r*((1/373)-(1/tpi)));

```

```

%Dimensionless Correlation
gasvel = (11.7/60*10^-3)*(tgas(i)/298)/(pi*0.115^2);
urel = abs(parvel-gasvel);
Re = pt*urel*d(i)/miut;
Pr = cpt*miut/lt;
Scs = miut/(pt*dh2om);
Shs = 2 + 0.6*Re^0.5*Scs^(1/3);
kcs = Shs*dh2om/d(i);
Nu = 2 + ((0.555*Re^0.5*Pr^(1/3))/(1+(1.232*(1/Re)*(Pr)^(-4/3))))^0.5;
h = Nu*lt/d(i);

%Constant Calculation
area(1) = pi*d(1)^2;
area(i) = pi*d(i)^2;

%Rate of Drying
if Drying == 1
nn(i) = (6*h*(tgas(i)-ta))/(hd*pwd*(mco(1)/(1+mco(1)))*d(i));
dryrate(i) = mco(1)*nn(i)*mi/area(i);
elseif Drying == 2
dryrate(i) = h*(tgas(i)-ta)/hd;
end

%Rate of Devolatilisation
kv(i) = av*exp(-ev/(r*tpi));
devolrate(i) = kv(i)*(ft-mv(i))/area(i);

%Ratio of CO/CO2 produced at particle surface
rat(i) = at*exp(-bt/(r*tpi));
psi(i) = 1/(1+rat(i));
vco(i) = 1-psi(i);vco2(i) = psi(i);
mech(i) = 2*(1-psi(i))+psi(i);

%Kinetic and Diffusion Coefficient
ko(i) = ao*exp(-eo/(r*tpi));
kc(i) = ac*exp(-ec/(r*tpi));
ks(i) = as*exp(-es/(r*tpi));
%ks(i) = 1.9E-3*pchar*diam/6/(P*fs);
kdot(i) = mech(i)*kdo*Tm(i)^0.75/d(i)*1E-3;
kdct(i) = kdc*Tm(i)^0.75/d(i)*1E-3;
kdst(i) = kds*Tm(i)^0.75/d(i)*1E-3;
hcomb(i) = hcd*((2/mech(i))-1)+hco*(2-(2/mech(i)));
qo(i) = 1/((1/kdot(i))+(1/ko(i)))*fo*P;
qc(i) = alphac*1/((1/kdct(i))+(1/kc(i)))*fc*P;
qs(i) = alphas*1/((1/kdst(i))+(1/ks(i)))*fs*P;
qt(i) = qo(i)+qc(i)+qs(i);
reaction(i) = -devolrate(i-1)*area(i-1)*hpyro +qo(i-1)*hcomb(i-1)-qc(i-1)*hcdg-qs(i-1)*hsg;
rate(i) = devolrate(i-1)*area(i-1)*dt+qt(i-1)*area(i-1)*dt;

% Transient Code algorithm
if mco(i-1) > inher
if tp(i-1) < ta
tp(i) = tp(i-1) + area(i-1)/(mt(i-1)*cpcoal)*dt*(e*sig*(tw^4-tp(i-1)^4)+h*(tgas(i-1)-tp(i-1)));
elseif tp(i-1) >= ta
mt(i) = mt(i-1)-(dryrate(i-1)*dt*area(i-1));

```

```

        tp(i) = tp(i-1) + area(i-1)/(mt(i-
1)*cpcoal)*dt*(e*sig*(tw^4-tp(i-1)^4)+h*(tgas(i-1)-tp(i-1))-dryrate(i-
1)*hd);
mco(i) = (mco(i-1)*mt(1)-dt*dryrate(i-1)*area(i-1))/mt(1);
if tp(i)<ta
        tp(i) = ta;
        end
        end
        if mco(i) < inher
                mco(i) = inher;
        end
        timedry = tf(i);
        disdry = distance(i);
        elseif mco(i-1)<=inher
mco(i) = inher;
        mt(i) = mt(i-1)-rate(i-1);
        mv(i) = mv(i-1)+devolrate(i-1)*area(i-1)*dt;
tp(i) = tp(i-1) + area(i-1)/(mt(i-1)*cpcoal)*dt*(e*sig*(tw^4-tp(i-
1)^4)+h*(tgas(i-1)-tp(i-1))+reaction(i-1));
d(i) = d(i-1)-2*qo(i-1)*dt/pdried;
if mt(i) <= unburnt,break,end
        end%-- exit from if mco < inher loopx
        err = abs((tp(i)-tpi)/tpi);
        tpi = tp(i);
tgas(i) = tgas(i);
        totconv(i) = (mi-mt(i))/mi;
end%-- Exit from for m= 1:50 loop
        if i == 2400
                ltf = lt;
                cpf = cpt;

        end
        fprintf('Time Step: %6d%10s:%10.4f Total
Conversion:%10.4f\n',i,'Error',err,totconv(i));
        i = i+1;
        if distance(i-1) <= 100
                iagain = 1;
                tf(i) = tf(i-1)+dt;
                if mt(i-1) <= unburnt
                        iagain = 0;
                        i = i-1;
                end
                if tf(i) >=0.0507
                        iagain = 0;
                        i = i-1;
                end
        else
                i = i-1;
                iagain = 0;
        end% -- Exit from if i > length(n)
        z = i;
end%-- From while iagain == 1

%Final Solution
tff = tf(1:i,1);tpf = tp(1:i,1);
mtf = mt(1:i,1);mvf = mv(1:i,1);mcof = mco(1:i,1);
qof = qo(1:i,1);qcf = qc(1:i,1);qs = qs(1:i,1);qtf = qt(1:i,1);
df = d(1:i,1);areaf = area(1:i,1);tgasf = tgas(1:i,1);
devolratef = devolrate(1:i,1);distancef = distance(1:i,1);

```

```

totconvf = totconv(1:i,1);

maxrate2 = gradient(devolratef,tff);
maxrate = gradient(maxrate2,tff);
index = find(maxrate==max(maxrate));
tdevol = tff(index);
tempdevol = tpf(index);
disdevol = distancef(index);
A = 5.012E11;%Fluent = 2.119E11;
Ea = 200000;%Fluent = 202700;
[miutff,ptff,cptff,ltff,do2mff,dn2mff,dco2mff,dh2omff,cvtff] =
Gprop(Tm,index,fo,fs,fc,fn);%J/molK
tignition = cvtff*(Tm(index)^2*r/Ea)/(hvol/18*0.33*A*exp(-
Ea/(r*Tm(index))));
fprintf('\nEnd of Calculation\n');

```

The function above can be invoked by:

```

clc
% clf
clear

fprintf('\n1.Air\n2.Oxy16\n3.Oxy21\n4.Oxy26\n5.Oxy31');
comb = 1;
mcoinput = 0.166;
% %XJC
% mcoinput = 0.262;
% %BC
% mcoinput = 0.058;
alphac = 1;
% if mcoinput == 0.14
%     inher = 0.098;
% elseif mcoinput == 0.22
%     inher = 0.176;
% elseif mcoinput == 0.3
%     inher = 0.27;
% end
inher = 0.1;
alphas = linspace(0,1,100);
if comb == 1
    a = 609;
    b = 771;
    c = 707;
elseif comb == 2||comb == 3||comb == 4||comb == 5
    a = 826;
    b = 1012;
    c = 938;
end
% shape(1,:) = '- ';
% shape(2,:) = ': ';
% shape(3,:) = '--';
% shape(4,:) = '-.';

for i = 1:1:length(alphas)

```

```

        [tff,tpf,qsf,qtf,qcf] =
Comb_function(mcoinput,comb,inher,alphas(i),alphac);
%     plot(tff*1000,tpf,shape(i,:))
%     hold all
        tp = tpf(c);
g(i,1) = tp;
        contri = qsf(c)/qtf(c);
        h(i,1) = contri;
        contrico = qcf(c)/qtf(c);
        j(i,1) = contrico;
%     contri50 = qsf(b)/qtf(b);
%     k(i,1) = contri50;
%     contrico50 = qcf(b)/qtf(b);
%     l(i,1) = contrico50;
%     tp2 = tpf(b);
%     m(i,1) = tp2;
end

```

D.3. MATLAB code to predict the ignition time of dense coal particle stream in a cylindrical cloud (Chapter 7)

Gas Composition in the furnace:

```
function [f] = gascomposition(steam,oxyfuel,comb)
% Steam option include 1. Without Steam Injection, 2. With Steam
Injection
% Oxy-Fuel option: 1. Conventional Air, 2. Oxy-Fuel Combustion
% Comb option: 1. 21%O2, 2. 25%O2, 3. 30%O2
if steam == 1
    fs = 0.13;
    if oxyfuel == 1
        fc = 0.12;
        if comb == 1
            fo = 0.21;fn = 0.54;
        elseif comb == 2
            fo = 0.25;fn = 0.5;
        elseif comb == 3
            fo = 0.30;fn = 0.45;
        end
    elseif oxyfuel == 2
        fn = 0;
        if comb == 1
            fo = 0.21;fc = 0.65;
        elseif comb == 2
            fo = 0.25;fc = 0.62;
        elseif comb == 3
            fo = 0.30;fc = 0.57;
        end
    end
elseif steam == 2
    fs = 0.26;
    if oxyfuel == 1
        fc = 0.1;
        if comb == 1
            fo = 0.21;fn = 0.42;
        elseif comb == 2
            fo = 0.25;fn = 0.39;
        elseif comb == 3
            fo = 0.30;fn = 0.34;
        end
    elseif oxyfuel == 2
        fn = 0;
        if comb == 1
            fo = 0.21;fc = 0.53;
        elseif comb == 2
            fo = 0.25;fc = 0.49;
        elseif comb == 3
            fo = 0.30;fc = 0.44;
        end
    end
end
end
f = [fo;fn;fc;fs];
end
```


Code to calculate reaction rate in gas phase:

```
function grate =  
gasreac(yo2,yn2,yco2,yh2o,ych4,yco,yh2,Tm,oxyfuel,cloudvol,rho)  
%This function file is to calculate the rate of gas-phase reaction rate  
%Reaction 1: CO + 1/2O2 --> CO2  
%Reaction 2: CH4 + 1.5O2 --> CO + 2H2O  
%Reaction 3: CO + H2O --> CO2 + H2  
%Reaction 4: H2 + 0.5O2 --> H2O  
%Reaction 5: CO2 --> CO + 0.5O2  
  
% totaln = 41.5/24;  
% Conv = totaln*10^-3*cloudvol/0.0415;  
% Conv = 101325*cloudvol/8.314/273;  
totalmol= yo2*32+yco2*44+yh2o*18+ych4*16+yco*44+yh2*2+yn2*28;  
  
if yh2 <0  
    yh2 =0;  
end  
if yh2o <0  
    yh2o =0;  
end  
if yco <0  
    yco =0;  
end  
if yco2 <0  
    yco2 =0;  
end  
if yo2 <0  
    yo2 =0;  
end  
if ych4 <0  
    ych4 =0;  
end  
  
%Mass source(kmol/m3s)  
qch4 = 5.03e11*exp(-  
200000/8.314/Tm)*(ych4*rho/totalmol)^0.7*(yo2*rho/totalmol)^0.8;  
qh2 = 3.48e13*exp(-47907/Tm)*(yh2o*rho/totalmol);  
qshift = 6.71e10*exp(-  
13688/Tm)*(yco2*rho/totalmol)*(yh2*rho/totalmol)^0.5;  
  
%Oxidation mechanism in oxy-fuel atmosphere (kmol/m3s)  
if oxyfuel == 1  
    qco = 2.239e12*exp(-  
170000/8.314/Tm)*(yco*rho/totalmol)*(yo2*rho/totalmol)^0.25*(yh2o*rho/to  
talmol)^0.5;  
    qco2 = 0;  
elseif oxyfuel == 2  
    qco = 2.239e6*exp(-  
41800/8.314/Tm)*(yco*rho/totalmol)*(yo2*rho/totalmol)^0.25*(yh2o*rho/tot  
almol)^0.5;  
    qco2 = 1.1e13*Tm^(-0.97)*exp(-  
328000/8.314/Tm)*(yco2*rho/totalmol)*(yo2*rho/totalmol)^-  
0.25*(yh2o*rho/totalmol)^0.5;  
end  
  
grate(:,1) = qco;
```

```

grate(:,2) = qch4;
grate(:,3) = qshift;
grate(:,4) = qh2;
grate(:,5) = qco2;

```

Reaction rate in particle phase:

```

function q = prate(tpi,do2m,dco2m,dh2om,Tm,d,yo2,yco2,yh2o)

%1 denote oxidation reaction
%2 denote char CO2 gasification reaction
%3 denote char steam gasification reaction

%Char oxidation kinetic
%Activation energy unit in J/mole
%Pre-exponential constant unit in kg/m2sPa
ao = 0.0024;eo = 69060;
ac = 0.0053;ec = 125500;
as = 2.09e6*615*8.4e-5/101325;es = 203802.7;
R = 8.314;
P = 101325;

%Particle phase equation
ko = ao*exp(-eo/(R*tpi));
kc = ac*exp(-ec/(R*tpi));
ks = as*exp(-es/(R*tpi));
kdo = 2*24*do2m*(1/(293)^1.75*1/R)*Tm^0.75/d*1E-3;
kdc = 24*dco2m*(1/(293)^1.75*1/R)*Tm^0.75/d*1E-3;
kds = 24*dh2om*(1/(293)^1.75*1/R)*Tm^0.75/d*1E-3;
qo = 1/((1/kdo)+(1/ko))*yo2*P;
qc = 1/((1/kdc)+(1/kc))*yco2*P;
qs = 1/((1/kds)+(1/ks))*yh2o*P;

q(:,1) = qo;
q(:,2) = qc;
q(:,3) = qs;
end

```

Code for calculating mass source in gas phase:

```

function Source = msourcep(qo,qch4,area,ndens)
%First column indicates mass sources for O2
%Second column indicates mass sources for CH4
%Third column indicates mass sources for CO
%Fourth column indicates mass sources for H2O
Source(1) = -qo*area/12/2 -2*qch4; %Sources in kmol/s
Source(2) = qv-qch4;
Source(3) = qo;

```

Main Code for Combustion calculation in cylindrical cloud :

```

function tignition = groupND(ndens)
%
%Input constant
massp = 1e-3/6; %Total Mass (kg)

```

```

v      = -0.1 ; %Gas velocity (m/s)
rad     = 0.005 ; %Reaction Zone Radius (m)
Rc      = 0.002 ; %Cloud Radius (m)
L       = 0.3 ; %Cloud Length (m)
pcoal   = 1200 ; %Coal Density (kg/m3)
diam    = 8.4e-5; %Particle Diameter (m)
tgas_i  = 300 ; %Initial Gas Temperature (K)
tgas    = 1200 ; %Gas Temperature (K)
tpi     = 300 ; %Reference Temperature (K)
P       = 101325; %Absolute pressure (kg/m2s2)
R       = 8.314 ; %Gas constant

%Enthalphy Value of Reaction (J/kmole)
ho      = 1.11e8;%C+O2->CO (EX)
hc      = 1.75e8;%C+CO2-->2CO (END)
hs      = 1.3e8 ;%C+H2O-->CO+H2 (END)
hm      = 8.89e8;%CH4+2O2-->CO2+2H2O (EX)
hco     = 2.83e8;%2CO+O2-->2CO2 (EX)
hh      = 2.86e8;%H2+1/5O2-->H2O (EX)
hcorev  = 2.83e8;%CO2-->CO+0.5O2
hcs     = 4.13e7;%CO+H2O-->CO2+H2 (EX)

%Gas composition and input
%fprintf('\nSteam Injection option\n\n1.Without Steam Injection\n2.With
Steam Injection\n');
%steam = input('Steam injection option =');
%fprintf('\nCombustion option\n\n1.Conventional Air\n2.Oxy-Fuel
Combustion\n');
%oxyfuel = input('Combustion mode =');
%fprintf('\nOxygen Concentration\n\n1.20%\n2.25%\n3.30%\n');
%comb = input('Combustion mode =');
steam = 2;oxyfuel = 1; comb = 1;
f      = gascomposition(steam,oxyfuel,comb);

%Calculated Constant
tspan   = linspace(0,0.2,100000) ;%Time Span (s)
h       = tspan(2)-tspan(1) ;%Delta t (s)
n       = length(tspan) ;%Total time indices
r       = linspace(0,rad,101) ;%Radius of cylindrical
Cloud (m)
m       = length(r) ;%Total position indices
rspan   = r(2)-r(1) ;%Delta r (m)
Rmix    = f(1)*32+f(2)*28+f(3)*44+f(4)*18 ;%Molecular mass of gas
mixture
Rspec   = R/Rmix ;%Universal gas constant for
specific mixture
areap   = pi*diam^2/4 ;%Area of single particle
pvool   = 4/3*pi*(diam/2)^3 ;%Volume of 1 coal particle
(m3)
cloudvol= pi*rad^2*L ;%Volume of cylindrical
cloud (m3)
ndens   = 1E7;
jj      = find(r==Rc) ;%Cloud Boundary

%Particle Phase Input
fv      = 0.4495 ; %Volatile mass fraction (ar)
cpcoal  = 1150 ; %Lignite heat capacity (J/kgK)

```

```

devolrat= 0 ; %Initial Coal Devolatilisation
Rate
e = 0.8 ; %Particle Emissivity
sig = 5.67e-8 ; %Stefan Boltzmann Constant
smass = pcoal*4/3*3.14*(diam/2)^3 ; %Mass of Single particle(kg)
ft = fv*smass ; %Mass of Volatiles in cloud(kg)
A = 0.01875 ; %Ash mass fraction dried basis
unburnt = A/(1-0.14)*smass ; %Mass of unburnt fraction
pcoal = 1150 ; %Coal Density (kg/m3)

%Reference value
Tm = (tpi+tgas)/2 ; %Mean Temperature (K)
pref = P/Rspec/tpi ; %Reference density value
[miut,pt,cpt,lt,do2m,dn2m,dco2m,dh2om,cvt] =
Gprop(Tm,f(1),f(2),f(3),f(4));
tmass = f(1)*32+f(2)*28+f(3)*44+f(4)*18;

%Array Initialization

tg = ones(m,n)*tgasi;
tp = ones(n,1)*tpi ;
mt = ones(n,1)*pt/ndens;
yo2 = zeros(m,n) ;
yn2 = zeros(m,n) ;
yco2 = zeros(m,n) ;
yh2o = zeros(m,n) ;
ych4 = zeros(m,n) ;
yco = zeros(m,n) ;
yh2 = zeros(m,n) ;
rho = ones(m,n)*pt ;
mv = zeros(n,1) ;

%Boundary Condition
yo2(m,:) =f(1)*32/tmass ;%Boundary Condition for Oxygen Mole
fraction
yn2(m,:) =f(2)*28/tmass ;%Boundary Condition for Nitrogen Mole
fraction
yco2(m,:) =f(3)*44/tmass ;%Boundary Condition for CO2 Mole fraction
yh2o(m,:) =f(4)*18/tmass ;%Boundary Condition for Steam Mole fraction
ych4(m,:) =0 ;%Boundary Condition for CH4 Mole fraction
yco(m,:) =0 ;%Boundary Condition for CO Mole fraction
yh2(m,:) =0 ;%Boundary Condition for H2 Mole fraction
tg(m,:) =tgas ;%Boundary condition for gas temperature

%Source Boundary Condition

wm(jj:m) =0 ;%Boundary Condition for mass source

%Initial Condition
yo2(:,1) =f(1)*32/tmass ;%Initial Condition for Oxygen mole fraction
yn2(:,1) =f(2)*28/tmass ;%Initial Condition for Nitrogen mole
fraction
yco2(:,1) =f(3)*44/tmass ;%Initial condition for CO2 mole fraction
yh2o(:,1) =f(4)*18/tmass ;%Initial condition for Steam mole fraction
tg(jj+1:m,1)=tgas ;%Initial Condition for gas temperature

```

```

q          =zeros(3,1)      ;%Initial condition for particle oxidation
rate

lambda    = v*h/(rspan) ;
tign      = zeros(n,1);
for j = 1:n/2-1              % Position as row
    for i = 2:m-1            % Time as column
        tmass
        =yo2(i,j)*32+yco2(i,j)*44+yh2o(i,j)*18+ych4(i,j)*16+yco(i,j)*28+yh2(i,j)
        *2+yn2(i,j)*28;
        hconv    =2*lt/diam      ; % Convective heat transfer
        coefficient
            Tm      =(tp(j)+tg(i,j))/2;
            yo       =yo2(i,j)*tmass/32      ;
            ycd      =yco2(i,j)*tmass/44      ;
            yho      =yh2o(i,j)*tmass/18      ;
            ych      =ych4(i,j)*tmass/16      ;
        yc         =yco(i,j)*tmass/28      ;
            yh       =yh2(i,j)*tmass/2       ;
            yn       =yn2(i,j)*tmass/28      ;

        %Gas phase Reaction Rate (kmol/m3s)

        grate      =
        gasreac(yo,yn,ycd,yho,ych,yc,yh,Tm,oxyfuel,cloudvol,pt);
        gaso2      = 32*(-grate(1)*0.5-grate(2)*1.5-
        grate(4)*0.5+grate(5)/2)      ;
        gasco2      = 44*(grate(1)+grate(3)-
        grate(5))      ;
        gash2o      = 18*(grate(2)*2-
        grate(3)+grate(4))      ;
        gash2       = 2*(grate(3)-
        grate(4))      ;
        gasco       = 28*(-grate(1)+grate(2)-
        grate(3)+grate(5))      ;
        gasch4      = 16*(-
        grate(2))      ;

        %Source Term Boundary Condition

        wm(1:jj)    =(q(1)+q(2)+q(3))*areap*ndens+devolrat*ndens      ;
        reac(1:jj)  =gaso2-
        0.5*32/12*q(1)*areap*ndens      ;
        reacd(1:jj) =gasco2-
        44/12*q(2)*areap*ndens      ;
        reaco(1:jj)
        =gasco+(28/12*q(1)+2*28/12*q(2)+28/12*q(3))*areap*ndens      ;
        reaho(1:jj) =gash2o-
        18/12*q(3)*areap*ndens      ;
        reah(1:jj)
        =gash2+2/12*q(3)*areap*ndens      ;
        ream(1:jj)
        =gasch4+devolrat*ndens      ;
        reac(jj+1:m)
        =gaso2      ;

```

```

        reacd(jj+1:m)
=gasco2                                     ;
        reaco(jj+1:m)
=gasco                                     ;
        reaho(jj+1:m)
=gash2o                                     ;
        reah(jj+1:m)
=gash2                                     ;
ream(jj+1:m) =gasch4                       ;

        if mt(j)<=unburnt
            reac(1:m)
=gaso2                                     ;
            reacd(1:m)
=gasco2                                     ;
            reaco(1:m)
=gasco                                     ;
            reaho(1:m)
=gash2o                                     ;
            reah(1:m)
=gash2                                     ;
            ream(1:m)
=gasch4                                     ;
        end

        %Source Term for Heat

        gasheat =grate(1)*hco+grate(2)*hm+grate(3)*hcs+grate(4)*hh-
grate(5)*hcorev;
        conheat(1:jj)=hconv*(tp(j)-tg(i,j))*areap*ndens;
conheat(jj+1:m)=0;

        %Continuity equation
        rup      =(r(i+1)+r(i))/2;
        rdo      =(r(i)+r(i-1))/2;
        rmid     =rup+rdo;

        rho(i,j+1) =rho(i,j)-lambda*(rho(i+1,j)-rho(i-1,j))+h*wm(i);
        mode      =h*5e-5/rho(i,j)/rspan^2;
        yo2(i,j+1) =yo2(i,j)+mode/r(i)*(rup*yo2(i+1,j)-
rmid*yo2(i,j)+rdo*yo2(i-1,j))-lambda*(yo2(i,j)-yo2(i-
1,j))+h/rho(i,j)*reac(i);
        yn2(i,j+1) =yn2(i,j)+mode/r(i)*(rup*yn2(i+1,j)-
rmid*yn2(i,j)+rdo*yn2(i-1,j))-lambda*(yn2(i,j)-yn2(i-1,j));
        yco2(i,j+1) =yco2(i,j)+mode/r(i)*(rup*yco2(i+1,j)-
rmid*yco2(i,j)+rdo*yco2(i-1,j))-lambda*(yco2(i,j)-yco2(i-
1,j))+h/rho(i,j)*reacd(i);
        yco(i,j+1) =yco(i,j)+mode/r(i)*(rup*yco(i+1,j)-
rmid*yco(i,j)+rdo*yco(i-1,j))-lambda*(yco(i,j)-yco(i-
1,j))+h/rho(i,j)*reaco(i);
        yh2o(i,j+1) =yh2o(i,j)+mode/r(i)*(rup*yh2o(i+1,j)-
rmid*yh2o(i,j)+rdo*yh2o(i-1,j))-lambda*(yh2o(i,j)-yh2o(i-
1,j))+h/rho(i,j)*reaho(i);
        yh2(i,j+1) =yh2(i,j)+mode/r(i)*(rup*yh2(i+1,j)-
rmid*yh2(i,j)+rdo*yh2(i-1,j))-lambda*(yh2(i,j)-yh2(i-
1,j))+h/rho(i,j)*reah(i);

```

```

        ych4(i,j+1) =ych4(i,j)+mode/r(i)*(rup*ych4(i+1,j)-
rmid*ych4(i,j)+rdo*ych4(i-1,j))-lambda*(ych4(i,j)-ych4(i-
1,j))+h/rho(i,j)*ream(i);

if yh2(i,j+1) <0
    yh2(i,j+1) =0;
end
if yh2o(i,j+1) <0
    yh2o(i,j+1) =0;
end
if yco(i,j+1) <0
    yco(i,j+1) =0;
end
if yco2(i,j+1) <0
    yco2(i,j+1) =0;
end
if yo2(i,j+1) <0
    yo2(i,j+1) =0;
end
if ych4(i,j+1) <0
    ych4(i,j+1) =0;
end

%Energy Balance

    tg(i,j+1) = tg(i,j)+mode/r(i)*(rup*tg(i+1,j)-
rmid*tg(i,j)+rdo*tg(i-1,j))-lambda*(tg(i,j)-tg(i-
1,j))+h/(rho(i,j)*cpt)*(gasheat+conheat(i));

end

%Symmetry Boundary Condition at r = 0
rho(1,j+1) = (4*rho(2,j+1)-rho(3,j+1))/3 ;
yo2(1,j+1) = (4*yo2(2,j+1)-yo2(3,j+1))/3 ;
yn2(1,j+1) = (4*yn2(2,j+1)-yn2(3,j+1))/3 ;
yco2(1,j+1) = (4*yco2(2,j+1)-yco2(3,j+1))/3 ;
yco(1,j+1) = (4*yco(2,j+1)-yco(3,j+1))/3 ;
yh2o(1,j+1) = (4*yh2o(2,j+1)-yh2o(3,j+1))/3 ;
yh2(1,j+1) = (4*yh2(2,j+1)-yh2(3,j+1))/3 ;
ych4(1,j+1) = (4*ych4(2,j+1)-ych4(3,j+1))/3 ;
tg(1,j+1) = (4*tg(2,j+1)-tg(3,j+1))/3 ;

%Particle Phase Reaction
%Pyrolysis Reaction
%Assuming Volatiles solely consisted of CH4

av = 5.18e16;
ev = 217270;
kv = av*exp(-ev/(R*tp(j))) ;
devolrat = kv*(ft-mv(j)) ;

if devolrat < 0
    devolrat = 0;
end

%Particle phase reaction rate

```

```

        tmassp =
yo2(jj,j)*32+yco2(jj,j)*44+yn2(jj,j)*28+yh2o(jj,j)*18+yh4(jj,j)*16+yco(
jj,j)*28+yh2(jj,j)*2;
        yop = yo2(jj,j)*tmassp/32;
        ycdp = yco2(jj,j)*tmassp/44;
        yhop = yh2o(jj,j)*tmassp/18;
        q = prate(tp(j),do2m,dco2m,dh2om,Tm,diam,yop,ycdp,yhop);
        mv(j+1) = mv(j)+devolrat*h;
        mt(j+1) = mt(j)-(q(1)+q(2)+q(3))*areap*mt(1)/smass*h-devolrat*h;
        if mt(j+1)<=unburnt
            mt(j+1) = unburnt;
        end
        heatp = 1/12*(q(1)*ho-q(2)*hc-q(3)*hs);
        tp(j+1) =
tp(j)+areap*mt(1)/smass/(mt(j)*cpcoal)*h*(e*sig*(tgas^4-
tp(j)^4)+hconv*(tg(jj+1,j)-tp(j))+heatp);
        if mt(j+1)<=unburnt
            tp(j+1) =
tp(j)+areap*mt(1)/smass*h/(mt(j)*cpcoal)*h*(e*sig*(tgas^4-
tp(j)^4)+hconv*(tg(jj+1,j)-tp(j)));
        end
        peak = find(tg(:,j)>1201);
        if isempty(peak)==0
            tignition=tspan(j)*1000;
        break
    end
end

```

These codes above can be invoked by :

```

ndens = linspace(1e7,1e9);
for i = 1:length(ndens)
    tign(i) = groupND2(ndens(i));
    fprintf('Iteration Completed = %d',i)
end

plot(ndens,tign)

```